



ScuDo
Scuola di Dottorato ~ Doctoral School
WHAT YOU ARE, TAKES YOU FAR

Doctoral Dissertation

Doctoral Program in Built and Landscape Heritage (29th Cycle)

**3D photogrammetric data modeling and optimization for
multipurpose analysis and representation of Cultural
Heritage assets**

By

Elisabetta Donadio

Supervisor:

Prof. Antonia Spanò

Doctoral Examination Committee:

Prof. Bonora Valentina, Referee, Università di Firenze
Prof. Malinverni Eva Savina, Referee, Università Politecnica delle Marche
Prof. Guarnieri Alberto, Università degli Studi di Padova
Prof. Rinaudo Fulvio, Politecnico di Torino
Prof. Chiabrandò Filiberto, Politecnico di Torino

Politecnico di Torino

2018

Declaration

I hereby declare that, the contents and organization of this dissertation constitute my own original work and does not compromise in any way the rights of third parties, including those relating to the security of personal data.

ElisabettaDonadio

2018

* This dissertation is presented in partial fulfillment of the requirements for **Ph.D. degree** in the Graduate School of Politecnico di Torino (ScuDo).

I would like to dedicate this thesis to my little Edo & Tommy

Acknowledgment

Writing this PhD thesis has been a great experience and many people have taken part in this process.

First of all, I would like to acknowledge my supervisor, Prof. Antonia Spanò, who taught me a lot and always encouraged me over these years.

I would to acknowledge my family, my husband, my parents and particularly my little twins, Tommy and Edo, whose liveliness made me a happier and stronger person.

I would to acknowledge Prof. Filiberto Chiabrando, who has always been available, always giving me valuable advices.

Finally, a great acknowledgment goes to all my colleagues, with whom I shared a lot of emotions and laughter in this three years.

Abstract

This research deals with the issues concerning the processing, managing, representation for further dissemination of the big amount of 3D data today achievable and storable with the modern geomatic techniques of 3D metric survey. In particular, this thesis is focused on the optimization process applied to 3D photogrammetric data of Cultural Heritage assets.

Modern Geomatic techniques enable the acquisition and storage of a big amount of data, with high metric and radiometric accuracy and precision, also in the very close range field, and to process very detailed 3D textured models. Nowadays, the photogrammetric pipeline has well-established potentialities and it is considered one of the principal technique to produce, at low cost, detailed 3D textured models.

The potentialities offered by high resolution and textured 3D models is today well-known and such representations are a powerful tool for many multidisciplinary purposes, at different scales and resolutions, from documentation, conservation and restoration to visualization and education. For example, their sub-millimetric precision makes them suitable for scientific studies applied to the geometry and materials (i.e. for structural and static tests, for planning restoration activities or for historical sources); their high fidelity to the real object and their navigability makes them optimal for web-based visualization and dissemination applications. Thanks to the improvement made in new visualization standard, they can be easily used as visualization interface linking different kinds of information in a highly intuitive way. Furthermore, many museums look today for more interactive exhibitions that may increase the visitors' emotions and many recent applications make use of 3D contents (i.e. in virtual or augmented reality applications and through virtual museums).

What all of these applications have to deal with concerns the issue deriving from the difficult of managing the big amount of data that have to be represented and navigated. Indeed, reality based models have very heavy file sizes (also tens of GB) that makes them difficult to be handled by common and portable devices, published on the internet or managed in real time applications. Even though recent advances produce more and more sophisticated and capable hardware and internet standards, empowering the ability to easily handle, visualize and share such contents, other researches aim at define a common pipeline for the generation and optimization of 3D models with a reduced number of polygons, however able to satisfy detailed radiometric and geometric requests.

This thesis is inserted in this scenario and focuses on the 3D modeling process of photogrammetric data aimed at their easy sharing and visualization. In particular, this research tested a 3D models optimization, a process which aims at the generation of Low Polygons models, with very low byte file size, processed starting from the data of High Poly ones, that nevertheless offer a level of detail comparable to the original models. To do this, several tools borrowed from the game industry and game engine have been used. For this test, three case studies have been chosen, a modern sculpture of a contemporary Italian artist, a roman marble statue, preserved in the Civic Archaeological Museum of Torino, and the frieze of the Augustus arch preserved in the city of Susa (Piedmont-Italy). All the test cases have been surveyed by means of a close range photogrammetric acquisition and three high detailed 3D models have been generated by means of a Structure from Motion and image matching pipeline. On the final High Poly models generated, different optimization and decimation tools have been tested with the final aim to evaluate the quality of the information that can be extracted by the final optimized models, in comparison to those of the original High Polygon one. This study showed how tools borrowed from the Computer Graphic offer great potentialities also in the Cultural Heritage field. This application, in fact, may meet the needs of multipurpose and multiscale studies, using different levels of optimization, and this procedure could be applied to different kind of objects, with a variety of different sizes and shapes, also on multiscale and multisensor data, such as buildings, architectural complexes, data from UAV surveys and so on.

Contents

1. 3D digital models for Cultural Heritage	1
1.1 Introduction: aims of the research and the case studies	1
1.1.1 The case studies	3
1.1.1 Lina, the gas doll by Andrea Bertotti	3
1.1.2 The roman loricata bust	4
1.1.3 The frieze of the Augustus' arch in Susa	5
1.2 The Cultural Heritage documentation needs and issues	7
1.3 3D models for multipurpose aims	10
1.3.1 Information and Communication Technology (ICT) for Cultural Heritage	10
1.3.2 3D models for web-based visualization	12
1.3.3 3D models for dissemination and didactic functions	15
1.4 Geomatic survey methods for Cultural Heritage	21
1.4.1 3D multisensor methods for close range surveys.....	22
1.4.2 Range or image based sensors?.....	31
1.4.3 Functions for errors determination in photogrammetric surveys.....	34
1.4.4 3D and 2D data extraction from the acquired data	38
2. The photogrammetric pipeline for Cultural Heritage small assets	43
2.1 State of the art in automated image-based 3D reconstruction.....	43
2.1.1 From traditional photogrammetry to SfM.....	44
2.1.2 The photogrammetric algorithms.....	46
2.2 The image processing pipeline applied to small assets.....	49
2.2.1 The acquisition phase.....	50

2.2.2	The processing phase	53
3.	3D data modeling and optimization of small assets	58
3.1	From the photogrammetric point cloud to a complete mesh.....	58
3.2	3D model optimization	61
3.2.1	3D model segmentation	62
3.2.2	NURBS models.....	65
3.2.3	Game Engine tools and entertainment technology for 3D modeling of small assets.....	66
3.2.4	3D model simplification and remeshing technique.....	67
3.2.5	Diffuse colors, bump, normal and displacement maps	70
3.2.6	Parameterization procedure	74
3.2.7	Retopology tools and quad-dominant mesh.....	78
3.2.8	SubDivision Surfaces and Displaced subDivision Surfaces	80
4.	Experimental section 1 - The image processing applied to the case studies	84
4.2	The case studies acquisition and processing	84
4.2.1	The photogrammetric acquisition of Lina.....	85
4.2.2	The data processing of Lina.....	86
4.2.3	The photogrammetric acquisition of the roman loriccate bust	88
4.2.4	The data processing of the roman statue.....	90
4.2.5	The photogrammetric acquisition of the frieze of the Augustus arch.....	94
4.2.6	The data processing of the frieze of the Augustus arch	96
5.	Experimental section 2 - 3D model optimization of the case studies.....	98
5.1	The optimization pipeline	98
5.1.1	Lina's 3D model optimization	106
5.1.2	Roman loriccate bust 3D model optimization	132
5.1.3	The frieze of the Augustus arch optimization.....	162
6.	Additional evaluations and conclusions	170
6.1	Comparisons through an automatic edge detection on extracted orthographic views	170
6.2	Final considerations	183

6.3 Conclusions and perspectives	185
7. References	187

List of Figures

Figure 1. The sculpture at the time of the acquisition.....	4
Figure 2. The statue as it is preserved in the museum in Torino	5
Figure 3. A view of the south side of the arch.	6
Figure 4. Sketchfab web page dedicated to Cultural Heritage and History	14
Figure 5. An example of a 3D model uploaded in Sketchfab, where it is possible to orbit and zoom around it.	14
Figure 6. A view of the 3DHOP gallery web page where some examples have been created by 3DHOP users and are online on their own website.	15
Figure 7. A view of the installation dedicated to Leonardo, Raffaello and Caravaggio. Source: http://www.mostreimpossibili.it/	17
Figure 8. An example of an Augmented Reality application applied to Aurelian wall at Castra Praetoria in Rome. Source: (Canciani et al., 2016).....	18
Figure 9. Graphical User Interface for the virtual museum tour of "Alt-Segeberger Bürgerhaus", a historic town house in Hamburg. Source: (T P Kersten et al., 2017).....	19
Figure 10. The virtual reality system HTC Vive in use (www.vive.com). The screen in the background shows the same sequence as appears to the user in the VR glasses (right). Source: (T P Kersten et al., 2017).....	20
Figure 11. The 3D scanner Faro Focus 3D. A phase shift laser which can be used for projects at architectural scale (1:100-1:50 - Range 0.60-330 m - Accuracy of point position 2 mm at 25 m.....	24
Figure 12. An example of a structured light system works and the fringe projection on the object.....	26
Figure 13. A Microsoft Kinect XBOX 360.....	26
Figure 14. Creaform Handyscan, Range 0.30 m and accuracy up to 0.030 mm.....	28
Figure 15. The Faro Freestyle	28
Figure 16. Insignificant level of roughness computed on the photogrammetric cloud. (less than 0.5 mm almost throughout the cloud) Roughness computed on the laser cloud presenting a considerable percentage of points affected by noise (2.5-3 mm)	29
Figure 17. The Faro ScanArm, range up to 3.70 m - accuracy of point position 0.025 mm.	30
Figure 15. A graphic representation of the concepts of Precision and Accuracy of a measure.	37

Figure 19. An example of DSM of the frieze of the arch of Augustus in Susa made from photogrammetric data and SfM technique. Source: the author in collaboration with the Geomatic Laboratory of Politecnico di Torino (F. Chiabrando, Donadio, Fernandez-palacios, Remondino, & Spanò, 2014).....	39
Figure 20. Planimetry, orthophoto of the vaults and contour lines of the hall of honor of the Stupinigi castle (Turin - Italy), made from photogrammetric data and SfM technique integrated with terrestrial laser scanner acquisition. Source: the author in collaboration with the Geomatic Laboratory of Politecnico di Torino	40
Figure 21. Progression of cross section through ceiling and wooden structure, in a 3D spatial view. Source: (Bertolini-Cestari et al., 2016)	40
Figure 22. Transversal section of the wooden beam and evaluation of the increasing depression of the wattle dropped ceiling. Source: (Bertolini-Cestari et al., 2016)	41
Figure 23. Ceiling plan of the room, in a bottom-up view. Isolines, derived from progressive planar sections each 1cm (indicated each 5cm step), show the depression of the dropped ceiling. Source: (Bertolini-Cestari et al., 2016)	41
Figure 24. From the 3D point cloud, it is possible to extract information useful for traditional 2D representation such as horizontal plans. In this representation a laser scanner survey has been applied to the Santa Maria Church of Staffarda. Above: an updated planimetry has been processed; below: a trasversal section with corresponding planimetry of the vaults with scalar field and isolines. Source: (Beltramo, Donadio, & Spanò, 2018; Donadio, 2013).....	42
Figure 25. Spatial configuration of the acquisition of an artefact. Source: (Martin-Beaumont et al., 2013)	52
Figure 26. A distortion of the point cloud calculated called blow effect	56
Figure 27. Computed normal on a dense point cloud of a column (software: CloudCompare 2.5.1; command: Compute normal). Source: (Minto & Remondino, 2014)	59
Figure 28. Segmentation of a column example. Source: (Minto & Remondino, 2014)	64
Figure 29. Semantic partition often requires interdisciplinary contributions that can help the identification of restorations. Source: (L Cipriani & Fantini, 2017)	64
Figure 30. NURBS model of an idealized cupola from surveyed data. Source: (Fantini & Pini, 2011)	66
Figure 31. Edge collapse decimation	68
Figure 32. Example of the Quadric Edge Collapse command in MeshLab.....	69

Figure 33. An example of structured remeshing: Irregular, semi-regular and regular. Source: (Alliez et al., 2008)	70
Figure 34. A sphere before and after the bump mapping. Source: lauraatnua.blogspot.it/2015/04/the-difference-between-bump-and-normal.html	71
Figure 35. A wall texture, a normal map and a bump map https://docs.unity3d.com/Manual/StandardShaderMaterialParameterNormalMap.html ..	71
Figure 36. Above: A stone wall with no normal map effect. The edges and facets of the rock do not catch the directional sun light in the scene. Below: The same stone wall with normal mapping applied. The edges of the stones facing the sun reflect the directional sun light very differently. Source: https://docs.unity3d.com/Manual/StandardShaderMaterialParameterNormalMap.html ..	72
Figure 37. Normal mapping across three polygons, viewed as a 2D diagram - Source: https://docs.unity3d.com/Manual/StandardShaderMaterialParameterNormalMap.html ..	73
Figure 38. Texture and normal map - the line-drawing is traced over the fused image of the statue. Source: (Pan et al., 2017).....	74
Figure 39. A mapping U puts a surface S of R^3 in one-to-one correspondence with a subset Ω of R^2 called the (u, v) parameter space. The inverse X of U is named a parameterization of S . Source: (Lévy, 2001)	75
Figure 40. An example of UV creation in Blender in which the user defines the cuts over the surface marking Seams and then the unwrapping creates the corresponding UV map.....	77
Figure 41. A) product of automatic parameterization. B) automatic parameterization of Low-Poly mesh from retopology after semantic partition. Source: (L Cipriani et al., 2014)	78
Figure 42. Above: base retopology example over a head; below: different topology from triangular to quadrangular mesh. Source: https://cloud.blender.org/p/blenderella/56040ecf044a2a00a515ada6	79
Figure 43. Left: High Poly model; right: corresponding Low Poly model from retopology realized with software Luxology Modo.....	80
Figure 44. The retopologized model, subdivision surface level 2, subdivision surface level 5.....	81
Figure 45. Control mesh, smooth domain surface and displaced subDivision surface. Source: (Lee et al., 2000)	82
Figure 46. Once converted in a displaced subdivision surface, it is possible to interactively increase and decrease the level of detail. Source: Adembri 2012	83
Figure 47. Visualization of the cameras position during the acquisition.....	85

Figure 48. Example of a masked image in which two targets used are visible.....	86
Figure 49. Tie point, dense cloud, mesh model and textured mesh model.	87
Figure 50. Automatic UV map processed in Photoscan	88
Figure 51. The camera used and a moment of the acquisition.....	89
Figure 52. An acquired image in which the targets used to scale the model are visible.....	89
Figure 53. Visualization of the cameras position during the acquisition.	90
Figure 54. An example of the masked image.....	90
Figure 55. The sparse cloud with tie points extracted, the dense cloud and the final 3D model viewed as smoothed mesh.....	91
Figure 56. In order to scale the model, the distances between the targets have been measured and then used as scale bars in Photoscan.....	92
Figure 57. UV maps extracted after the texture mapping. Above: UV map derived from the Generic mapping mode; below: UV map derived from the Spherical mode.....	93
Figure 58. Comparison between the texture made using generic mode (above) and the texture obtained with the spherical setting.....	94
Figure 59. Above: the acquisition step; below: the targets placed on the surface have been measured by a total station and referred to a global reference system.	95
Figure 60. Left: dense cloud; right: mesh model	96
Figure 61. Above: mesh model; middle-below: orthophoto of the north and south side.....	97
Figure 62. The proposed workflow for the HP model optimization.....	100
Figure 63. Left: HP model processed in Photoscan; right: HP model processed in 3DReshaper. Below: mesh statistics of Photoscan applied to the new edited mesh, the command Fix Topology is disabled since no more topological errors affect the mesh. .	108
Figure 64. HP model and decimated LP model (3000 faces).	109
Figure 65. Comparison between the HP model and the LP one. It is possible to notice that the 90% of the points of the LP have a displace between +0.001m and -0.001 m, which is a very low value.....	110
Figure 66. Comparison between section profiles extracted from the HP and LP models.	111
Figure 67. Marked seams (in red) and new UV map computed	112
Figure 68. XNormal interface to edit texture maps. The user chooses principally the size of the output image and the type of map.....	113

Figure 69. Left: Normal map generated in XNormal; right: Normal map generated in Blender. In both the images, the dimensions are set 2048*2048 pixels.....	113
Figure 70. Normal map generated in Photoshop.....	114
Figure 71. Graphs of the radiometric frequencies applied to the Blender (above) and Photoshop (below) normal maps, calculated on the red sections.....	115
Figure 72. Graphs of the radiometric frequencies applied to the Blender (above) and XNormal (below) normal maps, calculated on the red sections.....	116
Figure 73. Visualization of the Photoshop Normal map and its projection over the LP model. The so generated mesh is more detailed but offers information only about the material texture lacking the geometric detail.	117
Figure 74. Left: LP model with Blender NM applied; right above: LP model; right below: original HP mesh.....	118
Figure 75. Visual comparison of a render of the HP model (left) and a render of the LP model with NM applied (right). Below: on a zoom it is possible to notice that the LP model with normal map applied (right) has a more smoothed contour due to the greater size of the triangles.	120
Figure 76. Left: automatically generated diffuse color map; right: new diffuse color map keeping the UV map edited in Blender.	121
Figure 77. Node editor of Cycles Render. It is possible to notice both image textures (color diffuse and NM) that have been projected over the LP model as color and normal information for the rendering stage.....	122
Figure 78. Comparison between the LP with diffuse color map and without the Normal map (left) and the LP with diffuse color map and normal map applied (right).	123
Figure 79. Retopologized model and retopologized model with subdivision surface modifier applied (Level 6).	125
Figure 80. Deviation errors between the HP model and the retopolgized one and profile sections extracted with corresponding number of points.	127
Figure 81. Left: calculated displacement map; right; projection and generation of the displaced subdivision surface; below: Displace modifier.	128
Figure 82. Left: HP model; right: displaced subdivision surface.....	129
Figure 83. Deviation error between the HP model and the Displaced subdivision surface and comparison of the extracted polylines. The discards are mostly around 0.000 m.	130
Figure 84. New diffuse color map calculated keeping the UV of the reparametrized retopologized model.....	131

Figure 85. Original HP mesh and textured displaced subdivision surface.	131
Figure 86. Zoom on the Photoscan mesh in wireframe mode in which the topological errors and the noise are visible.....	133
Figure 87. The Photoscan mesh statistics table which reports the presence of topological errors in the mesh and allows to automatically fix them. Unfortunately, the user cannot personally control the operation, editing any factor.	133
Figure 88. The mesh created with 3D Reshaper. Generation with the two steps tool: the user sets the mean triangles dimension and, in a further step, the deviation error in order to refine the final mesh.	134
Figure 89. Final textured model of the statue and final textured model of the cut bust.	135
Figure 90. Quadric Edge Collapse Decimation applied to the whole statue in MeshLab.....	136
Figure 91. Left: the decimated mesh - Level 1; middle – right: the decimated mesh - Level 2.....	137
Figure 92. Ultra decimated Low Polygon (LP) surface - 7000 faces.....	137
Figure 93. Comparison between the decimated surfaces and the High Polygon one. Left: comparison between Level 1 and HP; middle: comparison between Level 2 and HP; right: comparison between Level 3 and HP.	138
Figure 94. Left: Comparison between the high detailed bust and the LP bust. It is possible to notice that the 90% of the points of the LP have a displace between -0.001 m and +0.001 m which is a very low value; right: extracted section profiles.....	139
Figure 95. Section profiles extracted from the HP (red) and LP (green) models.	140
Figure 96. Examples of manually marked seams, highlighted in red.	141
Figure 97. New UV map calculated for the bust which has been unwrapped dividing the front size from the back side. Image dimension 2048*2048.....	142
Figure 98. New UV map calculated for the whole statue that has been unwrapped according to the automatic <i>Smart UV project</i> . Above: the parameter used for the unwrapping. Image dimension 2048*2048 pixels.....	142
Figure 99. Normal map generated for the whole statue and for the bust.	143
Figure 100. Above: Render views of the bust model with normal map applied; below: LP model viewed as Object mode and texture mode with NM applied.....	144
Figure 101. Visual comparison between HP model (above-left), LP one (above - right) and the same LP model with NM applied (below).....	145

Figure 102. New diffuse color maps calculated in Photoscan on the decimated models and according to the edited UV maps.....	146
Figure 103. LP with diffuse color and Normal Map(left) and LP with just diffuse color (right).	147
Figure 104. Results of the LP with diffuse colour and normal mal applied (left) and LP object mode (right).	148
Figure 105. Left: original HP model; right: final rendered result LP model with NM applied.....	149
Figure 106. Shrinkwrap modifier and an example of quadrangular polygons generation over the HP mesh.	150
Figure 107. Above: Retopologized model of the statue and of the bust portion. Below: new UV map calculated on the retopo bust model.	151
Figure 108. Above: section profiles extracted on the HP and retopologized models. Below: deviation error between the HP model and the retopologized one. It is possible to notice that in this case the mean value is higher.	153
Figure 109. Retopologized bust after the SubDivision Surface modifier – level 6.	154
Figure 110. Displacement map and its projection over the retopologized model. Below: The Displace modifier.	155
Figure 111. New diffuse color map computed on the retopologized model.....	156
Figure 112. Final displaced subdivision surface.....	157
Figure 113. LP model with NM, Displaced SubDivision Surface and original HP model, without and with diffuse color texture.	158
Figure 114. Zoom on LP model with NM, Displaced SubDivision Surface and original HP model.	159
Figure 115. Displacement between the original HP model and the Displaced SubDivision Surface	160
Figure 116. Section profiles extracted from the HP (red) and the Displaced SubDivision Surface (green) models.	161
Figure 117. HP model of the north frieze.	162
Figure 118. LP model generated in MeshLab – 15.000 faces.....	163
Figure 119. On the left the Normal map computed in Blender; on the right the diffuse color map recalculated in Photoscan keeping the edited UV map.	163
Figure 120. LP model with the NM applied.	164
Figure 121. Textured LP model with NM and diffuse color maps applied.	165

Figure 122. Retopologized mesh projected over the HP model.....	166
Figure 123. Above: Retopo mesh; middle: subdivided surface; below: displaced subdivision surface.....	166
Figure 124. Displacement map	167
Figure 125. Above: zoom over the displaced subdivison surface; below: zoom over the HP mesh	167
Figure 126. Final displaced subdivision surface without and with diffuse color map	168
Figure 127. Above: original HP orthophoto; middle: orthophoto from LP model without NM applied; below: orthophoto from LP model with NM applied.	169
Figure 128. An example of the edge detection performed by Canny algorithm. Source: (Canny, J., 1987).....	172
Figure 129. Above: original HP model; middle: LP model with NM; below: displaced subdivision surface.....	173
Figure 130. An example of the syntax applied with default values.....	174
Figure 131. Canny filter HP. Threshold [0.03 0.08] sigma (0.8).....	175
Figure 132. Canny filter - LP model with NM applied. Threshold [0.03 0.08] sigma (0.8).....	177
Figure 133. Canny filter default value – Displaced subdivision surface. Threshold [0.03 0.08] sigma (0.8).....	179
Figure 134. Sobel edge detection. Default value.	179
Figure 135. Canny edge detector applied on a zoomed portion of the frieze – HP model- Threshold 0.2, sigma 3.....	180
Figure 136. Canny edge detector applied on a zoomed portion of the frieze. Threshold 0.2, sigma 3.....	181
Figure 137. Canny edge detector applied on a zoomed portion of the frieze - Displaced subdivision surface. Threshold 0.2, sigma 3.	182

List of Tables

Table 1. Evaluation of the factors influencing the acquisition and processing pipeline of both active and passive sensors.	34
Table 2. Visualization of the calculated errors of the control points used for scaling the 3D data.	87
Table 3. Visualization of the errors of the scale bars used for scaling the 3D data ...	92
Table 4. Control points errors propagation	96
Table 5. Decision support system of the tested methodologies	99
Table 6. The Pipeline applied to the test cases.	102
Table 7. Comparison between the HP mesh generated in Photoscan and 3DReshaper	108
Table 8. Report of the faces and KB reduction from the HP model to the LP one..	124
Table 9. Report of the file sizes involved in the optimization process	124
Table 10. Report of the faces and KB reduction from the HP model to the LP one.	132
Table 11. Report of the file sizes involved in the optimization process	132
Table 12. Comparison between the original Photoscan mesh and the 3D Reshaper one.....	134
Table 13. The results of the decimated mesh model compared to the original one.	137
Table 14. Report of faces and KB reduction from the HP model to the LP one.....	149
Table 15. Report of the file sizes involved in the optimization process	149
Table 16. Report of the faces and KB reduction from the HP model to the retopologized one.....	156
Table 17. Report of the file sizes involved in the optimization process	156
Table 18. Report of the file sizes involved in the optimization process as well as the KB reduction from the HP model to the LP one.....	165
Table 19. Report of the file sizes involved in the optimization process	165
Table 20. Comparison of the file sizes of the faces and KB reduction from the original HP model to the LP one.....	167
Table 21. Report of the file sizes involved in the optimization process.	167

Acronym Index

AG	Augmented Reality
API	Application Programming Interface
BA	Bundle Adjustment
BBA	Bundle Block Adjustment
BSDF	Bidirectional Scattering Distribution Function
BIM	Building Information Model
CCD	Charge-Coupled Device
CG	Computer Graphics
CH	Cultural Heritage
CIPA	Comité International de la Photogrammétrie Architecturale
CP	Check Point
DOF	Depth Of Field
DoF	Degrees of Freedom
DSM	Digital Surface Model
DTM	Digital Terrain Model
FEM	Finite Elements Methods
GCP	Ground Control Point
GNSS	Global Navigation Satellite System
GPS	Global Positioning System
GSD	Ground Sampling Distance
HP	High Polygon
ICH	Intangible Cultural Heritage
ICOM	International Council of Museum
ICOMOS	International Council on Monuments and Sites
ICP	Iterative Closest Points
ICT	Information and Communication Technologies
ISPRS	International Society of Photogrammetry and Remote Sensing
LIDAR	Light Direction and Ranging
LoG	Laplacian of Gaussian
LoD	Levels of Detail
LP	Low Polygon

MSER	Maximally Stable Extremal Regions
MVS	Multi-View stereo
NM	Normal Map
NURBS	Non-Uniform Rational B-splines surfaces
RANSAC	RANdom SAmples Consensus
RMS	Root Mean Square
RMSE	RMS Error
SDS	Smooth domain surface
SfM	Structure from Motion
SGM	Semi Global Matching
SIFT	Scale Invariant Feature Transform
SLR	Single Lens Reflex
SLS	Structured Light Sensor
SUBD	SubDivision
SURF	Speed Up Robust Feature
TOF	Time Of Flight
UAV	Unmanned Aerial Vehicle
UNESCO	United Nations Educational, Scientific and Cultural Organization
UTI	Ultrasonic Tomographic Imaging
VR	Virtual reality

Chapter 1

3D digital models for Cultural Heritage

1.1 Introduction: aims of the research and the case studies

Nowadays the modern Geomatic techniques of 3D metric survey allow to collect and store highly detailed 3D data, useful for multipurpose aims and applications and many institutions and museums are interested on the possibility to easily share and disseminate 3D digitized contents and related information with the public. The research here presented deals with the issues concerning the processing, managing, representation and dissemination of the big amount today processed in any Cultural Heritage documentation phase. In particular, this thesis is focused on the managing and optimization process in application to 3D photogrammetric data of Cultural Heritage assets. The photogrammetric pipeline represents a valid process for a low cost digitization of artefacts and the presented optimization can facilitate the access to the data, the promotion of interdisciplinary studies and their widespread dissemination.

The high resolution and textured 3D models, today achievable with modern Geomatic techniques, represent a base for multidisciplinary aims, from scientific studies focused on the geometry and materials, to visualization and dissemination applications via web or in museum contexts, but they have very heavy file sizes (also tens of GB) that makes them difficult to be handled by common and portable devices, published on the internet or managed in real time applications.

Even though recent advances produce more and more sophisticated and capable hardware, empowering their ability to easily handle, visualize and share such contents, other researches aim at define a common pipeline for the generation of 3D models with a reduced number of polygons but able to satisfy detailed radiometric and geometric requests. Starting from these issues, this research is inserted in this second scenario and tested the 3D models optimization processing, in application to three case studies: a modern sculpture of a contemporary Italian artist, a roman marble statue, preserved in the Civic Archaeological Museum of Torino and the frieze of the arch of Augustus of Susa. This process consisted in the attempt to reduce the file size of the final textured models (otherwise hard to be handled) through the generation of Low Polygons mesh, with very low byte file size (few KB), while maintaining the highest degree of detail as possible, comparable to the original High Polygons one. To do this several tools borrowed from the game industry and game engine have been tested. The main activity of this work consisted, starting from High Polygons 3D models (made by millions of polygons), in the generation of Low Polygons models (constituted by hundreds of polygons), obtained testing different decimation and optimization procedures (remeshing and retopology), with different Level of Detail (LoD), able to show however a high detail comparable to the original 3D model, by means of the fake detail offered by the projection of particular texture maps, usually used in game engine and entertainment applications.

This application may meet the needs of multipurpose and multiscale studies and, for this reason, different optimization and decimation process have been tested, editing and comparing different levels of detail. The process here presented is focused on assets and to photogrammetric data, but such optimization can be tested to any kind of object with a variety of different sizes and shapes and on multiscale and multi-sensor data, such as buildings, architectural complexes, data from Unmanned Aerial Vehicle (UAV) surveys and so on.

The final generated models have been then analyzed and compared to original ones in order to define the quality of information that can be extracted and related accuracy in relation to multipurpose analysis and dissemination aims.

Indeed, what it is interesting to analyze is what the optimized models are still able to say, once they are reduced. The geometry is hardly decimated, using different methods, but they look like the original high detailed models.

- Which information can be extracted from the optimized models, from a geometrical and radiometric point of view?

- How to evaluate the differences, the quality and precision of the final output data, also in comparison to the original detailed models?
- How to compare them from a metric point of view? Which objective method can be used?

These are some of the questions that raised looking at some of the achieved results. The optimized models are quiet similar but depending on the type of optimization they look a little bit different in the rendering stage. So one of the aims of the thesis is also to find an objective and sharable approach able to compare the differences presented in the optimized models and define their possible application fields.

The thesis is structured in 6 chapters, in the first one the state-of-the-art about the Cultural Heritage documentation needs is presented, as well as the available 3D multi-sensor survey methods. In the second chapter the photogrammetric pipeline and image matching algorithms are presented. In the third section, the 3D data modeling and optimization process and tools are explained. The fourth and the fifth chapters present the experimental sections, the image processing applied to the case studies is presented and then the proposed optimization process is tested and evaluated. In the last chapter some additional evaluation and comparison applied to the optimized models, the conclusion and future perspective are presented.

1.1.1 The case studies

The case studies of this thesis have been chosen according to the aims of the work and considering different level of details, scales and decorative elements.

In order to validate the applied tools and the proposed optimization pipeline which aims to meet multipurpose needs, three case studies have been chosen, which differs for decorative elements and dimensions:

- a terracotta sculpture of a contemporary Italian artist;
- a marble roman bust, preserved in the Civic Archaeological Museum of Torino;
- the frieze of the Augustus' arch preserve in the Archeological site of the city of Susa.

1.1.1 Lina, the gas doll by Andrea Bertotti

Lina is a terracotta sculpture of the contemporary italian artist Andrea Bertotti. The statue represents the shape of a gas cylinder that has the appearance of a female figure. With this artwork the artist aims to interpret the concept of containment vs expansion, assuming

that human desire pushes him to expansion, without limits. Lina has rounded and soft limits showing its freedom. According to the artist: "*we were gas and we will be gas again*". The sculpture has been surveyed before the cooking operation in the studio of the artist.



Figure 1. The sculpture at the time of the acquisition

1.1.2 The roman loricate bust

This bust, named "loricate" because of its decorated armour, was found, with another one very similar, in 1802 in the city of Susa, after a demolition of a stroke of the fortifications. Now it is possible to admire the statues in their completeness since in the nineteenth century, a restoration action completed both of them adding the missing heads, low parts of the legs and the arms. The surveyed bust represents a Julio-Claudian emperor and is an exceptional witness of the north Italian sculpture during the first imperial age (Cadario, 2005). In the decorated armor, goddess Athena (identified with the Palladium, the sacred statue that Enea brought from Troia) is represented surrounded by two dancing maidens giving her weapons, whose presence contributes to create a sacred atmosphere suitable for the veneration of the goddess. This representation had the aim to invokes the mythical origins of the gens Iulia (Cadario, 2005). Under the armor, the statue presents

the *pterigi*, which are fringes that form a sort of decorative skirt used by the ancient Greek and Roman soldiers under the armor.

The dimensions of the statue are about 2 m high and 0.5 m wide and it is now located over a pillar.

The marble grain makes the statue suitable for a photogrammetric survey. Indeed, as reported in (Guidi, Remondino, Russo, & Spinetti, 2009; Nicolae, Nocerino, Menna, & Remondino, 2014) marble, which derives from the aggregation of small packed grains of calcite realizing a crystalline rock, may generate errors and noise if surveyed with an active sensor, due to heterogeneous reflection properties that may be encountered if the marble surface is too smoothed and shiny.



Figure 2. The statue as it is preserved in the museum in Torino

1.1.3 The frieze of the Augustus' arch in Susa

The Arch of Augustus in Susa (Piedmont - Italy) was built with white marble in 8 BC by King Cottius in memory of the treaty between the Romans and the Gauls (Figure 3). It is

one of the oldest existing and well preserved Roman arches and it was part of a great building program for the construction of the new capital of the Alpes Cottiae Province (Agostoni, Barello, Borghi, & Compagnoni, 2016). It is placed along the ancient road that leads to Gaul, near the Praetorium, the headquarters of the Roman praefectus. Its illustrated and well preserved friezes are an exceptional historical testimony of the meeting of two different cultures (Roman and Gauls). The representations depict religious ceremonies and administrative procedures that took place immediately after the political agreement (13 BC) between the Roman Empire and the local dynast M. I. Cottius, who obtained, on that occasion, Roman citizenship and the title of Prefect. The architectural design is typical of the Roman architecture of the period and shows all the effort to provide the new capital with typical infrastructure and monuments of contemporary Roman city planning.

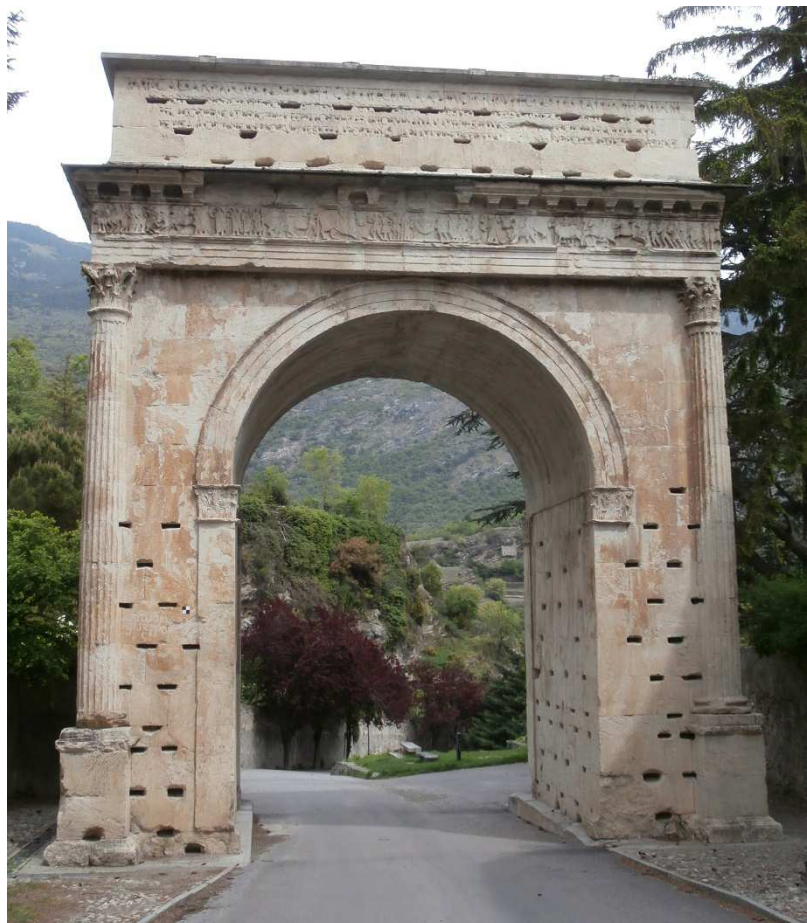


Figure 3. A view of the south side of the arch.

1.2 The Cultural Heritage documentation needs and issues

Every day architectural heritage around the world must face continuous and damaging challenges and deformations due to human factors, such as unregulated urban development, tourism, pollution and wars, as well as physical factors such as aging, humidity, dust, natural disasters and pressure (Sužiedelytė-Visockienė, Jūratė Bagdžiūnaitė, Malys, & Malienė, 2015). For these reasons, the preservation, documentation and dissemination of Cultural Heritage are important tasks and also a duty to be pursued for transmit them to future generations.

The Cultural Heritage (CH) documentation is a complex process which requires the collaboration of many multidisciplinary activities that include surveying, monitoring, gathering and sharing a big amount of information. The different technical apparatus, methods and aims requested by different scientists involved in this process, usually produce heterogeneous datasets, stored in different media types, data formats, models of different quality and spread around different institutions (Auer, Agugiaro, Billen, Loos, & Zipf, 2014).

The documentation and monitoring is a very challenging phase, also due to the different sizes of the objects that have to be preserved as well as the variable required quality and resolution. For these reasons it is difficult to establish common documentation standards. Main guiding concepts of the Cultural Heritage documentation have been presented in many researches, i.e. (D'Ayala & Smars, 2003; Patias, 2006). As most important concepts to be pursued they include:

- the objectivity of the documentation which influences further actions;
- the values importance, considering that what now can be seen uninteresting, may appear extremely valuable in the future;
- the learning process;
- the continuity of the documentation process over time;
- the integration of multidisciplinary sources and methods;
- the redundancy of the data and the possibility to link information about the data quality.

Already in the 60's, International organizations have been facing the need of issuing guidelines for standards of the documentation. The most important ones are represented by the International Council on Monuments and Sites, ICOMOS and UNESCO, with the well-known Venice Charter, The International Charter for the Conservation and Restoration of Monuments and Sites, 1964, and the International Committee for Heritage Documentation, CIPA, (<http://cipa.icomos.org/>), founded in 1969 by ICOMOS and the

International Society of Photogrammetry and Remote Sensing (ISPRS) with the main aim to connect an international community interested in the improvement of all methods for surveying the Built Heritage. Another important organization is the ICOM, the International Council of Museum (<http://icom.museum/>), created in 1946 by and for museum professionals and committed to improve the conservation and protection of cultural goods. Nowadays, the ICOM Code of Ethics for Museums represents a reference for the global museum community, establishing a set of standards for professional practices and designing the main goals for museums. The museum sector has been one of the first sectors that developed shared standards, and by now it is well-known the importance of the virtual digital component and the online sharing of information, 3D models included.

The common features stated in the years by the international agreement are:

- recording 4D (3D plus time) multidisciplinary information, of different sources, formats and contents, and their sharing and distribution to the users;
- 3D digital inventories enriched, when possible, by dated historical images, texts;
- visualization and communication of the data in a user-friendly way, allowing different possible users to manage and query the data, selecting useful information according to their interests, using Internet and others visualization techniques.

In latest years, the digitization process of Cultural Heritage has increased a lot. Indeed, in recent years almost all the developed countries have invested in the creation of free digital archives in which their digitized Cultural Heritage is stored and viewable (for some examples see 1.3). Nowadays, in the 3D survey and modeling field, the developed technological advances allow to digitally preserve the memory of built heritage thanks to available and accurate instruments and methods, and the achievement of digital data represented by highly detailed 3D models has changed the cognitive model and working approach. For many years, the documentation and communication of Cultural Heritage was based on printed materials (texts, images) or in some cases videos. By now, high resolution digital reproduction of Cultural Heritage represents not just a simple copy of the objects but an increase in its communication skills: an enhanced vision that can provide a useful service for its enhancement. Indeed, 3D digital replicas efficiently communicate information about scenes or objects characterized by important 3D shapes if compared to more traditional 2D representations such as photos, videos or drawings (Manferdini & Remondino, 2012). Such kind of 3D data are, in fact, more and more dynamic and interactive. An object can be viewed both in its entirety or focusing on its minimal details. The user can directly choose the dimension, the viewpoint to access each single artifact and different levels of detail, focusing on specific elements which can be

sometimes hardly visible also to the naked eye. An architectural object, for example, can be navigated in the context where it is situated today, but can also be seen in its original place, which may have been virtually 3D reconstructed (Ott & Pozzi, 2011).

In latest years, Geomatic methods have reached great popularity in different Cultural Heritage sectors: documentation, diagnosis, restoration, conservation, communication and fruition. The continuous evolution and improvement of 3D survey methods, as well as their integration, involve multi scale contexts, from small artefacts, artistic and archaeological heritage to many other types of assets, architectural complexes and landscapes (Chiabrandò, Spanò, Sammartano, & Teppati Losè, 2017; Ramos & Remondino, 2015; Dall'Asta, Bruno, Bigliardi, Zerbi, & Roncella, 2016).

One of the main issues that such detailed 3D in their management is due to their heavy file size. Final processed 3D models are constituted by millions of polygons and high resolution textures, with very large data volumes, which may become very difficult to be handled and visualized by common computers, portable devices with low performance (e.g. Smartphones and tablets) or on the Internet. Even though many technological improvements have been done in hardware and software, the recovering of large polygonal models may, in fact, led to several management problems, i.e. too long processing and editing time or bad real-time visualization too limited by the hardware performance (Jiménez Fernández-Palacios, Morabito, & Remondino, 2017). With regard to this, nowadays the scientific community is trying to develop new ways to optimize and share such 3D digital contents, in order to guarantee fast access to the data and their effective communication (e.g. in dissemination and valorization applications of Virtual and Augmented Reality), providing low resolution 3D models easy navigable and viewable (Cipriani & Fantini, 2017; Guarnieri, Pirotti, & Vettore, 2010). Some critical considerations about the contradiction between the great increase in digitization projects of cultural assets in the last decade and the problems that today are an obstacle to their massive sharing on the web can be found in (Scopigno, Callieri, Dellepiane, Ponchio, & Potenziani, 2017)

From these considerations, about the needs and the new available approaches, derives the aims of this thesis.

1.3 3D models for multipurpose aims

Cultural Heritage increasingly requires interdisciplinary researches and the possibility to share, compare and integrate them, is desirable and essential. Among the potential users there are architects, engineers, restorers, CH curators, museum visitors and scholars.

Reality based 3D models offers great opportunity for specialistic studies on the geometry and materials, with high precision, but also for dissemination or visualization aims. As explained in the following 1.4, different representation are achievable and different data can be extracted.

In the model processing stage, it is always necessary to establish the needs that the 3D model have to fulfil, which determine the final level of geometrical and radiometric accuracy, size and visualization, but with the constant aim of not losing quality and information. Different purposes led to different processing choices and different optimization levels, depending on the final aim to pursue, whether it is a specialized analysis (Gonizzi Barsanti & Guidi, 2017), or a communication application (Kai-browne, Kohlmeyer, Gonnella, & Bremer, 2016).

The possible use of 3D models for further specialized studies needs high detailed acquisition and processing to generate detailed copies as close as possible to the shape and contents of the real one (Balletti, Adami, Guerra, & Vernier, 2012). In this case, the models must be particularly dense and rich in information with very high accuracy and high geometrical and radiometric resolution.

When the aim is dissemination and web visualization, 3D models must be suitably processed to make them easy to be handled. In this case, the information density can decrease depending on the communication purpose, and, with the aim of maintaining high adhesion to the original object, the optimization of surfaces, involving remeshing techniques and other textures techniques tested in this research, seems to be a very promising perspective.

1.3.1 Information and Communication Technology (ICT) for Cultural Heritage

In the important study of David Bolter and Richard Grusin (Bolter & Grusin, 1996), the concept of remediation is defined as the process in which a newer medium replaces an older one, borrowing and reorganizing its writing characteristics and reforming its cultural space. An example of refashioning is represented by the shift, in Western Europe,

from handwritten codex to printed books, as well as the more recent shift to electronic writing.

Even before, in the Sixties, Levine and McLuhan (Levine & McLuhan, 1964) stated that "the 'content' of any medium is always another medium" meaning that "The content of writing is speech, just as the written word is the content of print, and print is the content of the telegraph."

Nowadays, the access to heritage objects is re-mediated through networks. Starting from this point, hypermedia applications can be considered as acts of remediation, since they import preceding media within a new digital space in order to rebuild and "refashion" them. Modern digital media application that aim at a total virtual immersion and immediacy (such as in virtual reality and virtual games) can be viewed as acts of remediation.

Information and Communication Technologies (ICT) have been giving a growing support to Cultural Heritage preservation and exploitation from many years.

ICT may contribute to spread cultural patrimony among people, increasing communication, education and concretely contributing to the recognition of the importance of the past (Ott & Pozzi, 2011).

At first, the focus of ICT applications was on transferring paper catalogues into the corresponding digital metadata, cataloguing CH and related metadata, then on the digitization of documents and multimedia objects such as photos and audiovisual recordings. More recently, developments of ICT allow to enrich and augment the original preserved information, making it easier to retrieve and explore such information (Haus, 2016).

Providing an augmented access to Cultural Heritage knowledge, ICT significantly changes the way Cultural Heritage can be studied and communicated. In fact, ICT allows:

- An enhanced and multi-perspective view of digitized objects, available in a digital form.
- Entertaining: Development of interactive games designed to be also educational. This is known as "Edutainment", a combination of education and entertainment, a concept more and more popular and pursued by museums insiders (Martina, 2014).
- To better understand: for example, with application of virtual or augmented reality and virtual museums.
- Interactivity: CH visitors aim to learn something during their visit and interactivity allows contents to be more easily impressed. The users can select the level of information they would to achieve, according to their interests and capabilities.

- Usability: If the application is too complicated to be used, the visitor's commitment is too focused on how the system works, rather than the content itself. For this reason, it is essential to develop as far as possible user-friendly application that enable the user to easily receive the content he look for (Owen Ruth, Buhalis Dimitrios, & Pletinckx Daniël, 2005).

- Intangible cultural Heritage (ICH) preservation: while traditional CH concerns information mostly related to the material world – such as buildings, monuments, books, artworks, artefacts, and even natural heritage such as landscapes and biodiversity – in the virtual domain ICH can be preserved and exploited (Haus, 2016).

In recent years almost all the developed countries increased their production of digital archives in which their Cultural Heritage is digitized. Some examples are the MINERVA EC4 (eContentPlus), a thematic network in the field of cultural, scientific information and didactic material, working on the digitization and online sharing of cultural contents and digital preservation across the Europe; The MICHEAL project⁵ (e-TEN) a European trial to create digital collections from museums, archives, libraries and other cultural European institutions (Ott & Pozzi, 2011). Also big Internet players has been advocated as a fundamental support in this attempt: some examples are Google Book Search and Google Art Project that dominate the international scene (Bonacini, 2013).

1.3.2 3D models for web-based visualization

As already stated, an interesting potentiality that modern 3D models offer is to conceive them both as visualization container and/or as intuitive interface for the representation of different kinds of data. For the resource management, research and public-educational dissemination of built heritage, it is essential to improve and simplify the access to 3D models and their related attribute data. Since the amount of data grows over time and they may be stored in different archives and databases, a common attempt should be the integration of all information together, granting their easy access, for example through web-based solutions. In this purpose, 3D models can be used as a valid and potential graphical interface to further access the data behind (Auer et al., 2014).

The visualization of the 3D content in web pages has arrived with a significant delay in comparison to other kind of digital media such as texts, images, videos or sounds. Originally, 3D data were managed only locally, then, several different approaches have been developed and tested for their distribution and visualization on the web (e.g. VRLM, X3D). The first attempts showed some disadvantages, since the 3D data was confined to a simple visualization tool, developed as a plug-in that the user should explicitly install. This approach did not meet the needs of the CH community, where probable users may

not be ICT experts, and a request of installation of a new software may frequently discourage from a further exploration (Ponchio et al., 2014).

The debut of the WebGL standard in 2009 represented a big change in this scenario. WebGL is a new component of the OpenGL ecosystem, developed as a JavaScript Application Programming Interface (API), which enables the implementation of 3D data within web pages without the need to install other plug-ins or Java applets. All major browsers have at least a partial support implemented. The WebGL based technology allows a direct access to the rendering pipeline of the graphics card, the so called programmable pipeline of OpenGL ES 2.0 (Auer et al., 2014). Since WebGL is a low-level API, thereafter others higher-level libraries have been implemented to enable the design and implementation of applications also by non-expert users. These new libraries use different programming paradigm, ranging from scene-graph-based interfaces, such as X3Dom (Behr, Eschler, Jung, & Zöllner, 2009), to procedural paradigms, like SpiderGL (Di Benedetto, Ponchio, Ganovelli, & Scopigno, 2010).

The advent of WebGL brought an enormous potential for CH applications development. First of all because it is not necessary to install specific plugins and also because thanks to WebGL 3D data can be managed in a web page, immersed in the full multimedia context (Di Benedetto et al., 2014). However, a WebGL application entirely leans on the JavaScript engine that the browsers use to interpret the application code and, differently to desktop applications, does not allow a direct control over the memory management. For this reason, it is indispensable to apply a reasoned strategy of data loading and unloading when dealing with detailed 3D models. A good practice is represented, for example, by incrementally loading 3D data as parts and with different resolutions according to the visible field, the distance between the observer and the object and viewing angle (Auer et al. 2014).

A well-known web database of 3D models is Sketchfab (<https://sketchfab.com/>), a web platform where it is possible to publish, share and discover 3D, VR and AR contents.

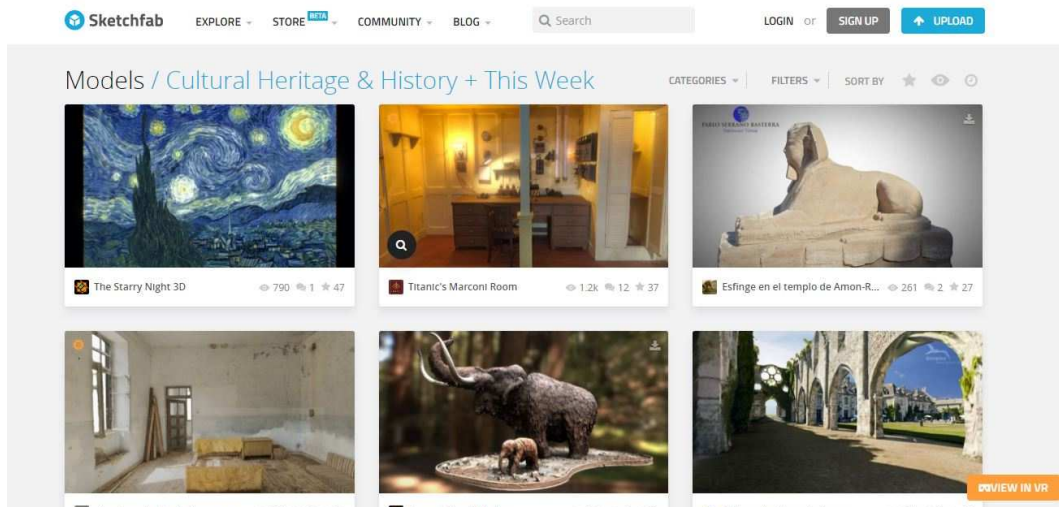


Figure 4. Sketchfab web page dedicated to Cultural Heritage and History



Figure 5. An example of a 3D model uploaded in Sketchfab, where it is possible to orbit and zoom around it.

Another interesting platform is 3DHOP (3D Heritage Online Presenter) (<http://vcg.isti.cnr.it/3dhop/index.php>) that is an open-source software package that

allows the interactive Web implementation of high-resolution 3D models, principally aimed to the Cultural Heritage domain. The 3DHOP package may represent an interesting tool for museum curators, CH institutions, Web designers, students, up to companies that develops web-based applications.

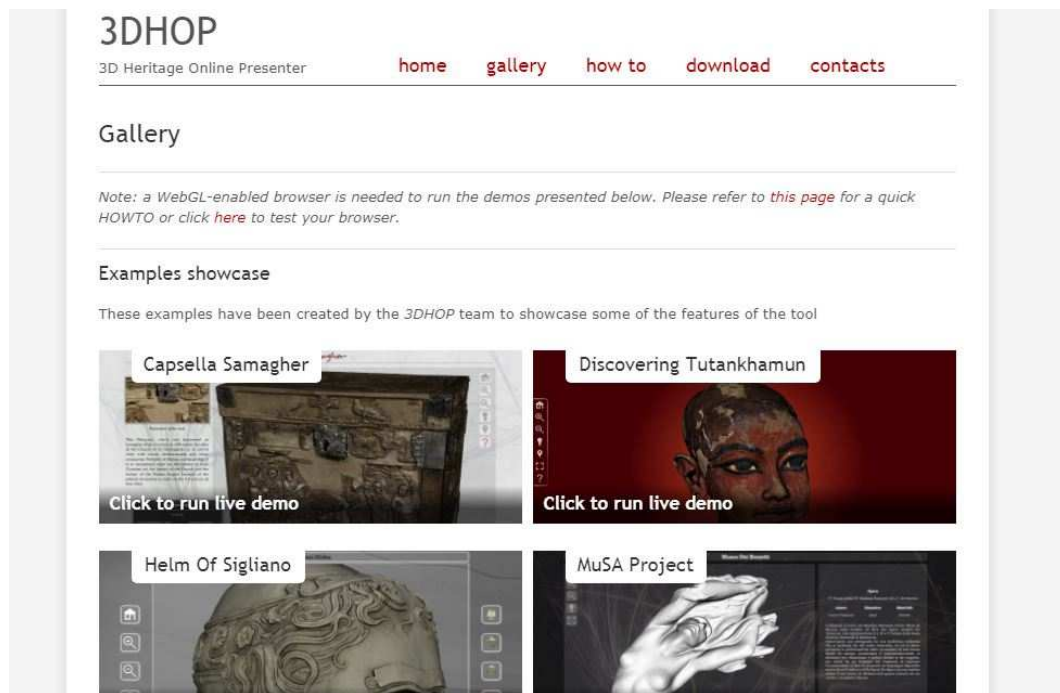


Figure 6. A view of the 3DHOP gallery web page where some examples have been created by 3DHOP users and are online on their own website.

1.3.3 3D models for dissemination and didactic functions

The contribution of the cultural sector to the European Economy is extremely important and each country could take great advantages which are both social and economic.

In latest years, museums and other CH institutions have been increasingly investing money and attention not only on cutting edge documentation and information systems, but also on the introduction of new multimedia technologies, encouraging more consolidated relationships with their visitors.

Many museums look today for more interactive exhibitions which involve and increase the visitors' emotions enhancing the museum interactive experience and in recent years, museums' role changed from a simple "container" of cultural objects to a "narrative

space" able to show and describe in a more captivating way the preserved historical material (Donadio, Barellò, & Mazza, 2016).

Cultural institutions offer new experiences to their visitors: mobile multimedia devices that guide the visitor during his visit or virtual museums with online content. These technologies offer the great opportunity of delivering personalized content connected to user interests, age and cultural background. From the museum professionals point of view, this kind of application may offer many advantages, such as monitoring of the visitors patterns, interests, and, in some cases, real time communication.

By now, the developed application in this field strengthen the divulgation opportunities through:

- interactivity;
- multimedia: images, texts, videos...etc.;
- hypertext: links that refer to other databases;
- increasing diffusion and degree of remote accessibility to goods;
- multiplication of information;
- benefits for poorer categories;
- multilingualism of messages;

On the other hand, the disadvantages may be in some cases:

- decontextualization of fruition;
- cultural banalization.

A key to success is certainly to invest in interoperability of CH digital archives. Interoperability implies that the owners of different CH archives agree to join their digital contents, so that users can navigate multiple archives transparently as a single, larger one. For example, the complete production of a great painter, whose paintings are probably exhibited in a number of different museums and art galleries, could be experienced in a single virtual gallery thanks to the interoperability among institutions' archives (Haus, 2016). A good example of a web digital transformation is represented also by the Tate with its "fifth gallery" online (<http://www.tate.org.uk/about-us/digital>).

Another similar attempt is represented by "Le mostre Impossibili", realized starting from 2003 and dedicated to Caravaggio, Leonardo and Raffaello, which present, in a single and real exhibition space, the complete work of a painter in the form of high-definition reproductions, making use of digital technologies that allow reproductions absolutely in conformity with the original works (<http://www.mostreimpossibili.it/progetto.html>).



Figure 7. A view of the installation dedicated to Leonardo, Raffaello and Caravaggio. Source: <http://www.mostreimpossibili.it/>

Among the ICT applications of CH divulgation, four applications are particularly useful for data visualization and interpretation:

- Augmented Reality (AR): a technology that superimposes a digital image (or a 3D model) on a user's view of the real world. In this way it creates a composite view using mobile devices such as tablets and shareware software (Canciani, Conigliaro, Del Grasso, Papalini, & Saccone, 2016; de la Fuente Prieto, Castaño Perea, & Labrador Arroyo, 2017; Pierdicca et al., 2015).



Figure 8. An example of an Augmented Reality application applied to Aurelian wall at Castra Praetoria in Rome. Source: (Canciani et al., 2016)

- Interactive Museum Installation: computer-based systems, used within the site, where the user gives an input to the system that in turn affects the output.
- Mobile Multimedia Guide: An enhancement of traditional audio guides constituted by wireless devices where multimedia can be presented and have also the capability to track the user's position accordingly sending information (Owen Ruth et al., 2005)
- Virtual Museums: The lack of space is one of the main reasons why virtual museums should be considered, as most of museums display only a small part of their collection. These applications use multimedia contents, such as texts, images, sounds and animated 3D models, creating interactive platforms where digital collection can be explored time- and location-independently, or panorama-based virtual tours and even interactive apps for smartphones or tablets (Kersten, Tschirschwitz, & Deggim, 2017). They are becoming an integrative and widespread way for museums to present their collections and information (Rodríguez Miranda, Valle Melón, Calparsoro, & Iñáñez, 2017).



Figure 9. Graphical User Interface for the virtual museum tour of "Alt-Segeberger Bürgerhaus", a historic town house in Hamburg. Source: (T P Kersten et al., 2017)

- Virtual Reality immersion systems, CAVE: Virtual reality is a technology of mediation which aims to create "immersive" spaces. Its purpose is to disappear, surrounding the user with a computer-generated world. With a display mounted on the head, virtual reality gives a first-person point of view where the viewer should forget the computer interface and see the virtual reality that is offered as a visual world. In this kind of application, digital medium aims to completely delete itself, so that the user acts in this reality as he would if he were in the real world (original medium). Ideally, there should be no difference experiencing an artwork through a digital medium or seeing it in person, even though this is almost impossible to reach. The computer presence is always felt anyway, for example if the user must click on a icon or slide a bar to view what he desires or if the digital image (or the 3D model) may appear grainy or with distorted colors (Bolter & Grusin, 1996).



Figure 10. The virtual reality system HTC Vive in use (www.vive.com). The screen in the background shows the same sequence as appears to the user in the VR glasses (right). Source: (T P Kersten et al., 2017)

With regard to museum assets, recent extensive digitalization projects aimed at achieving multilingual information archives that make digital libraries accessible to everyone. This is the main mission of Europeana project, (<https://www.europeana.eu/portal/it>), but also of other institutions as the Getty Foundation or the Smithsonian institution which are devoted to the preservation of Cultural Heritage (CH), promoting research, culture and educational activities or directing efforts towards the achievement of standards for CH and the realization of digital inventories.

Another interesting project is the 3D-ICONS (3D Digitisation of Icons of European Architectural and Archaeological Heritage) project, funded by the European Commission, which aims at generating 3D models of architectural and archaeological monuments of remarkable cultural importance for Europeana. The main aim of this project is to realize about 3,000 3D models, that have to be processed both as high resolution 3D content and in a further decimated form, in order to be easily visualized on common computers connected to a 3D web database. To reach this goal, (Guidi, Gonizzi Barsanti, Micoli, & Russo, 2015) presents a suitable pipeline for the digitization of Cultural Heritage assets and connected attributes.

NUBES is a research project which aims at develop an information platform at architectural scale. It consists in an online implemented system for documenting, visualizing, analyzing and sharing detailed 3D models of CH objects. The NUBES platform represents a efficient way to virtually visit distant places, for the promotion, education and communication of CH sites and objects and, finally, for storing, disseminating and sharing the related information. However, even if NUBES represents

an efficient container of different kinds of data for different purposes, one of the fundamental issues that encountered concerned the difficult online visualization of large reality-based 3D models (Fernandez-Palacios, Remondino, Stefani, Lombardo, & De Luca, 2013a).

The MayaArch3D project – a collaboration of the German Archaeological Institute (DAI), with the Chair of GIScience Heidelberg University and the 3D Optical Metrology Research Group of the Bruno Kessler Foundation (FBK) Trento - is a web-based research platform for the Maya archaeology site of Copán. In this application an attempt to combine and integrate both georeferenced and ungeoreferenced 2D and 3D data, and thematic information has been tested and implemented (Auer et al., 2014).

1.4 Geomatic survey methods for Cultural Heritage

Creating reality based 3D models of real artefacts and landscapes with a high degree of fidelity represents a very challenging task that demands advanced knowledge of digitization techniques and computer graphics. The digitization of artefacts and monuments represents a field of continuous research and development and technologies such as 3D scanning and photogrammetry have changed the whole digitization process.

In the Cultural Heritage field, 3D detailed models of built heritage, architectural complexes, archaeological objects and sculptures offer great advantages in any documentation, maintenance and restoration phase, as mentioned before, and the digitization process enables the detailed store of the information about their shape and appearance, against the possibility of their damage or lost over time. Unfortunately, Cultural Heritage assets are not always placed or preserved in the best places for a 3D survey, limited sometimes by narrow spaces and/or uncontrolled light conditions, and many other variables, for these reasons many different technologies are today available and usable on many different case studies. It is now well established that over the past two decades, Geomatic techniques have gained great popularity revolutionizing the documentation and recording of CH items and their following dissemination (Campana, 2014; Minto & Remondino, 2014). Such methods enable the acquisition and storage of a big amount of data with high metric and radiometric accuracy, also in the very close range field, and to process very detailed 3D textured models which communicate in a more efficient way information about objects with relevant 3D characteristics, with the further possibility to enrich them with descriptive data and efficient search and retrieval functionalities (Scopigno et al., 2017). Such representations are a powerful tool for many multidisciplinary purposes, at different scales and resolutions, from documentation, conservation and restoration to visualization and education. In most of the application, the

acquired 3D data aim to historical documentation, monitoring of shape (Di Pietra, Donadio, Picchi, Sambuelli, & Spanò, 2017), colors and decay monitoring (Robleda, Caroti, Martínez-Espejo Zaragoza, & Piemonte, 2016), data sharing in 3D GIS and HBIM systems (Kivilcim & Duran, 2016; Oreni et al., 2014), virtual reality/computer graphics applications (Jiménez Fernández-Palacios et al., 2017; Verykokou, Ioannidis, & Kontogianni, 2014), web-based geographic systems (Aliaga, Bertino, & Valtolina, 2011; Alsadik, 2016; Fernandez-Palacios, Remondino, Stefani, Lombardo, & De Luca, 2013b; Manferdini & Remondino, 2012), multimedia museum exhibitions (Fantini & Pini, 2008; Donadio et al., 2017), visualization and creation of replicas via 3D prints (Caterina Balletti et al., 2012) or in other cases virtual reconstruction of objects according to the original aspect after their lost (Project Mosul - <https://projectmosul.org/>) (Vincent et al., 2015). Focusing on small assets, the developed technologies of 3D digitization allows to fulfill the requests of the institutions involved in the conservation and documentation process, such as museums, arranging a massive and increasingly efficient digitization of their preserved objects (Tucci, Cini, & Nobile, 2011). An example of this scenario is offered by the Cultlab3D system (Santos et al., 2014) which focuses on the standardization and automation of the whole 3D digitization pipeline of artifacts by means of cutting-edge active sensors and illumination techniques integrated into a defined digitization laboratory. (Gattet et al., 2015) present another effort in this direction. In this research a low-cost and versatile 3D acquisition and processing workflow for collecting archaeological objects on the field is tested, from the acquisition step to the web sharing one.

1.4.1 3D multisensor methods for close range surveys

In the last decade, the development in 3D survey techniques was rapid and continuous producing new, more effective methods in terms of automation, acquisition and processing speed, quality and precision of the output data. Nowadays multisensor techniques are available, range and image based, and by now, it is well recognized that the integration of multisensor methods may provide more complete and detailed data than standalone acquisition (C. Balletti, D'Agnano, Guerra, & Vernier, 2016; Magda Ramos & Remondino, 2015). The integration of these two technologies led to some benefits. One of them is to take the advantage of the range sensors capability to directly acquire dense colored point clouds with the flexibility offered by the photogrammetric pipeline to be used also in exceptional condition and to provide high resolution textures.

Generally speaking, the employed sensors are commonly distinguished in active and passive ones, basing on the emission of an electromagnetic signal.

Active sensors, such as Time Of Flight (TOF), phase-shift or triangulation based laser scanners and stripes projection systems, measure angles and distances sending a signal (i.e. laser beams or infrared lights) and recording the reflected answer. Whereas passive sensors, used for photogrammetric surveys, use the ambient light to make measurements, recording the electromagnetic energy, i.e. visible light, emitted by the objects.

In the close range field, the 3D survey of objects that require a very high accuracy (around 1 mm) can be carried out typically with triangulation-based range sensors and pattern projection sensors or passive sensors (image-based techniques). Some of the available sensors and systems for the close range survey are explained in the following section, both active and passive and also hybrid sensors. The presentation is divided in macro families, according to the way the instrument acquires and its accuracy. The type of presented instrument is chosen considering its great diffusion in the close range survey field or because it has been used by the author herself in some applications.

Time of Flight (TOF) scanning systems

Time Of Flight (TOF) scanning, also known as LiDAR (Light Direction and Ranging), emits a laser pulse towards the object of interest and generates a dense point cloud calculating the time that the laser pulse takes to return back to the scanner. Such instruments are not limited by the need of a fixed distance between laser source and sensor. Furthermore, time-of-flight scanners can be employed in great object-to-sensor range (from 1-2 m up to several hundred meters) enabling imaging of large objects and sites with accuracies ranging from several millimeters to centimeters (depending on the acquisition distance) and even in poor light condition. For closer range surveys, phase shift scanners offer higher accuracy, measuring the phase difference (shift) of the returning laser pulse to calculate distances (Figure 11). The phase difference is proportional to the signal travelling time, reason why these instruments belong to the ToF category.



Figure 11. The 3D scanner Faro Focus 3D. A phase shift laser which can be used for projects at architectural scale (1:100-1:50 - Range 0.60-330 m - Accuracy of point position 2 mm at 25 m.

During the surveying, the instrument must be placed for a fixed time in different locations around the object ensuring a minimal overlapping of 60% between adjacent scans. The results of scanner acquisitions are as many point clouds as the number of scans, constituted by millions of points, which can be also coloured thanks to the RGB camera integrated in the instrument. The data processing always starts with the necessary errors and outlier's filtering, noise reduction, followed by the mutual registration of the clouds into a unique reference system in order to produce a single point cloud. The registration can be generally done following two steps: manual alignment recognizing targets or homologous points or automatic registration using the data itself, according to the shape of the clouds, and final global alignment based on Iterative Closest Points (ICP) or Least Squares method procedures (Manferdini & Remondino, 2012). This operation may require several hours, depending on the resolution of the scans and the operator skills. This kind of instruments may offer an accuracy of millimeters, reason why for the very high accuracies triangulation-based range sensors and pattern projection sensors are more appropriate.

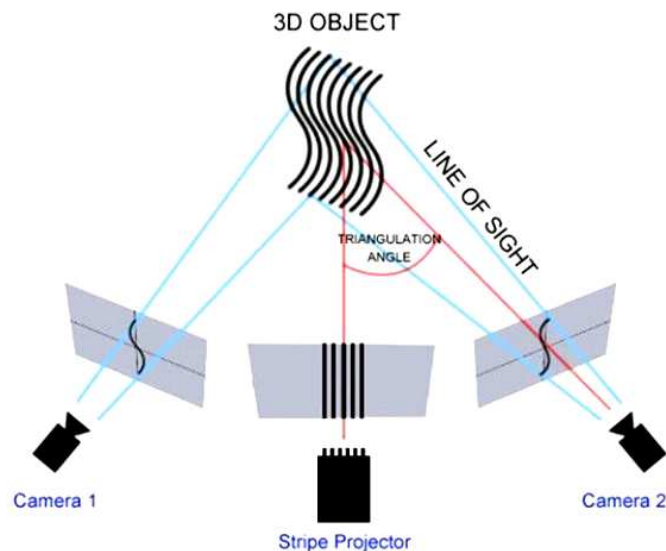
Triangulation-based scanning

Time-of-flight scanning is not accurate enough and does not produce fine documentation in detail for high scale surveys. In these cases, others range sensor systems are available, that typically work according to the triangulation principle. For most museum artefacts, for example, triangulation-based scanning is more appropriate to achieve adequate accuracy for architectural details, statues, ornamentation and small objects (Silver, 2016). These systems are able to compute the XYZ coordinates of a dense point cloud, because there is a fixed, known distance between the laser source and sensor (optical receiver) and a CCD camera takes a picture of the spot on the object. For many years these systems

were very expensive, but in more recent years, new low-cost systems are available and the quality, the quantity of the recorded data and their reliability are studied in some recent applications (Kersten, Omelanowsky, & Lindstaedt, 2016). Usually, such systems are used for scan objects at ranges less than 5m and some of them also considerably shorter (15 cm to 30 cm range) with a good accuracy (up to 50 μ m) (Payne, 2013).

Structured light scanners

Systems such as structured light scanners consist of one or more camera(s) and an active light source, that projects on the object a known pattern. The 3D object coordinates can be measured and recovered in few seconds, basing on a measuring principle similar to the triangulation one (Akca, 2006). Indeed, these systems works on principles of both passive and active systems: they capture 2D images of the light reflected from the objects of interest, like photogrammetry, and like a laser scanner they project a light themselves, though in this case the light is not just a single spot but a bi-dimensional image. The principle on which the measures are based is that this know pattern (i.e. a stripe of light) projected on a 3D surface results distorted when viewed from different projector's positions. The object geometry is reconstructed since the relation between projector and sensor and the distortion of the pattern are known. When the surface (or a specific section) is entirely covered in such patterns, its geometry can be extrapolated. Other more complicated patterns, such as fringe projection or changing patterns, like a Gray code, can also improve accuracy (Hindmarch, 2015).



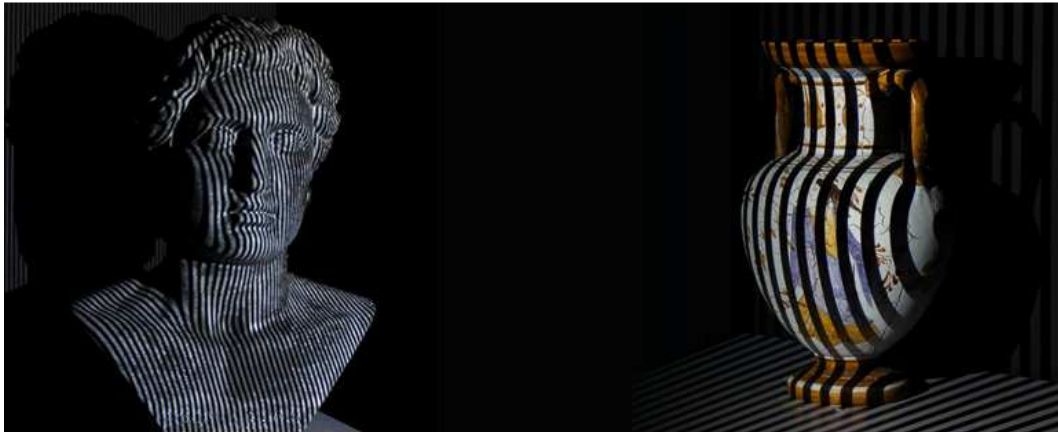


Figure 12. An example of a structured light system works and the fringe projection on the object

Microsoft Kinect

The Microsoft Kinect, a gaming accessory of XBox360 console launched in 2010, consists of an infrared projector that emits a pattern of infrared dots, an infrared camera and an RGB camera. From each frame taken by the RGB camera, several features are detected and positioned in 3D space using the depth map. Subsequently, they are matched in adjacent frames and a coloured 3D point cloud is gradually generated. The sensor is based on ToF principle, which is a quite recent technology for the range imaging.



Figure 13. A Microsoft Kinect XBOX 360

In (Lachat, Macher, Landes, & Grussenmeyer, 2015) a test employing a Kinect V2 is applied to a 3D object. The results obtained in this and other tests shows that such system can reach accuracies still far from the photogrammetric ones (about 1 cm vs sub-millimetric accuracy of photogrammetric survey) and have some limitations related to the application field: mainly indoor survey, applied to objects.

The potentialities of the Kinect are also tested in (Kersten, Omelanowsky, et al., 2016) in comparison with the low-cost recording systems DAVID SLS-1 (Structured Light Sensor) for evaluating its sustainable use in application to small objects. Geometrical investigations demonstrated that the two low-cost systems, DAVID SLS-1 and Microsoft Kinect, produce worse results in comparison to an image-based reconstruction approach, fulfilled with digital Single Lens Reflex (SLR) cameras. However, the author stated that these systems offer some advantages, such as the on-line control of recording of the object and/or of the object space during the digitization process. Final considerations highlight that the complete package DAVID SLS-1 should be used when the aim is to produce digital 3D models of small objects with limited accuracy and in a short time, whereas the system Microsoft Kinect/ReconstructMe may produce better results but requires more repetition and/or major practical experience of the user. In conclusion, the authors state that such systems benefit from a low cost and a quick way of generating 3D data for visualizations and could offer great potentials for public applications but their metrological value have to be improved.

Time of flight Cameras

Time of Flight (TOF) cameras are range-imaging systems that resolve distances basing on the known speed of light, practically measuring the TOF that a light signal needs between the camera and the object for each point of the image. Such sensors, as well as Kinect-like sensors are nowadays known source for 3D data but their use for Cultural Heritage objects is still rare.

Hand-held scanner

Another kind of instruments for close range survey is represented by hand-held 3D scanners, considered an potential supplement to terrestrial laser scanning. Thanks to their simple handling and, for some solutions, also to their favorable price, these systems may potentially become significant competitors to the more expensive and accurate structured light projection systems in some applications. These instruments operate on the triangulation based principle but allow more flexible movements around the object (Grussenmeyer, Landes, Doneus, & Lerma, 2016).

Well-known of this family is the HandyScan, that appeared in 2005 and ensures a sub-millimetric precision. The operating principle is based on the integration of two operations: a laser plotter and a system that automatically trace the position of the instrument itself in relation to the surveyed object. Firstly, this recognition was ensured placing reflecting circular target over the surface (Bonfanti, Chiabrando, & Spanò, 2010).



Figure 14. Creaform Handyscan, Range 0.30 m and accuracy up to 0.030 mm.

In 2015 two hand held scanners have been launched, the Faro Freestyle122 and Artec Spider123. Both scanners use the same principle of the Kinect – a structured light creates a depth map image, and implemented algorithms allow to register each frame into a coloured 3D point cloud. Differently to the Kinect, however, these scanners provide accurate and dense point clouds.



Figure 15. The Faro Freestyle

In particular, the Faro Freestyle is a hybrid system that implements a structured light technology, consisting in two infrared cameras that generate “stereo pair” images looking at a known structured light pattern. A laser sensor enables the measurement of the object of interest within an acquisition range of 0.5-3 m, (3D point accuracy about 1-2 mm) and an RGB camera recovers the radiometric information. Its relatively low cost makes such technique suitable and ideal for small objects modelling and addressable for many different uses. Compared to others more popular and tested hand-held scanner, the Faro Freestyle offer some advantages that make it attractive for Cultural Heritage documentation, which are its portability (i.e., it can reach the extension of small rooms

and narrow spaces and it can easily capture objects in situ), its ease to use, fast data acquisition, real-time visualization, colored point clouds acquisition, and finally its low cost with respect to many other systems.

In (Donadio et al., 2017), a photogrammetric survey and a hand-held 3D scanner, the Faro Freestyle, have been applied to an Egyptian statue in order to provide a detailed 3D model for a 3D Ultrasonic Tomographic Imaging (UTI) test, aimed at the evaluation of the interior persistency of visible damages and also in order to compare the accuracy of the hand held scanner in comparison to the photogrammetric 3D models assumed as reference. Some comparisons about the roughness of both the point clouds showed that the laser point cloud has a quite higher level of noise compared to the photogrammetric one and measuring samples of discards between the photogrammetric cloud, assumed as the reference cloud, and the freestyle one, we estimated that the second one has residuals mostly around 1-2 mm probably due to alignment operation and its intrinsic roughness. However, the final range-based 3D model allows to fulfill the requests of the 3D Ultrasonic test, and this is a great result.

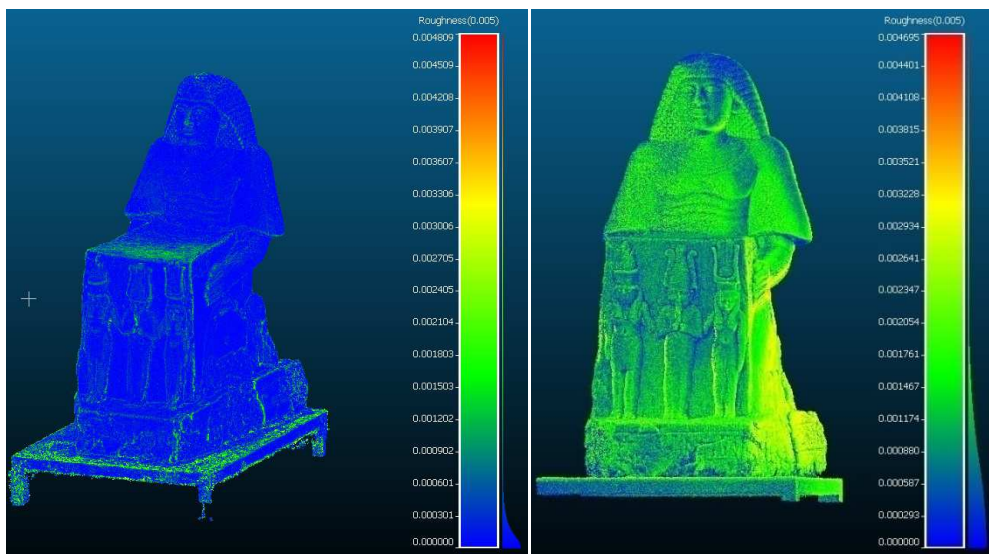


Figure 16. Insignificant level of roughness computed on the photogrammetric cloud. (less than 0.5 mm almost throughout the cloud) Roughness computed on the laser cloud presenting a considerable percentage of points affected by noise (2.5-3 mm)

Other tests are presented in (Kersten, Przybilla, Lindstaedt, Tschirschwitz, & Misgaiski-Hass, 2016) in which an evaluation of the geometrical performances of hand-held scanners for the close range field in comparison to two structured light projection systems (AICON smartSCAN and GOM ATOS I 2M) and to a photogrammetric survey is presented. The tests demonstrated that the evaluated scanning systems currently do not reach the accuracies and the quality of the reference data produced by high-end structured

light systems and also that the acquisition requirements (scanning by slow, homogeneous movements around and over the object) needs appropriate user experience, whereas the results of the Nikon D800 were the best of all systems.

Arm scanners

With regard to the field of metrology systems for very high accuracies ($\pm 25\div 30\mu\text{m}$), new developed scanning systems, such as arm scanners, combine moveable arms together with high definition hand-held scanners. This instruments are still expensive and usually used in rapid prototyping and reverse engineering fields. The measurement device is connected with a mechanical arm, from which the 6 degrees of freedom (DoF), i.e. 3 rotation angles and 3 translations, can be deduced. Therefore, the registered point clouds are referenced in real-time in the coordinate system (Grussenmeyer et al., 2016)

In addition, nowadays there are stereomicroscopes for art conservation and high-powered and high-resolution microscopes using digital imaging in 3D that can be used for studying glass, ceramic and stone objects (Silver, 2016).



Figure 17. The Faro ScanArm, range up to 3.70 m - accuracy of point position 0.025 mm.

Photogrammetric method and image matching

For 3D survey of small and detailed objects, the photogrammetric pipeline have well-established potentialities and it is sought as one of the principal technique to provide, at low cost, 3D model reconstructions (Dall'Asta et al., 2016; Lo Brutto, Garraffa, Pellegrino, & Di Natale, 2015; Menna et al., 2016; Sužiedelytė-Visockienė, Jūratė Bagdžiūnaitė et al., 2015).

The transformation of a 2D image measurements into a 3D information is possible through a mathematical formulation (Luhmann, Robson, Kyle, & Harley, 2006). In recent years, the development made on digital cameras and in calibration technology, in connection with very competitive costs, and especially thanks to the integration of image matching and Structure from Motion (SfM) algorithms, meant that photogrammetry is more and more used to recover objects with high accuracy (Samaan, Héno, Pierrot-Deseilligny, Pascal, & France, 2013). An in depth view of the photogrammetric pipeline is presented in Chapter 2.

The pipeline is more and more automatic, although the expertise of the user ensures a check on the final accuracy and precision of the output data. The final processed point cloud can be scaled and referenced in a geographic or local coordinate system (which can be the same of the laser point cloud) by means of the recognition on the images of points with known coordinates, named Ground Control Points (GCPs) and then integrated to range data and processed to obtain a detailed 3D textured model. Such points are also used to determine the precision and accuracy of the survey. Focusing on small assets, usually scale bars with known length are positioned in the scene and use to scale the data.

A great number of studies demonstrated how the close-range photogrammetry can be used to survey objects with different levels of complexity and for different aims, i.e. for reconstructing missing elements in the larger object, fulfilling high quality requirements and implying few restrictions (Barazzetti, Remondino, & Scaioni, 2010; Clini, Frapiccini, Mengoni, Nespeca, & Ruggeri, 2016; Lerma, Navarro, Cabrelles, & Villaverde, 2010; Sužiedelytė-Visockienė, Jūratė Bagdžiūnaitė et al., 2015).

1.4.2 Range or image based sensors?

Facing a new survey, from the surveyor's point of view, it is important to ensure a detailed digital recovery of the shapes, colours, materials and decay of the object that has to be documented, pursuing the better balance between the prefixed representation scale and the level of accuracy achievable in the survey.

To identify the most appropriate technology and sensor, in any 3D digitalization several aspects have always to be considered:

- characteristics of the object (i.e. its shape, dimension, colour, type of material and relative reflectivity and homogeneity, etc.),
- the acquisition place (if internally or externally, with natural or artificial light, with the possibility to move the object or not),
- the aim of the survey (documentation, analysis, mapping, dissemination, virtual reality and real time applications),

- time and budget constraints.

Since 2000, range sensors have been used for many different applications and continuous developments and technological advancements have been made in both hardware and software. Thanks to their potentialities, range sensors have increased their popularity and, for more than a decade, they have represented the fundamental source for dense point clouds generation, 3D recording, mapping and visualization purposes in multi-scale applications, while photogrammetry was not sufficiently able to generate comparable detailed 3D point clouds. Consequently, range sensors have become the lead technology for dense 3D documentation, replacing photogrammetry in many application fields. In the last decade, thanks to significant improvements made in hardware and algorithms (such as Structure from Motion (SfM) and image-matching algorithms, borrowed from the Computer Vision field), photogrammetry has returned to be a competitive technology and we are now witnessing a renaissance of automated photogrammetric methods. Image-based techniques and modern tools of 3D modelling can now generate, in quite rational time, output data that offer geometric levels of detail comparable to those obtained by range based sensors. Therefore, the market, previously mostly dominated by range sensors, nowadays has seen the advent of new image-based measurement tools for 3D recording and modelling (Remondino, Spera, Nocerino, Menna, & Nex, 2014).

Trying to make a comparison among the potentialities of active and passive sensors, some considerations can be carried out.

Laser scanner technology is usually competitive in case of indoors surveys, allowing to automatically and quickly record 3D spaces even in poor light conditions (Pepe, Ackermann, Fregonese, & Achille, 2016). On the other hand, range sensors give notoriously poor results scanning black or shiny materials, since the surfaces tends to absorb the light beams precluding the point acquisition. Another problem can be represented by the data bulkiness, which might be problematic in some survey campaigns and research projects.

The photogrammetric image-based pipeline is generally preferred for example when dealing with regular geometric shapes, small objects with free-form shape, low-budget projects, deformation and material analyses, etc. (Manferdini & Remondino, 2012). Digital photogrammetry allows to reach better results on the material appearance (texture) of the 3D models, thanks to the high resolution images used to generate the diffuse color texture. However, the image-based approach may encounter some limits if big and/or complex objects must be acquired computing detailed and high resolution models. In such applications, a higher level of attention must be kept during the acquisition step, especially with regard to a reduced depth of field; moreover, additional equipment, such

as tripods, artificial lights, etc., could be indispensable and this could increase the acquisition and the following editing time as well (Pepe et al., 2016).

The algorithms applied to the photogrammetric processing may encounter problems dealing with low quality images (i.e. noise, low radiometric quality, shadows, etc.) or facing certain type of surface materials (shiny or textureless surfaces) which represent a limit for the feature extraction and can led to noisy point clouds (F. Remondino et al., 2017). Focusing on the surface materials issue, on one hand image matching algorithms may present limits on some difficult surfaces, but in some test cases they proved to be more efficient with materials that cause unsolvable reflective problems for range sensors. On the other hand, texture less surfaces are almost impossible to be geometrically reconstructed with image matching algorithms but successfully registered with range methods (Magda Ramos & Remondino, 2015).

In the following table, the main characteristics of both methods are summarized, according to those proposed in (M. M. Ramos & Remondino, 2015).

	RANGE BASED METHOD	IMAGE BASED METHOD
ACQUISITION STEP		
Portability	Medium	High
Network design	Fixed stations in multiple positions	Multiple shots from easy to move station positions
Target/spheres/markers	Necessary to speed up the alignment phase or to georeference data	It is necessary to measure GCPs to scale and orientate the model
Acquisition time	Depending by the number of stations, the resolution desired and the geometry of the object to be acquired	Depending by the object geometry and the resolution desired
Ambient light	Independent	To be controlled
Reflective objects	May give problems	May give problems
Textureless surface	Not influenced	May give problems
Transparent materials	Give problems	Give problems
Humidity, wet surfaces	May give problems	Not influenced
Fundamental requirements	Target or Control points have to be visible in multiple scan stations	Ensuring an image overlap (about 60-80%)

Radiometric resolution	Low (when a camera is integrated)	High
Level of experience	Low	High
PROCESSING		
Processing steps	Point clouds registration	Calibration, orientation (bundle-adjustment), dense matching
Software available	Proprietary and open source solutions	Proprietary and open source solutions
3D information available	Directly, in each single scan	After a computation process on a set of images
Texture	Low resolution	High resolution
Corner and edge detection	Problematic	Very good
Scale of the acquired data	1:1	Must be provided
Processing time	Medium	High
Level of experience	Medium	High in order to obtain scaled and accurate objects

Table 1. Evaluation of the factors influencing the acquisition and processing pipeline of both active and passive sensors.

1.4.3 Functions for errors determination in photogrammetric surveys

As showed in the preceding paragraphs, 3D data from range and image based techniques ensure high level of precision and accuracy. However, it is always advisable to evaluate and quantify the errors that may be present in the processed data (firstly in the point cloud and thereafter in the mesh) in order to determine the quality of the acquired data in absolute terms. For example, the type of material may influence the level of noise on range based data and the radiometric quality of the acquired images is responsible of the final accuracy of a photogrammetric survey.

For the photogrammetric pipeline, the most common functions to detect systematic errors have been studied considering additional parameters to model the effects of radial and tangential distortion as well as affine errors in the image coordinate system and by now some of them are well established.

Recently (F. Remondino et al., 2017) have synthesized the main functions in a review research of automated photogrammetric processing of large datasets. Another contribution that explains common photogrammetric terms and abbreviations is represented by Photogrammetric Terminology: Third Edition (Granshaw, 2016) which is an official document of the International Society for Photogrammetry and Remote Sensing (ISPRS).

Point cloud error determination

In order to evaluate and compare the quality of the processed point clouds, several functions can be applied to them.

- **Re-projection error:** is the Euclidean distance between an image point (manually or automatically measured) and the projected position of the corresponding 3D point in the same image. This value usually differs from zero due to noise in image measurements, inaccurate camera poses and un-modelled lens distortions.

- **Standard deviation, variance, mean and median:** in statistics, the *standard deviation*, σ , is the square root of the *variance*. The *variance*, in turn, measures the spread, or variability, of a set of measures from their mean value μ and is calculated with the mean of the squared deviations of the variable x from its *mean* value μ .

The *median* is the ‘middle’ value of a sample of measures, separating it in two halves, containing the higher and the lower values.

$$\sigma = \sqrt{\frac{1}{n} * \sum_{i=1}^n (x_i - \mu)^2}$$

$$\mu = \frac{1}{n} * \sum_{i=1}^n x_i$$

- **Root Mean Square (RMS) and RMS Error (RMSE):** the RMS is the square root of the mean of the squared differences between the variables and their most probable values, whether the RMSE is calculated considering a specific measured reference,

obtained by an independent method (reference values can be the coordinates of check points measured for example with GNSS methods or total station).

RMSE computed on check points (CPs):

$$RMSE_x = \sqrt{\frac{1}{n} * \sum_{i=1}^n (x_{comp_i} - x_{Ref_i})^2}$$

$$RMSE_y = \sqrt{\frac{1}{n} * \sum_{i=1}^n (y_{comp_i} - y_{Ref_i})^2}$$

$$RMSE_z = \sqrt{\frac{1}{n} * \sum_{i=1}^n (z_{comp_i} - z_{Ref_i})^2}$$

$$RMSE = \sqrt{RMSE_x^2 + RMSE_y^2 + RMSE_z^2}$$

**Comp* indicates the coordinates determined with the bundle adjustment (BA) and *Ref* report the reference values.

- **Accuracy:** Represents how close the measurements, calculation or process are to a reference value. If the set of measurements have been filtered from gross errors, it can coincide with *precision*. This term is widely used as a general term for quality (Granshaw, 2016; Thomas Luhmann, Stuart Robson & Kyle, 2014). To determine the *accuracy* value, it is necessary to compare a set of observations within dependent measures, such as measured reference coordinates or reference lengths.

- **Precision:** it consists in a quantitative measure that describes the variability of results and allows to highlight the presence of big random errors, following a Gaussian or normal distribution (Granshaw, 2016). It is strictly connected to the concept of reproducibility and repeatability, which is the ability to recover the same result measured in the same conditions.

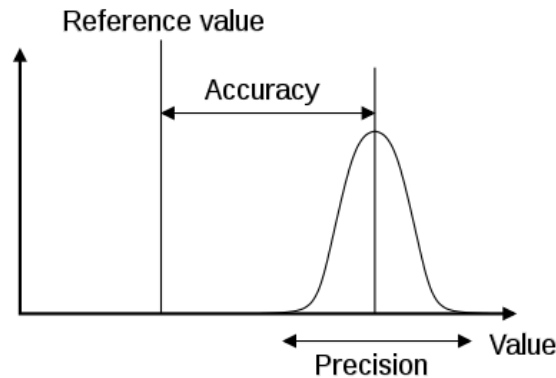


Figure 18. A graphic representation of the concepts of Precision and Accuracy of a measure.

- **Reliability:** indicates with a measure how gross or systematic errors can be identified and deleted from a set of measurements in an adjustment process. It is influenced by redundancy and geometrical acquisition configuration (Thomas Luhmann, Stuart Robson & Kyle, 2014).

- **Redundancy and multiplicity:** *redundancy* represents the surplus of observations (e.g. image points) related to the minimum number necessary (e.g. 3D object coordinates) in an adjustment process (e.g. Bundle Adjustment - BA). In photogrammetry, the redundancy is represented by the number of images in which a defined point is visible/measured and is commonly defined as multiplicity or number of intersecting optical rays. A high level of redundancy ensures a better quality in the computed 3D points.

- **Ground sample distance (GSD):** It derives from the projection of the camera pixel in the object space and represents the distance between two pixel centers measured on the ground. It is expressed in object space units and reflects the resolution of the survey.

- **Roughness or noise:** Level of deviation from the true value. A high level of noise in the point cloud produces a mesh affected by great topological errors.

Mesh model error determination

- **Topological errors:** These kind of errors may affect a mesh model generated from a noisy point cloud and it is necessary to further delete them. They include self-intersecting triangles such as triangles that cross each other or more than two triangles that share the same side.

- **Holes:** when the sensor cannot achieve some portions of the object of interest, before the point cloud and then the mesh will present voids and holes that have to be filled in order to obtain a complete surface. This operation requires good skills in the tools and in the knowledge of the object.

- **Non Manifold faces:** represent areas that are not watertight. They arise when an edge incident to more than two faces, two or more faces are connected only by a vertex and not by an edge or if adjacent faces have normals pointing in opposite directions. Non-manifold geometry can be problematic for some tools and operations, such as rendering of refractive effects, fluid simulations, Boolean operations, 3D printing.

1.4.4 3D and 2D data extraction from the acquired data

The processed detailed 3D models are very useful for the visualization of the object of interest which can be rendered on computers or on a portable device, using zoom and orbit tools to look at specified details according to the user needs. The same 3D model can be seen smoothed, with or without texture and in wireframe mode, visualizing the triangulation quality.

Moreover, the processed data can be considered as 3D archives from which it is possible to extract many other information and useful representation that may help restorer, historians and other scientists to study and further, represent their knowledge in a more captivating and descriptive way. Digital models can provide, in fact, the base with which both accurate 2D and 3D information can be extracted and processed, with a variety of different approaches, which have demonstrated in many applications to contribute to the documentation of complex buildings, detailed decorative elements and other architectural structures (Chiabrandò, Donadio, Sammartano, & Spanò, 2016; Sužiedelytė-Visockienė, Bagdžiūnaitė et al., 2015).

The modern photogrammetric pipeline ensures the generation of DSM/DTM (Digital Terrain Model / Digital Surface Model) and true orthophotos in an increasingly automatic way (Filiberto Chiabrandò, Donadio, & Rinaudo, 2015). DSM/DTM are very useful representation for study, for example, the discards between two surfaces, the deviation between two walls, or in other cases to study the shapes of vaulted systems in order to detect possible anomalies (Sammartano, 2018). The orthophoto is a very useful metric product for Cultural Heritage documentation, combining both radiometric information and real measures. Moreover, from the point of view of the researchers working in the restoration or requalification field, this is an efficient support for mapping materials,

deteriorations or other important effects that damage the object of interest (Koska & Křemen, 2013; Rijdsdijk, 2014). Finally, the processed orthophoto can be also used as a base to integrate traditional drawings with more descriptive information, or also as texture for virtual reality based applications and 3D modeling purposes.

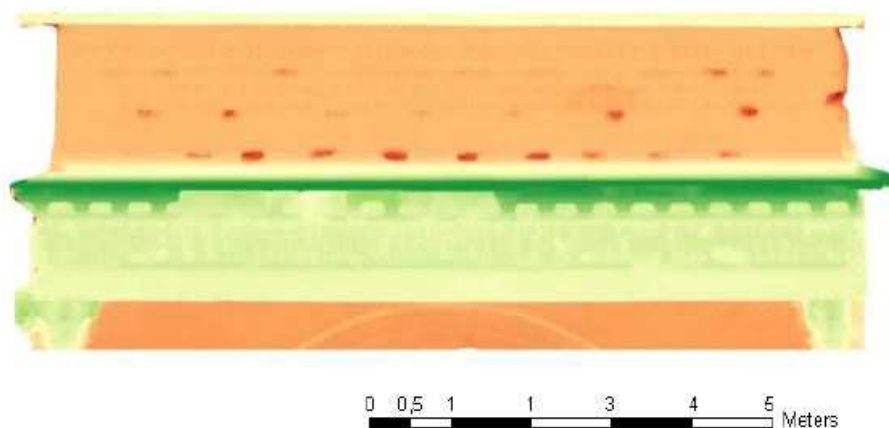


Figure 19. An example of DSM of the frieze of the arch of Augustus in Susa made from photogrammetric data and SfM technique. Source: the author in collaboration with the Geomatic Laboratory of Politecnico di Torino (F. Chiabrando, Donadio, Fernandez-palacios, Remondino, & Spanò, 2014)

From the 3D model it is possible to automatically extract 3D polylines at defined steps by the user, along X, Y or Z axes or along a defined axe by the user. This tool, when applied on the Z axe, creates a isolines curves representation which can be very useful for study the morphology and geometry of structures, such as vaults, domes and walls (Filiberto Chiabrando, Donadio, Sammartano, & Spanò, 2015; Luca Cipriani, Fantini, & Bertacchi, 2014).

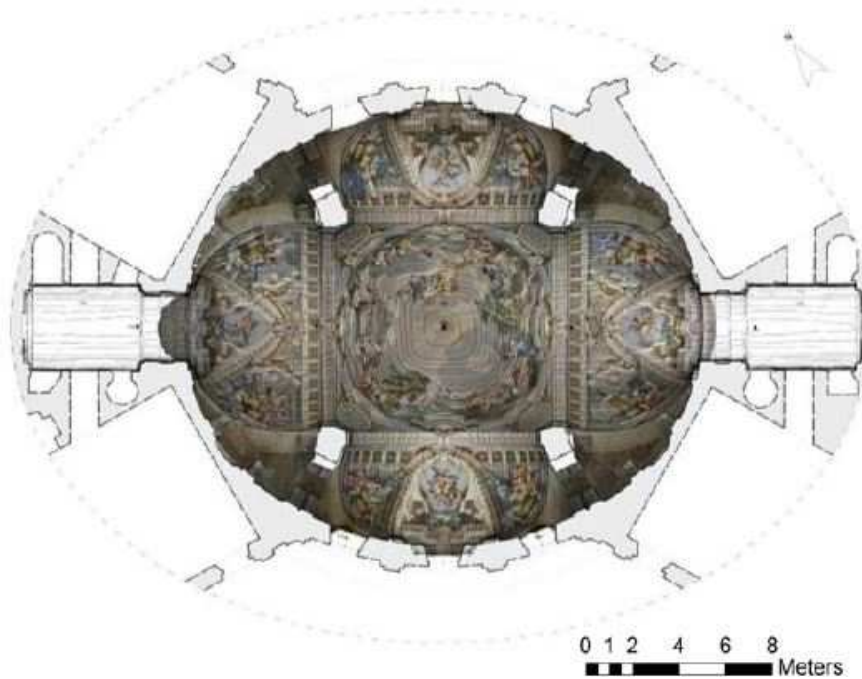


Figure 20. Planimetry, orthophoto of the vaults and contour lines of the hall of honor of the Stupinigi castle (Turin - Italy), made from photogrammetric data and SfM technique integrated with terrestrial laser scanner acquisition. Source: the author in collaboration with the Geomatic Laboratory of Politecnico di Torino

For example, in (Bertolini-Cestari et al., 2016), the extraction of progressive isolines allowed the exploration of the depression trend of the suspended wattle ceiling.

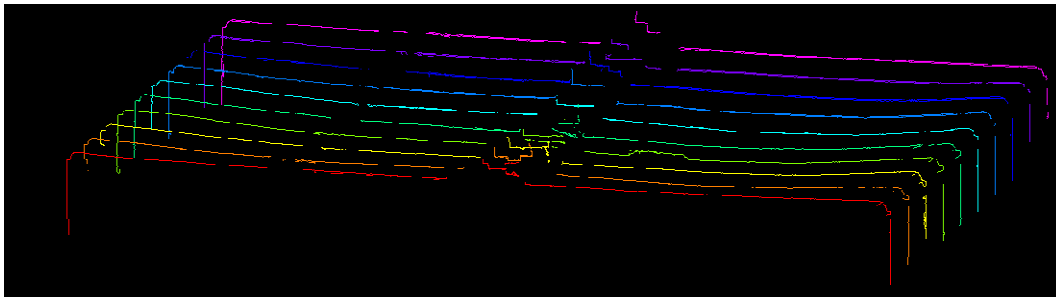


Figure 21. Progression of cross section through ceiling and wooden structure, in a 3D spatial view. Source: (Bertolini-Cestari et al., 2016)

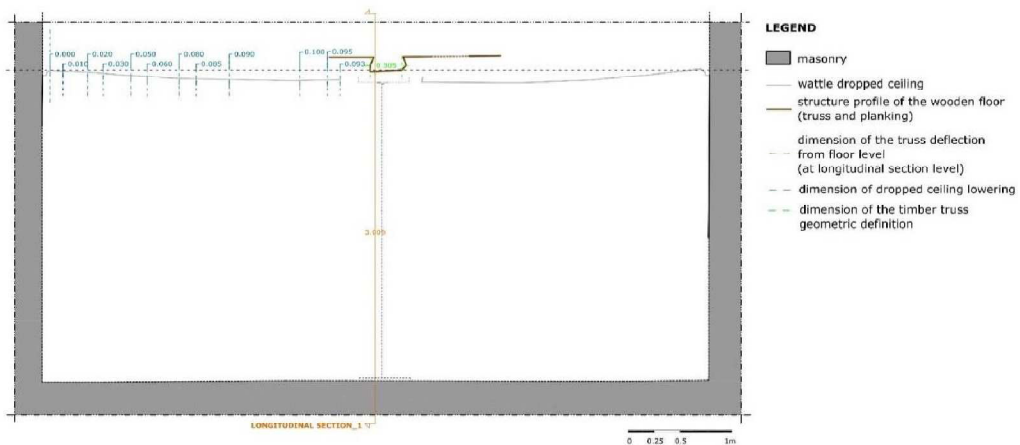


Figure 22. Transversal section of the wooden beam and evaluation of the increasing depression of the wattle dropped ceiling. Source: (Bertolini-Cestari et al., 2016)

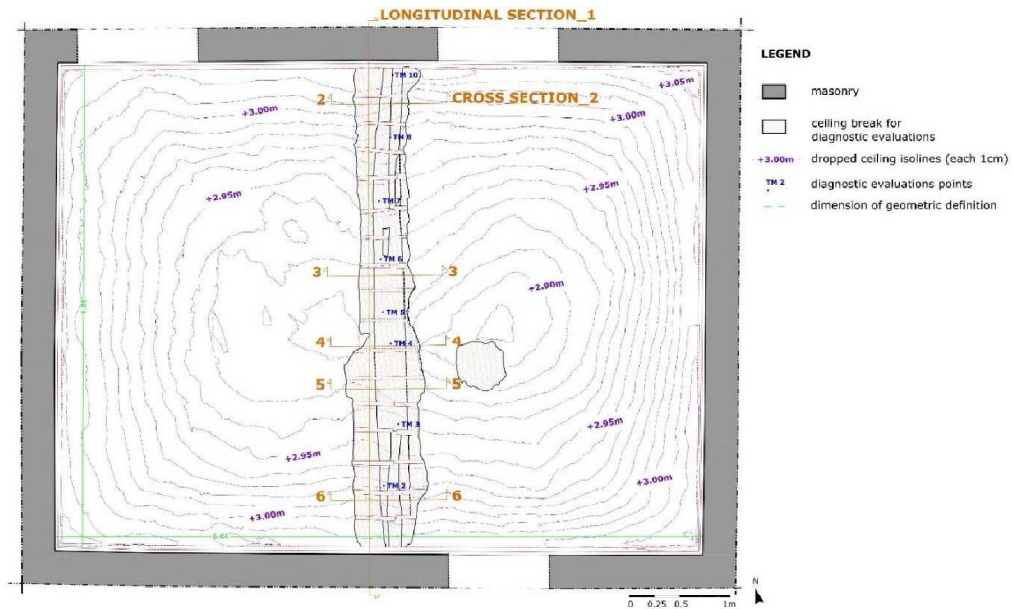


Figure 23. Ceiling plan of the room, in a bottom-up view. Isolines, derived from progressive planar sections each 1cm (indicated each 5cm step), show the depression of the dropped ceiling. Source: (Bertolini-Cestari et al., 2016)

Furthermore, from the point cloud, it is possible to extract infinite bi-dimensional orthogonal views, chosen by the user, that are different from an orthophoto since they have a lower resolution, limited by resolution of the point cloud. However, these representations offer great potentialities. The ability to extract infinite section planes in sensitive zones of the building, is very useful for bi-dimensional standard architectural drawings, such as prospects and horizontal and vertical sections (Filiberto Chiabrando et al., 2017)

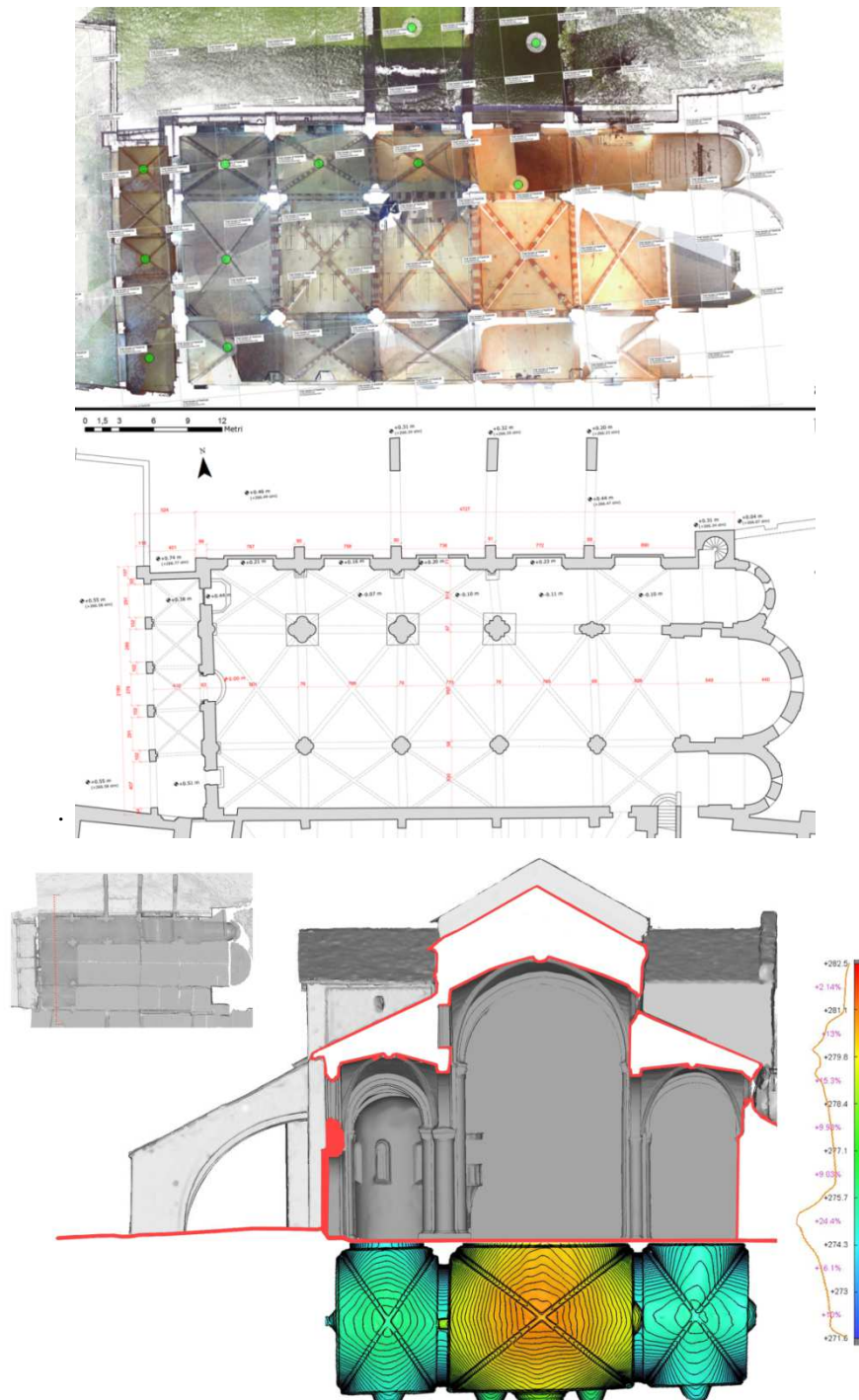


Figure 24. 2D representations such as horizontal plans from the 3D point cloud. In this representation a laser scanner survey has been applied to the Santa Maria Church of Staffarda. Above: an updated planimetry has been processed; below: a trasversal section with corresponding planimetry of the vaults with scalar field and isolines. Source: (Beltramo, Donadio, & Spanò, 2018; Donadio, 2013)

Chapter 2

The photogrammetric pipeline for Cultural Heritage small assets

2.1 State of the art in automated image-based 3D reconstruction

Image matching is a technique that allows the identification of correspondences between two or more images. In particular, dense image matching methods enable the generation of dense point clouds and detailed 3D models processing a set of un-oriented images acquired from different viewpoints.

In the last years, thanks to the developments made on hardware and software algorithms, image-based reconstruction has re-emerged as an effective alternative to range sensors offering comparable accuracy and resolution, and also due to its lower cost demanding, with reduced time and location constraints. Some of these evaluations have been reported in (Filiberto Chiabrando & Spanò, 2013; Menna et al., 2016; Nocerino, Menna, & Remondino, 2014; Fabio Remondino & Rizzi, 2010). In the last ten years, many algorithms for image processing in connection to geomatic field have been improved. The MSER: Maximally Stable Extremal Regions (Matas, Chum, Urban, & Pajdla, 2004), SIFT: Scale Invariant Feature Transform (Lowe, 2004a), SURF: Speed Up Robust Feature (Bay, Tuytelaars, & Van Gool, 2006), SURE: Surface Reconstruction from imagery (Rothermel & Wenzel, 2012), are some of the most important algorithms that helped digital photogrammetry to become more competitive.

The first applications of image-matching methodology have been tested on Remote Sensed data. Initial efforts has been oriented to provide orientation solutions and then to perform the extraction of DTM/DSM from aerial or satellite strips with high density (Zhang & Gruen, 2006).

By now, such methods are widely used also in the Cultural Heritage field, as the acquisition of images using digital cameras has proved to be an efficient method to retrieve 3D detailed data useful for documentation purposes. This techniques can be employed in many different applications relevant to the Cultural Heritage field including documentation, conservation, for an appropriate planning of surfaces restoration activities, geometric deformation analysis, monitoring, visualization and painting analyses (Filiberto Chiabrando, Lingua, Noardo, & Spano, 2014; Luca Cipriani et al., 2014; Dall'Asta et al., 2016; Di Pietra et al., 2017).

In the close-range field, in which a millimetric precision is required, photogrammetry is increasingly preferred over other techniques, offering great potentialities when applied for data acquisition and processing of architectural structures, small objects of irregular shape, for mapping applications or, in other cases, for reconstruction of missing elements of a greater object (Lo Brutto et al., 2015).

Starting from these considerations and the mentioned experiences, the 3D surveys applied to the case studies presented in this thesis have been conducted by means of photogrammetric method.

In the following paragraphs the principles and algorithms regulating the photogrammetric pipeline are explained as well as the acquisition and processing procedures.

2.1.1 From traditional photogrammetry to SfM

Image matching method, often called stereo correspondences problem (Szeliski, 2011a) has been developed in the 1990s by the computer vision community, which is the science that develops mathematical techniques aimed at the extraction of spatial and structural information from images; whereas the implementation of automatic feature-matching algorithms dates back to the Eighties. A brief description of the first principles of Structure from Motion is presented in (Westoby, Brasington, Glasser, Hambrey, & Reynolds, 2012).

The extraction of 3D data from a set of images is strictly connected with the possibility to retrieve corresponding points (features) in images shooting the same object from different viewpoints. This process allows to produce depth maps in image space assigning relative

depths to each pixel of an image and generating 3D pointclouds. In traditional analogical photogrammetry, this operation has always been performed manually, while in digital photogrammetry, this procedure has become more and more automatic. After a first revolution phase that has sought the transition from analytical to digital, producing an automation of the photogrammetric pipeline (points extraction, orientation, digital plotting etc.), in latest years we have been witnessed a second revolution, that has pushed digital photogrammetry (still semi-automatic) to the SfM technique. This new approach is naturally related to photogrammetric basis (measures, accuracy etc.) but is very close to the computer vision logic: fully automatic with a measurement approach not so important.

Traditional photogrammetry requires the 3D location and the position of the camera, or the 3D coordinates of a series of control points in order to extract a 3D scene. In the former case, it is necessary to mount a GPS (Global Positioning System) and electronic compass on the camera, otherwise a triangulation can be used to build the scene geometry, while in the second case, a series of control points have to be manually identified in the acquired images, and then the so-called resectioning process, or camera pose estimation, determines the camera locations (Westoby et al., 2012).

The great innovation in the image matching process consists in the implementation of the Structure from Motion approach, which requires neither of the above mentioned conditions to reconstruct the scene since it simultaneously computes the calibration parameters of the camera, the camera poses and a set of sparse 3D point cloud. To do this, it uses a highly redundant bundle adjustment which retrieves corresponding image features from a set of overlapping images captured by a camera moving around the object (Verhoeven et al, 2012). These features are sought and traced in each image of the dataset, enabling the estimation of camera positions and object coordinates. A further step iteratively refines the estimated values using non-linear least-squares minimization.

The difference of the process consists in the fact that unlike traditional photogrammetry, the data derived with SfM process lack the scale and orientation, traditionally ensured by measured ground-control coordinates. In this way, the 3D point clouds refer to a relative 'image-space' coordinate system, which need to be subsequently scaled and rototranslated in order to be aligned to a measured 'object-space' coordinate system. Usually, the transformation from the relative image-space coordinates to an absolute coordinate system can be performed using a 3D similarity transformation based on Ground-Control Points (GCPs) with known coordinates. If no GCPs are available, a scale bar with known length should be placed in the scene and shoot in some images in order to scale the model.

By now, it is clearly admitted that these techniques allow everyone to do photogrammetry, even non-expert operators about photogrammetric principles. Every day a large number of people is attracted by the potentialities of image-based 3D reconstruction and modeling tools, but some critical issues raised in the years about the quality of the derived 3D models, the ability to derive accurate 3D results without any shape deformation and the suitability of SfM under every network configuration. After an initial enthusiasm, a deeper analysis on the real potentiality for CH documentation of these techniques has been conducted in many studies (Chiabrando et al., 2015; Nocerino et al., 2014; Pierrot-Deseilligny, De Luca, & Remondino, 2011). These questions are less crucial if a 3D model is produced for communication and visualization aims, for web sharing or AR needs, but are fundamental for documentation, conservation, preservation and replica purposes. Nevertheless, it is undoubted that such new automatic tools, if properly used, have potentialities never offered before. Originally computer vision, and in particular the SfM approach, was in fact not considered sufficient suitable for metrology applications due to the lack of results in term of accuracy and reliability of the process. By now some advances have been done in SfM software, that allows using the SfM pipeline also in metrological context producing final products with comparable feature (Lo Brutto et al., 2015).

2.1.2 The photogrammetric algorithms

The algorithms for retrieval 3D information can be distinct into two main categories (Konrad Wenzel, Rothermel, Haala, & Fritsch, 2013). The first category ensures the determination of image positions and orientation parameters retrieving, with manual or automatic procedures, distinct features in the collected images, followed by a bundle adjustment (BA). The second category includes all the surface reconstruction methods, where dense image matching algorithms operate the previously derived orientation of the images to generate the 3D surface reconstruction. Nowadays the image matching procedure can be realized using stereopairs (stereomatching) (Hirschmüller, 2011) or through the identification of correspondences in multiple images (Multi-View stereo – MVS) (Pierrot-Deseilligny, Marc and Paparoditis, 2006). As explained by (Fabio Remondino et al., 2014), according to (Szeliski, 2011b), stereo methods work locally or globally. Local stereo methods compute disparity at a given point, using the intensity values within a finite region, applying implicit smoothing assumptions and a local “winner-take-all” optimization on each pixel; whereas global stereo methods make explicit smoothness assumptions and solve for a global optimization problem applying an energy minimization approach.

In the previous orientation step, Structure from Motion process works through the automatic identification of matching features in multiple images. This process works without specifying a network of targets a priori. Such features are then tracked on each image and further iteratively refined using non-linear least-squares minimization approach, generating an initial estimation of camera poses and object coordinates. Feature detection and description has been a very active area of research for decades. The Computer Vision community intensively studies and tests detectors in intensity images and, nowadays, different point detection algorithms are available. There is not a single method that is always best for every application, however, all the point detection algorithms are designed to be invariant against moderate scale and viewpoint changes. The mentioned MSER detector, for example, identifies groups of pixels that are best separable from their surroundings. The SIFT (Scale Invariant Feature Transform) algorithm extracts feature points in a four step approach: scale-space extrema detection, keypoints localization, orientation assignment and key points descriptor. In the first step, it uses the difference of Gaussian function to retrieve potential points of interest, that has to be invariant to scale and orientation (difference of Gaussian is used instead of Gaussian to speed up the computation time). In the key point localization step low contrast points are refused and the edge response are eliminated. The Hessian matrix is employed to determine the principal curvatures and eliminate those points that have a ratio between the principal curvatures greater than the ratio. An orientation histogram is created from the gradient orientations of sample points within a region around the key point, in order to get an orientation assignment (Lowe, 2004b). Sometimes SIFT data processing can be slow (Lingua, Marenchino, & Nex, 2009), reason why many researches are focusing on the improvement of the algorithms speed. In (Bay et al., 2006) the *SURF: Speeded Up Robust Features* algorithm is introduced. As the name suggests, it is a speeded-up version of SIFT. While in SIFT, Lowe approximated Laplacian of Gaussian (LoG) with Difference of Gaussian to determine scale-space, SURF goes a step further approximating LoG with a box filter. This approximation offers some benefits. For example, convolution with box filter can be easily computed with the help of integral images and it can be calculated concurrently for different scales. The SURF is also based on determinant of Hessian matrix for both scale and location. For orientation assignment, SURF uses wavelet responses in horizontal and vertical direction for a neighborhood of 6 pixel size; adequate Gaussian weights are adopted. For feature description, SURF uses again wavelet responses in horizontal and vertical direction (the use of integral images makes the process easier). A neighborhood of 20x20 pixel size is considered around the key point, it is then divided into 4x4 pixel sub-regions and for each sub-region, horizontal and vertical wavelet responses are used. Another important improvement is the adoption of

sign of Laplacian (trace of Hessian Matrix) for underlying interest point. The sign of the Laplacian distinguishes bright blobs on dark backgrounds from the reverse situation. In the matching stage, we only compare features if they have the same type of contrast. This minimal information allows for faster matching, without reducing the descriptor's performance. Summarizing SURF implements adding features that improve the speed in every step and making this approach 3 times faster than SIFT, while performance is comparable to SIFT. SURF offers the advantage of handling images with blurring and rotation, but it is less performing dealing with viewpoint illumination changes.

Nowadays the most used commercial and non-commercial software are based on SIFT (Bundler, PMVS) or on a modified version of SIFT (MicMac, Photoscan, 3DF ZephyrPro, Pix4D) in the first step of the pipeline.

After this first phase, a bundle block adjustment or a similar transformation is computed and then dense matching is processed. Most software solutions implement multi-view stereo (MVS) algorithms to compute 3D dense reconstruction of the object surface (G. Verhoeven, Taelman, & Vermeulen, 2012). This step allows the generation of detailed 3D dense point clouds or triangular meshes, operating on the pixel values instead of on the feature points. Another performing algorithm is the Semi Global Matching (SGM), developed by Hirschmuller (Hirschmüller, 2011), originally for aerial application. This approach implements both global and local stereo methods for an accurate, pixel-wise matching with greater stability. In comparison to others global matching methods that may suffer from high computational efforts, SGM provides efficient computations at low runtime. It works estimating a disparity map for each pair and then merging those disparity maps that share the same reference view into a unique final point cloud. Within a premodule, a network analysis and selection of suitable image pairs for the reconstruction process is computed. Epipolar images are then generated and the SGM algorithm is applied to produce depth maps, in a time and memory efficient process. Through a conversion process, the maps generate 3D coordinates, using a fusion method based on geometric constraints that both allow to reduce the number of outliers and increase precision. SGM approach is able to retrieve reliable results also for repetitive or low textured images and so, it is particularly recommended (Remondino et al., 2014).

Another process available is constituted by SURE (Rothermel & Wenzel, 2012) that is a MVS method for the generation of dense and precise 3D point clouds given a set of oriented input images. It is based on the SGM approach, followed by a fusion step in which the redundant depth estimations across single stereo models are merged.

2.2 The image processing pipeline applied to small assets

Considering the potentialities of the developed tools which are object of interest also for non-expert users or public institutions, the scientific community found necessary over these latest years to have an extensive reflection on these tools, trying to propose some guidelines for the whole digitization pipeline. Recent works are focusing on finding new solutions for decreasing the acquisition time and pursuing a better coverage of the objects. For example, as reported in (Gattet et al., 2015), since 2012, the MAP laboratory (Modèles et Simulations pour l'architecture et le Patrimoine), in partnership with ENSG and IGN, is developing optimized photogrammetric acquisition protocols for the documentation of Cultural Heritage artifacts (archaeological fragments, paintings, sculptures, furniture, architectural elements, buildings, sites, etc.) basing on the parameterization of the APERO /MICMAC tool chain (Pierrot Deseilligny & Clery, 2011).

In the case of close range photogrammetric survey applied to small artefacts and assets, we immediately tend to think of museum objects. In this context the more the pipeline is standardized, the more digitization process of the objects is facilitated and can be increased. In this scenario, the TAPENADE project (Tools and Acquisition Protocols for Enhancing Artifacts Documentation) (Pierrot-Deseilligny et al., 2011), developed as a collaboration between IGN (France), CNRS Marseille (France) and FBK Trento (Italy), aimed at defining a common pipeline, available for every user, for managing the entire process, from the acquisition step to the generation of a 3D documentation in a web-based open-source pipeline. In particular, it contains specific acquisition protocols for different kind of objects (i.e. about which equipment to use, how to take photos, etc.) and, shows a processing performed with the open source software MICMAC. In (Nicolae et al., 2014) the authors tested the processing of 3D models of artefacts stored in a museum with problematic surfaces – reflective, translucent and homogenous materials. This study showed how a careful planning and a correct image acquisition allow to generate accurate and faithful 3D textured models without the need of moving the object from the museum and employing low-cost photographic equipment.

Starting from all of these application experiences, in the following paragraphs, the main steps of the acquisition and processing phase of a photogrammetric survey are explained.

2.2.1 The acquisition phase

The acquisition of artefacts, for example preserved in a museum, may result problematic due their surfaces– i.e. facing reflective, translucent and homogenous materials - and also due to many constraints defined by the location (i.e. narrow and restrictive spaces, uncontrollable lights conditions, etc.). Indeed, as already mentioned, passive techniques are hardly influenced by ambient lighting conditions, more than range sensors.

Each guideline about the principles of the photogrammetric acquisition foresees as mandatory a quick onsite analysis of the scene and its conditions and environment, in order to define the possible constraints (complexity, morphology, material, dimensions, environment, occlusions, light, inaccessibility, etc.).

In every application, the aimed density and resolution defined by the Ground Sampling Distance – GSD) of the final dense point cloud can be achieved choosing an adequate image sensor (properly setting photographic parameters, such as exposure time, sensitivity settings ISO, aperture value and then Depth Of Field - DOF) and adopting the appropriate geometrical acquisition configuration (network design) (Konrad Wenzel et al., 2013). The type of sensor influences the image quality, especially dealing with objects affected by large illumination differences and contrasts or sparse texture, in which a camera with large sensor and high dynamic range is advisable. In general, a short focal length helps the image orientation due to a stable bundle adjustment and also the image acquisition is more effective. The camera settings must always guarantee the sharpness on the whole object, which is mandatory to compute an efficient features extraction and the surface reconstruction. To achieve this, a proper short exposure time, less than 1/100s (e.g. 1/160s) is recommended for handheld acquisitions. In order to ensure a sufficient depth of field over the whole surface, the aperture should be closed as much as necessary. Generally, the ISO value should be as low as possible. In those cases, in which the acquisition place is too dark, it may be slightly increased, but only if a good sensor is operated and the level of noise is low. In such cases the use of a tripod is also desirable in order to ensure an adequate quality. Furthermore, it is important to optimize the field of view, trying to cover the great part of the sensor with the object of interest (Nicolae et al., 2014).

The exact number of photographs to be acquired has to be determined case-by-case, considering the occlusion, shape complexity and scale.

Another essential component is to design the optimal configuration in order to achieve the desired resolution and completeness in the output data. The optimal network can be sometimes complex to be determined, in particular dealing with objects with strong depth

variations, acquired at short distances. A wrong photogrammetric planning can lead to a general deformation (bending effects) in the 3D results. Similarly, the spatial density and resolution of the final outputs can be enhanced by decreasing the distance between the camera and object of interest and increasing the spatial resolution of the photograph (Westoby et al., 2012).

In (Nocerino et al., 2014) different configuration layouts, with normal and convergent images, are analyzed. Since photogrammetric process is based on angle observations, principles for an optimal network configuration are independent to the image scale. According to this, same principles can be followed for acquiring small objects, as well as for recording sculptures or buildings, and also for terrestrial and aerial imagery. The study showed that the inclusion of convergent images considerably strengthens the network geometry and help to avoid global deformation of the 3D results.

Also in (Nony et al., 2012), several principles about the acquisition process have been highlighted:

"Illumination conditions and luminosity affect the speed and acquisition parameters of the camera and therefore whether a tripod is necessary or not (which slows down the image acquisition step). The presence of obstacles implies a change in the acquisition location or the use of different focal length. Also, homogeneous and transparent materials, reflections and windows cannot be correctly processed. The employed digital camera must be preferably calibrated in advanced following the basic photogrammetric rules in order to compute precise and reliable interior parameters.[...] It is also important to keep a reasonable base-to-depth (B/D) ratio: too small baselines guarantee more success in the automatic tie points extraction procedure but strongly decrease the accuracy of the final reconstruction. The number of images necessary for the entire survey depends essentially on the dimensions, shape and morphology of the studied scene and the employed focal length"

In (Martin-Beaumont, Nony, Deshayes, Pierrot-Deseilligny, & De Luca, 2013; Pierrot-Deseilligny et al., 2011) a series of acquisition protocols for the museum's photographs are explained. For example, the protocol "all around a simple artefact", shows how to acquire an artifact with a simple shape, located in an easy context. In particular, this mode of acquisition requires a set of "master" images and several neighbors associated images (at least 4, with low ratio base to distance and high overlapping) and, in order to assure the connection during the orientation step, a sufficient number of intermediary images between each master image.

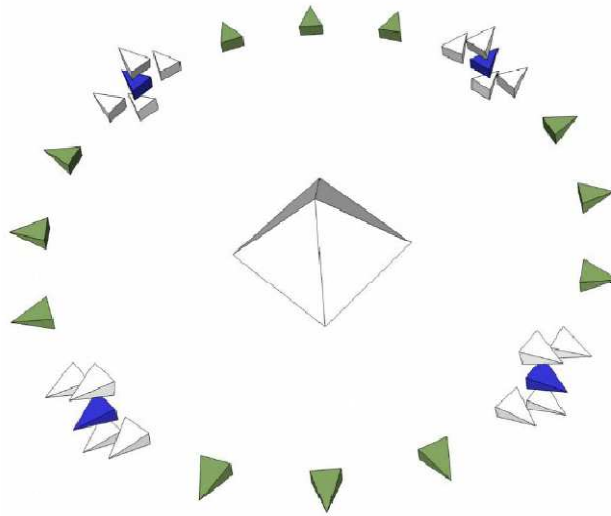


Figure 25. Spatial configuration of the acquisition of an artefact. Source: (Martin-Beaumont et al., 2013)

In (K Wenzel, Rothermel, Fritsch, & Haala, 2013) a guideline for the acquisition of images for photogrammetric survey is presented. In this paper relevant aspects such as the selection of the sensor, the self-calibration, the importance of the sharpness and the camera settings are explained.

These application highlight also the importance of controlling the quality of the lights and related factors such as artificial light positioning, their size and orientations in each photograph.

Natural lights coming from windows or mixed color light temperature deriving from different light sources must be controlled, especially dealing with reflective surfaces. As before mentioned, an inspection of the location is always necessary to control the light over the artefact and to check the available space around the object.

Facing lights constraints, it is often advisable to mount the camera on a stable tripod. To avoid the presence of unpleasant shadows, theoretically a light source should be originated exactly from the centre of perspective of the objective lens. Since this is an impossible condition to be ensured in practice, lights must be positioned symmetrically with respect to the optical axis of the camera to overcome this problem. In this way, the shadows produced by a light source can be filled from those produced by the symmetrical lamp. A diffuse light produces a similar effect similarly, being the source of light virtually uniformly diffused around the object (Menna et al., 2016).

In some cases, it is also advisable to rotate the object (when allowed) rather than rotate the camera around it. This procedure enables to reduce the space needed for the photographic acquisition and also the acquisition time. Using this approach and especially

capturing with limited depth of field, the distance between camera and object can be much more controlled, with respect to continuously move the camera and the tripod around the object and, when used, lamps and their stands. On the other hand, acquiring with turning tables has the disadvantage that there are only relative movements within the image scene between the artefacts and its surrounding environment. Therefore, if automatic photogrammetric orientation is used, it is necessary to mask the images for removing parts not belonging to the artefacts. In some cases, when possible, this kind of problem can be solved placing a homogeneous background.

2.2.2 The processing phase

Today, different software are available to automatically perform the image matching procedure, either commercial like Photomodeler (<http://www.photomodeler.com>), Agisoft Photoscan (<http://www.agisoft.com>), Pix4D or open-source like Bundler (Snavely, 2008), MICMAC (Pierrot Deseilligny & Clery, 2011) and VisualSfM (Wu, 2011). Interesting new tools, implemented for example in Pix4D, allow also to extract desired frames from videos, directly in their environment (without the need to add another software in the procedure).

The initial processing step consists in the automatic identification of common features in single photographs to be used for image correspondence. After this step:

- the relative orientations of camera poses at the moment of image acquisition are computed;
- the internal camera parameters (focal length, principal point position, radial and tangential distortion coefficients) are automatically determined;
- a 3D sparse point cloud is processed defining the scene geometry.

To do this, usually the mentioned SIFT algorithm is used to recognize in the photographs those features that result invariant to image scaling and rotation and partially invariant to changes in illumination conditions and 3D camera viewpoint (Lowe, 2004). Such points of interest, called 'keypoints', are iteratively searched and identified in each image of the dataset and a feature descriptor is associated to them. This value is computed by transforming local image gradients into a representation that is indifferent to variations of illumination and orientation. The number of detectable keypoints in an image depends primarily on image texture and resolution, so that high resolution images offers better results (Westoby et al., 2012).

Following keypoints identification and descriptor association step, a sparse bundle adjustment is applied to retrieve camera poses and generate a low-density sparse point cloud. Keypoints correspondences set constraints on camera pose orientation, which is

computed applying a similarity transformation, while minimization of errors is ensured through a non-linear least squares calculation (Szeliski and Kang, 1994; Nocedal and Wright, 1999). The sparse point cloud can be then intensified in a following step using for example Multi View Stereo (MVS) techniques (Konrad Wenzel et al., 2013).

In this thesis, Photoscan is the software used to process all the datasets. This choice is due to the fact that it has well-known potentialities and its outputs data have been validated in many applications, also conducted by the author herself and applied to similar test cases (for scale and resolution). In addition, since the aim of this thesis is not to test the processing itself but the following 3D data optimization phase, Photoscan seemed to be the best choice, ensuring to reach the desired high quality and resolution of the output data with a semi-automatic procedure.

In the following part the entire pipeline implemented is presented.

Photoscan processing

Photoscan is an advanced image-based processing software produced by the Russian AgiSoft LLC company aimed at processing high detailed 3D data from a set of overlapping images. It has a simple user-friendly interface and allows the generation of sparse, dense point cloud, detailed 3D textured models and other representations such as DSMs and orthophotos (Geert Verhoeven, 2011). It has been built to operate on Windows systems but it is also available on Linux and OS as well., allowing to operate with many different formats, JPEG, TIFF, PNG, BMP or MPO files. The reconstruction process is constituted by three main steps, in which the user can control a series of parameters. For example, at any step, the user can disable/enable single photographs, mask uninteresting parts of the images or import textures and models created in external software. The only prerequisite to ensure the 3D data extraction is to provide a set of overlapping images of the object/scene of interest. As mentioned before, the SfM technique is implemented to compute the images alignment, camera calibration and to reconstruct 3D scene geometry and camera motion. The process of image features extraction is realized by means of a modification of the Lowe SIFT algorithm, since this is protected by the copyright. Subsequently, the movement of the feature points is computed throughout the image dataset and a local descriptor is assigned to each point, basing on its local neighborhood, which is then used to detect point correspondences through the entire dataset (G. Verhoeven et al., 2012). For this operation, robust methods, such as a modified version of RANSAC, are applied. After this computation, the camera interior and exterior parameters and its positions and motion are determined and identified in a local reference system. The output data is a sparse 3D point cloud which correspond to the extracted feature points. This step considerably influences the final achievable accuracy of the 3D

model, so it is recommended to always check the image alignment quality and the computed projection errors after this computation.

In the second step a dense point cloud can be processed basing on the calculated camera poses. The program computes depth maps for each camera to be combined into a single dense point cloud. The settings allow to choose the quality requested and offer several depth filtering modes to remove possible outliers among the points.

In the third step, the computationally most intensive operation, stereo reconstruction method allows to build 3D geometric scene. In this phase, the dense reconstruction algorithm works on the pixel values in order to generate detailed 3D meshes. The computation time principally depends on the resolution and quantity of the images and on the desired level of detail.

To achieve this, Photoscan allows to choose among several dense stereo-matching algorithms (i.e. Arbitrary or Height Field), that affect the way in which the individual depth maps will be merged into the final 3D model. The result is a polygonal mesh, viewable in a solid, shaded and wireframe mode and comparable to a DSM. It is important to highlight that the results of this process are expressed in a local coordinate system, derived from the relative orientation. Since Geomatic applications and Cultural Heritage surveys, always require scaled models inserted in a known coordinate system, in order to ensure the measurement of distances, volumes and areas, Photoscan allows to define a coordinate system setting Ground Control Points (GCPs) coordinates or, when available, camera coordinates (this latter is usually used for aerial data where the acquisition may be connected to GNSS and an IMU).

GCPs are essential to produce georeferenced, scaled and more accurate data. Such points define constraints that establish a reference coordinate system, its origin, orientation and scale (F Remondino, Del Pizzo, Kersten, & Troisi, 2012). Three GCPs is the minimum but it is recommended to have between 5-10 GCPs, well distributed over the object of interest, to be used as weighted observations inside the least squares minimization. When abundant GCPs are available in a project, some of them can be also used as Check Points (CP). These points are not take into account for processing and calibrating the model but only to assess the absolute accuracy of the project, fully independent on the processing. The introduction of the checkpoints is used to estimate their 3D position as well as potential errors in the clicks and, in particular, to calculate the RMSEs with respect to the computed object coordinates. In this way, the relative accuracy of the area of the checkpoints may be improved. In some software, the difference between the initial and the computed positions of the checkpoints is displayed in the quality report, giving an estimation of the absolute accuracy of the model in the region.

In this part of the data processing, Photoscan defines a simple affine transformation to the final model in order to minimize the RMS error on GCPs. It is also possible to optimize the camera alignment based on camera or marker coordinates to fix non-linear distortions of point cloud mode (the so called blow effect).

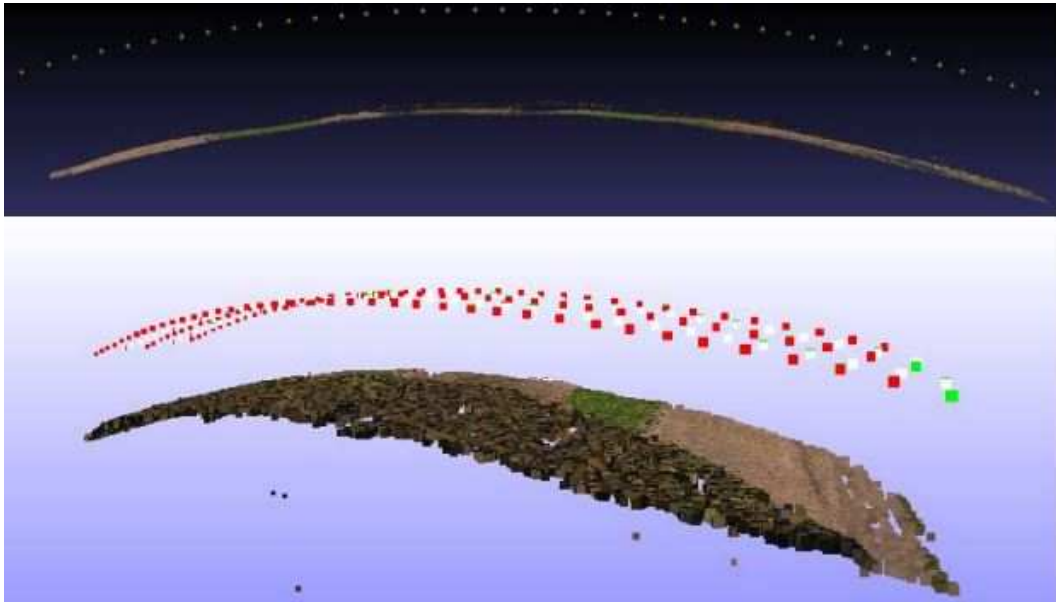


Figure 26. A distortion of the point cloud calculated called blow effect

To do this, it probably computes an adjustment based on Gauss-Markov linear model. This operation allows the user to accurately check the final output in order to control that any distortion does not affect the final 3D model. This workflow differs from traditional aerial photogrammetric pipeline, in which georeferencing, performed by traditional Bundle Block Adjustment (BBA), sometimes assisted by data from a GNSS IMU system, precedes the 3D mesh reconstruction.

Another important factor involved in the photogrammetric process is related to the radiometric color representation. Besides the reconstruction of a 3D surface, it is later possible to calculate the color information for each vertex of the model, storing it as an attribute. These colors are calculated as an average of the corresponding pixel values from the source photos and, in the model rendering, they are then interpolated for each polygon face, which is then filled by a color gradient. This representation is not enough accurate for many of the Cultural Heritage purposes. For this reason, it is usually necessary to calculate and apply a separate texture mapping. Photoscan allows to compute a diffuse color texture calculating a so-called texture atlas from one or more source photographs. After this calculation process, each model vertex stores its 3D coordinates in this texture atlas, a 2D parameter space also known as UV map (in 3.2.5 and 3.2.6 an

in depth examination of the UV map creation and the parameterization procedure is presented). During 3D rendering, these coordinates are used to project the 2D texture image onto the 3D model surface, providing a very rich texture for each polygon in the model.

Photoscan offers different texture mapping modes that determine how the object will be projected in the texture atlas. Other texture generation parameters control the way how pixel values from different photos will be combined in the final texture. They are chosen according to different needs and the kind of object, if it is made at most by flat parts or if it is more spherical. In this second case the spherical mapping mode allow for continuous texture atlas being exported, so that it is much easier to edit it later. The *Keep UV* mapping mode generates texture atlas according to a determined texture parametrization and it is very useful, as demonstrated in the following paragraphs, for those models that are parametrized in external software and then re-imported in Photoscan.

As already mentioned in 1.4.4, the described pipeline allows to generate, beside a detailed textured 3D model, other useful and metric representation, such as true orthophotos in an increasingly automatic way (G. Verhoeven et al., 2012). Today all the software implementing the image matching approach allow to quickly and easily generate orthophotos but an accurate check is always preferable in order to validate their final real accuracy. To do this, several points not involved for image orientation and adjustment in the matching software can be measured.

Chapter 3

3D data modeling and optimization of small assets

3.1 From the photogrammetric point cloud to a complete mesh

Before any conversion of the processed 3D point-cloud into a surface mesh it is generally necessary to operate a pre-processing phase in which erroneous data, outliers and noise are eliminated. The so-cleaned point cloud represents already a database from which it is possible to extract information, but navigating through it can be an unusual environment for inexperienced users, since solid walls can appear transparent. It is easier to interpret and interact with 3D objects when represented as a surface mesh and particularly when photo textures or enhanced visualizations are added (Corns, Deevy, Devlin, Kennedy, & Shaw, 2015).

For this reasons, the generation of surfaces from point clouds is a fundamental step in every digitization and survey activity.

A polygon mesh is a surfaces constituted by vertices, edges and faces that defines the shape of a 3D object. The faces usually consist of triangles, although quadrangular shapes can be also used. Quad-dominant meshes are valid data structures much used in computer graphic field and some applications of modeling, simulation, rendering, etc. are better suited for quad meshes than for triangle ones.

Many processing steps are needed to generate a complete reality based 3D model, starting from the dense point cloud before generated, that are often related to the computer vision and computer graphics fields.

Depending on the employed geometric algorithm, normals are often computed before generating a polygonal surface. A normal is a vector perpendicular to a surface, in the case of point clouds the plane tangent of the point, whose direction indicates what is considered the “inside” and the “outside” of a surface. In computer graphics, normals are used to increase the realism of rendering as they "reflect light" and describe the shadows behavior on the surface. They can be estimated analyzing the neighboring points, setting a value of radius around the considered point (Minto & Remondino, 2014).

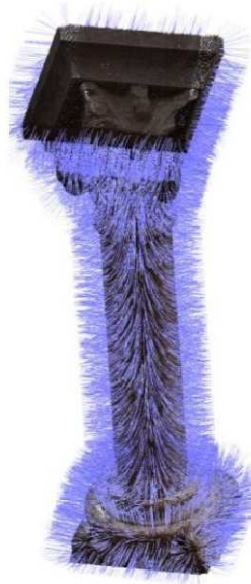


Figure 27. Computed normal on a dense point cloud of a column (software: CloudCompare 2.5.1; command: Compute normal). Source: (Minto & Remondino, 2014)

About reconstruction algorithms, it is hard to provide an overall classification and many studies have focused on this issue. In (Remondino, 2003) the issues and solutions of transforming a point cloud into a realistic 3D polygonal mesh that can satisfy high modeling and visualization needs are identified and discussed. These algorithms aim to produce the most faithful geometric model representation on the basis of the available data.

The mesh can be obtained in various ways and with various techniques starting from:

1. points, keeping their original coordinates (E. A. Ramos & Sadri, 2007), by means of triangulation algorithms and tetrahedralization (e.g. Delaunay, Poisson, etc.);

2. surfaces (tessellation algorithms, in particular for the rendering of curved surfaces);
3. data volumes (volumetric data, iso-surfaces, etc.) (Minto & Remondino, 2014).

A very well-known and used algorithm for mesh generation is the Poisson surface reconstruction method (Hoppe, Kazhdan, & Bolitho, 2006), implemented in MeshLab, which produces a polygonal surface starting from a point cloud with normal information. It works making an average of the neighborhood normal for every point of the input dataset in order to reduce the noise. Starting from the set of all normals, the algorithm derives an initial shape solving what is seen as a Poisson problem, hence the name. Unlike others mesh generation processes, which usually require mesh editing procedure of filtering and refinement, the Poisson algorithm directly implements smoothing filters providing a continuous geometry (Rodríguez-González, Nocerino, Menna, Minto, & Remondino, 2015).

As previously explained, image matching software allow to automatically generate mesh models, giving the users the possibility to choose some editing parameters according to the final detail requested by the purpose. According to (Tucci, Bonora, Conti, & Fiorini, 2015) it is possible to suppose that Photoscan uses a meshing algorithm similar to the Poisson algorithm.

However, once processed the 3D mesh, it may request a further user intervention since many topological errors or voids could be present in the model, worsening the final look of the model, that have to be solved. Therefore, further time-consuming post processing operations are mandatory to achieve an accurate and satisfactory visual appearance of the final 3D model. The main operations that have to be realized are holes filling, smoothing, removal of noise and/or parts not belonging to the object, possible topological error correction and definition of new polygons in those areas not reachable in the acquisition phase. The editing time needed for complete a mesh, may be long and responsible for as much as 90% of the total time of the 3D processing. After the creation of a complete and topologically correct 3D surface, a decimation operation, based on spatial resolution and/or setting a number of triangles, is often needed, in order to adapt the model resolution to the aims of the research. In the following paragraphs the most known practices of 3D model optimization are presented.

3.2 3D model optimization

Nowadays, 3D modeling and editing tools are quite popular and the software market offers a great set of solutions for many different purposes, responding to the most variable audience needs.

As explained in Chap. 1, one of the most important limiting factor for the dissemination of 3D models by the Cultural Heritage community is related to their heavy structure, which contrasts for example with traditional CAD models, represented in a more compact form by set of mathematical surfaces (Guidi & Angheluddu, 2016).

The final detailed 3D models include a big amount of geometric details, millions of polygons and high resolution images, which produce very large data volumes, difficult to be handled and visualized by common computers, portable devices or on the Internet, giving also problems for their further management operations, such as, for example, for segmentation procedures and visualization issues in virtual reality applications (Manferdini & Remondino, 2012; Spangher, Visintini, Tucci, & Bonora, 2017).

The irregularity and huge size of highly detailed surface models present challenges in management, animation, visualization, rendering, dissemination, and storage. Meshes are expensive representations since they store:

- the irregular connectivity of millions of faces;
- the (x,y,z) coordinates of each vertex;
- texture parameterization stored in (u,v) coordinates linked to the vertices;
- texture images, such as for example color images and bump maps, referenced to this parameterization.

For these reasons, in latest years the scientific community is testing new ways to optimize and share such 3D digital contents, in order to guarantee fast access to the data and their effective communication, providing low resolution 3D models easy navigable and viewable (Cipriani & Fantini, 2017; Guarnieri, Pirotti, & Vettore, 2010)

The challenge is to find a compromise between file size, final accuracy and visualization in order to ensure a fluent and efficient real-time interaction of detailed 3D scenes.

However, when it is necessary to deal with huge datasets (millions of polygons and GB of texture files), it is difficult to establish a common pipeline of the optimization process. Each case presents different characteristics and the optimization procedure is related to the density of the original mesh, the aimed level of detail as well as the object dimensions, shape and complexity (Fernandez-Palacios et al., 2013a).

In all cases, it is necessary to establish the needs that the 3D model has to fulfill, which determine the final level of geometrical and radiometric accuracy, size and visualization, but with the constant aim of not losing quality and information. Different purposes led to different processing choices and different optimization levels, whether it is a specialized analysis, which may require to maintain the geometric detail in the final mesh (Di Pietra et al., 2017), or a communication application which needs a lower data volume (Kai-browne et al., 2016)

In this effort many different applications are available which differs by the final aim that have to be pursued. From a metric point of view, in all of these cases it is important to evaluate the quality and accuracy of the final 3D optimized product, in comparison with the original ones.

Many applications optimize 3D models through a semantic segmentation (see 3.2.1) in order to share descriptive information in connection to 3D elements for multidisciplinary studies (i.e. for the implementation in HBIM or 3D GIS systems) (Murphy, Mcgovern, &Pavia, 2009; Oreni et al., 2014; Quattrini, Malinverni, Clini, Nespeca, & Orlietti, 2015). In other researches, in which the aim is the model visualization via web or in museum installations, optimization techniques such as re-meshing and game engine tools from entertainment technology (see the following paragraphs) allow to generate and edit Low Poly Models, textured with particular maps which simulate the original high detail of the original High Polygon mesh. In other applications, as the web-based 3DHOP, the HP model representation is based on progressive mesh proposed in (Hoppe, 1996) and foresees the use of different level of details (LoD) to reduce the latency time before the first visualization and enabling the rendering capabilities of different devices. It is based on a multi-resolution data structure which allows the client to efficiently perform view-dependent visualization (Potenziani et al., 2015).

In the following paragraphs the main characteristics of the available optimization techniques as well as some application tests are reported.

3.2.1 3D model segmentation

With the aim to simplify their polygon complexity and to pursue the chance to further link to them other heterogeneous and descriptive data, 3D models can be subdivided in several sub-components and organized according semantic rules. In Cultural Heritage field, semantic segmentation foresees the identification of sub-elements characterized by uniform properties, such as their belonging to precise historical, artistic or cultural contexts, the use of determined building techniques, the reference to classical orders or

particular certain conservation conditions. One of the aims is to connect geometry with other semantic information and many useful application involves such kind of models inside searchable databases in knowledge ontology contexts also in web-based systems for geo-visualization, data querying and sharing, educational purposes, communication, etc. (Manferdini & Remondino, 2012).

Different segmentation techniques are available, performed using manual or automatic procedures. The automatic approach aims to imitate the human visual perception, helping to automatically recognize sub-elements and define their hierarchical organization. In latest years, many researchers have investigated and developed *automatic segmentation* tools of 3D geometries. In (Minto & Remondino, 2014) the possible methodologies to automatically segment 3D data are reported:

- a) Segmentation by identifying the principal planes of the object: which can be in case of a building, the single façades or portions of them in the case of more complex structures.
- b) Segmentation techniques using region growing and principal component analysis that try to group sets of individual entities that have common properties.
- c) RANdom SAmple Consensus (RANSAC), which is an iterative method for the estimation of parameters of a mathematical model from a set of input data that produces a correct result with a given probability that increases with the increase of the iterations.

It is important to highlight that the wide range of case studies and the typical complex shape of the objects that it is possible to find in the Cultural Heritage field makes difficult to connect them to recurrent and classified examples and therefore to establish standardized rules and often a manual segmentation solution is more suited to a subdivision according to the architectural vocabulary. Although more time consuming, a *manual approach* allows to identify the main geometric elements and, if necessary, to follow rules dictated by the architectural language (column, pillar, arc, etc.) (Manferdini & Remondino, 2012).

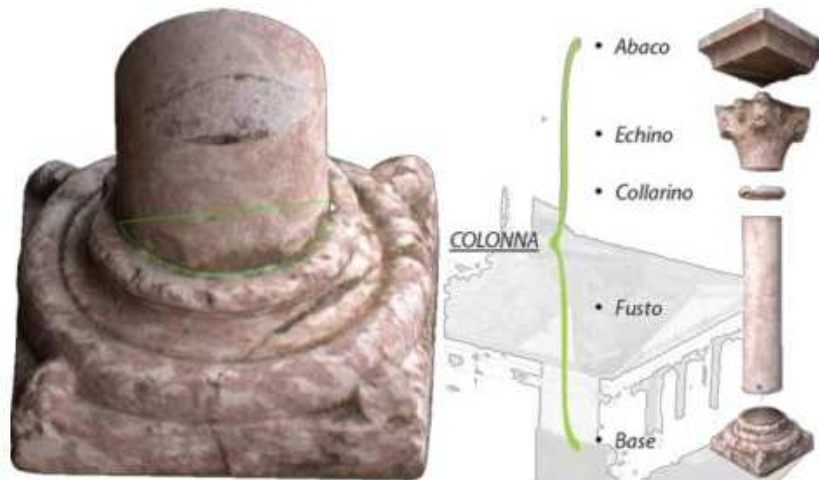


Figure 28. Segmentation of a column example. Source: (Minto & Remondino, 2014)

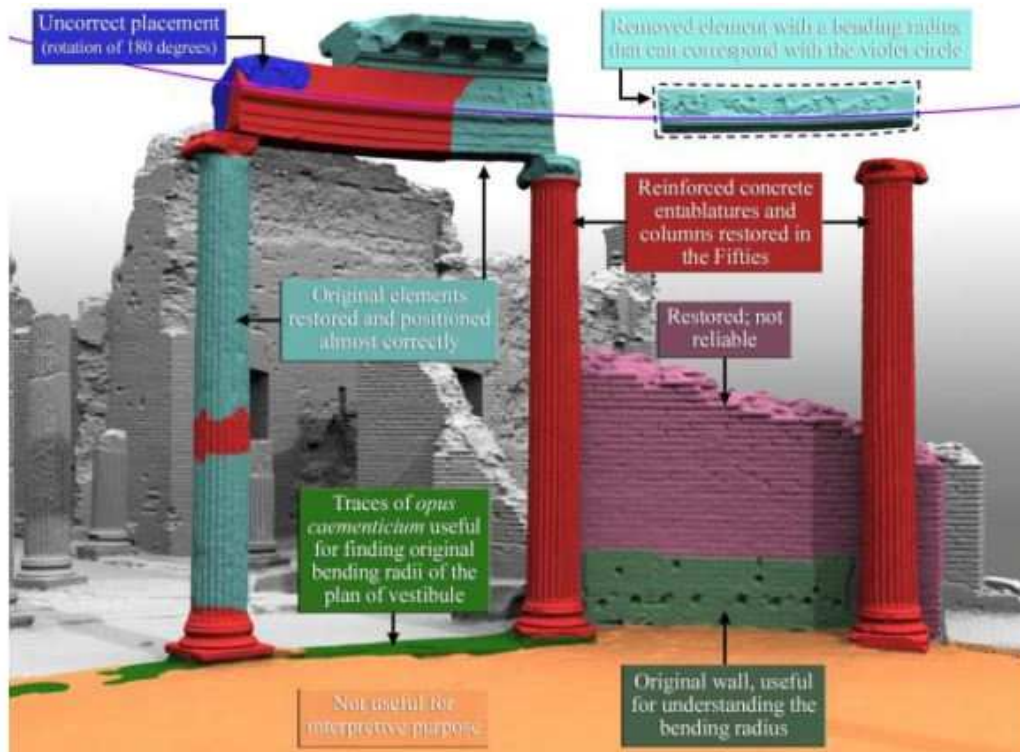


Figure 29. Semantic partition often requires interdisciplinary contributions that can help the identification of restorations. Source: (L Cipriani & Fantini, 2017)

Such processing is the base of Building Information Model (BIM) which have been developed with the aim to describe building elements according to their geometry, topology and semantic characteristics. These systems are generally designed and organized to ensure the managing of a big amount of data, allowing an enlarged access,

also remotely, for different multidisciplinary purposes (Auer et al., 2014). In latest years these tools have been adapted also to build heritage, in Historical Building Information Modeling applications (Baik, Alitany, Boehm, & Robson, 2014; Kivilcim & Duran, 2016; Oreni et al., 2014).

An example of a 3D platform to query semantic information on segmented models, is the QueryArch3D project (Agugiaro et al., 2011) developed to manage multi-resolution 3D models where the geometric data is organized in different Levels of Detail (LoD), enriched with geometric and semantic hierarchies and with attributes linked from external data sources.

3.2.2 NURBS models

Non-Uniform Rational B-splines surfaces (NURBS) are produced by means of two different approaches: reverse modelling and direct modelling. In general, the first approach convert high resolution meshes into mathematical models formed by a clean and continuous set of surfaces called “patches” by means of automatic or semi-automatic procedures based on various steps (detection of regions, feature curves, etc.). The other approach consists in sectioning the point cloud or the high resolution mesh along specific planes (offset of the ground plane, symmetry planes, radial array of planes centred on a specific axis, etc.) for extracting polylines or spline curves that once exported to modelling software can be used as references for the construction of a simplified 3D model (Adembri, Di Tondo, & Fantini, 2012). It is important to highlight that both reverse modelling and direct modelling (from a collection of sections) provide simplified version of the original survey, more a geometric idealization than a real documentation, reason why they are not suitable for scientific analysis or in some visualization application where the material texture is important. NURBS modelling tools are in fact designed for the development of new projects more than documenting the irregularities caused by degradation, decay, cracks and deformation which may be encountered in the Cultural Heritage objects. In others applications they are used for Finite Elements Methods (FEM) analysis, representing the ideal shape of the object to be simulated (Gonizzi Barsanti & Guidi, 2017).

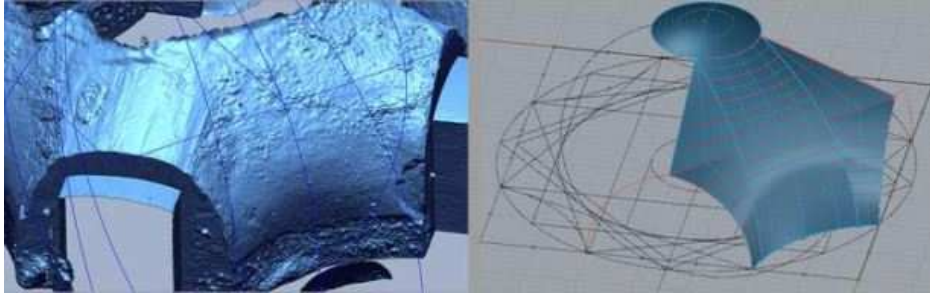


Figure 30. NURBS model of an idealized cupola from surveyed data. Source: (Fantini & Pini, 2011)

3.2.3 Game Engine tools and entertainment technology for 3D modeling of small assets

Gaming applications need a smoothly navigation through 3D virtual environments, also enabling quick dynamic actions. Such visualization requires the generation of continuous rendered frames of 3D content in fractions of a second. In order to respond to these requests, gaming industry have developed, in the years, solutions for hardly decimate the size of 3D models. In particular, nowadays any 3D model animated in videogames is usually constituted by an ultra-simplified polygonal surface, on which particular visual features able to make such simplified model much more complex and visually convincing are projected. Game engine and entertainment software, in fact, provide several useful tools to process and generate Low Polygon models, which show however a good level of detail on the surfaces, in a very low byte files, by means of particular texturing techniques. The trick of projecting visual features that simulate the geometric detail is very useful in visualization application as many researchers have already demonstrated. However, this is just a visual effect and, for this reason, this method is often considered not rigorous enough by 3D digitization scientists which aim at maintaining available all the amount of 3D metric information generated by multi-sensor acquisition methods (Guidi et al., 2016). From a geomatic point of view, approaching this kind of 3D optimization, it is important to monitor all the steps of the decimation process, in particular the entity of the geometrical error introduced in the modelling process by the transition from multi-sensor 3D data to game engine. In this thesis, one of the aims is therefore the evaluation of the final accuracy of the optimized model in comparison to the original one, considering the extractable data and their quality.

In the following paragraphs different game engine optimization tools are explained and tested in the following operative section.

3.2.4 3D model simplification and remeshing technique

Among the available processes that allow to generate new meshes, with lower polygon count or with better topology, there are the simplification and remeshing techniques.

Simplification of polygonal meshes has been studied in depth in many studies over the last 30 years and it can now be considered a consolidated technology. By now, many algorithms are available for the simplification of triangle meshes, implemented in the most common modeling packages like Maya, Blender or MeshLab (Tarini, Pietroni, Cignoni, Panozzo, & Puppo, 2010).

The mesh simplification consists, starting from a mesh as input, in the creation of another one with less faces, edges and vertexes. Most triangle mesh simplification algorithms employ an adaptive meshing, with the primary aim to generate a reduced mesh model that approximate as much as possible the original shape reducing the number of triangles.

In the study presented in (Rodríguez-Gonzálvez et al., 2015), the authors present a simplification and optimization pipeline with the aim of generating a reduced product that maintain the maximum amount of significant information. According to this research:

"Ideally, considering equilateral triangular meshes, the target number of triangle (N) could be derived applying simple geometrical considerations:

$$N = \frac{4 * A}{\sqrt{3} * L^3}$$

where A is total lateral area of the meshed object, L is the face edge length (equal to the user-defined spatial resolution) and N the number of triangles."

According to (Minto & Remondino, 2014) a possible classification of the available decimation algorithms can be the following:

1. Iterative decimations: automatically decreases the number of vertices or faces or edges of the mesh, depending on the specific decimation ratio specified by the user, re-triangulating the resulting holes. Such algorithms work very fast and are excellent for the elimination of redundant elements. This method has also simple implementation, achieves a good approximation and preserves the topology of the original mesh. However, it does not use an evaluation of error (Campomanes-Alvarez, Damas, & Cordon, 2012).
2. Vertex-merging: collapses two or more vertices into a single new one which may be then joined to other vertices in further stages. A subclass of these methods is based on edge-collapsing. Using this method, it is important to control the scheme that can be used to decide which vertices must be joined and in which order.

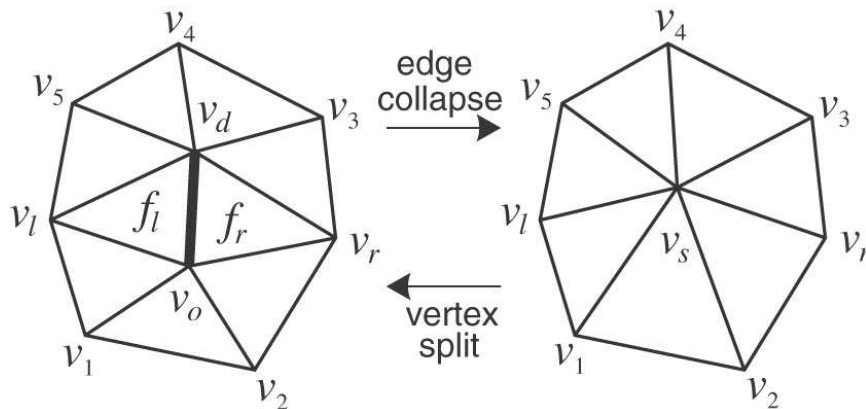


Figure 31. Edge collapse decimation

3. Adaptive subdivisions: a simple base mesh is recursively divided to approximate more and more the original surface model, editing multi-resolution surfaces and preserving the topology.

Among the vertex merging algorithms, the quadratic edge collapse algorithm developed by (Garland & Heckbert, 1997) is one of the most used since it can rapidly produce high quality approximations of High-polygon models. The algorithm applies an iterative contractions of vertex pairs (not just edges) to decimate models, maintaining surface error approximations using quadric matrices and joining unconnected regions of models. The primary advantages of this algorithm are the ability of rapidly simplify complex models, the high fidelity to the original surface, since their primary features are maintained even after strong simplification, and the capability to merge unconnected regions of the resulting model with a process called "aggregation". MeshLab, for example, implements the Quadric edge collapse algorithm, which is able to decimate the faces of a 3D mesh preserving boundaries and/or normals. If the model is textured, there is also an option properly oriented (with texture) that allows to keep the textures positioned properly.

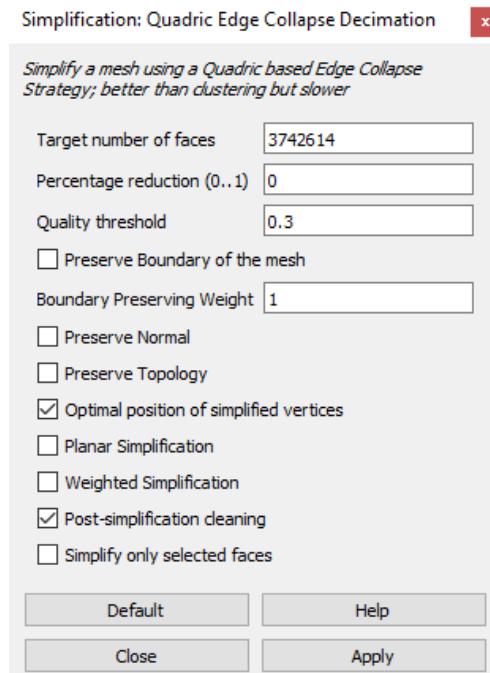


Figure 32. Example of the Quadric Edge Collapse command in MeshLab

This mechanism ensures that this system also supports non-manifold surface models, which are surfaces that does not completely enclose a volume. A "Non-Manifold" mesh does not represent a problem for conventional meshes, but it may rise to unpleasant artifacts dealing with subdivided meshes (see 3.2.8) and generate problems for the calculation of the normal vectors.

Another algorithm of edge contraction is the iterative edge contractor by (Hoppe, DeRose, Duchamp, McDonald, & Stuetzle, 1993). This kind of algorithms have been designed in application to manifold surfaces, even though edge contractions can be also applied on non-manifold surfaces, since they perform successive edge contractions. They can close holes in the object but they cannot join unconnected regions.

Compared to triangle-based meshes, simplification of quad-dominant meshes sets additional challenges, because quads are less adaptive and more delicate structures than triangles. A practical quad mesh simplification is presented in (Tarini et al., 2010).

A different topic to create a simplified mesh model is the "re-meshing" technique that indicates the whole process of computing, given a 3D mesh, a completely new mesh whose elements respect some specific quality requirements, while approximating the original input acceptably (Alliez, Ucelli, Gotsman, & Attene, 2008). The aim of remeshing is not necessarily just at lower complexity, since it can be used also for improving the quality of an input mesh, producing a new one with superior quality and better topology. Remeshing approach requires to solve more complex issues compared to

mesh decimation (like new parametrization, or identification of principal curvature direction) which are difficult to tackle robustly and often it can be less robust to noise issues (Tarini et al., 2010). Furthermore, remeshing approach produces higher deviations from the original model if compared to those obtained by decimation in comparison to the original input (Minto & Remondino, 2014). It is important to highlight that this technique cannot always be used with any kind of 3D model. It can be difficult when dealing with urban surveys, due to the presence of a big amount of occlusion effects (Merlo, Dalco, & Fantini, 2012). Indeed, quad dominant re-meshing requires “waterproof” meshes lacking topological errors, and such models are very hard to completely fulfill these requests.

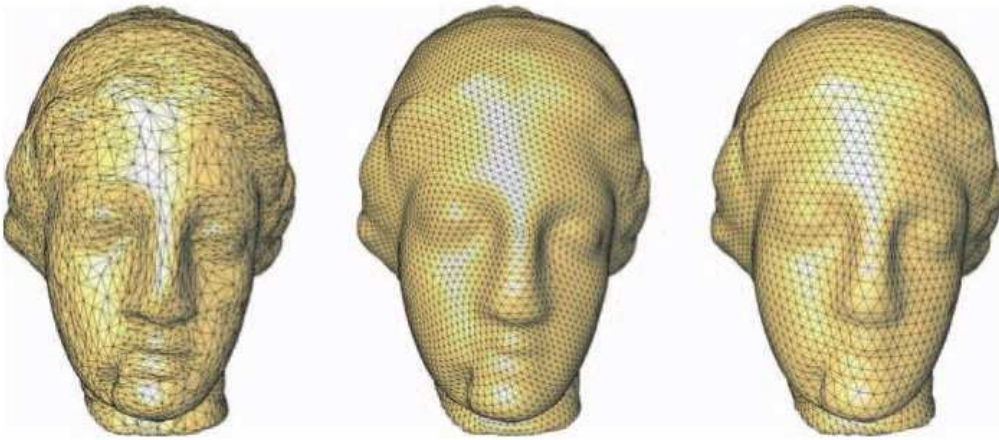


Figure 33. An example of structured remeshing: Irregular, semi-regular and regular. Source: (Alliez et al., 2008)

3.2.5 Diffuse colors, bump, normal and displacement maps

The idea of coding a mesh with small details, mapping them on a new simplified version (Low Polygon surface), rather than really representing them geometrically with tiny 3D polygons, has been studied since the early Computer Graphic applications.

This shading technique uses texture images mapped onto a surface in a 3D scene, in order to define and encode many surface parameters. The aim is to produce realistic and visually rich 3D models, creating a specific correspondence between the 3D coordinates of the model vertexes and 2D images (Lévy, 2001). This idea raised by the need of simplifying the geometrical complexity of 3D models, trying, however, to maintain a good visual quality level at the rendering stage. The aim is to only simulate the detail rather than render the detail itself, with optical illusion effects which are less computationally intensive than the original 3D rendering would be. As reported in (Guidi & Angheldu, 2016), several techniques working at pixel level are available. Such

methods allow to locally alter the lighting of a material through the projection of a particular image map, whose coded attributes alter the computational lighting model. Such parameters might be for example: the local light reflectance encoded in Bump Mapping, that simulates bumps and wrinkles using a single channel image (grayscale) (Blinn, 1978), or the orientation of the normal vector for simulating the details as made in Normal Mapping.

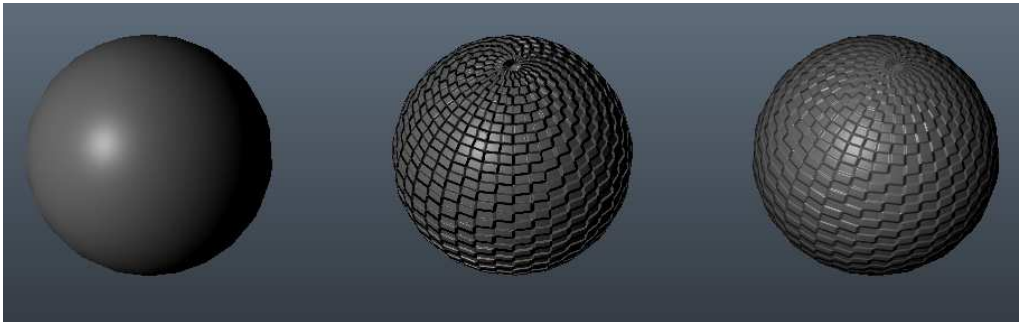


Figure 34. A sphere before and after the bump mapping. Source: lauraatnua.blogspot.it/2015/04/the-difference-between-bump-and-normal.html

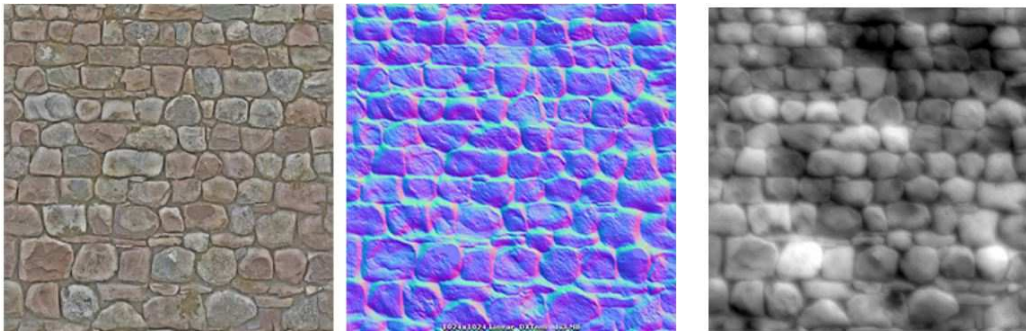


Figure 35. A wall texture, a normal map and a bump map
<https://docs.unity3d.com/Manual/StandardShaderMaterialParameterNormalMap.html>





Figure 36. Above: A stone wall with no normal map effect. The edges and facets of the rock do not catch the directional sun light in the scene. Below: The same stone wall with normal mapping applied. The edges of the stones facing the sun reflect the directional sun light very differently. Source:

<https://docs.unity3d.com/Manual/StandardShaderMaterialParameterNormalMap.html>

These kind of texture maps are bitmap images that are obtained by baking processes between the original High Polygon (HP) model and the Low Polygon (LP) one, wrapped in a UV bi-dimensional space. The baking process consists in an operation whereby the software computes information about the geometry and colour of the HP mesh and stores them in an RGB or grey scale image built on a specific UV reference system (Merlo, Sánchez Belenguer, Vidal Vendrell, Fantini, & Aliperta, 2013). Such tools have a fundamental role in the optimization process since may store information about normal vectors on each surface point, defining its shading, or about the points position in the space (see Displaced Subdivision Surfaces, in 3.2.8). With the projection of these images, such as bump maps, normal maps and displacement maps, the LP improves its appearance and it can be in some cases visually perceived as the HP ones (Merlo, Fantini, Aliperta, Lavoratti, & López Hernández, 2013).

In this thesis, greater attention has been paid to normal and displacement maps, focusing on their potentialities of simulating the detail and in order also to make some comparison about the quality of the rendered detail.

A normal map is an image that contains the surface normal vector of the original High Poly mesh, stored as a RGB value in the pixel. It stores a normal behaviour as follows:

- Red maps from (0 - 255) to X (-1.0 - 1.0)
- Green maps from (0 - 255) to Y (-1.0 - 1.0)
- Blue maps from (0 - 255) to Z (0.0 - 1.0)

Once calculated and projected to a Low-poly mesh, the normal map simulates the behavior of light reflections from the original model adjusting the shading of the low-detail model, which looks again like the original HP model but in a very lower byte file size.

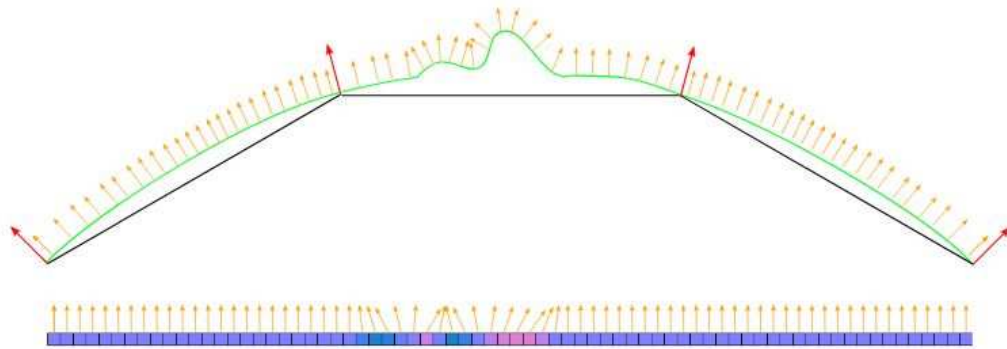


Figure 37. Normal mapping across three polygons, viewed as a 2D diagram - Source: <https://docs.unity3d.com/Manual/StandardShaderMaterialParameterNormalMap.html>

A displacement map is, instead, a grey scale image, in which each shade of grey represents the deviation between the original HP model and the optimized one. Unlike the normal map, the displacement map, once applied to the Low Poly model, really displaces its vertices basing on the deviations calculated in the baking process (Merlo, Sánchez Belenguier, et al., 2013).

In order to compute such 2D representation, it is essential to firstly process the UV map of each 3D model by unwrapping it in a 2D coordinate system (u, v) which ensures the spatial link between the (x,y,z) coordinates of the mesh and the image. This process consists in the parameterization procedure, which will be discussed in the next paragraph. In latest years many different applications of these tools have been developed and applied to multi-scale objects and with different aims. (Pan, Tang, Xu, & Da, 2016), for example, present a method for the generation of a detailed orthogonal projection of a 3D model merging normal map and texture information in gradient domain. This non-photorealistic projection is both geometry-aware and texture-aware and helps the recognition of subtle details which would be otherwise hard to be seen in the texture image or the normal map alone.



Figure 38. Texture and normal map - the line-drawing is traced over the fused image of the statue.
Source: (Pan et al., 2017)

In (Merlo et al., 2012) an optimization procedure using the mentioned texture maps have been processed and applied to the 3D model of the fortification complex of Pietrabuona Castle with the further aim to use such data in a 3D GIS.

(Jiménez Fernández-Palacios et al., 2017) report an experience of optimization with the aim to use such models in virtual reality solutions.

As shown in these experiences, the need to operate an optimization of a 3D model by means of the mentioned techniques may derive from different research's field and with different aims and this makes such tools very attractive from many points of view.

3.2.6 Parameterization procedure

As explained in the previous paragraph, in order to realize a texture map, it is necessary to create a 2D space on which project the 3D model. Texture space is the 2D space of surface textures and Object space is the 3D coordinate system that contains 3D geometry such as polygons. The processing that retrieves the correspondences between 2D texture space and 3D object space is called parameterization of the surface space and the mapping of the 3D object space to 2D space generates a UV map (Hu et al., 2010). Basically, the parameterization is a function that puts a 3D surface to be textured in one-to-one correspondence with a 2D space. In a UV map each vertex of the polygonal mesh gets assigned to 2D coordinates (u, v) that define how each part of the image will be mapped. The process that generates these UV maps is also called “unwrap”, since it works as if the mesh were unfolded onto a 2D plane. Thanks to the parameterization, it is possible to texture-map the surface by coding specific information in the parameter space with an image.

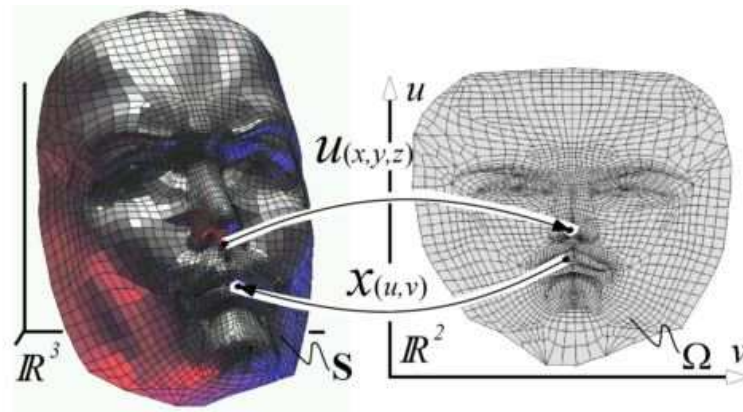


Figure 39. A mapping U puts a surface S of \mathbb{R}^3 in one-to-one correspondence with a subset Ω of \mathbb{R}^2 called the (u, v) parameter space. The inverse X of U is named a parameterization of S .
Source: (Lévy, 2001)

Since some mesh models, as the ones achievable by multisensor survey methods, are not generated, – unlike NURBS – with natural parameterization, Computer Graphics researchers tried to provide an easy way to map such complex polygonal models on the 2D reference system (u,v) . From the end of the Nineties, the field of entertainment software for 3D modeling has been focused on producing advanced texturing techniques. Some researches proposed at international conferences on Computer Graphics (Lévy, 2001; Piponi & Borshukov, 2000) focused on the parameterization procedure and gave interesting inputs to software developers for the implementation of new tools inside 3D modeling applications. The fundamental issue these studies faced was the need to find a simplified and intuitive way to unwrap in a 2D system a complex 3D surface, in order to use a 2D space for texture mapping. The intuition of a kind of digital “pelting” presented in (Piponi & Borshukov, 2000) reached great popularity in the entertainment software field. The pelting method consists in the identification, by the operator, of a series of consecutive edges belonging to the LP model and forming a "connected tree", that is a chain of adjacent edges: along these geometrical entities a "cut" will be made to the mesh model that allows its development in the 2D (u, v) reference system. In practical, this solution simulates what happens when the skin of an animal (pelting) is spread on a plane: the cutting edges are used as the limits to which a special algorithm is applied. In the early years of the 21th century, the most important software companies working in this field have implemented different tools for the interactive parameterization of 3D polygonal surfaces. An important issue in parameterization procedure is that complex shapes cannot be unwrapped into the (u,v) reference system without applying distortions and cuts and for this reason in the last ten years many studies on parameterization have been focused on the implementation of new more performing and automatic algorithms,

also considering that the parameterization procedure is not just limited to the texture mapping operation, since it now allows other detail transfer processing which include morphing, mesh completion, remeshing and surface fitting (L Cipriani, Fantini, & Bertacchi, 2014).

Many studies aim to control two main aspects of the parameterization process: the creation of a low number of island in the (u, v) space and the maintenance of a noteworthy balance between the area occupied by individual polygons in space (x, y, z) and their homologous surface in (u, v) , making them directly proportional. To a Low-poly mesh that approximates a specific number of polygons in the Hi-Poly mesh, should correspond a UV map able to contain a sufficient number of pixels in order to store adequate geometrical information during the baking process. The UV map needs also that the polygons do not overlap, otherwise it loses any correlation between the points of the model and their corresponding developed on the same plane. In (Lévy, Petitjean, Ray, & Maillot, 2002) an interesting research aimed at finding a solution to surface parameterization is presented. The aim of this study is to reduce texture errors along boundaries, exploiting a uniform sampling in (u,v) space and properly and completely using the parameter space (no waste of useful pixels). In particular, the researchers proved the need to reduce the number of cuts along connected trees of triangles edges in order to reduce as much as possible the number of islands in (u,v) space.

Many software packages allow to automatically generate sub-optimal UV parameterization within the 3D acquisition and processing pipeline but often the final result may give rise to some misinterpretation. This typically happens to 3D surfaces derived from automatic meshing processes, with respect to a (u, v) parameterization generated according user intervention, as in manually designed 3D models with Computer Graphics (CG) functions (Guidi & Angheluddu, 2016).

Focusing on the Cultural Heritage field and its related documentation methods and processing software, it is important to highlight that the parameterization procedure – crucial in 3D model texturing process – has always been considered as a secondary topic, up to the introduction of SfM techniques. In fact, most of applications for point cloud and mesh processing implements only automatic and not interactive parameterization, that in most cases produces an un-controlled and un-editable number of islands in the (u,v) parameter space (Merlo, Sánchez Belenguer, et al., 2013) (see 2.3.2).

Thanks to the implementation of SfM algorithms into photo-modelling applications, the problem of parameterization assumed a new and more important role in Cultural Heritage geometric modelling field. The main reason is due to the uncontrolled quality achievable by automatic parameterization solutions implemented in most photo-modelling software:

high detailed 3D models from SfM may have very poor parameterization, that as a consequence compromises their texturing quality.

Furthermore, the photogrammetric data acquisition step may be influenced by lighting conditions and shadows or overexposed areas cannot be corrected if a bad parameterization is realized, compromising so the texture quality. A correct parameterization is essential to achieve a high quality texture mapping but also for the editing and optimization of highly portable, multipurpose 3D models, able to store and disseminate information, through real-time interactive applications.

From this point of view, the geometric modeling programs for entertainment are not comparable to SFM processing software, since the latter create reference systems (u, v) in an automatic way without significant possibility of intervention by the operator.

Too many islands, in fact, make the model texture not editable and so it is not possible to operate any correction. For example, a column UV map may derive from a cylindrical wrapping, but reverse modelling and SfM software are not able to automatically recognize and produce such kind of parameterization. SfM software creates a big amount of islands (atlas), that broke the polygons continuity in many small portions that the operator is not able to recognize in an easy way. For this reason, the final texture is very difficult to be later corrected in other software such Photoshop, where the radiometric quality can be improved. Furthermore, the 3D model deriving from an image matching pipeline may present topological errors as dangling faces, isolated polygons, overlapping faces, holes, etc.

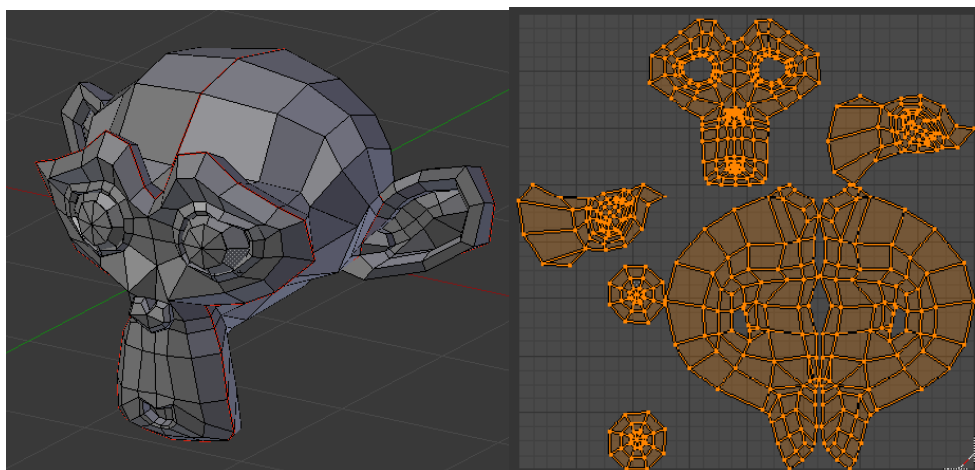


Figure 40. An example of UV creation in Blender in which the user defines the cuts over the surface marking Seams and then the unwrapping creates the corresponding UV map.

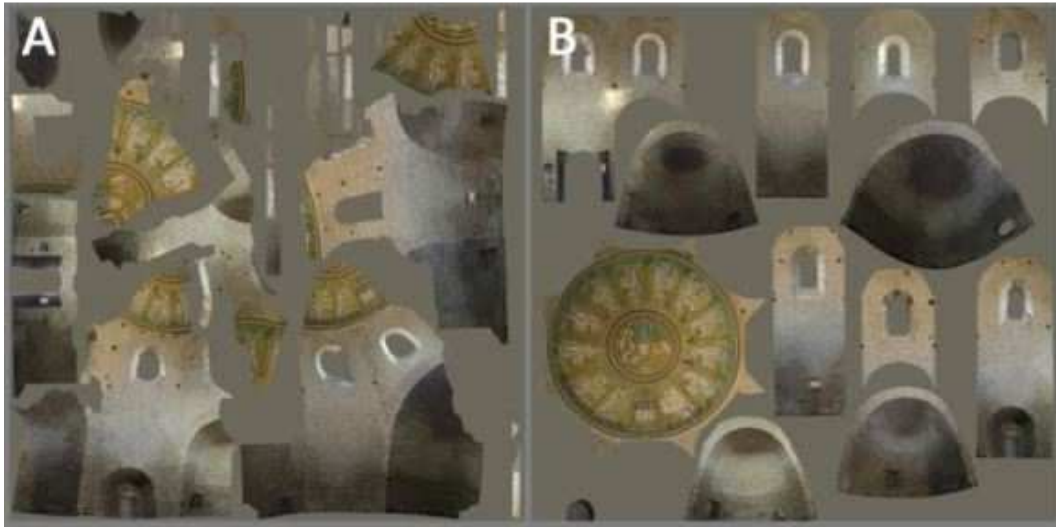


Figure 41. A) product of automatic parameterization. B) automatic parameterization of Low-Poly mesh from retopology after semantic partition. Source: (L Cipriani et al., 2014)

Entertainment software, instead, offer a wide set of tools aimed at texture calculation and application. For these reasons, software such as Agisoft Photoscan allows to export the processed 3D models, in .OBJ or .PLY formats, in reverse modelling software where it is possible to correct possible topological errors and later re-import them for the final texturing phase, allowing to obtain UV maps with better quality.

Starting from this considerations, it is evident that in an optimization process it is necessary to integrate different software, in order to obtain high quality parameterization.

3.2.7 Retopology tools and quad-dominant mesh

The retopology technique allows the achievement of Low Poly models in a different way compared to automatic decimation. It consists in a manual (or in some software automatic) tracing of the High Poly mesh with a quadrangular mesh of lower density, called "quad-dominant mesh". This process requires a skilled and experienced operator and may take long time.

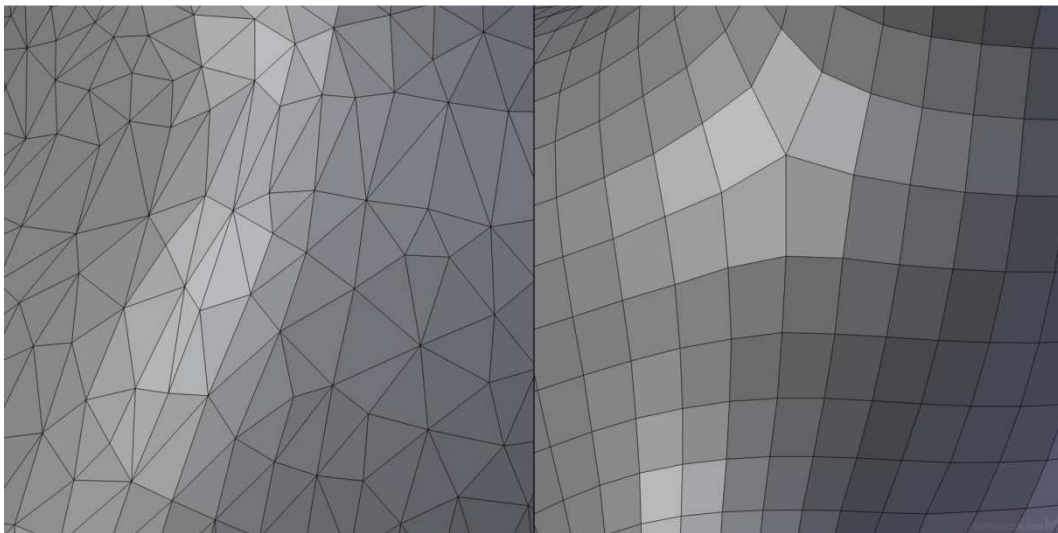
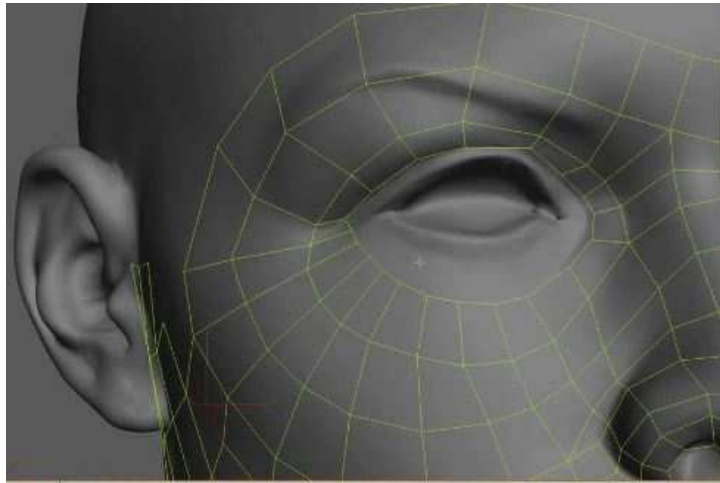


Figure 42. Above: base retopology example over a head; below: different topology from triangular to quadrangular mesh. Source: <https://cloud.blender.org/p/blenderella/56040ecf044a2a00a515ada6>

The reason of making this kind or retopologized models are:

- In a triangles based mesh, the number of polygons is fixed, while retopology tools produce quad-dominant Low Poly models, that support the conversion into Catmull-Clark SubDivision surface, which is a variable LoD model, that is usually considered a prerogative of NURBS modelling application and may be interactively increased in different output scales by adjusting the level of subdivision (Merlo, Sánchez Belenguer, et al., 2013);
- Both automatic and manual retopology approaches can be applied to generate smart quadrangular polygon loops following objects' formal features and their selection in

entertainment applications is easier if compared with unstructured triangular meshes. (Merlo, Sánchez Belenguer, et al., 2013).

When manually editing such mesh, the user must constantly take under control the quality of the quadrangular polygon, the regularity and size of its edges, in order to not generate too sparse or too dense a mesh. The final quad meshes, constituted entirely of quadrilaterals, represent important data structures in computer graphic field and several applications of modeling, simulation, rendering, etc. works better for quad meshes than for triangulated ones (Tarini et al., 2010).

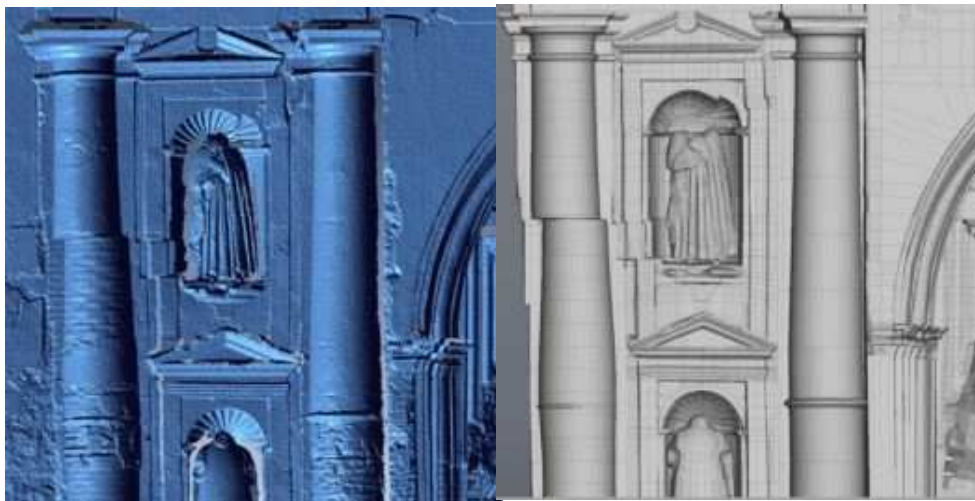


Figure 43. Left: High Poly model; right: corresponding Low Poly model from retopology realized with software Luxology Modo

Almost every entertainment software (Pilgway 3D Coat, Pixelmachine Topogun, Autodesk Mudbox, Pixologic Zbrush, Luxology Modo, Blender etc.) implements efficient automatic or manual solutions and this confirms the efforts of software developers to improve this kind of re-meshing approach.

3.2.8 SubDivision Surfaces and Displaced subDivision Surfaces

SubDivision (SubD) surfaces is a kind of surface originated using methodologies for the modeling of assets borrowed from character animation. These methodology make a surface a variable-detail model, in which the geometry of the mesh (and the number of polygon) may be interactively increased or decreased setting the level of subdivision (Figure 44). These surfaces are generated applying a subdivision process to a polygonal mesh that forms a manifold, M^0 , to produce a new higher resolution mesh M^1 . This process is then iterated to form meshes M^0, M^1, \dots that better approximate the limiting

mesh M^∞ . The subdivision scheme is defined in order to guarantee that under reasonable conditions the limiting surface is smooth (Piponi & Borshukov, 2000).

One of the most known subdivision schemes defining smooth surfaces is the one introduced by Catmull and Clark (Catmull & Clark, 1978) (mentioned in 3.2.5). It is the most implemented in open-source and commercial 3D software packages. As already mentioned, this criterion is more effective with quad-dominant surfaces, that are not a common in the field of remote sensing (Luca Cipriani & Fantini, 2017). For this reason, time consuming re-topology process is always necessary to create coarse quad-meshes from triangles ones, suitable for the conversion into displaced subdivision surfaces.

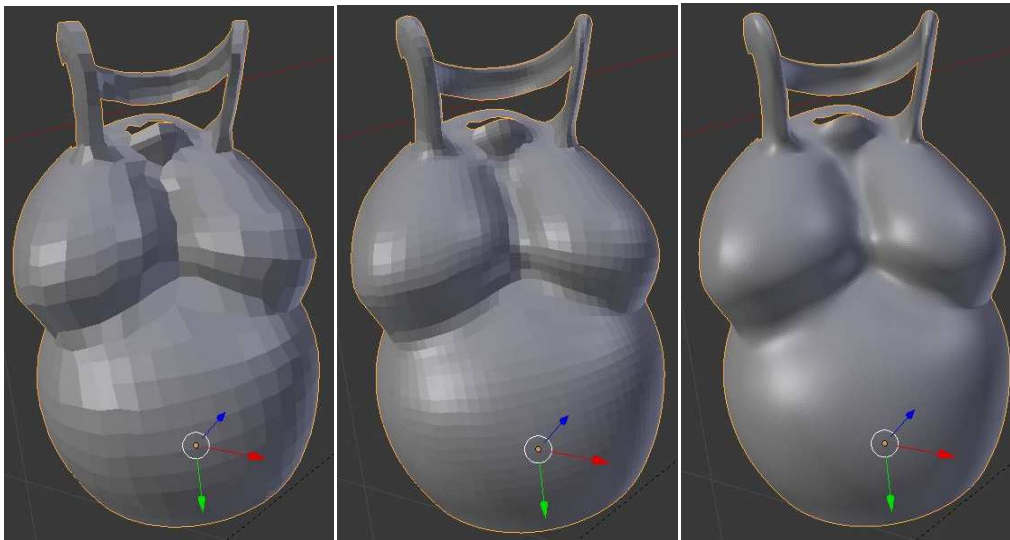


Figure 44. The retopologized model, subdivision surface level 2, subdivision surface level 5.

A Displaced subDivision surface represents a surface model that derives a high level of detail from a scalar-valued displacement over a smooth subdivided domain surface. The implementation of a Level of Detail model, with a very low polygon count, and the detail ensured by the displacement map allow to store in the final model detailed and decorative elements without the need of a radical decimation.

Displaced subDivision models are often used in the field of computer graphics, when it is necessary to animate virtual character obtained by digital sculpting or made by an artist and then scanned (Adembri et al., 2012).

Compared to a high detailed surface model, a displaced SubDivision Surfaces ensures a number of advantages (Lee, Moreton, & Hoppe, 2000):

- geometry editing, animation, scalability and adaptive rendering;

- the domain surface is constituted by a control mesh which is a simplified copy of the original HP mesh;
- fine details are stored as a scalar-valued function in a displacement map which is more compact than traditional vector-valued geometry;
- the parameterization of the displaced surface is congruent with the one of the smooth domain surface and therefore it is not necessary to explicitly store it;
- the fine detail can be easily modified since it is a scalar field.

The main aspect of displaced subD is the capability to increase the geometric resolution during the computation of the rendered image thanks to the displacement map, that re-establish the detail of the high resolution model (Adembri et al., 2012) (Figure 46).

In the field of Cultural Heritage these models offer great advantages, as compression of morphologic detail, high portability and different output scales.

The approach presented in (Lee et al., 2000) consists of a control mesh and a scalar field that locally displaces the subdivided surface along its normal.

The main steps are:

- Control mesh generation: a coarse and simplified model that traces the shape of the HP model with a quadrangular topology (after retopology);
- Smooth domain surface (SDS) computation: a LoD model obtained converting the Control mesh in SubDivision surface.
- Displacement map computation and projection: an image that stores a scalar field that locally displaces the associated subdivision surface along its normal.

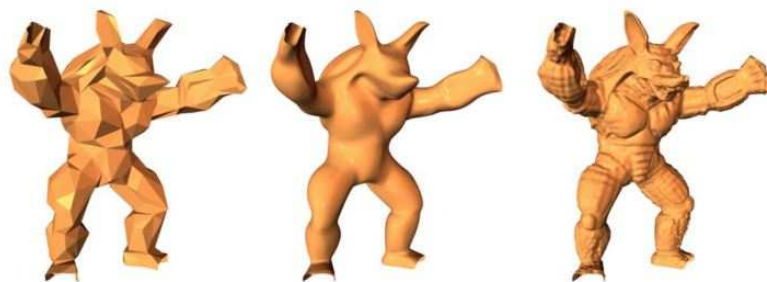


Figure 45. Control mesh, smooth domain surface and displaced subDivision surface. Source: (Lee et al., 2000)

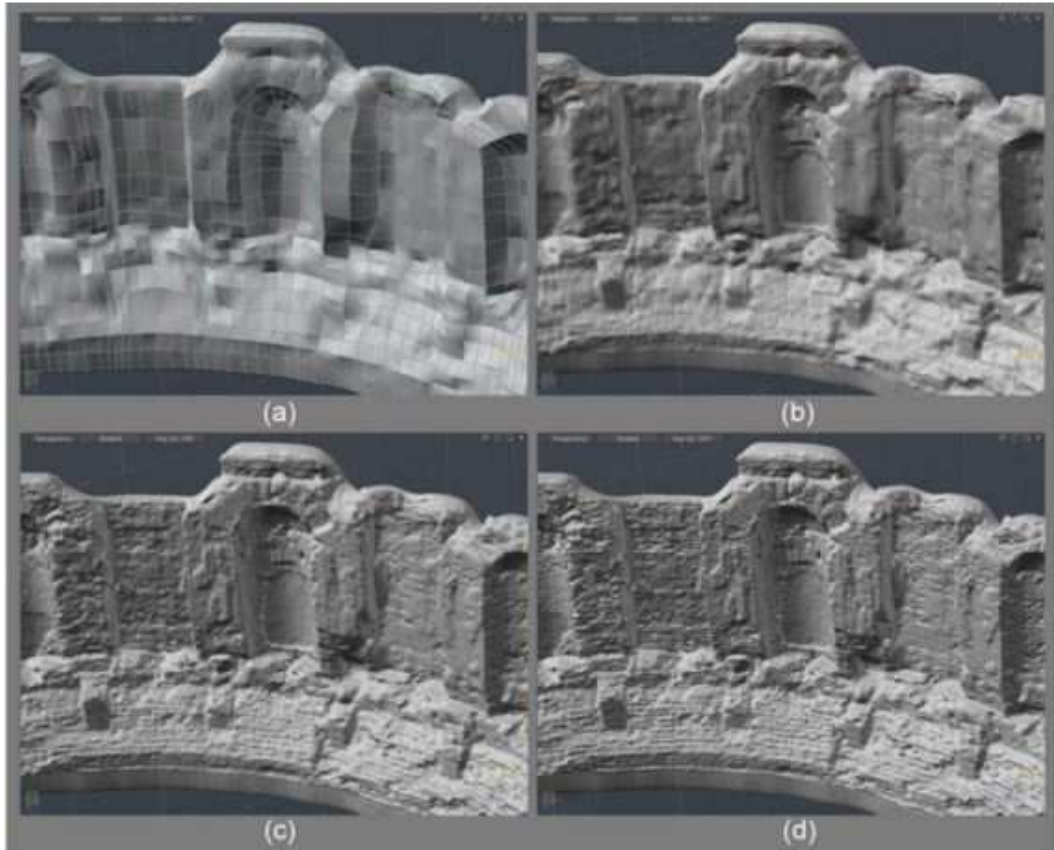


Figure 46. Once converted in a displaced subdivision surface, it is possible to interactively increase and decrease the level of detail. Source: Adembri 2012

Chapter 4

Experimental section 1 - The image processing applied to the case studies

4.2 The case studies acquisition and processing

In the following paragraphs the photogrammetric acquisition and processing steps of each test case will be presented, highlighting the different camera parameters, the chosen acquisition configuration and the processing settings.

The acquisition phases have some parameters in common but different techniques have been used to scale and georeference the data. The acquisition of Lina and of the roman bust was carried out in indoor space and to better control the exposure time, influenced by dim light, the camera was mounted on a stable tripod and artificial lights have been also used. Whereas, in the frieze case, just natural light has been used.

Three different methods have been use to scale and assign a reference system:

- In the Lina test case, the photogrammetric model has been scaled using a laser point cloud as reference;
- In the roman bust test case, several lengths have been manually measured placing some targets on the wall, since a total station was not available;
- In the frieze test case, a specific micro geodetic network has been previously measured using GNSS techniques and then linked to the frieze measuring several targets placed on its surface with a total station.

These applications demonstrate how different approaches can be applied to pursue the same aim, according to the available resources at the acquisition time.

4.2.1 The photogrammetric acquisition of Lina

The aim of the survey was to process a detailed textured model of the sculpture. The photogrammetric acquisition was carried out inside the professional artist's studio. The statue has been placed over a stool in the center of the room and the camera has been mounted on a stable tripod.

Regarding the illumination, the room was very dark and it has been considered necessary to add to natural light also two artificial lights, mounted over a tripod and properly oriented, in order to produce a quite homogeneous illumination on the object, without strong shades and reflections.

Unfortunately, it was not possible to rotate the object, so the acquisition has been made moving around it.

The statue has been surveyed with a Canon EOS-1Ds Mark II (pixel size 4.24 μm , sensor size 24x36mm) equipped with a 24 mm focal length, with the focus locked. The imaging acquisition distance was about 0.5 m all around the object assuming an image scale of about 1:20 with a GSD of 0.1 mm/pixel. 75 images have been acquired at three different heights all around the statue.

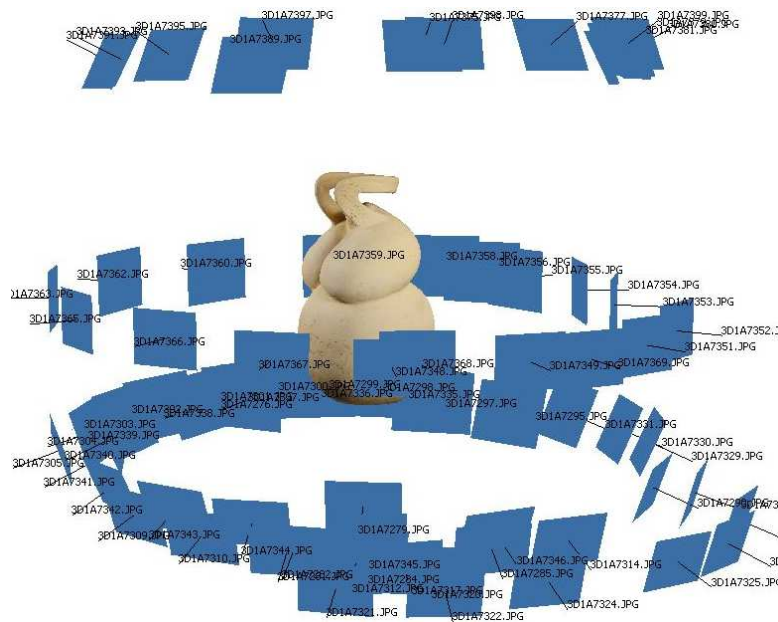


Figure 47. Visualization of the cameras position during the acquisition.

At the same time, a laser acquisition has been conducted by means of the terrestrial laser Faro Focus 3D, whose purpose has been also to provide a reference system (the one automatically set in the laser at the time of the acquisition) in order to further scale the photogrammetric model. To ensure this, several targets have been placed on the walls and objects around the sculpture, paying attention to acquire them in more images, in order to further read their coordinates in the laser point cloud and then assign them in the photogrammetric process.

4.2.2 The data processing of Lina

The acquired images have been processed by means of the SfM technique and image matching algorithms in Photoscan.

Once imported in the software, all the images have been masked in order to remove the walls and the objects behind the sculpture in the calculation that could produce noise in the calculation process (with the exception of the targets).

The alignment phase has been processed with High settings and a sparse cloud composed by 124.511 tie points has been calculated.



Figure 48. Example of a masked image in which two targets used are visible.

The Dense cloud has been processed using High settings and the Moderate depth filtering for remove outliers, which brings results that are in between the Mild and Aggressive approaches. The result is a dense cloud of 10,126,633of points. The mesh model has been processed with High settings, the Arbitrary parameter, suggested for modeling this kind of object and the Mild depth filtering. A mesh model of 2.022.311 faces has been

created. The RMS, re-projection error is about 0.914 pix and the final GSD is 0.134 mm/pix (Figure 49).

In order to scale the photogrammetric results, a local reference system has been assigned to the model, basing on the coordinates of the targets extracted from the laser point cloud (referred to the center of the instrument at the time of acquisition) (Table 2)

Label	X error (mm)	Y error (mm)	Z error (mm)	Total (mm)
1	-1.5335	-0.822835	-1.32132	2.18508
2	0.138029	2.25245	1.80127	2.88741
3	1.52609	-0.382	-1.32077	2.0541
4	-0.130583	-1.04769	0.840821	1.3497
Total	1.0859	1.32233	1.36399	2.18819

Table 2. Visualization of the calculated errors of the control points used for scaling the 3D data.

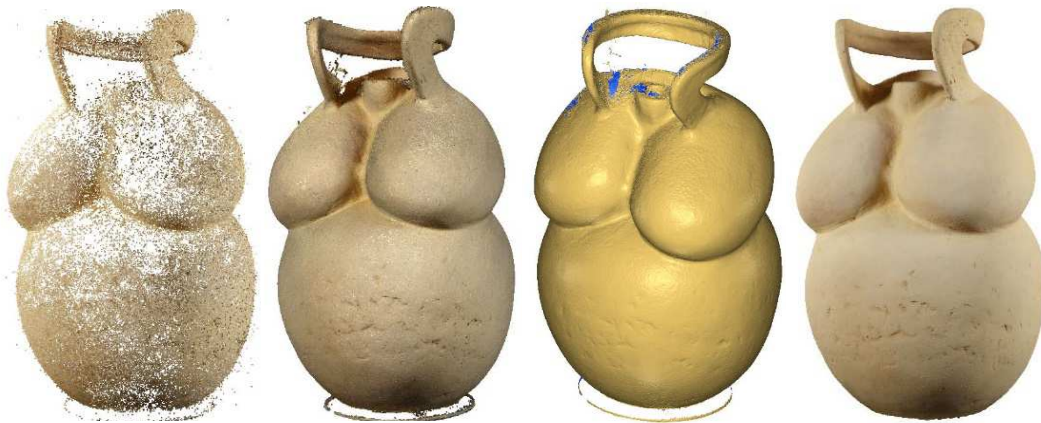


Figure 49. Tie point, dense cloud, mesh model and textured mesh model.

The texturing step has been processed with the Generic mapping mode, that tries to create as uniform texture as possible, and the Average generation parameter, that uses the weighted average value of all pixels from individual photos.

An interesting evaluation regards the UV maps that automatically are generated during the texture generation in the texture space. As visible in (Figure 50), the automatic process generates a big amount of indiscriminate atlas, difficult to be recognized and possibly modified. For this reason, the following optimization process presented in the next Section aims also on the generation of a more controlled UV map and resulting texture, which would be more easily controlled and corrected from the radiometric point of view in external software.

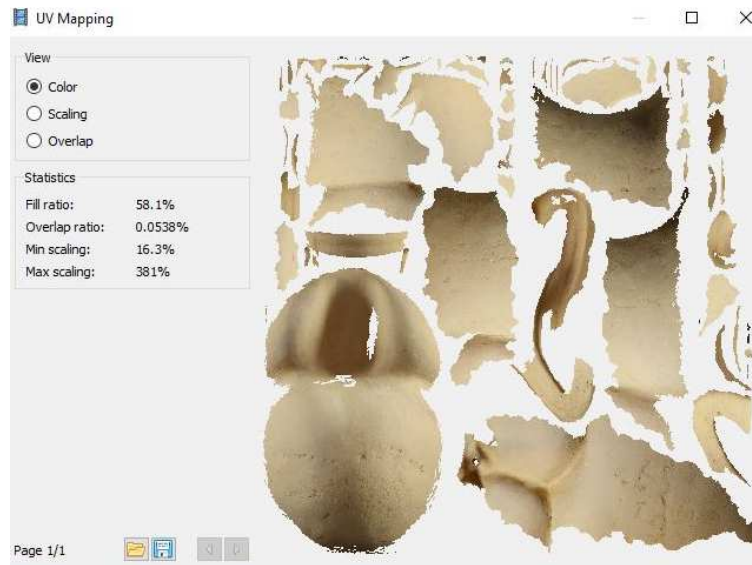


Figure 50. Automatic UV map processed in Photoscan

4.2.3 The photogrammetric acquisition of the roman loricated bust

The aim of the 3D survey was to process a textured model of the busts as it is today and the way it was before the addition of the nineteenth century restoration, which completed the bust with the lower part of the legs, the arms and the head. The photogrammetric acquisition was carried out during the museum closing day. The bust is exposed in a big hall of the museum, between two big windows, and plenty of natural light comes inside. The statue is located over a pillar, so the head reaches a height over two meters from the ground. For this reason, it has been necessary to use a scaffolding for the acquisition of the higher portions, moving it all around the object. During the acquisition, the camera has been mounted on a stable tripod.

Regarding the illumination, it was considered necessary to add to natural and artificial illumination present in the museum, two artificial lights mounted over a tripod in order to produce a quite homogeneous illumination on the object, without strong shades and reflections.

One important issue that influenced the acquisition operation was the insufficient space behind the statue, between the statue itself and the wall. Unfortunately, it was not possible to move the object from the pillar or to rotate it, so it has been difficult to acquire information on the backside of the sculpture. In other cases, it would be interesting and efficient to use other acquisition systems, range based, such as a Freestyle Laser Faro, since it is more applicable in narrow spaces but, in order to process a high detailed

textured surface high resolution images should be captured anyway and this strategy would require more acquisition time.

The statue has been surveyed with a Canon EOS-1Ds Mark II (pixel size $7.2\ \mu\text{m}$, sensor size $24\times 36\text{mm}$) (Figure 51) equipped with a 50 mm focal length with the focus locked. The imaging acquisition distance was about 1 m all around the object assuming an image scale of about 1:20 with a GSD of $0.1\ \text{mm}/\text{pixel}$.



Figure 51. The camera used and a moment of the acquisition.

In order to scale the data in the processing phase, in this second test case a different procedure has been applied: five targets have been placed on the wall behind the statue and have been measured with a measuring tape. In order to ensure the scalability, it has been ensured their visibility in more than three pictures.



Figure 52. An acquired image in which the targets used to scale the model are visible.

About 120 images have been captured at 3 different heights all around the statue.

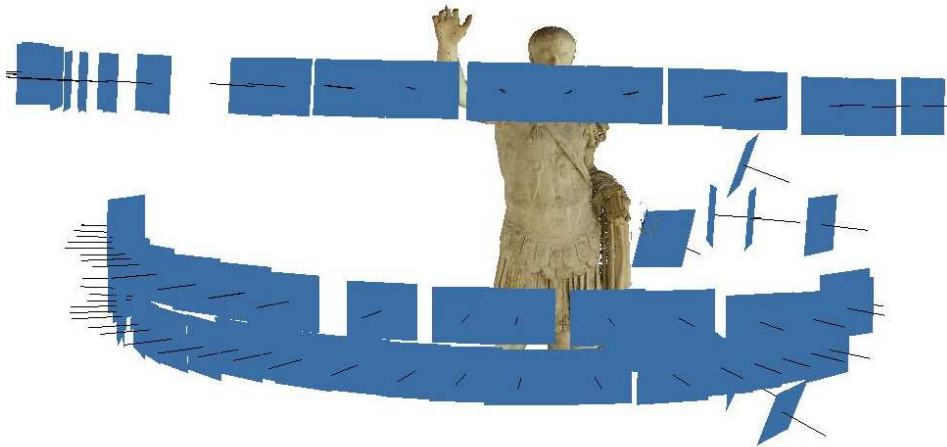


Figure 53. Visualization of the cameras position during the acquisition.

4.2.4 The data processing of the roman statue

The acquired images have been processed by means of the SfM technique and image matching algorithms in Photoscan.

Once imported in the software, all the images have been masked in order to remove in the calculation the wall behind the statue (with the exception of the targets) and the window of its right that may produce noise and issues in the alignment phase.



Figure 54. An example of the masked image.

The alignment phase has been processed with High settings and a sparse cloud composed by 4784 tie points has been calculated.

The Dense cloud has been processed using High settings and the Mild depth filtering for remove outliers, which is recommended for object or areas that contain small details. The result is a dense cloud of 12.289.323of points.

The mesh model has been processed with High settings, the Arbitrary parameter, suggested for modeling this kind of object and the Mild depth filtering. A mesh model of 2.457.864 faces has been created. The RMS, reprojection error is 0.692 pix and the final model as a mean GSD of 0.253 mm/pix.



Figure 55. The sparse cloud with tie points extracted, the dense cloud and the final 3D model viewed as smoothed mesh

In order to scale the photogrammetric results, a local reference system has been assigned to the model, basing on the targets measured in the acquisition phase.



Figure 56. In order to scale the model, the distances between the targets have been measured and then used as scale bars in Photoscan

Label	Distance (m)	Error (m)
3_2	0.509538	-0.000461509
3_4	0.555829	-0.000170887
4_5	0.424777	0.000776754
Total		0.000530892

Table 3. Visualization of the errors of the scale bars used for scaling the 3D data

The texturing step has been processed testing two different mapping mode: the default Generic mapping mode, that tries to create as uniform texture as possible, and the Spherical one, which is more indicated for ball-like object.

In both case the Average generation parameter, that uses the weighted average value of all pixels from individual photos, is used.

Also in this case the UV maps of the diffuse color texture have been checked for both the texturing modes. In both cases, the process generates a big amount of indiscriminate atlas, difficult to be recognize. In the first Generic mapping it is impossible to recognize any part of the model, whereas, in the second one, part of the decorated armor is visible but the remaining atlas are confused as well.

In the following optimization paragraph, a new user-controlled UV map will be generated and described, showing how the resulting texture would be easily controlled and corrected from the radiometric point of view in external software.

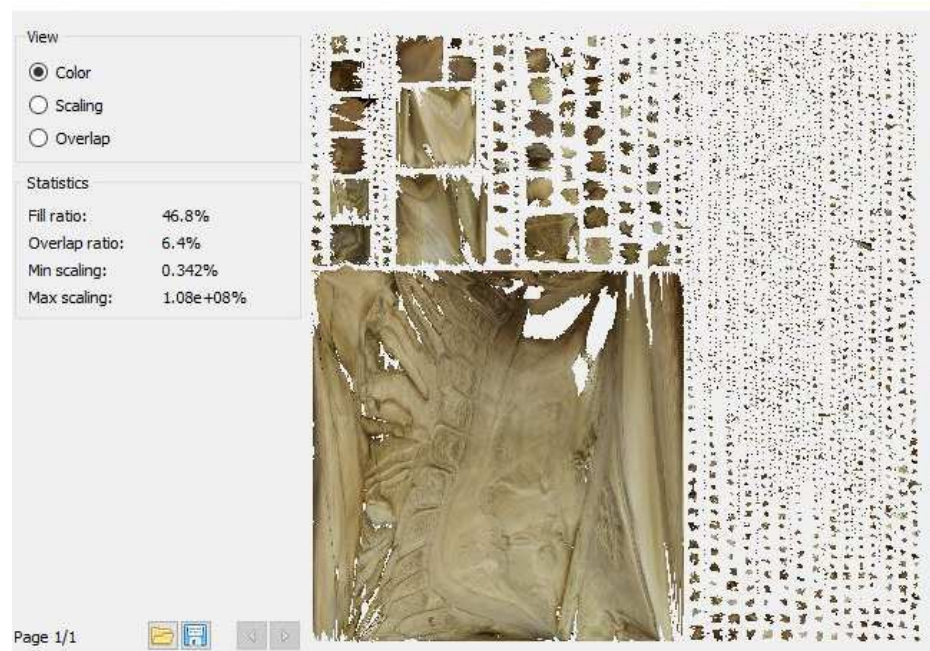


Figure 57. UV maps extracted after the texture mapping. Above: UV map derived from the Generic mapping mode; below: UV map derived from the Spherical mode.

Comparing the final textured model, the texture processed with the generic mode offers a greater visual quality, as visible in (Figure 58).



Figure 58. Comparison between the texture made using generic mode (above) and the texture obtained with the spherical setting.

4.2.5 The photogrammetric acquisition of the frieze of the Augustus arch

A multi-sensor complete survey campaign was performed in 2013 by Politecnico di Torino with 5x1000 funds and by some local authorities (the Piedmont Region, City of Susa, local cultural associations). The photogrammetric survey of the arch has been

focused on its friezes portions and has been realized with the help of a lift truck (Figure 59). A calibrated photogrammetric Canon EOS 5D Mark 2, with a 24 mm focal lens has been used, ensuring an overlapping of 80-90% between adjacent images. At the same time, several targets (GCPs) have been placed on the frieze and measured with a total station from a specific micro geodetic network (previously measured using GNSS techniques) (Figure 59). 49 images have been captured at a distance of about 1.5 m with a final GSD of 1.9 mm.



Figure 59. Above: the acquisition step; below: the targets placed on the surface have been measured by a total station and referred to a global reference system.

4.2.6 The data processing of the frieze of the Augustus arch

The alignment step extracted 229.195 tie points and a dense cloud of 12.488.000 has been then generated. The reprojection errors is of 0.555 pix.

The model has been scaled and georeferenced importing and assigning the coordinate of the measured targets (Table 4).

Label	X error (mm)	Y error (mm)	Z error (mm)	Total (mm)	Image (pix)
9	0.254105	-0.32913	0.575339	0.709867	1.541 (8)
10	-0.383959	-1.00861	0.769774	1.32562	0.882 (23)
11	-1.03537	0.0826666	1.21566	1.59896	0.721 (21)
12	-1.00631	0.416914	0.0308051	1.08969	0.504 (19)
13	-0.747074	0.0259294	0.565025	0.937041	0.581 (36)
14	-0.182564	0.784707	-0.136686	0.817177	0.844 (25)
15	0.0789931	0.581132	-0.495046	0.767479	0.391 (33)
16	1.50742	-0.703281	-0.741808	1.82132	0.816 (22)
17	0.691617	1.35201	0.0729961	1.52039	1.110 (27)
18	0.776789	0.612021	-0.0615989	0.99084	0.435 (25)
20	1.23072	-0.969331	-0.947042	1.83062	0.538 (17)
21	-0.628041	-0.413055	1.01686	1.26454	0.481 (10)
22	-1.1591	-0.899896	0.731523	1.63965	0.537 (12)
23	-0.24867	0.441325	-0.974687	1.09846	0.413 (25)
24	0.851438	0.0265963	-1.62112	1.83131	0.447 (19)
Total	0.828163	0.686685	0.799534	1.34039	0.703

Table 4. Control points errors propagation

A mesh model of 1.236.503 faces has been then generated setting the High quality command (Figure 60).

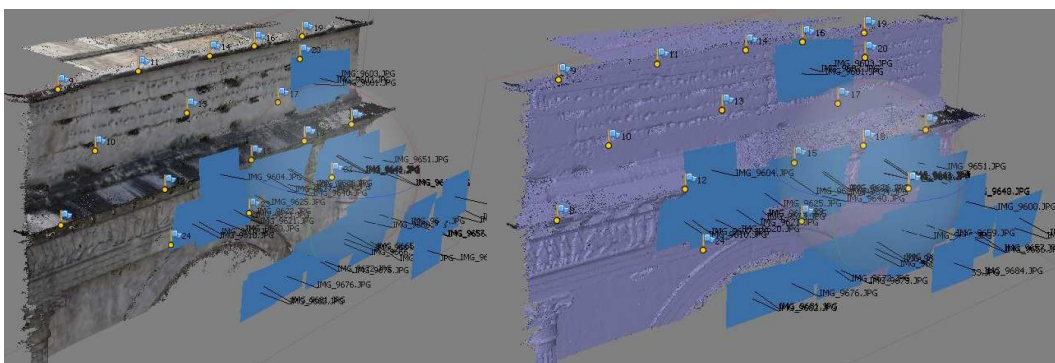


Figure 60. Left: dense cloud; right: mesh model

The texture has been processed with the *Orthophoto* mapping mode and the *Average Blending* mode. The orthophoto of both the sides of the frieze have been extracted with a 0.001 m pixel size.



Figure 61. Above: mesh model; middle-below: orthophoto of the north and south side.

Chapter 5

Experimental section 2 - 3D model optimization of the case studies

In the following paragraphs, different optimization process applied to the surveyed test cases are presented. The main aim has been to operate a hard reduction of the HP models testing different remeshing techniques, as the above mentioned tools of game engine and entertainment, in order to define the potentialities of the final optimized models in terms of visual quality and accuracy of the extractable metric information.

5.1 The optimization pipeline

In order to define the main operations applied to the models, a scheme of the optimization workflow has been outlined.

In particular, the proposed optimization pipeline (Table 5, Figure 62) follows two possible strategies which could respond to different aims, as highlighted in the following paragraphs, but with the common goal of reducing the file size while maintaining a high level of detail:

- *HP model hard decimation and baking and projection of a Normal Map* - The final optimized model loses the original geometrical detail but it visually looks like the HP;
- *Re-topology of the HP model with a quad-dominant mesh, and following computation and projection of a Displacement Map over the retopologized model before subdivided with Catmull and Clark function* - The final optimized model

offers the same geometrical detail of the original HP thanks to the computed displacement map.

In both cases a new diffuse color map has been computed according to the new user-defined UV map and projected on the optimized model.

	LP model + NM	Displaced SubDivision surface
High scale model	Suitable	Suitable
Low scale model	Suitable	Suitable
Object with tiny details and small decorative elements	Suitable	Less suitable for not expert users as the retopology process is more difficult
Planar surfaces (as terrain models from aerial surveys)	Suitable and the parameterization process is eased	Suitable and the parameterization and retopology process are eased
Type of acquisition sensor	Independent	Independent
Final geometric resolution	Low	High
Final radiometric resolution	High	High
Final file sizes involved	Very low	Low
Measurable	No	Yes
Details recognizability	Good	High
Visualization purposes (AR and VR applications)	Suitable	Suitable
Structural/static evaluations	Not Suitable	Suitable
Sections profiles extraction	Low accuracy in detailed geometries	High accuracy

Table 5. Decision support system of the tested methodologies

GENERAL OPTIMIZATION WORKFLOW

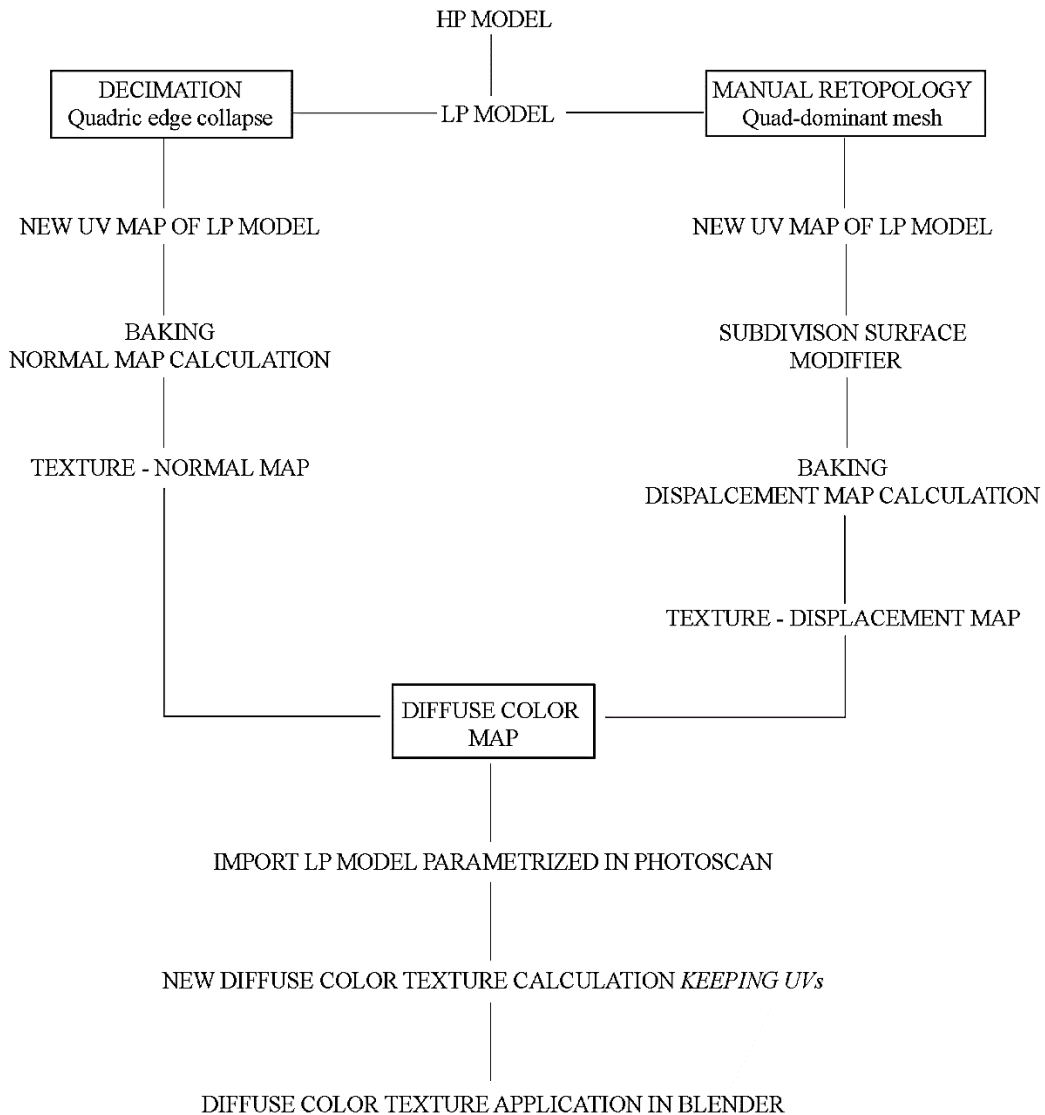


Figure 62. The proposed workflow for the HP model optimization

The three test cases have been processed according to this pipeline but applying different possible parameters, has showed in (Table 6.), also considering the different characteristics of their shapes: Lina has no decorative elements and tiny details whereas the roman bust and the frieze have bas-relief which have to be recognizable also in the optimized models.

In particular, some differences have been applied in the decimation process. The more the decimation is heavy, the less the detail will be recognizable and so a Normal map is advisable.

For Lina test case, an indiscriminate hard decimation has been applied to its smoothed surface and three different software (Blender, XNormal and Photoshop) have been tested to produce three different Normal maps, which have been then compared through some raster analysis tools implemented in QGIS. The Roman bust has been decimated testing three possible ways, comparing different decimation levels that may be interesting for different purposes. The frieze of the roman arch has been indiscriminately decimated in order to further project the Blender Normal map.

The second pipeline which foresees the generation of a displaced subdivision surface, after a manual retopology process, follows the same rules for each test case.

In each step of the process, it has been important to evaluate the quality of the output data in comparison to the original detailed model as well as the file size of the final optimized model. For this reason, in each test case, the LP model has been geometrically compared to the original HP one in order to define the range of discards, evaluating also a comparison between several 3D polylines extracted from the optimized model and the original HP one. Furthermore, the size of each file produced has been taken into account and compared.

Final evaluation concerns the possibility to extract specific and punctual information from the optimized model and are presented in the next Chapter 6. In order to detect the quality of the information extractable from the final optimized model some algorithms of edge detection have been applied to the edited models of the bust and of the frieze (Lina presents a too smoothed surface for this kind of test).

	LINA	ROMAN BUST	FRIEZE
SURFACE TYPE	Smoothed surface No decorative elements	Detailed surface with decorative elements	Detailed surface with decorative elements
MESH EDITING	Mesh editing topological errors removal	Mesh editing topological errors removal	Mesh editing topological errors removal

GEOMETRICAL DETAIL ONLY VISUAL	DECIMATION + NORMAL MAP	HP indiscriminate decimation MESHLAB New parameterization & UV map NORMAL MAP computation, comparison between: - Blender - XNormal - Photoshop Normal maps comparison QGIS	HP decimation 3 decimation levels MESHLAB New parameterization & UV map NORMAL MAP computed in Blender	HP indiscriminate decimation MESHLAB New parameterization & UV map NORMAL MAP computed in Blender
KEEP GEOMETRICAL DETAIL	DISPLACED SUBDIVISON SURFACE	Manual Retopology New param. & UV map SubDivision surface modifier DISPLACEMENT MAP computed in Blender	Manual Retopology New param. & UV map SubDivision surface modifier DISPLACEMENT MAP computed in Blender	Manual Retopology (only a portion) New param. & UV map SubDivision surface modifier DISPLACEMENT MAP computed in Blender
	FURTHER CONSIDERATIONS Evaluation of extractable information	No edge detection due to the smoothness of the surface	Edge detection algorithms on extracted orthographic views Comparison with HP model	Edge detection algorithms on extracted orthographic views Comparison with HP model

Table 6.The Pipeline applied to the test cases.

The employed software

To operate all of the mentioned and others passages presented in the following paragraphs, many software are available. In this thesis in particular the employed software are: 3D Reshaper and MeshLab, for the mesh editing and decimation step, and

Blender for the remeshing procedure and the generation of normal and displacement maps (Photoshop and XNormal have been also tested in 5.1.1).

PhotoScan tends to produce 3D models with excessive geometry resolution, so mesh decimation is usually a desirable step after geometry computation. Photoscan itself offers several mesh editing tools that can be applied to the mesh model processed:

- Decimation tool;
- Close Holes tool;
- Automatic filtering based on specified criterion;
- Manual polygon removal;
- Fixing mesh topology.

The decimation tool automatically decimates the polygon count according to the user settings. In this operation, it is necessary to pay attention that the mesh does not become too smoothed, losing too many details. The Close Holes tool allows to automatically close the holes present in the mesh but is not possible to set a maximum dimension of the hole so the software closes each hole that it meets. The Polygon filtering on specified criterion can be used since in some cases reconstructed mesh may contain small isolated polygons fragments not belonging to the object of interest.

More complex and sophisticated editing tools can be found in external 3D editing software. Indeed, PhotoScan allows to export mesh and then import it back for this purpose.

3D Reshaper (<https://www.3dreshaper.com>) is a proprietary software dedicated to the point cloud processing that offers many tools for point cloud editing and mesh generation (texturing, 3D inspection, polylines, CAD surfaces, etc). In particular, in this thesis, it has been employed for the point cloud cleaning and mesh generation and editing. Once imported in the program, a point cloud can be filtered according to the user needs and the noise that may affect the data can be removed/reduced. The mesh processing offers different interpolation approaches. In the test cases of this thesis, all the mesh has been generated using a triangulation in two steps: in the first one the desired mean dimension of the triangles has to be set and in a second step the max deviation error from the point cloud is fixed, in order to refine the output.

MeshLab (Cignoni et al., 2008) is an open source tool designed for the visualization and processing of 3D models. It represents a mesh viewer application, in which a 3D object, stored in various kinds of formats, can be loaded and interactively navigated in an easy way. It is oriented to the management and processing of large, unstructured triangular meshes and point clouds providing a set of tools for measuring, checking, cleaning, healing, inspecting, rendering and converting 3D meshes.

For mesh editing, the user can apply a wide suit of direct parametric filters, that automatically process tasks like smoothing, re-meshing or decimation, by means of interactive tools. The most useful operations are:

- Interactive user-oriented selection and deletion, smoothing and coloring of mesh portions. Even for large models;
- Input/output in many formats;
- Mesh Cleaning Filters: – removal of duplicated, unreferenced vertices, null or non-manifold faces, small isolated components, coherent normal unification and flipping and automatic holes filling;
- Remeshing filters: – High quality edge collapse simplification (also with the possibility to preserve texture coordinates), Subdivision surfaces (loop and butterfly), Feature preserving smoothing and fairing filters;
- Various Colorization/Inspection filters – Gaussian and mean curvature – Border edges, geodesic distance, from borders – Non two-manifold edges and vertices – Self intersecting faces – Ambient Occlusion that can be computed and stored per vertex;
- Measuring tools;
- A slicing tool that allows to export planar sections of a mesh in SVG format;
- 3D Scanning tools – Alignment: ICP based range map registration tool. – Merging of multiple meshes - the Poisson surface reconstruction.
- OpenGL Shader based rendering and large rendering of very large images.

For the following 3D models decimation, MeshLab has been chosen since it offers a very performing decimation algorithms (quadric edge collapse algorithm). In fact, also 3DReshaper and Blender provide decimation tools but those implemented in MeshLab demonstrated to offer better results, comparing the readable details on the LP models generated, with same number of polygons and same file size.

For the Quadric Edge Collapse Decimation, it is necessary to set the number of faces to be maintained or the percentage of reduction. The quality Threshold tool requires to enter a value between 0 and 1. 0 accept any kind of face (no penalties), 0.5 penalize faces with quality < 0.5, proportionally to their shape"; the higher the value the harder MeshLab tries to stick to your original model's shape.

The further optimization procedure has been fulfilled in Blender. Blender is an open source 3D creation suite that supports the entirety of the 3D pipeline from modelling, rigging, animation, simulation, rendering, compositing and motion tracking up to video editing and game creation. Blender offers different remeshing tools and it has been used in particular for the retopology process, for the generation of new UV maps for each LP model and for the texture maps computation and projection.

Once realized a LP mesh (through a decimation or a retopology approach) the unwrapping process allows to generate a new UV map associated, more rational and functional, if compared to those automatically generated in Photoscan which have an uncontrolled number of atlas. In fact, thanks to this new parameterization, each texture map generated on this UV structure can be more easily modified, if necessary, in others software. This is interesting, for example, handling a diffuse color map that presents bad shadows or radiometric errors. In this way, it is possible to import the image in external software to more easily correct the radiometric information and the aberrations, since each part of the object is more easily recognizable. For most simple 3D models, Blender has an automatic set of unwrapping algorithms that you can easily apply, although for more complex 3D models, regular Cubic, Cylindrical or Spherical mapping, is usually not sufficient. In these cases, it is advisable that the user mark himself the seams over the LP mesh where to unwrap the model or to use the automatic *smart UV project* tool.

Furthermore, Blender allows also to modify the structure of the UV map itself, when necessary. After the unwrap, it is possible to arrange the UV map into something that can be more logically textured or painted. The main editing operations are:

- Stitch some pieces (UV maps) back together.
- Minimize wasted space in the image.
- Enlarge the faces where you want more detail.
- Re-size/enlarge the faces that are stretched.
- Shrink the faces that are too grainy and have too much detail.

With a minimum of dead space, the most pixels can be dedicated to giving the maximum detail and fineness to the UV texture.

With specific regard to the texture mapping generation, many software are today available to process and generate any kind of texture maps. Depending on which application is used, they can differ from each other's. For the test cases, Blender has been used, since it offers a quite easy pipeline for the baking process and very good results at the rendering stage, and both normal and displacement maps have been generated in this software. The main steps involved in making and using a Normal or Displacement Map are:

- In a layer, import a HP model.
- In another layer, import a LP model.
- Bake the Normal or the Displacement map, according to the UV map generated and setting the dimension of the new image.

Other software for the generation of texture mapping are available, for example the widely used Photoshop or the open-source XNormals, which have been tested and compared in 5.1.1.

In Photoshop, for example, the way to create bump and normal maps is very easy, but it differs from the process used in Blender, since it does not require the baking process among the HP and LP model, but it calculates the image mapping just applying some filters on a single 2D image texture.

From the 3D filter menu, it is possible to choose to generate Bump Maps and this will bring up the Generate Bump Map dialog box which shows an interactive 3D preview, with controls on how to generate the grayscale image that will make up the Bump map.

When Bump Maps are not enough accurate and in certain angles they do not look very realistic, it is possible to generate Normal Maps with a bit different approach. It is also possible to download a NVIDIA Texture Tool plugin for the Normal Map generation in Photoshop. It creates normal maps from grayscale height maps with powerful 3D preview and a variety of filtering options.

XNormal is another free tool to bake texture maps more similar to the Blender 3D approach, baking Low Polygons models with High Polygons ones. What it is essential in XNormal is to generate LP mesh as a CAGE mesh, which entirely contains all the polygons of the HP one; it is an essential condition to compute any texture map. Some comparisons between this three software will be presented in the experimental section. (see 5.1.1).

The projection of the computed texture maps has been realized in Blender.

The Normal maps have been projected through the node editor that allows to combine more images on the same model. Whereas, in order to project the displacement map on the retopo model it is necessary to apply the *Displace* modifier linking the new calculated displacement map. This modifier displaces vertices in a mesh basing on the intensity of a texture. The displacement can be along a particular local axis, along the vertex normal, or the separate RGB components of the texture can be used to displace vertices in the local X, Y and Z directions simultaneously (sometimes referred to as *Vector Displacement*). In the test cases presented, chose direction is the Normal direction.

5.1.1 Lina's 3D model optimization

The image matching pipeline allowed to process a very detailed 3D model, textured with the images used for its generation. However, even though the parameters for the mesh processing were set to very high and with the automatic interpolation disabled, the

mesh presents some topological errors, as visible in (Figure 63), so it has been decided to further edit the model in 3DReshaper.

Mesh editing

The generated dense point cloud has been imported in 3DReshaper and modeled. A new mesh of 2 mm of resolution has been generated, setting a refinement with a deviation error of 1 mm (Figure 63). In comparison to the one generated by Photoscan, the new mesh provide a high level of detail without topological errors and in a smaller file size (see Table 7.). The final mesh has been imported and textured in Photoscan and, checking the mesh statistics, it is possible to notice that no topological errors are found anymore (Figure 63).

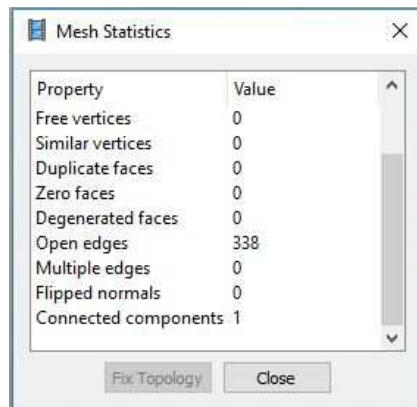
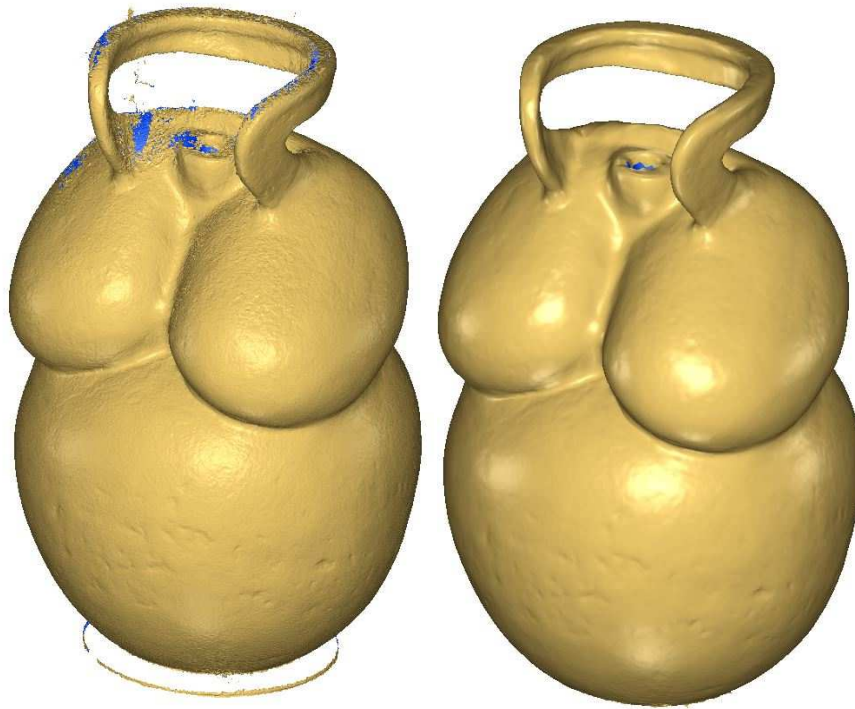


Figure 63. Left: HP model processed in Photoscan; right: HP model processed in 3DReshaper. Below: mesh statistics of Photoscan applied to the new edited mesh, the command Fix Topology is disabled since no more topological errors affect the mesh.

	N. Points	N. Triangles	N. independent pieces	N. of holes or free contours	KB .obj file
Mesh PS	1.082.869	2.022.311	4.926	9.759	147.323
Mesh 3DR	186.592	372.854	1	2	17.794

Table 7. Comparison between the HP mesh generated in Photoscan and 3DReshaper

Optimization with LP model and Normal maps

Once generated a HP lacking of topological errors, the first optimization process started with its decimation, generating a Low Poly model on which further project the details of the High Poly one, by means of a Normal Map computed in the baking process.

To do this, initially, the HP model has been imported in MeshLab. Several cleaning and repairing automatic filters have been applied throughout the model before the decimation:

- Remove duplicate faces;
- Remove duplicate vertices;
- Remove faces from non-manifold edges;
- Remove isolated pieces.

Subsequently the decimation has been run with the Quadric Edge collapse decimation algorithm and a mesh constituted by only 3000 faces has been generated. Since the model has a uniform level of detail and does not present particularly decorated portions, a uniform decimation throughout the model has been performed.

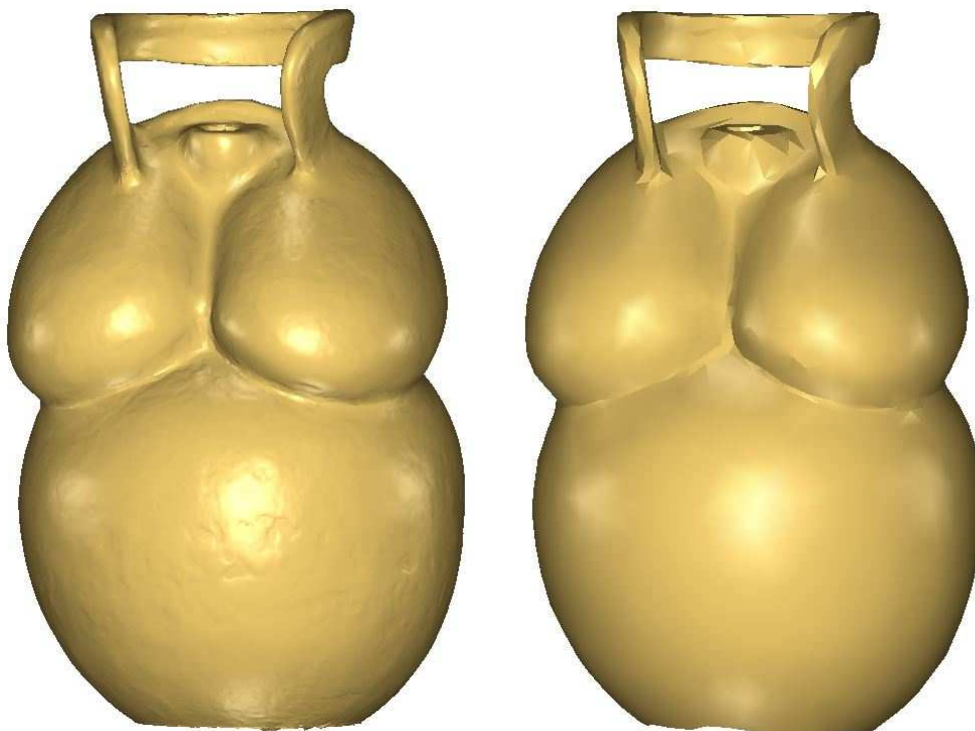


Figure 64. HP model and decimated LP model (3000 faces).

A comparison between the HP model and the LP one, as visible in (Figure 65), shows a very low deviation error throughout the model, mostly ranging from -0.001 m and + 0.001 m, which is a very good result of the decimation process. Also extracting some 3D polylines from both the models, it is possible to notice that the discards are very low (max neg. value: -0.002, max pos. value: +0.001) (Figure 66). Obviously, compared to the following roman bust and frieze case studies, Lina has far less details and therefore it is possible to operate a more aggressive and indiscriminate decimation, without the risk to lose too many details.

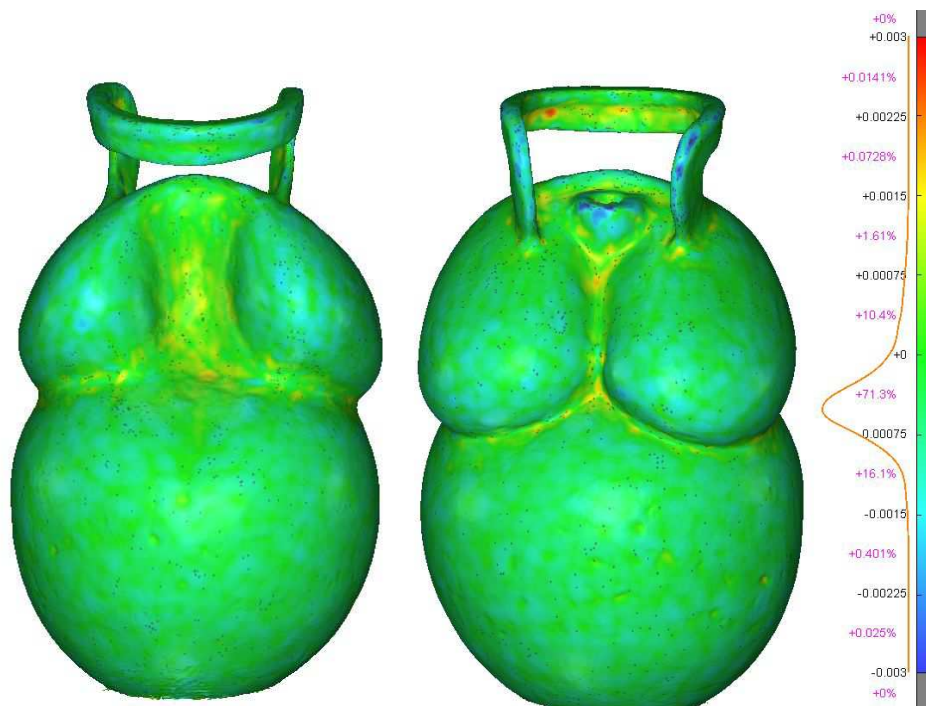
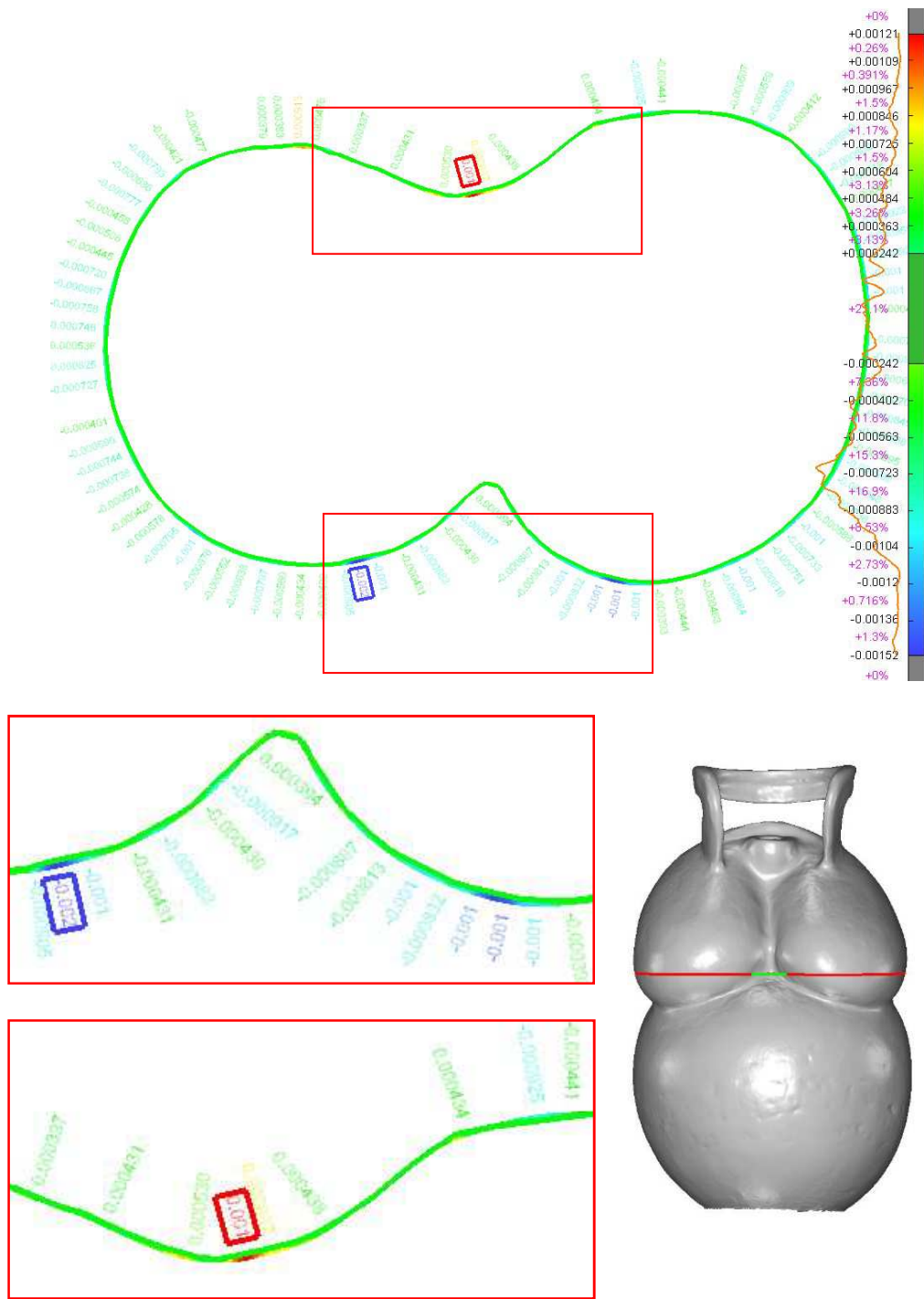


Figure 65. Comparison between the HP model and the LP one. It is possible to notice that the 90% of the points of the LP have a displacement between +0.001m and -0.001 m, which is a very low value.



	N. of points
HP polyline	1207
LP polyline	117

Figure 66. Comparison between section profiles extracted from the HP and LP models.

Once processed the LP model, the object has been imported in Blender in order to compute a controlled UV map and to process and project a Normal Map able to reproduce the high detail of the original HP mesh. Since Photoscan did not produce a satisfying UV map, as shown in paragraph 4.2.2 (Figure 50), a new one has been computed in Blender after having manually marked the seams in which cut and project the model. The seams manually identified, in fact, guide the unwrapping process. Once manually marked the cut profiles, it is possible to automatically generate the new UV map, unwrapping the so defined mesh that presents a better quality in terms of number of "atlas" and their distinctiveness (Figure 67).

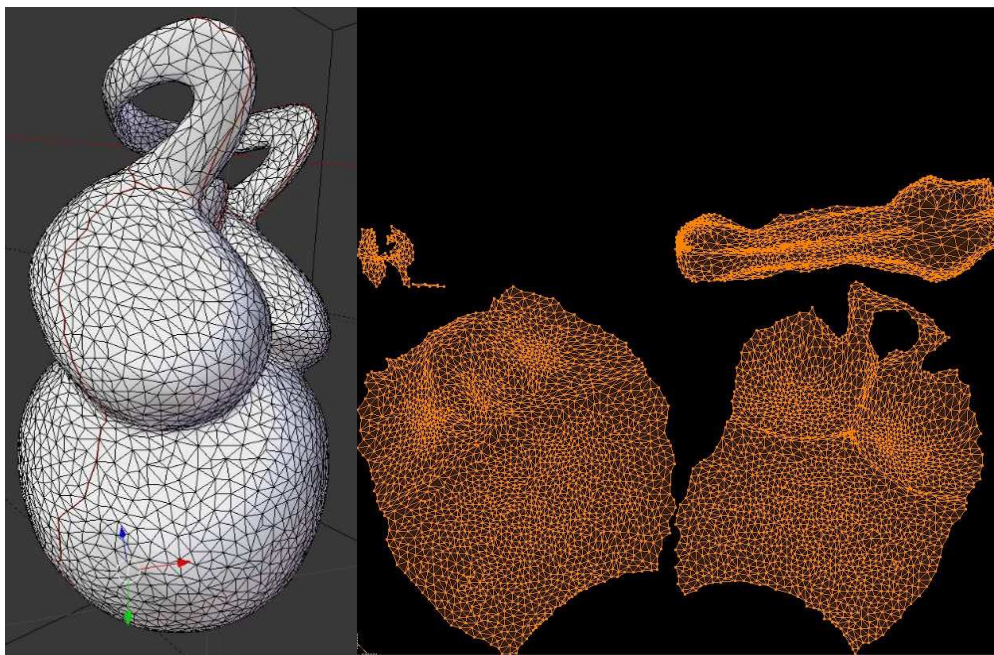


Figure 67. Marked seams (in red) and new UV map computed

The following step of the optimization consisted in the generation of the Normal Map, that has to be generated baking the Normal vector from higher resolution geometry (HP model) and storing it as a RGB value according the new defined UV map. In this case study, three different NM have been created testing three different software: Blender, XNormal and Photoshop, in order to make some comparisons.

XNormal, already mentioned in previous paragraphs, is able to bake texture maps similar to the Blender 3D approach, baking Low Polygons models with High Polygons ones. The interface is very easy to use, it is necessary to import the HP model and the LP one choosing then some settings for the automatic generation of texture maps as Normal, Bump and Displacement Maps (Figure 68).

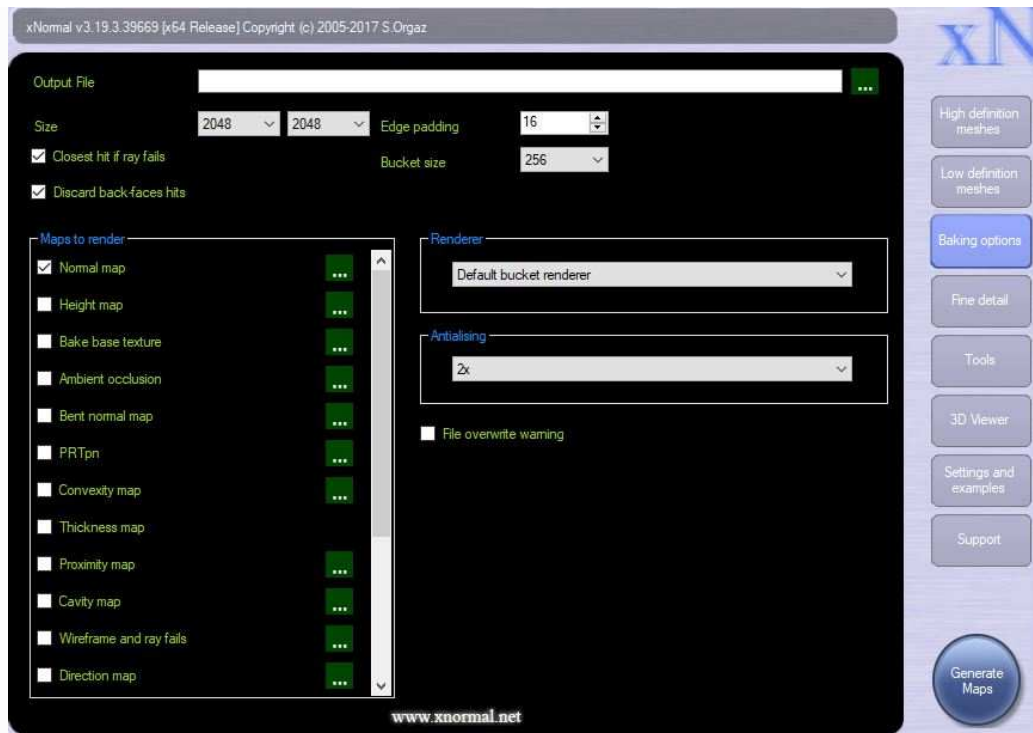


Figure 68. XNormal interface to edit texture maps. The user chooses principally the size of the output image and the type of map.

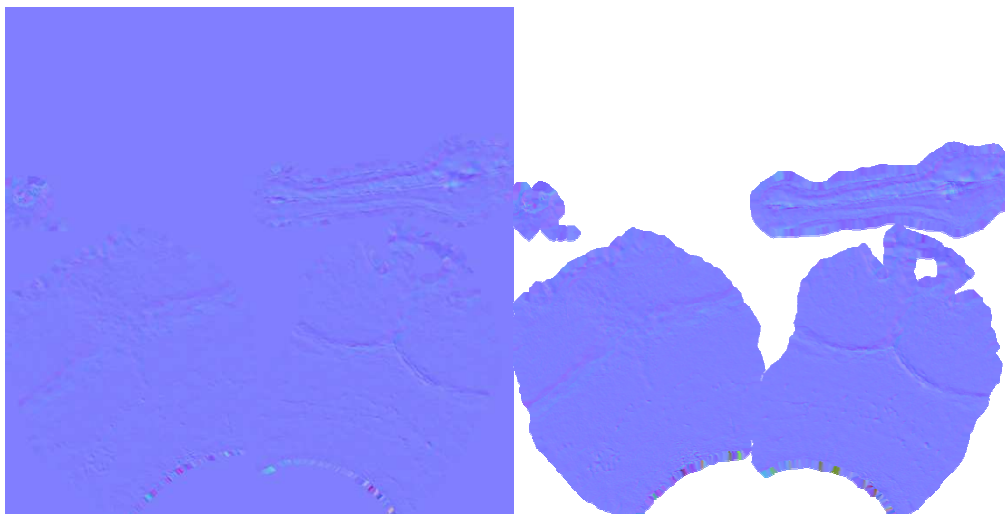


Figure 69. Left: Normal map generated in XNormal; right: Normal map generated in Blender. In both the images, the dimensions are set 2048*2048 pixels.

Photoshop, as well, has some plug-in that allows to create Normal Maps, such as the Nvidia filter (Figure 70). It differs from the others two software since the output is calculated basing only on the texture image rather than on the geometries of a HP and LP models. For this reason, the result is rather different from Blender and XNormal and the

reflection of the light over the surface is calculated only basing on the pixel value of the texture image.

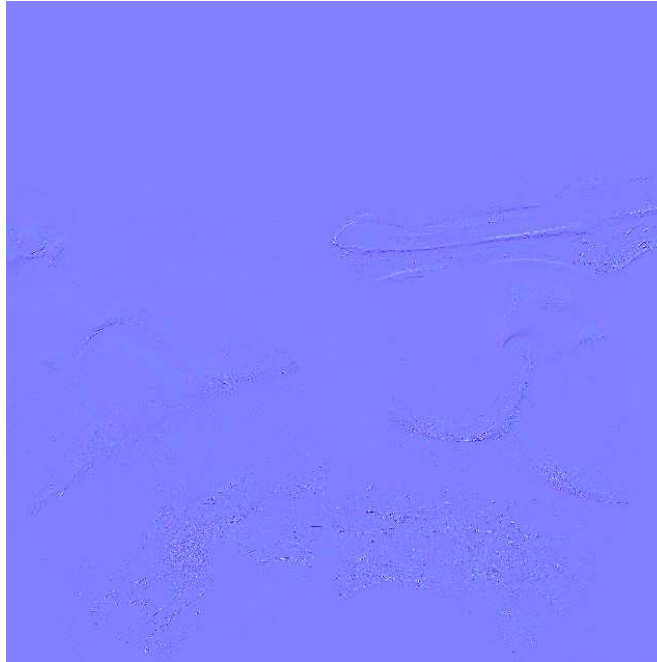


Figure 70. Normal map generated in Photoshop

It is well visible also to the naked eye the difference between the so generated images, but in order to evaluate the results with a more objective method, such images have been imported in the software QGIS, trying to analyse them with some raster analysis tools. The PlugIn *profile tool* allows to extract the radiometric frequency for each color band in specific profile sections defined by the user. The three normal maps generated have been in this way analysed. As it is possible to see in (Figure 71), the Blue band has the highest value, defined by the type of image itself. Whereas the red and green have much lower frequencies. In the normal map generated in Blender the red and green bands have great discontinuities where the geometry of the model changes, in proximity of protrusions and indentations (Figure 71, above). Whereas in the normal map generated in Photoshop, the frequencies of the red and green bands are dominated by the material discontinuities, that for its nature are thicker and more tight (Figure 71, below).

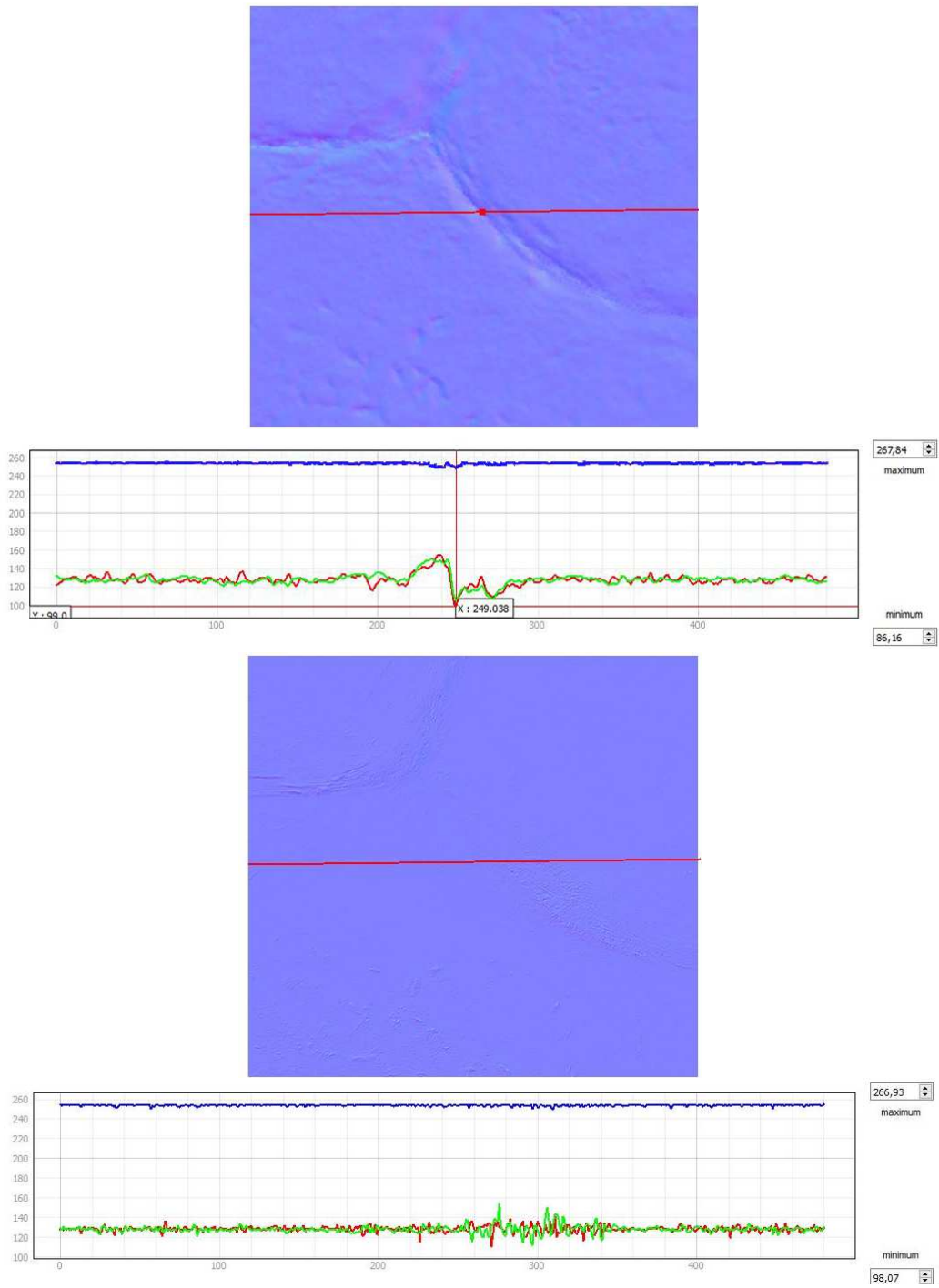


Figure 71. Graphs of the radiometric frequencies applied to the Blender (above) and Photoshop (below) normal maps, calculated on the red sections.

The same calculation has been applied to compare the Blender and XNormal normal maps. In this case, the graphs show a quite similar behaviour in each of the three bands and so the images can be almost indifferently used (Figure 72).

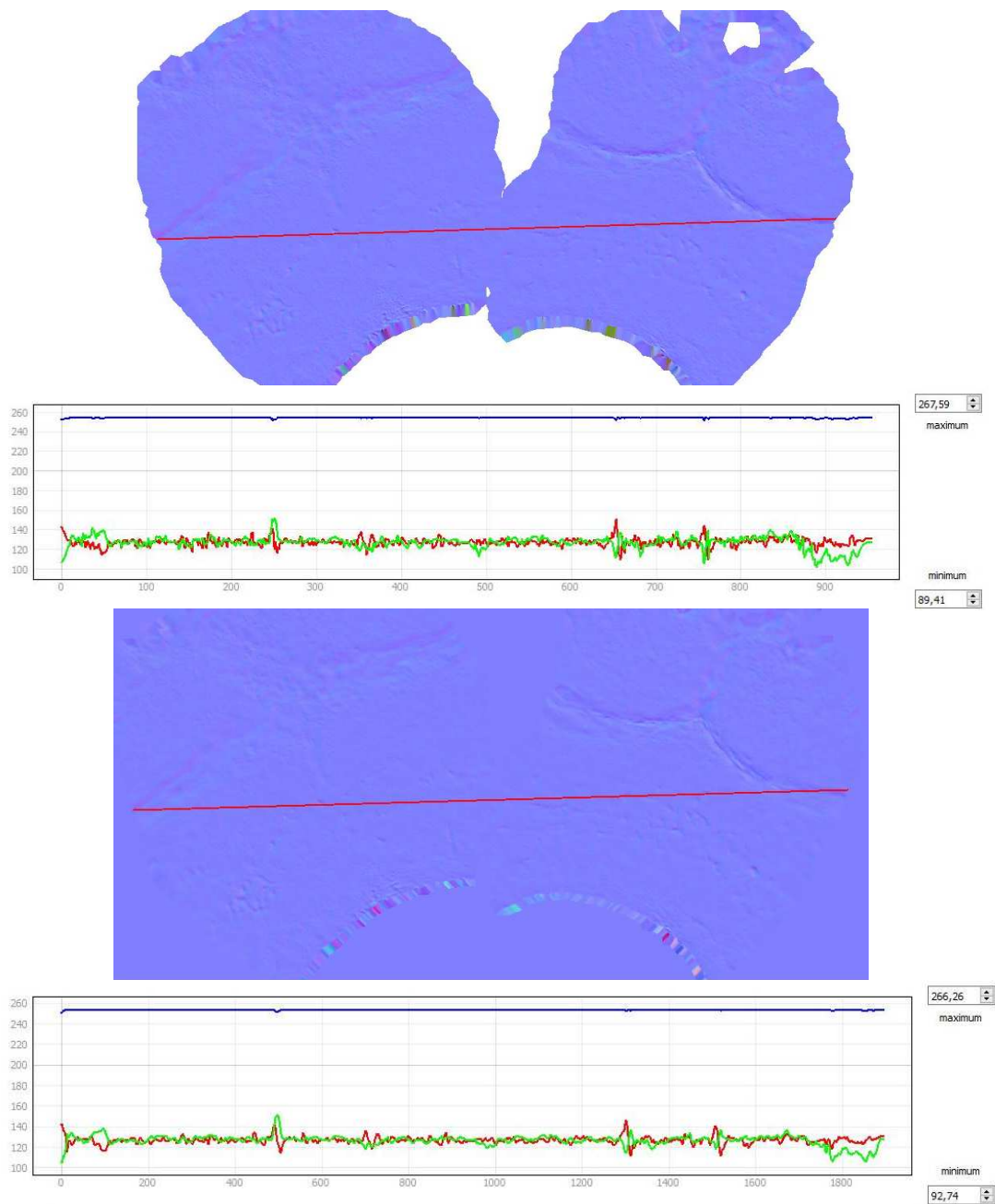


Figure 72. Graphs of the radiometric frequencies applied to the Blender (above) and XNormal (below) normal maps, calculated on the red sections.

Once projected on the LP model, the different normal maps produce a quite different rendering output. As visible in (Figure 73) the LP model with the Photoshop NM applied shows some irregularities on the surface deriving from the material grain but it offers less information about the geometry and shape of the model, which are the desired details aimed in this test.

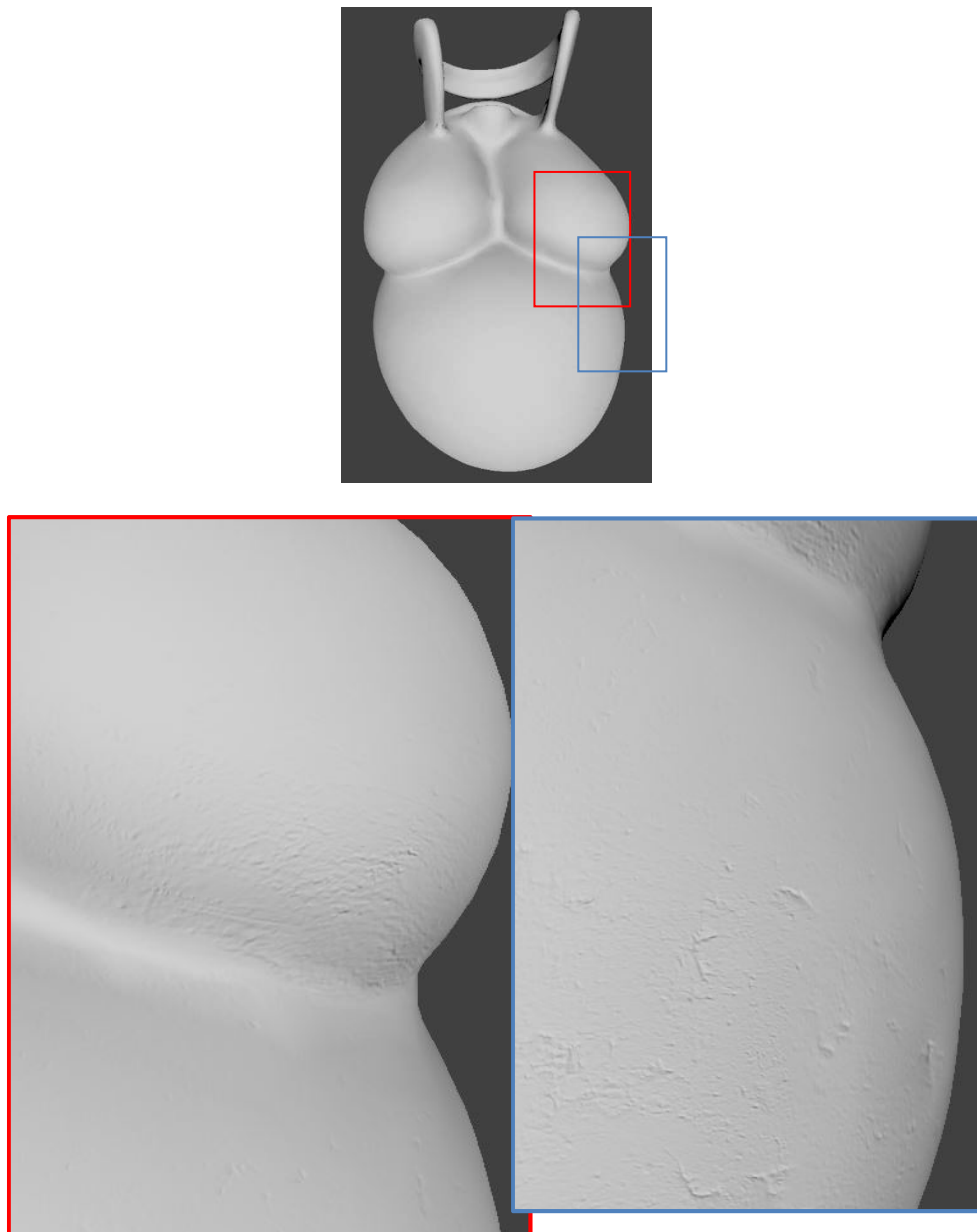


Figure 73. Visualization of the Photoshop Normal map and its projection over the LP model. The so generated mesh is more detailed but offers information only about the material texture lacking the geometric detail.

Starting from these considerations, it seemed to be more appropriate to use the Blender approach rather than the Photoshop one, more purposed to the geometry quality aspect.

The Blender Normal map, once projected over the LP model, allows to render the high level of detail of the original HP mesh reproducing accurately its geometry (Figure 74 - Figure 75).

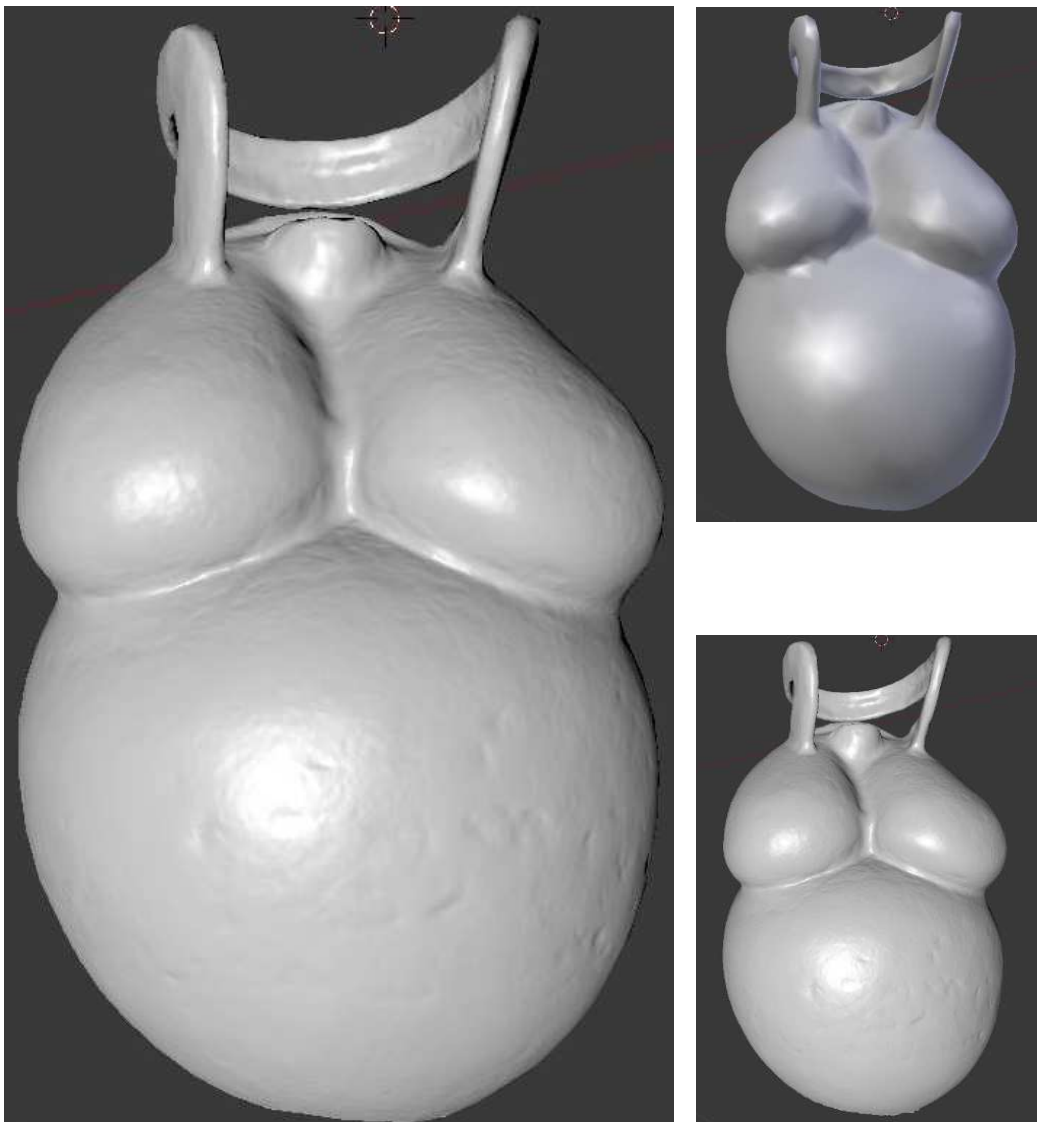


Figure 74. Left: LP model with Blender NM applied; right above: LP model; right below: original HP mesh.

Thereafter a visual comparison has been realized between the HP model and the processed LP model with NM. As it is visible in (Figure 75), the optimized LP model offers a level of detail comparable to the HP model but, zooming on its boundaries, it is possible to notice that the model presents a rougher surface due to the greater dimension of the triangles. For these reasons, this type of optimization allows to represent a high level of detail for a simple visualization but does not ensure the possibility to extract detailed geometric information, for example, if it is necessary to vectorialize specific profiles or a traditional 2D drawing of the object.

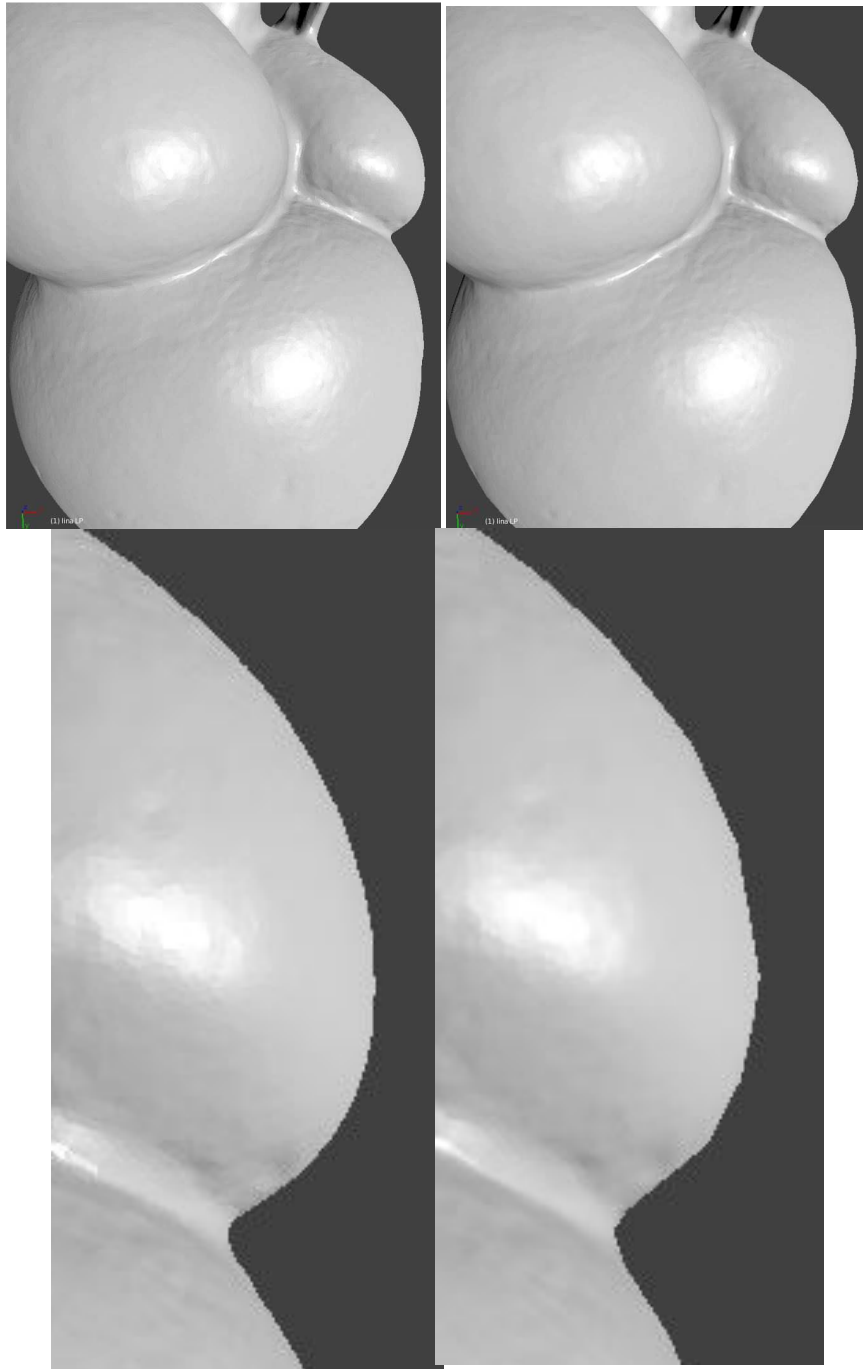


Figure 75. Visual comparison of a render of the HP model (left) and a render of the LP model with NM applied (right). Below: on a zoom it is possible to notice that the LP model with normal map applied (right) has a more smoothed contour due to the greater size of the triangles.

Since the so processed model still lack the radiometric information, furthermore, the re-parametrized LP model has been imported in Photoscan in order to compute a new diffuse color map, selecting the "*Keep UVs*" texture generation mode (according to the

new UV map generated in Blender) (Figure 76). In this way, Photoscan computes a new texture map according to the same UVs that are associated to the LP model, making possible to import this image in Blender and project with the same UV coordinates to the optimized model. This processing allows to produce a new diffuse color texture with a controlled number of atlas which can be easier recognized by the user and, if necessary, easily modified in order to improve the radiometric quality of the final representation.



Figure 76. Left: automatically generated diffuse color map; right: new diffuse color map keeping the UV map edited in Blender.

In Blender, in order to project more than one image on a model, the render nodes editing tools have been used (Figure 77). In this way it is possible to combine more textures, as color diffuse map and normal maps, defining what aspect they have to control (color or normals). The *image texture* node has been inserted twice, in order to import both the diffuse color and the normal map. Then the diffuse color map has been directly linked to the *Diffuse BSDF* (Bidirectional Scattering Distribution Function) node, which is used to add Lambertian and Oren-Nayar diffuse reflection, and in particular to the *Color* input, that control the color of the surface, or physically speaking, the probability that light is reflected or transmitted for each wavelength. Whereas the Normal map has been linked to the *Normal Map* node, which controls the normal quality output, and then to the *Normal* input of the *Diffuse BSDF* node, which is used for shading the model. Lastly the *Diffuse BSDF* node is linked to the *Surface* input of the *material Output* node.

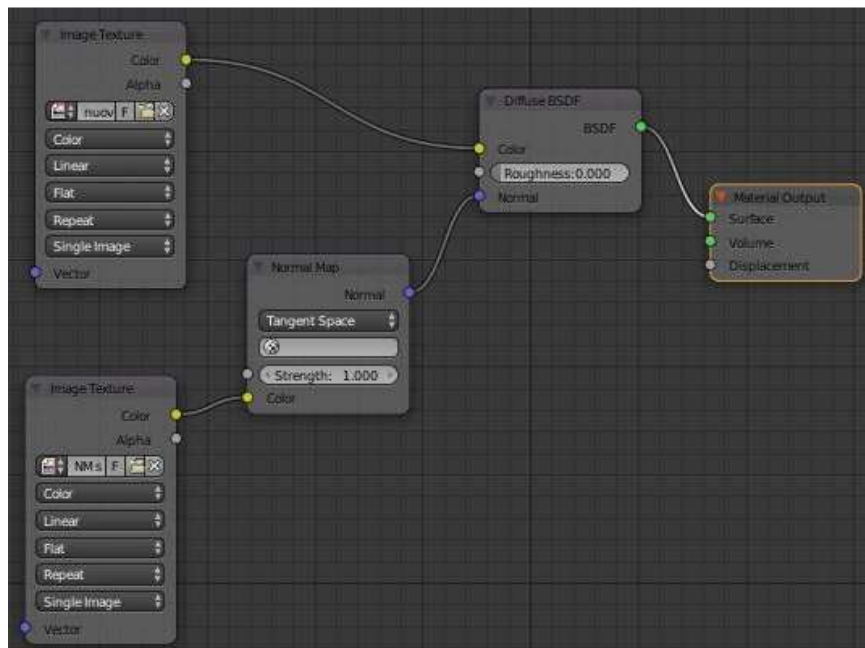


Figure 77. Node editor of Cycles Render. It is possible to notice both image textures (color diffuse and NM) that have been projected over the LP model as color and normal information for the rendering stage.

The detail offered by the projection of the calculated Normal map can be also evaluated comparing the so optimized model with the same textured LP but without the Normal map applied. Even though Lina does not have many geometrical details, the shadows projected by the Normal map allow nevertheless to better appreciate the shapes of the sculpture (see Figure 78).



Figure 78. Comparison between the LP with diffuse color map and without the Normal map (left) and the LP with diffuse color map and normal map applied (right).

A final interesting evaluation concerns the determination and comparison of the file size of the so optimized model in comparison to those of the original HP mesh, as reported in (Table 8 - Table 9).

	N. vertices	N. of faces	KB file	% Faces reduction	% KB reduction
Original HP mesh	186.592	372.854	17.794	-	-
LP mesh	1.514	3000	231	-99,2%	-98,7%

Table 8. Report of the faces and KB reduction from the HP model to the LP one.

	KB file
Original HP mesh	17.794
LP mesh	231
Normal Map	829
Diffuse color map	292

Table 9. Report of the file sizes involved in the optimization process

The tested optimization process allows to significantly reduce the file sizes involved, so facilitating the data managing and sharing and this aspect fulfils the aims of this test. However, it is important to reaffirm that the final LP model has some limits if the user needs to extract punctual information on some details.

Optimization with Displaced subdivision surface

The second test applied to the model aimed at the creation of a Displaced SubDivision Surface in order to define the potentialities of a real displacement applied to the vertices of a subdivide surface. As explained in 3.2.6, this kind of model foresees the computation of a displacement map and a retopologized quad-dominant mesh that supports the conversion in subdivision surface of Catmull& Clark.

The manually performed re-topology process requires much attention in order to build a quadrangular mesh without topological errors that recovers the HP model (Figure 79).

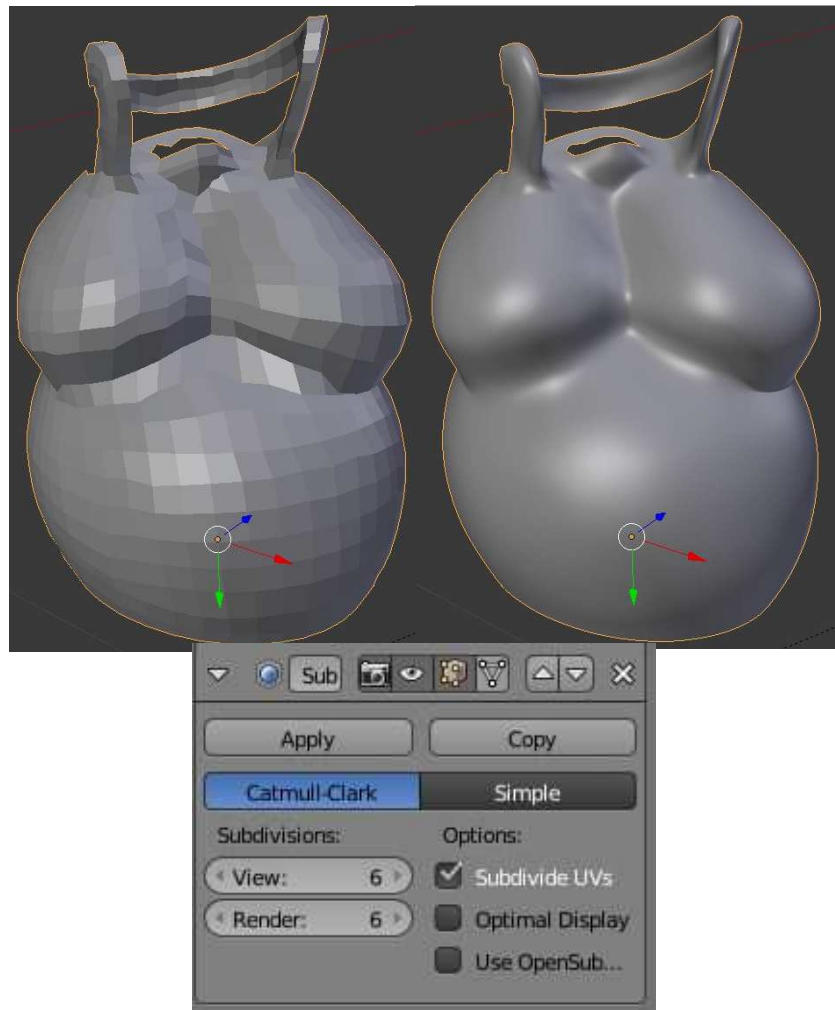
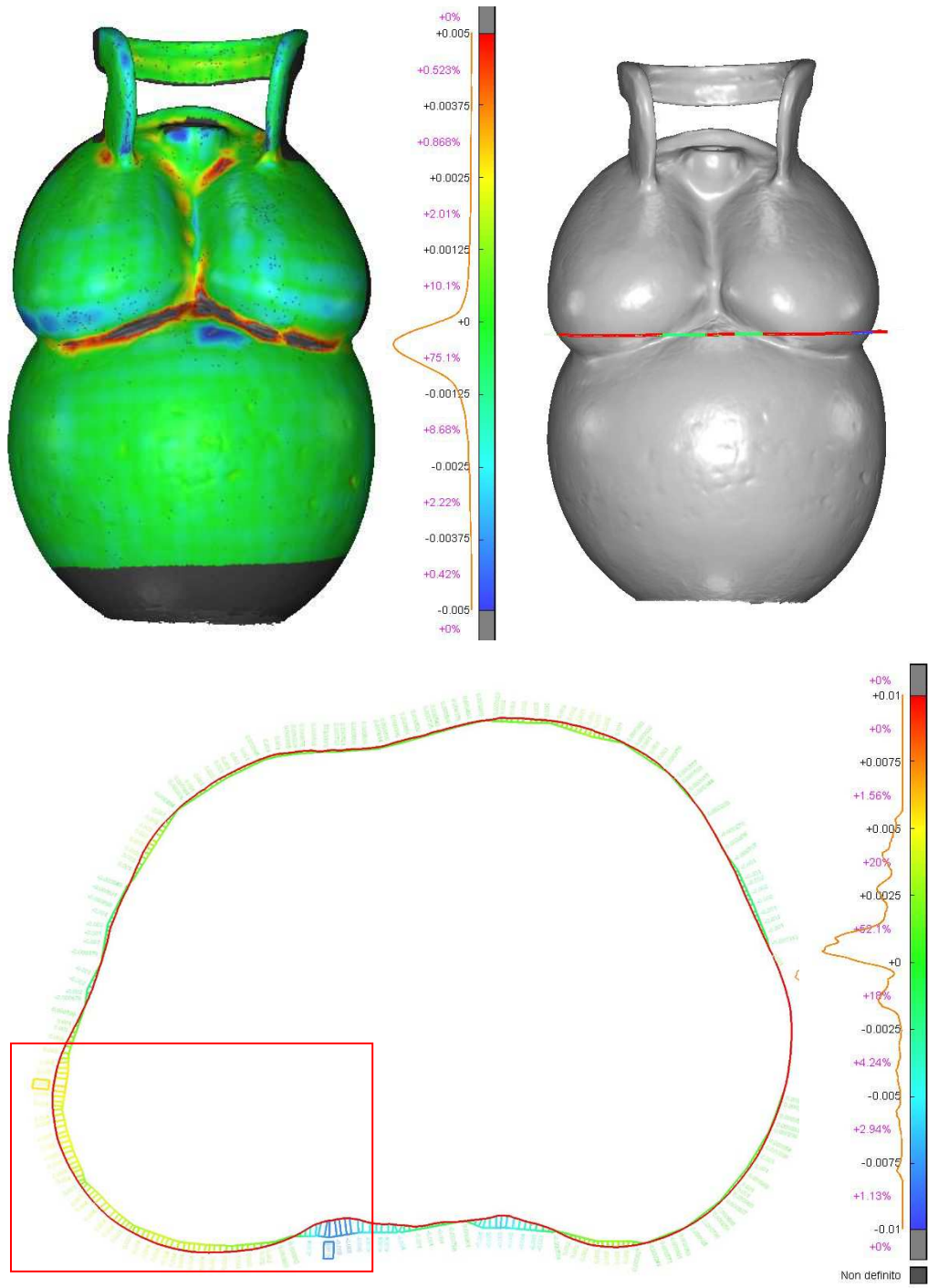
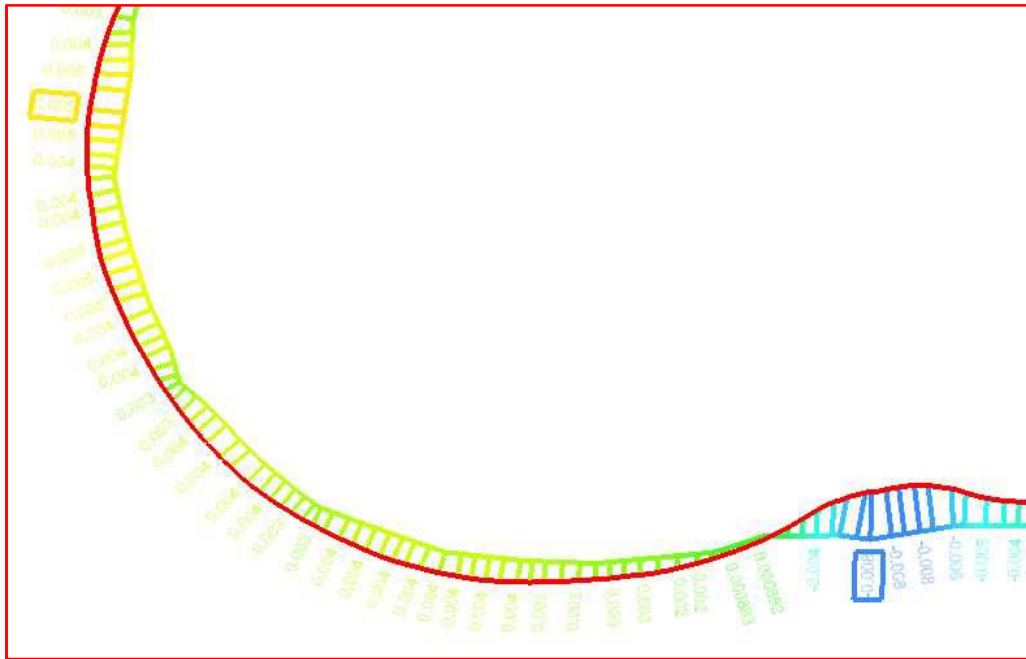


Figure 79. Retopologized model and retopologized model with subdivision surface modifier applied (Level 6).

The so retopologized model, compared to the HP one, shows higher discards than the previous decimation process, even though they are limited by the fact that the surface is quite smoothed (Figure 80). The majority of them (85%) stays in a range between -0.001 and +0.001 mm but extracting a sample of section profile the deviation has maximum positive discard of +0.005 and maximum negative discard of -0.008 mm.





	N. of points
HP polyline	1207
Retopologized model polyline	89

Figure 80. Deviation errors between the HP model and the retopologized one and profile sections extracted with corresponding number of points.

Subsequently the subdivision surface modifier of Catmull & Clark has been applied to the retopo model in order to generate different LoDs and a smoother surface (Figure 79).

A new UV map has been computed and the displacement map has been generated baking the displacement between the HP and the new subdivided retopologized model, setting a dimension of the final image of 2048*2048 pixels (Figure 81).

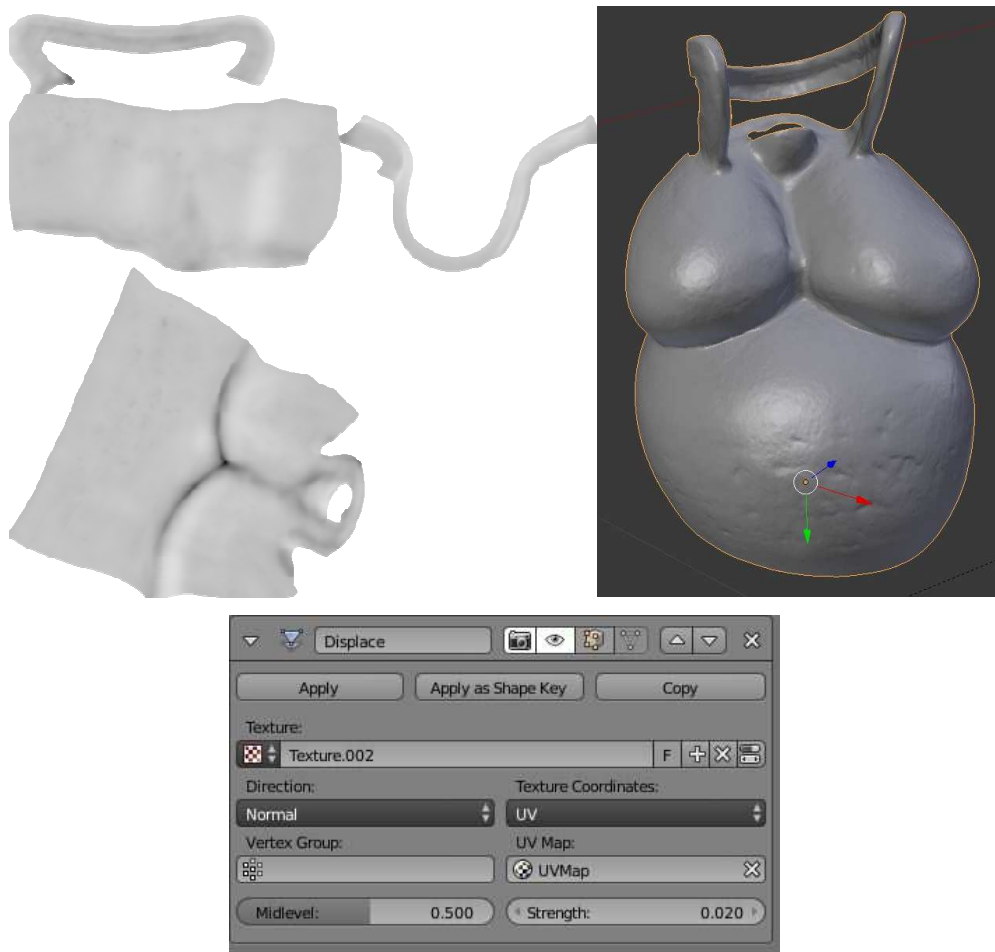


Figure 81. Left: calculated displacement map; right; projection and generation of the displaced subdivision surface; below: Displace modifier.

In order to project the displacement map on the retopo model it is necessary to apply the *Displace* modifier linking the new calculated displacement map. After the calculation, it is possible to see the result in the render mode. The final optimized model offers a great level of detail since its vertices are displaced according to the Displacement map applied, unlike the Normal Map which only simulates the detail (Figure 82).

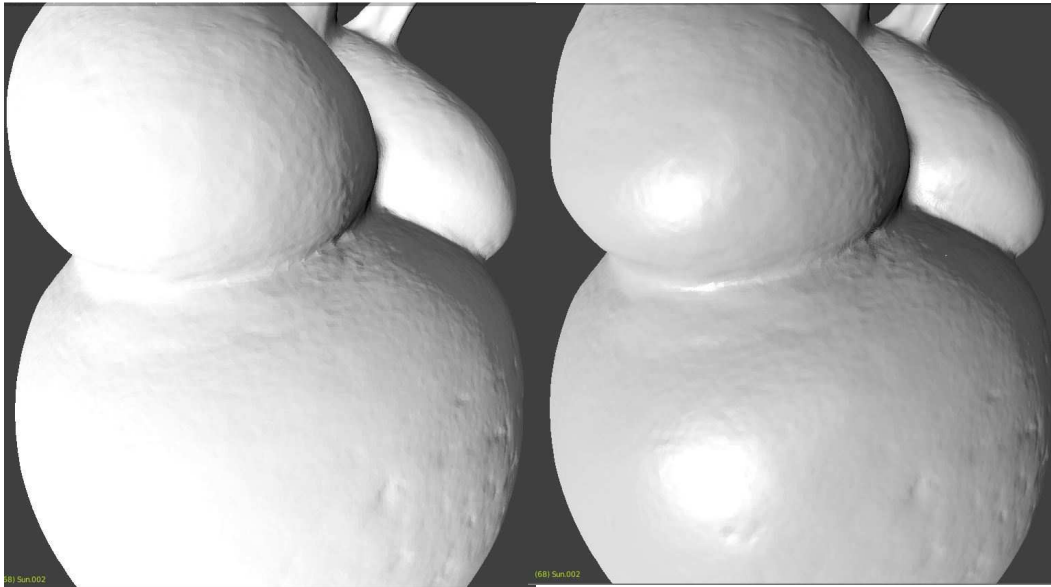


Figure 82. Left: HP model; right: displaced subdivision surface.

Also in this case the final displaced subdivision surface has been exported and compared to the original HP model (Figure 83). This operation showed that the discards are around 0,000 mm and the optimized model offers great accuracy. Therefore, this optimization approach allows to produce more faithful data also from the geometric point of view. From these kinds of models, it is possible to extract measures or other punctual analysis. In particular, their multi-scale nature (LoDs) makes them suitable for many purposes.

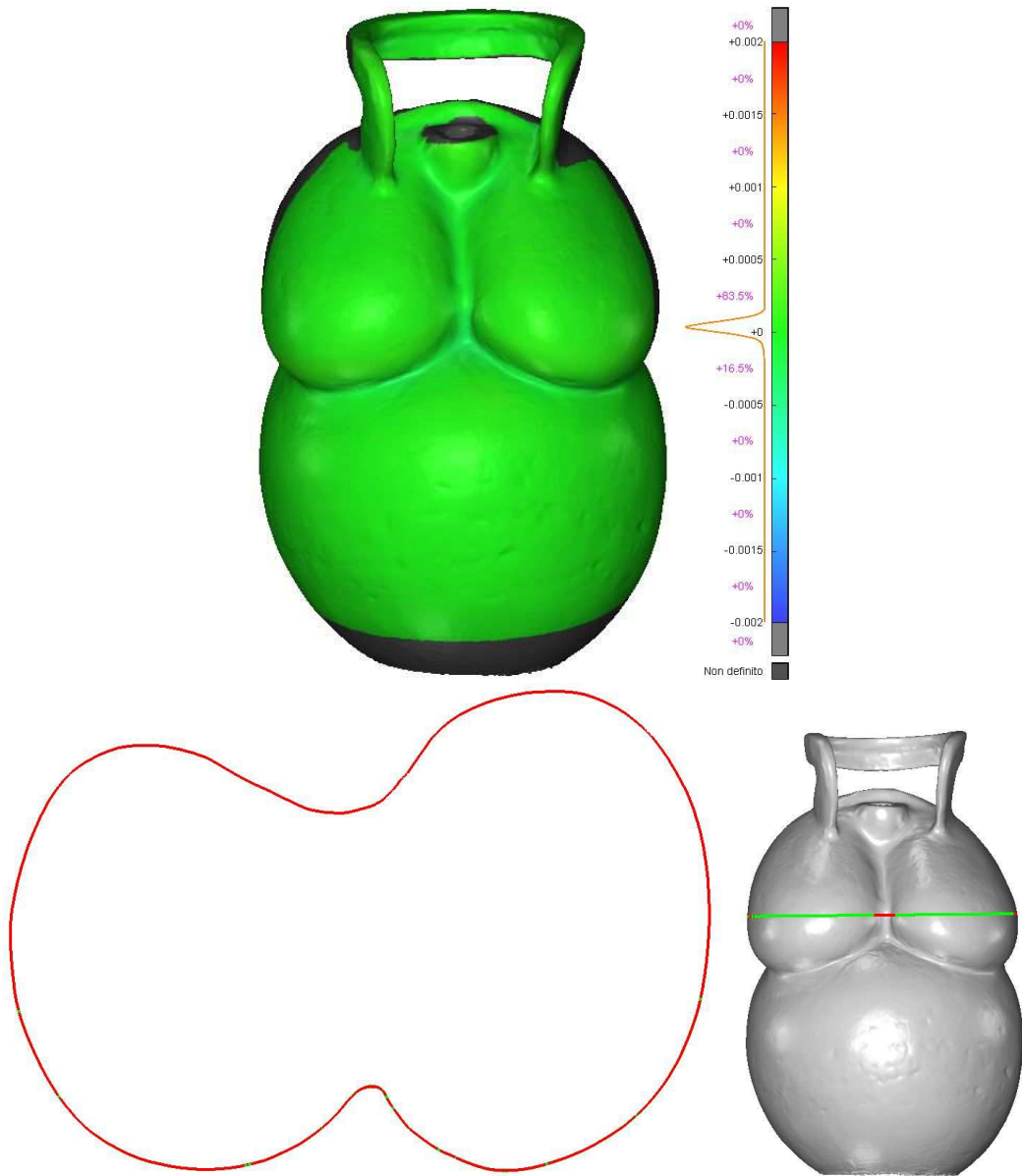


Figure 83. Deviation error between the HP model and the Displaced subdivision surface and comparison of the extracted polylines. The discards are mostly around 0.000 m.

A new diffuse color map has been also generated importing the raw retopologized model in Photoscan (Figure 84), according its UV map, and then it has been projected on the Displaced SubDivision surface



Figure 84. New diffuse color map calculated keeping the UV of the reparametrized retopologized model.



Figure 85. Original HP mesh and textured displaced subdivision surface.

The final textured model visually communicates the same level of information as the HP one and stores also the same geometrical detail.

The final file size of the optimized model in comparison to the original HP mesh are reported in (Table 10 - Table 11). The retopologized model has a very small number of vertices and faces, in comparison to the HP one, in an extremely compact file size, which is awesome. However, the subdivision surface modifier, depending on the level of subdivision, increases the polygon count, so it must be adequately controlled.

	N. vertices	N. of faces	KB file	% Faces reduction	% KB reduction
Original HP mesh	186.592	372.854	17.794	-	-
Retopo mesh	1.057	963	122	-99,7%	-99,3%

Table 10. Report of the faces and KB reduction from the HP model to the LP one.

	KB file
Original HP mesh	17.794
Retopo mesh	122
Displacement Map	1.885
Diffuse color map	376

Table 11. Report of the file sizes involved in the optimization process

5.1.2 Roman loric bust 3D model optimization

The image matching pipeline allowed to process a detailed 3D model, textured with the images used for its generation. However, even though the parameters for the mesh processing were set to very high and with the automatic interpolation disabled, the mesh presented a bad topology especially in the arm and the neck part as visible in (Figure 86). For these reasons, some editing tools have been applied on the mesh in order to remove errors and improve the mesh quality.

The mesh editing

Photoscan offers a decimation tool that has been applied to the model and automatically reduced it from 2.457.684 triangles to 1.800.000 triangles (a lower number made the mesh too smoothed). In a second step the command “Fix Topology”, which is active if there are any topological problems, has been ran to solve such problems (Figure 87).

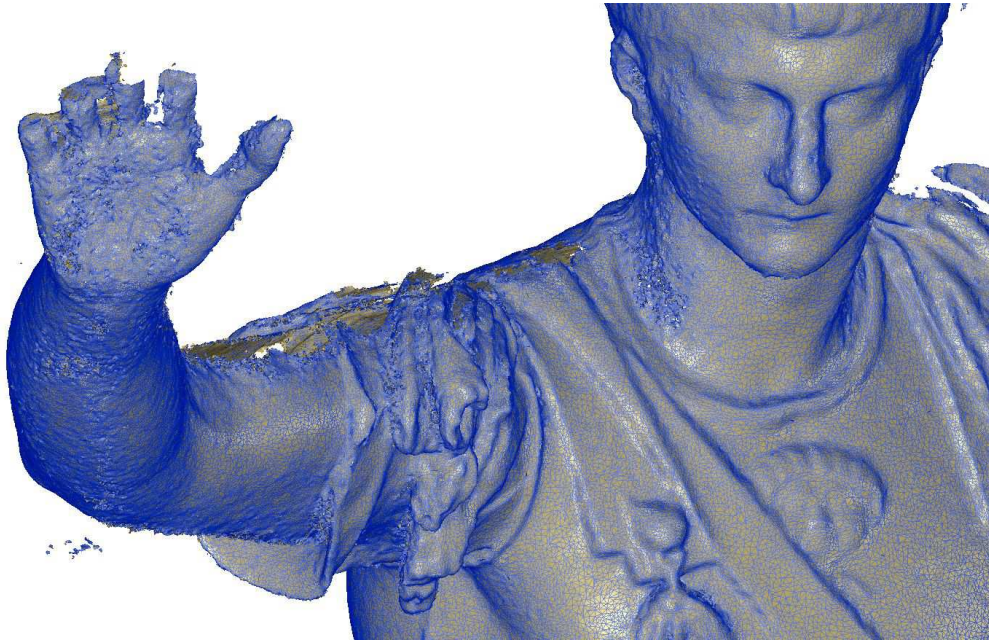


Figure 86. Zoom on the Photoscan mesh in wireframe mode in which the topological errors and the noise are visible.

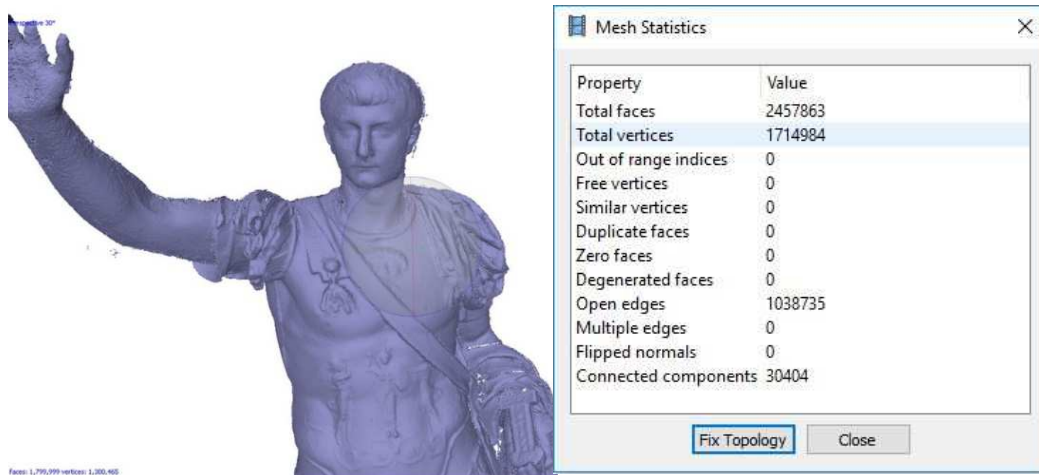


Figure 87. The Photoscan mesh statistics table which reports the presence of topological errors in the mesh and allows to automatically fix them. Unfortunately, the user cannot personally control the operation, editing any factor.

Since topological errors and noisy parts still occur in the mesh, a second attempt has been made exporting the generated dense cloud in the software 3D Reshaper, with the aim to test a new mesh generation. A new mesh has been processed setting a triangle size of 2 mm and refining the mesh with deviation error of 1 mm. The final mesh offers better results, fewer topological errors and it is possible to manually close the remaining holes.

The higher quality offered by the 3D Reshaper mesh is also due to fact that the operator has higher power in the generation process.



Figure 88. The mesh created with 3D Reshaper. Generation with the two steps tool: the user sets the mean triangles dimension and, in a further step, the deviation error in order to refine the final mesh.

Moreover, it is interesting to highlight the number of triangles of both the mesh and the resulting file size. As visible in (Table 12), the original Photoscan mesh has a greater number of points and triangles but also a higher number of errors as independent pieces and holes or free contours, and then a higher file size.

	N. Points	N. Triangles	N. independent pieces	N. of holes or free contours	KB .obj file
Mesh PS	1.720.221	2.457.684	30.405	71.075	110.309
Mesh 3DR	374.774	741.327	2	264	37.390

Table 12. Comparison between the original Photoscan mesh and the 3D Reshaper one.

Moreover, as mentioned at the beginning, in order to represent the bust before the additions of the nineteenth century, the added lower part of the legs, parts of the arms and the head have been cut in a copy of the model.



Figure 89. Final textured model of the statue and final textured model of the cut bust.

Optimization with LP model and Normal maps

This first optimization process started with the generation of a Low Poly model on which project the details of the High Poly one, by means of a Normal Map.

To do this, initially, the 3D Reshaper model has been imported in MeshLab.

Several cleaning and repairing automatic filters have been applied before the decimation:

- Remove duplicate faces;
- Remove duplicate vertices;
- Remove faces from non-manifold edges;
- Remove isolated pieces.

Subsequently the decimation has been processed with the Quadric Edge collapse decimation algorithm. Several steps of decimation, which can respond to different purposes, have been tested and compared on this object in (Donadio, Sambuelli, & Spanò, 2018):

- In a first level, the mesh is indiscriminately and automatically decimated with the *Quadric Edge Collapse Decimation* tool. In this process, it is not possible to reduce that much the mesh if you do not want to lose completely the geometric and visible detail. For this reason, the decimation was set from 741.327 to 100.000 faces. The file size changed from 37.390 KB to 2.483 KB but visually the mesh still has a good level of detail, although it is more smoothed (Figure 91).
- In a second level, the aim was to maintain the original high level of detail in the high detailed portions (the decorated armour and the *pterigi* part - the fringes that form a sort of decorative skirt used by the ancient Greek and Roman soldiers under the armor), hardly decimating just flat parts such as the legs and the arm. In this way, the file size is reduced a little less but the detail on the decorated portion is still very high (Figure 91).
- In the third level of optimization, the aim was to reduce at most the mesh, making use of the texture maps to just visually simulate the detail. The mesh has been decimated to 7000 faces, with the aim to generate a very low file size to the detriment of the geometric accuracy. The mesh so generated has been then imported in Blender for the baking process of a Normal map (Figure 92).

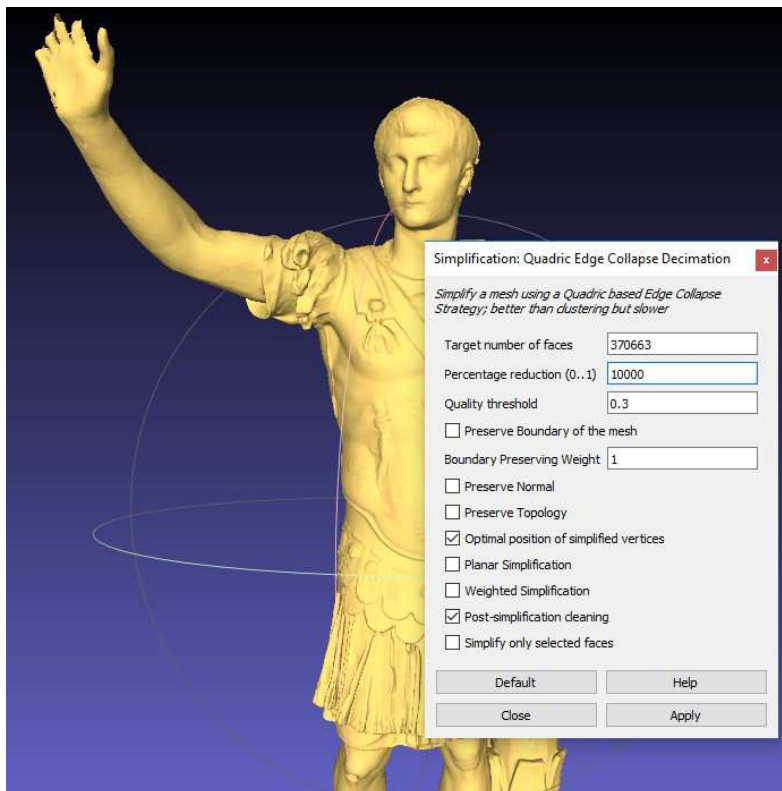


Figure 90. Quadric Edge Collapse Decimation applied to the whole statue in MeshLab.

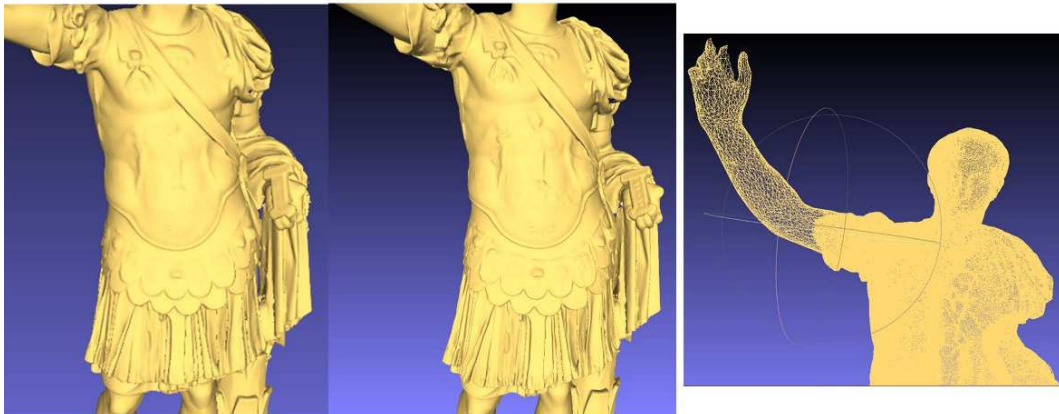


Figure 91. Left: the decimated mesh - Level 1; middle – right: the decimated mesh - Level 2.



Figure 92. Ultra decimated Low Polygon (LP) surface - 7000 faces.

A comparison between the resulting file sizes of the decimated models is reported in (Table 13) and the evaluation of the discards in comparison to the original model is shown in (Figure 93).

	N. vertices	N. of faces	KB file .obj	% Faces reduction	% KB reduction
Original HP mesh	374.774	741.327	37.390	-	-
Level 1	52.622	100.000	8.599	-86,5%	-77%
Level 2	147.754	288.165	25.200	-61%	-32,6%
Level 3	3.874	7.000	575	-99%	-98%

Table 13. The results of the decimated mesh model compared to the original one

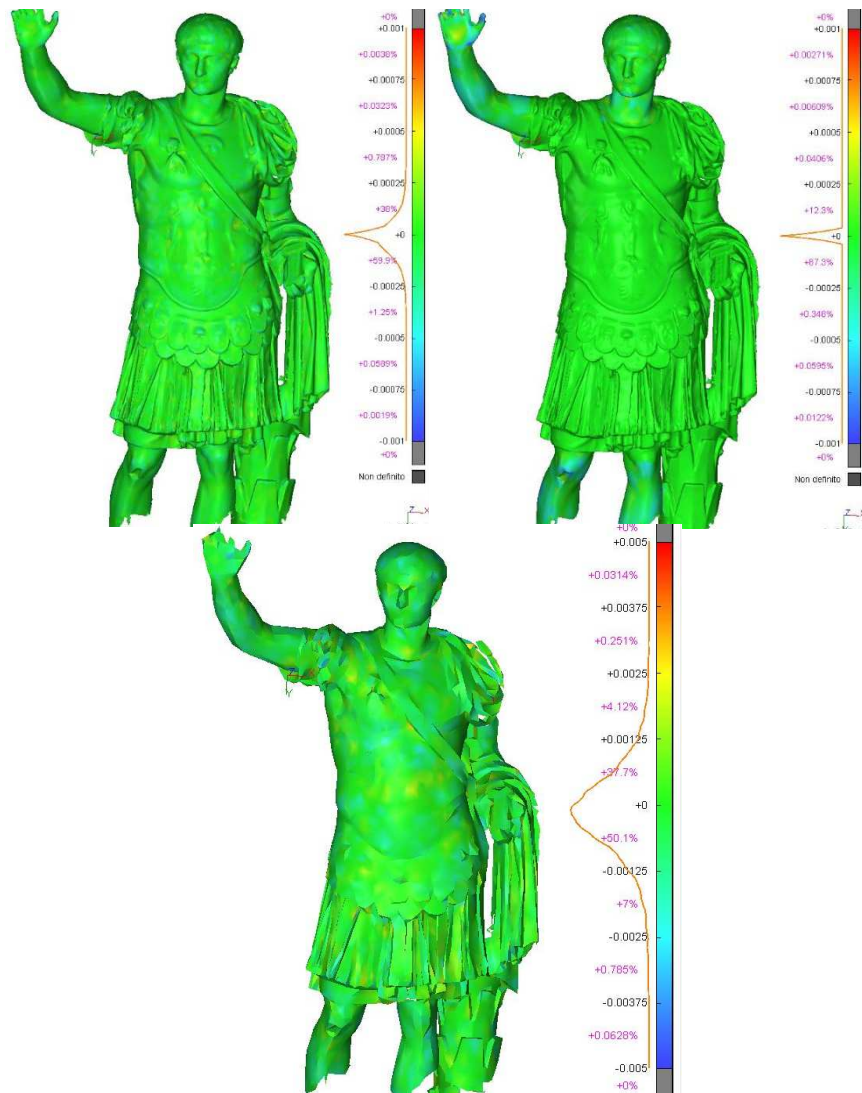


Figure 93. Comparison between the decimated surfaces and the High Polygon one. Left: comparison between Level 1 and HP; middle: comparison between Level 2 and HP; right: comparison between Level 3 and HP.

The same operation has been applied over the cut bust and a LP model has been created, maintaining just 5000 faces. A first evaluation consisted in the comparison between the LP model generated and the HP one. As visible in (Figure 94) the deviation error is very low throughout the model, mostly ranging from -0.001 m and + 0.001 m. This is a very good result, offered by the decimation algorithm implemented in MeshLab, also dealing with a decorated surface.

Another comparison can be done extracting some section profiles from the HP and the LP models, in particular in sensitive zones such as the *pterigi* part which is more

detailed and decorated. As it is possible to see in (Figure 94- Figure 95), the Polyline extracted from the LP model has a much reduced number of points that approximate the geometry of the object. However, the discards are low, with a maximum positive value of +0.003m and maximum negative value of - 0.004 m.

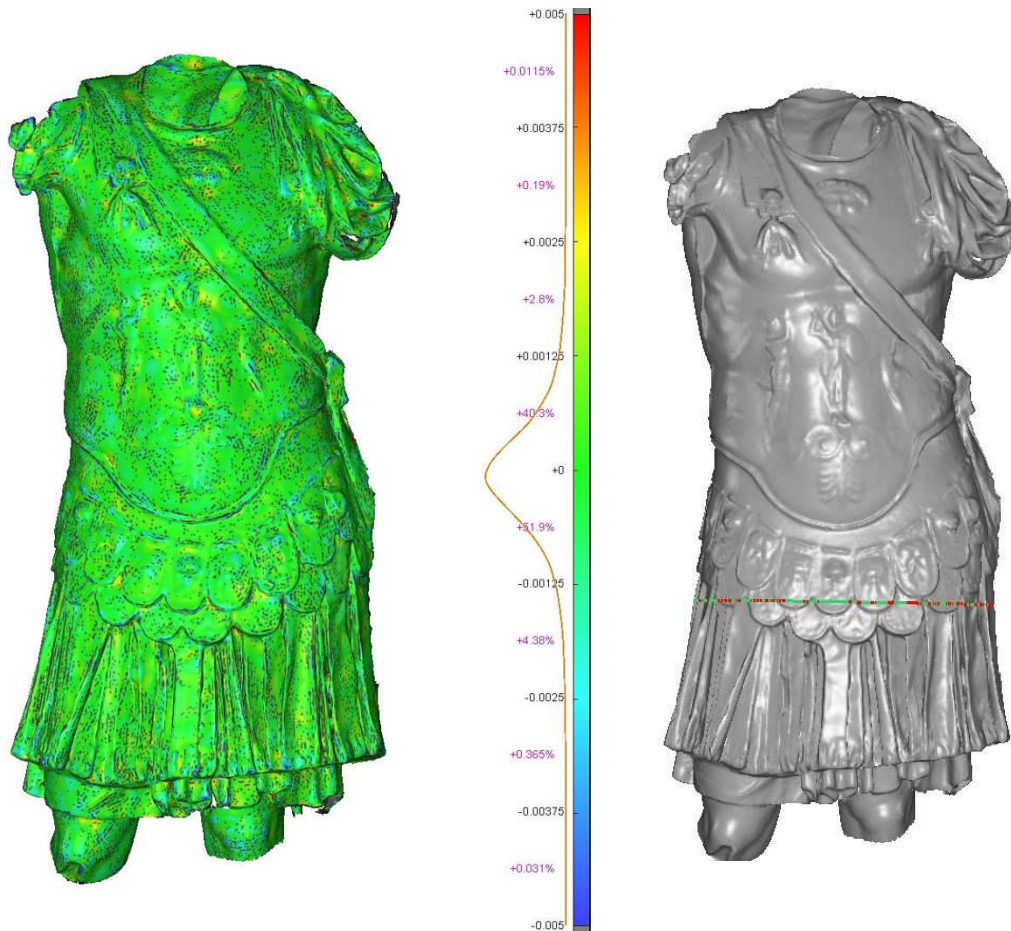


Figure 94. Left: Comparison between the high detailed bust and the LP bust. It is possible to notice that the 90% of the points of the LP have a displace between -0.001 m and +0.001 m which is a very low value; right: extracted section profiles.

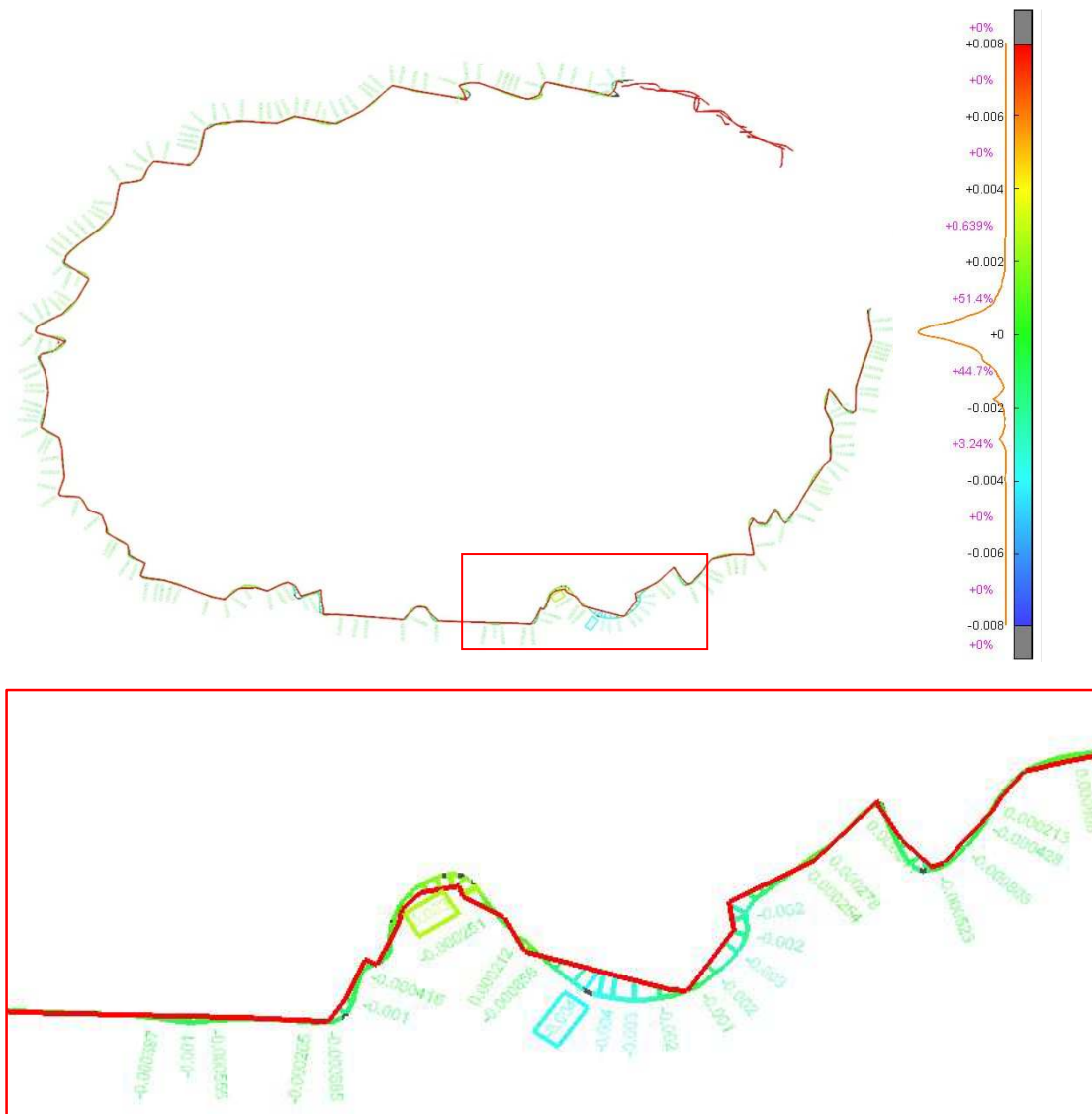


Figure 95. Section profiles extracted from the HP (red) and LP (green) models.

Once processed the Low Polygon mesh, the object has been imported in Blender in order to compute a controlled UV map and to process and project the Normal map. As already shown in 4.2.4 (Figure 58-Figure 59), Photoscan automatically created a UV map to compute the diffuse color texture map, but it is too confused, divided in too many atlas. For this test case, the parameterization has been processed both basing on the cuts defined by the user and also following the *smart UV project* tool proposed by Blender.

Once manually marked the cut profiles (Figure 96), a new UV map has been generated unwrapping the so defined mesh (Figure 97). Since it is not always easy to create such cut profiles for a non-expert user and dealing with a complex model, a second attempt tested the *smart UV project* tool for the LP model of the entire statue. As it is visible in (Figure 98), this automatic procedure allows to fix some parameters to guide the process; the final result has still many islands, as the one of Photoscan, especially in the *pterigi* part, however it offers a better reading of the main parts of the statue and is more automatic.

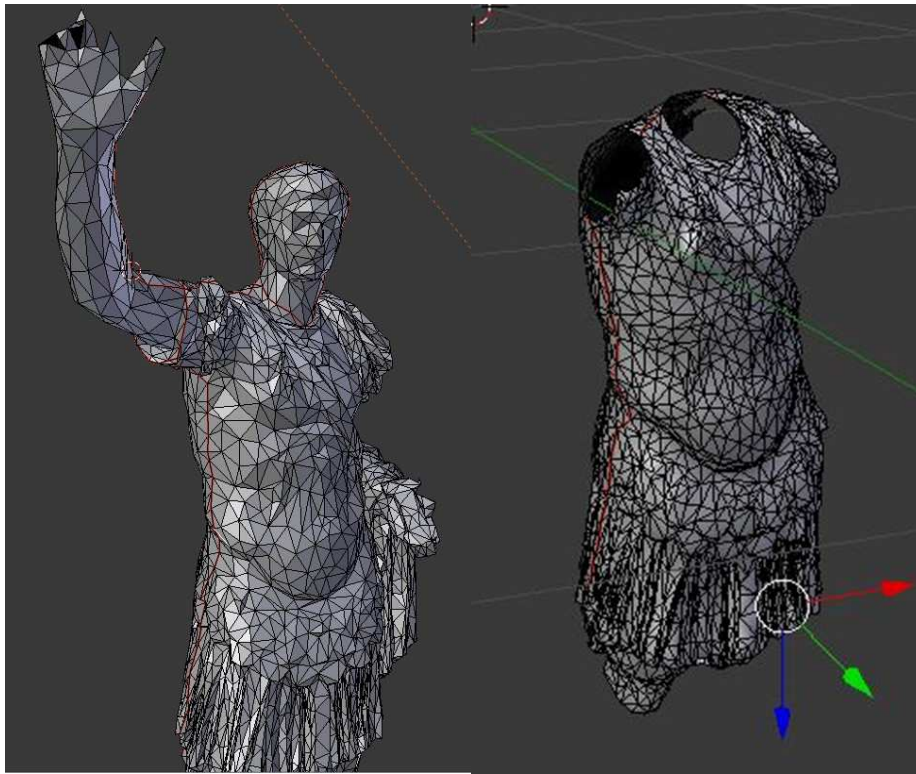


Figure 96. Examples of manually marked seams, highlighted in red.

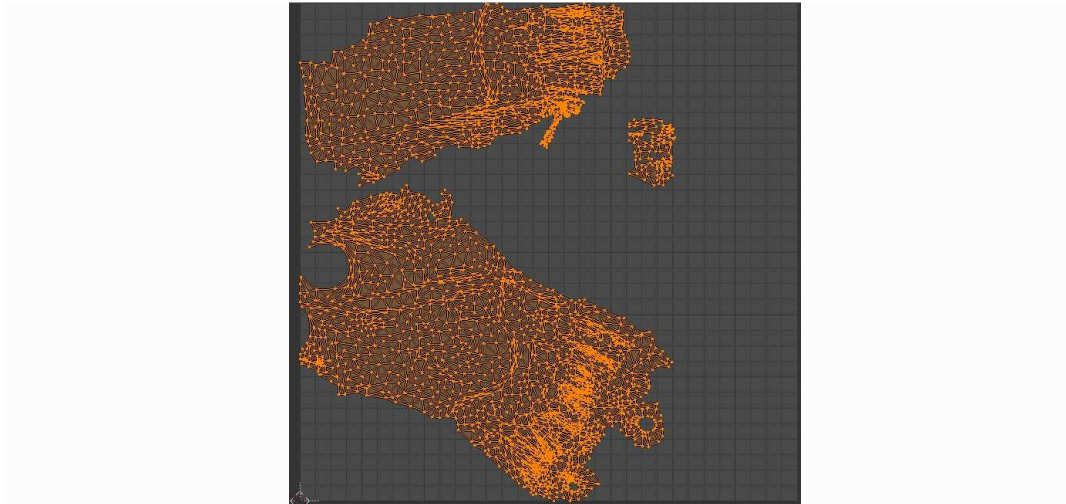


Figure 97. New UV map calculated for the bust which has been unwrapped dividing the front size from the back side. Image dimension 2048*2048.

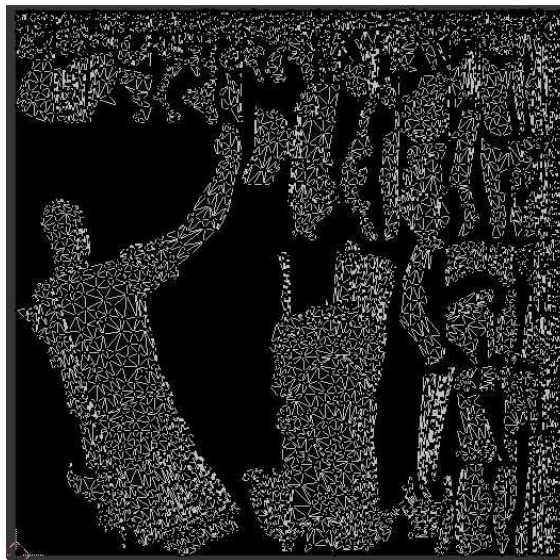
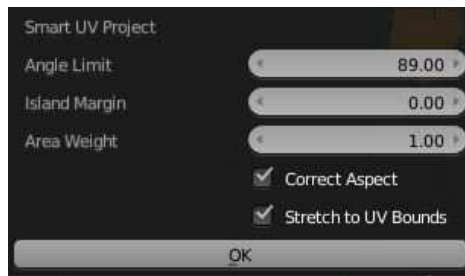


Figure 98. New UV map calculated for the whole statue that has been unwrapped according to the automatic *Smart UV project*. Above: the parameter used for the unwrapping. Image dimension 2048*2048 pixels

The following step of the optimization consisted in the creation of the Normal Maps, that has been generated baking setting a dimension of 2048*2048 pixel (Figure 99).

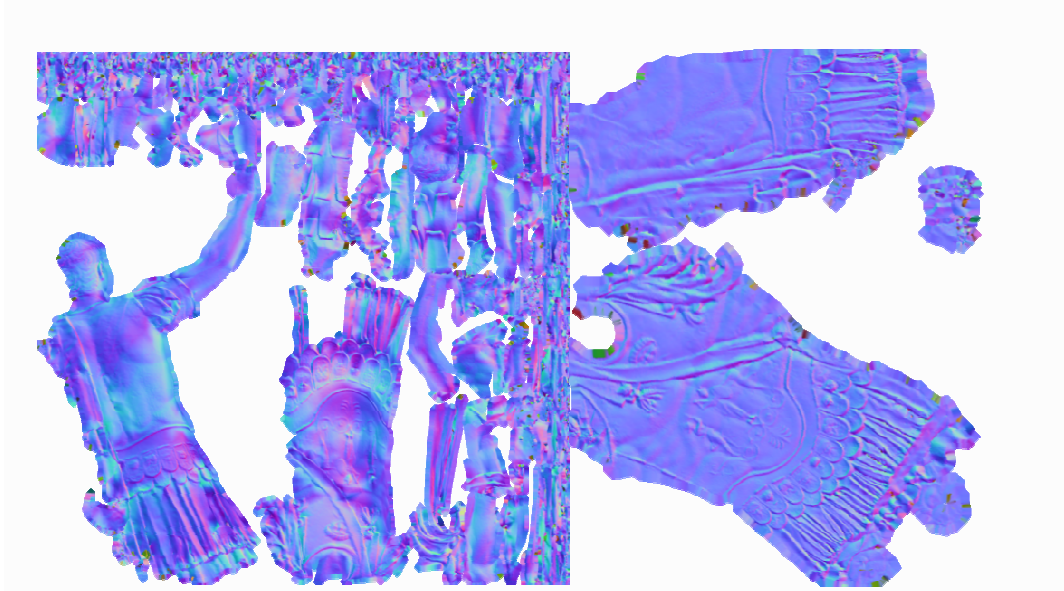


Figure 99. Normal map generated for the whole statue and for the bust.

After this computation, it has been possible to project the maps over the LP model, using the common coordinate system generated from the UV layout. After this computation, in the texture visualization, the LP model shows again a high level of detail, compared to its real surface, and it appears visually identical to the HP mesh, except with less vertices (Figure 100- Figure 101).

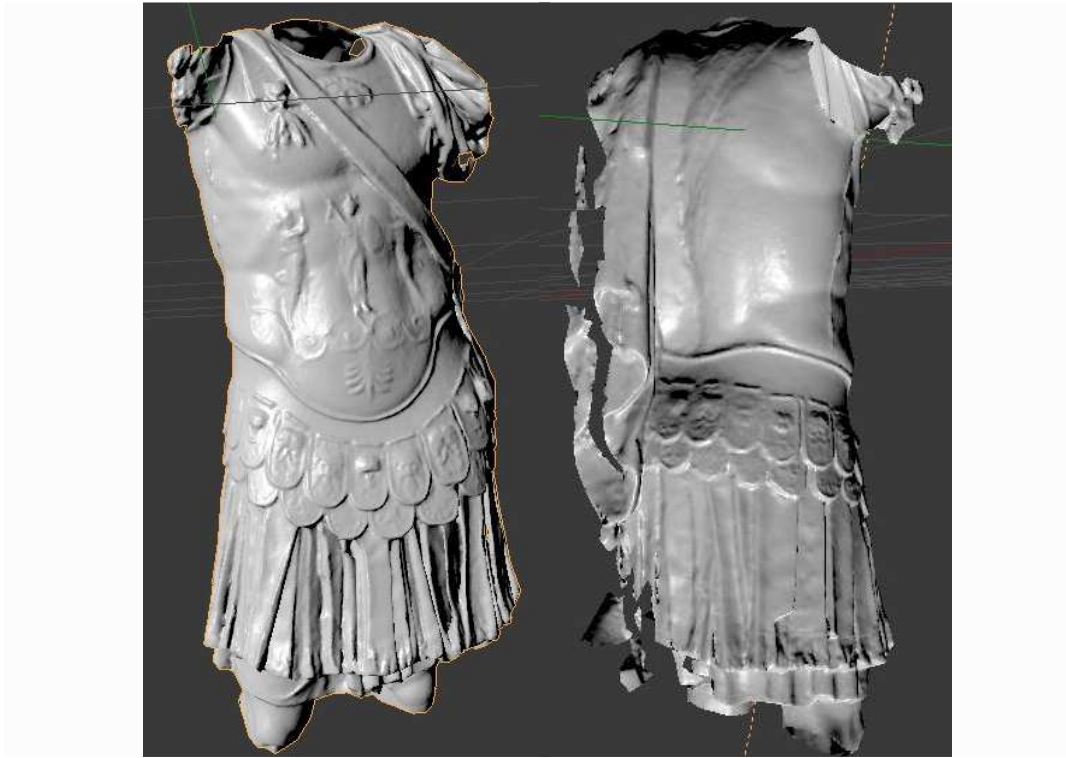


Figure 100. Above: Render views of the bust model with normal map applied; below: LP model viewed as Object mode and texture mode with NM applied.

Also in this case, making a visual comparison between the original HP model and the so optimized LP one, it should be noted that the LP model has more sharp edges due to the greater dimension of its triangles. However, considering the high smoothness and the low level of detail of the coarse LP surface, the NM projection allows to render a remarkable result and the representation achieved so far demonstrates to satisfy the aims to reduce the file size without losing the perception of the geometrical detail. However, it necessary to underline that such model lack the real geometric detail which is only simulated and so it is impossible to extract punctual accurate measures.



Figure 101. Visual comparison between HP model (above-left), LP one (above - right) and the same LP model with NM applied (below).

Since the model still misses the colour information, a further step consisted in the projection of the diffuse colour map over the LP optimized model. To do this, the new

parametrized model has been imported in Photoscan and a new texture calculation has been run, setting the *Keep UV* mode (Figure 102).

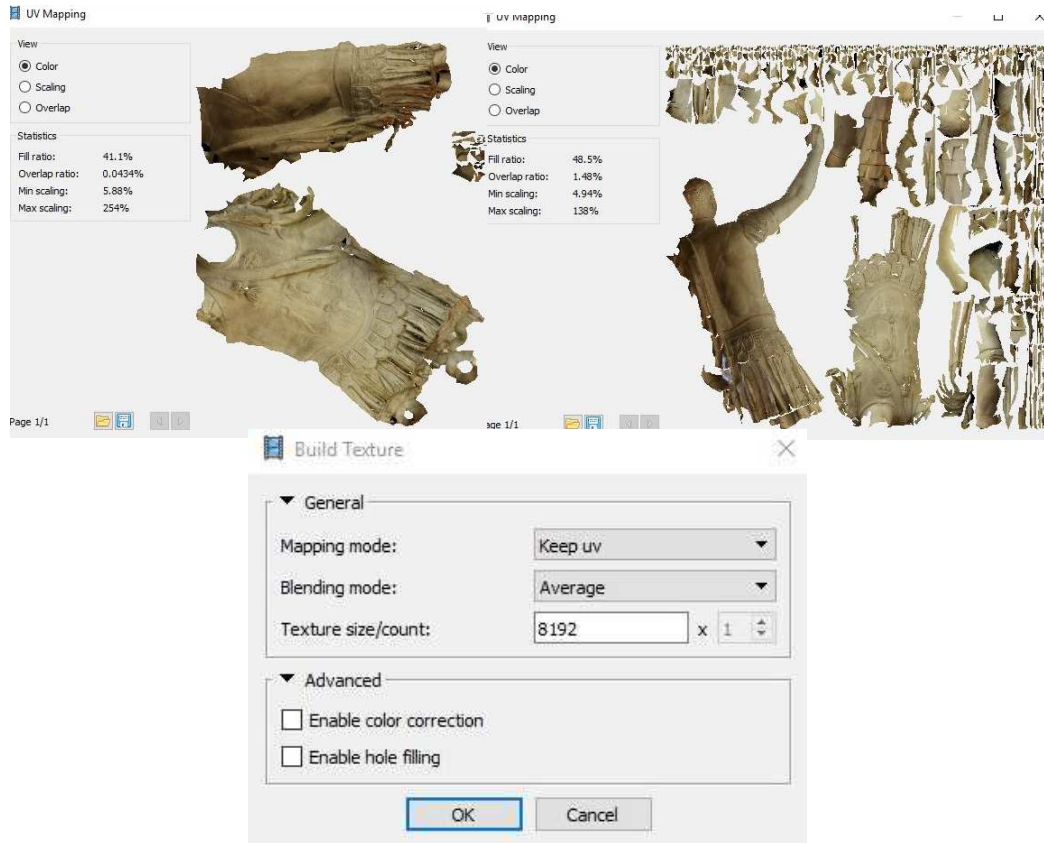


Figure 102. New diffuse color maps calculated in Photoscan on the decimated models and according to the edited UV maps.

The new diffuse color has been projected with the NM over the LP model through the Node editing tools. Once projected both the texture maps, it is possible to see and evaluate the results (Figure 104). Also in this case, the so processed colored 3D model looks like the HP one, but has a very small file size (see Table 14-15).

Certainly, the only diffuse color map provides a good representation of the details on the LP smoothed model, but the Normal map and its shadows allow to render a more detailed surface, as visible in (Figure 105). In fact, making again a comparison between the so optimized surface and the LP with only the diffuse color map projected and without the NM, it is possible to state that the 3D profiles of the surface are more defined and so the whole geometry is more faithful to the original one (Figure 103).



Figure 103. LP with diffuse color and Normal Map(left) and LP with just diffuse color (right).



Figure 104. Results of the LP with diffuse colour and normal map applied (left) and LP object mode (right).



Figure 105. Left: original HP model; right: final rendered result LP model with NM applied.

	N. vertices	N. of faces	KB file	% Faces reduction	% KB reduction
Original HP mesh	212.512	420.565	34.955	-	-
LP mesh	2.685	4.985	434	-98,8%	-98,8%

Table 14. Report of faces and KB reduction from the HP model to the LP one.

	KB file
Original HP mesh	34.955
LP mesh	434
Normal Map	1.071
Diffuse color map	396

Table 15. Report of the file sizes involved in the optimization process

Optimization with Displaced subdivision surface

The second test applied to the LP model aimed again at the creation of a Displaced SubDivision Surface in order to define the potentialities of a real displacement applied to the vertices of a subdivided surface. As explained in 3.2.8, this kind of model requires the computation of the displacement map and a quad-dominant mesh that support the conversion in subdivision surface of Catmull & Clark.

The re-topology process, as mentioned, can be fulfilled with different approaches. To do this on the roman statue, it started with the creation of a plane that with the Subdivision Surface modifier has been subdivided in smaller planes, which constituted the quadrangular polygon of the mesh, and with the Blender *Shrinkwrap* modifier has been subsequently projected over a surface of reference (the HP), with an offset set by the user. In order to cover the whole HP model, some manual-traced lines provided the guide for the creation of new quad-polygons (Figure 106.).

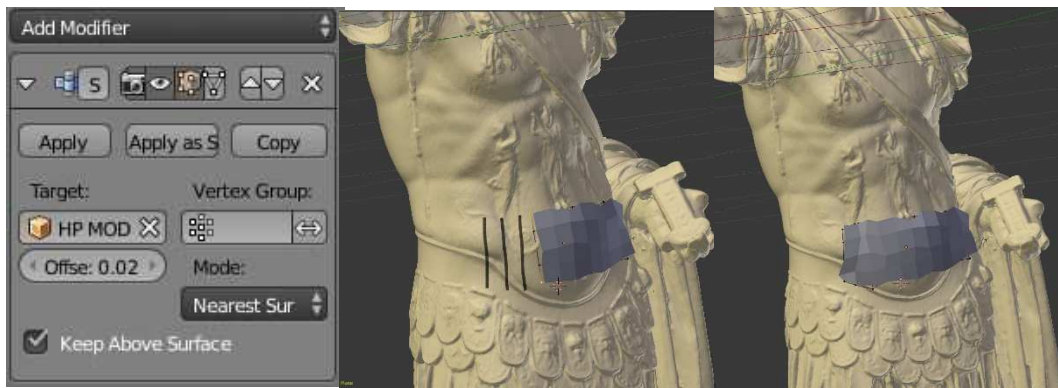


Figure 106. Shrinkwrap modifier and an example of quadrangular polygons generation over the HP mesh.

The Retopo process has been applied on both, the statue mesh and the bust one but further operations have been applied only to the cut bust model. Once the retopo LP model has been completed, a new UV map has been computed, based on the marked seams by the user (Figure 107).

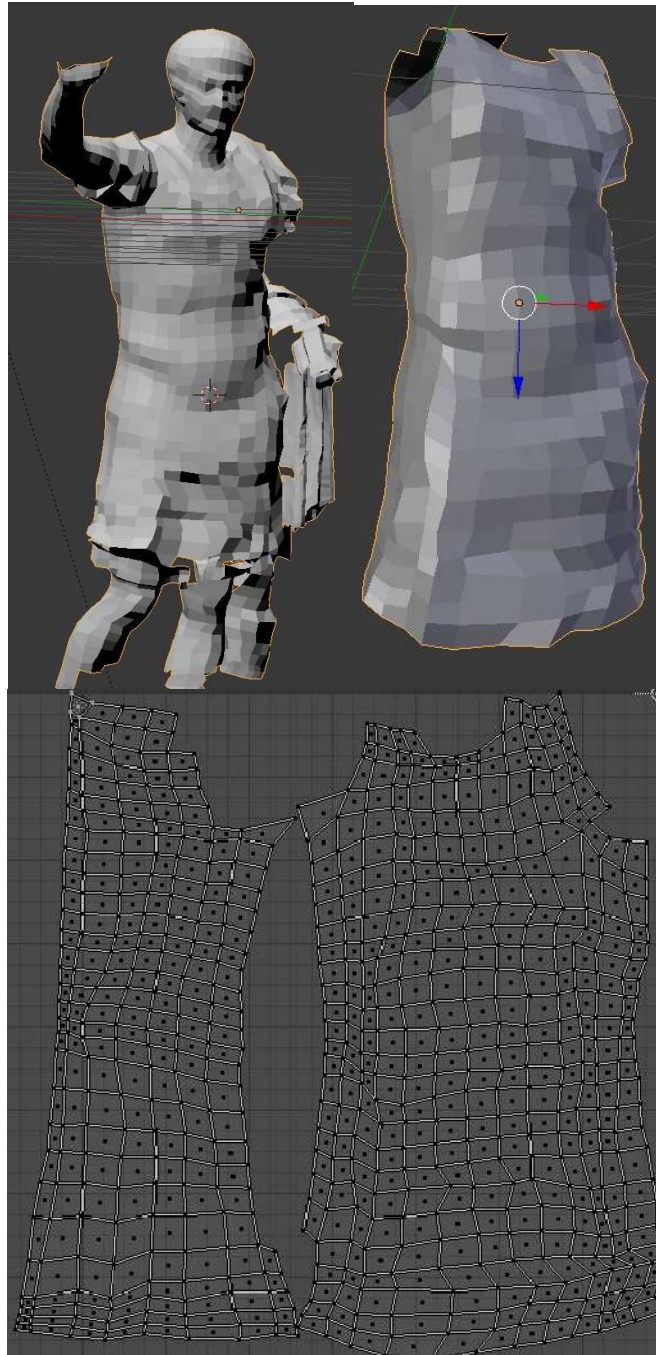
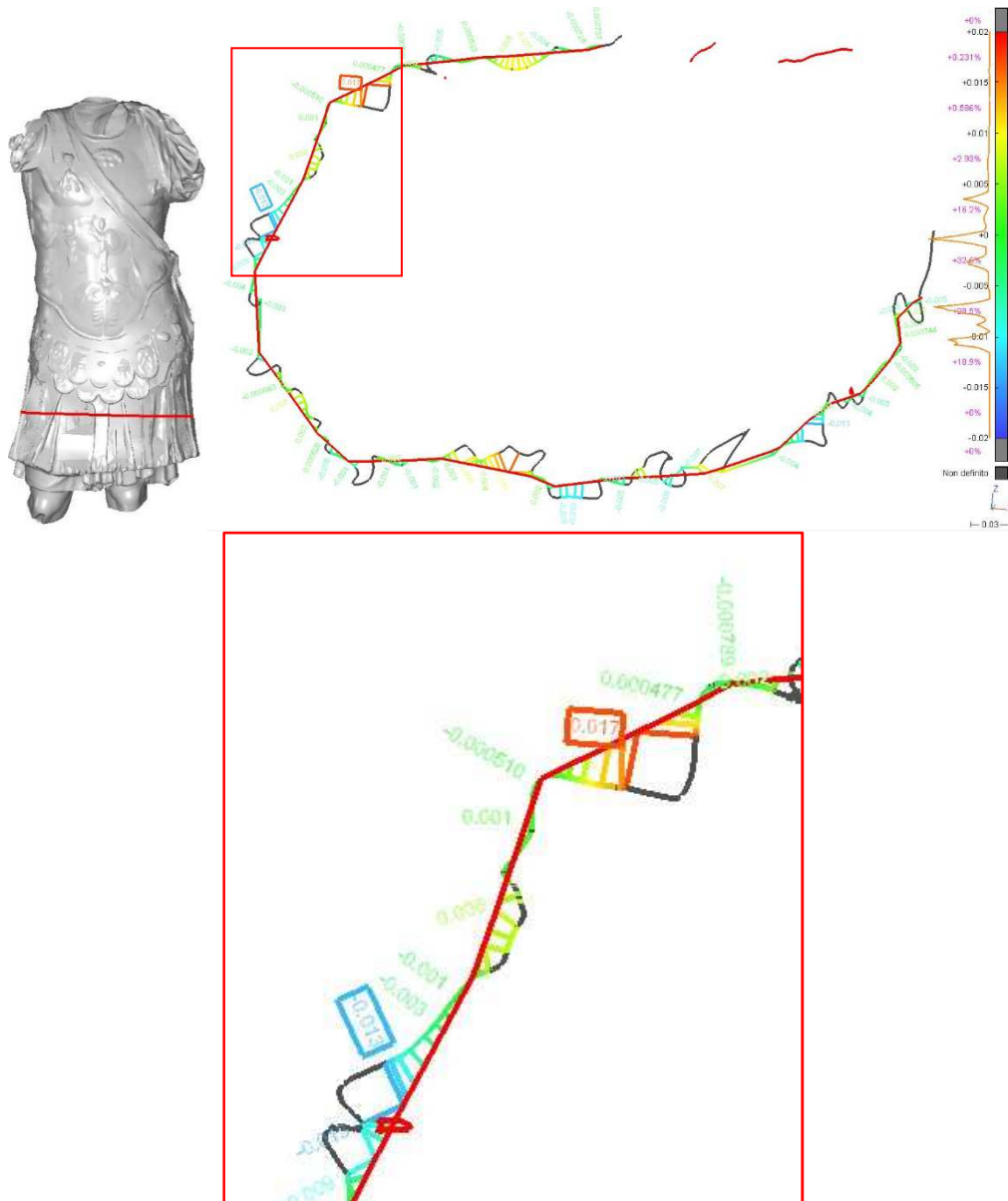


Figure 107. Above: Retopologized model of the statue and of the bust portion. Below: new UV map calculated on the retopo bust model.

Also in this second optimization attempt, the deviation between the HP model and the retopologized one (before the subdivision surface modifier) has been computed. In this case, the deviation error, as expected, is much greater since the retopo procedure

produced a very low polygon model which, without any modifier, has lost most of the information about the geometry of the original model. The 90% of the vertices of the retopo model as a deviation of +/-0.005 mm from the HP one (Figure 107 -Figure 108). Extracting a sample of section profile in a sensitive zone (the detailed pterigi part) the discards evaluation shows a maximum positive discard of +0.017 m and a maximum negative discard of -0.013 m.



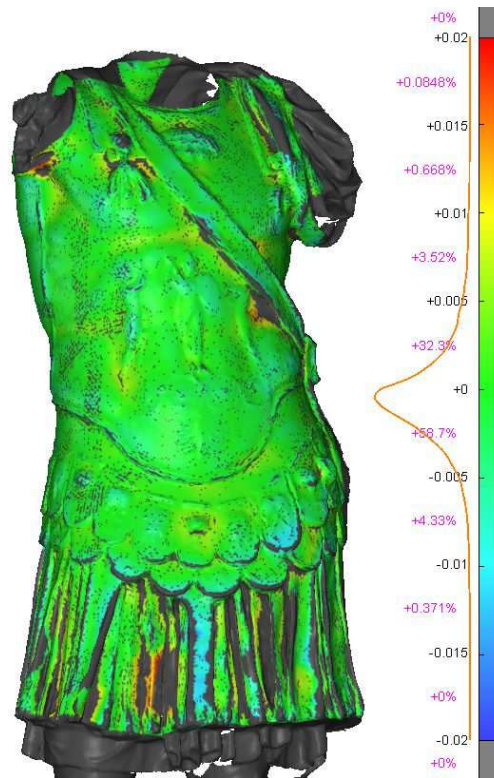


Figure 108. Above: section profiles extracted on the HP and retopologized models. Below: deviation error between the HP model and the retopologized one. It is possible to notice that in this case the mean value is higher.

Thereafter, before the computation of the Displacement Map, the SubDivision Surface modifier has been applied to the LP model. In this way it is possible to subdivide the LP model in different LoDs, increasing or decreasing the polygon count (Figure 109) to be calculated both for the view or the rendering mode. In this application, the level of subdivisions has been set to 6.

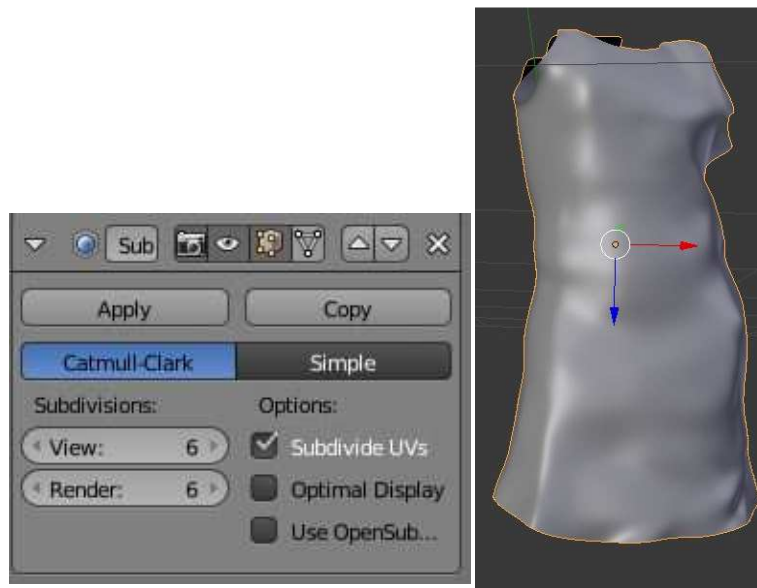


Figure 109. Retopologized bust after the SubDivision Surface modifier – level 6.

The following step consisted in the computation of the Displacement Map. As well as for the Normal map computation, it requires the selection of the HP mesh and the LP sub-surfaced one, in order to compute the scalar vector to be stored in the pixel value. The Displacement map generated has been saved with a dimension of 2048*2048 pixels.

In order to project the displacement map on the retopo model, the *Displace* modifier has been applied (Figure 110) linking the new calculated displacement map. After the calculation, it is possible to see the result in the render mode. The final optimized model offers a great level of detail since its vertices are displaced according to the Displacement map applied, unlike the Normal Map which only simulates the detail (Figure 110).

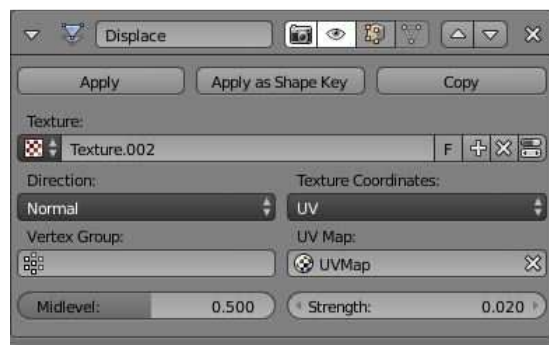
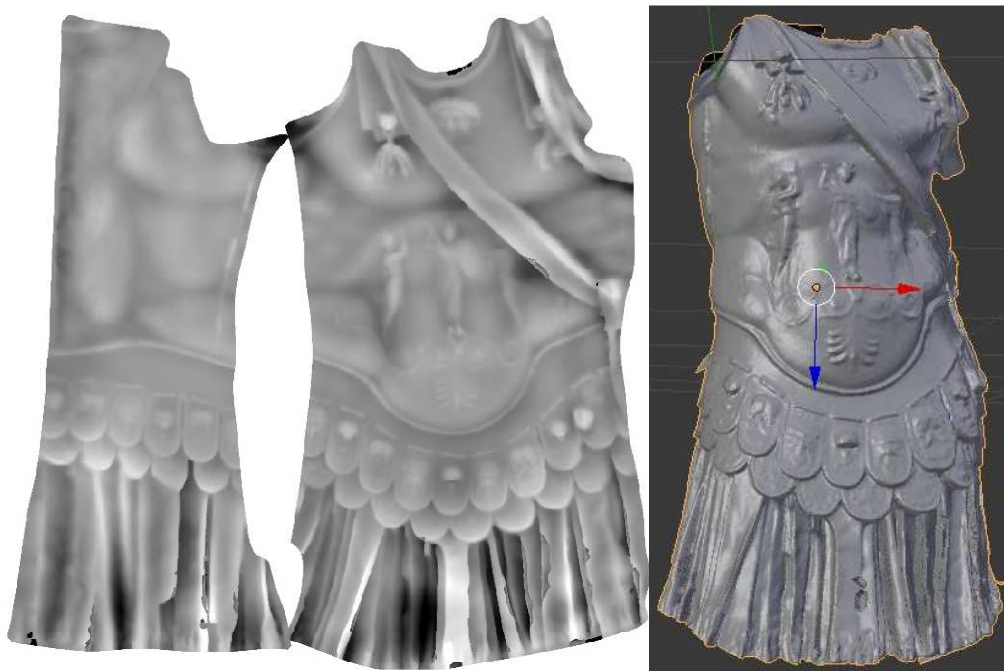


Figure 110. Displacement map and its projection over the retopologized model. Below: The Displace modifier.

As well as for the first optimization case study, a new diffuse color map has been computed in Photoscan importing the re-topologized and parametrized LP model and setting the *Keep UV* texturing mode.



Figure 111. New diffuse color map computed on the retopologized model.

Subsequently, the diffuse color has been projected over the LP model using the Node editor tool (Figure 112).

Also in this case the file sizes of each object involved in the process has been computed (Table 16-17). Again the retopologized model shows its extreme compactness, however, as already mentioned, it is necessary to take into account the level of subdivision subsequently applied to generate the displaced subdivision surface, which influences the rendering process time.

	N. vertices	N. faces	KB file	% KB reduction	% faces reduction
HP mesh	212.512	420.565	34.955	-	-
LP retopologized mesh	595	538	67	-99,8%	-99,7%

Table 16. Report of the faces and KB reduction from the HP model to the retopologized one.

	KB file
Original HP mesh	34.955
Retopo mesh	67
Displacement Map	2.736
Diffuse color map	389

Table 17. Report of the file sizes involved in the optimization process



Figure 112. Final displaced subdivision surface

What it is interesting to evaluate on the final Displaced SubDivision Surface is not just the comparison with the original HP model, but also the discards and the visual quality in comparison with the LP model with the NM applied (Figure 113).

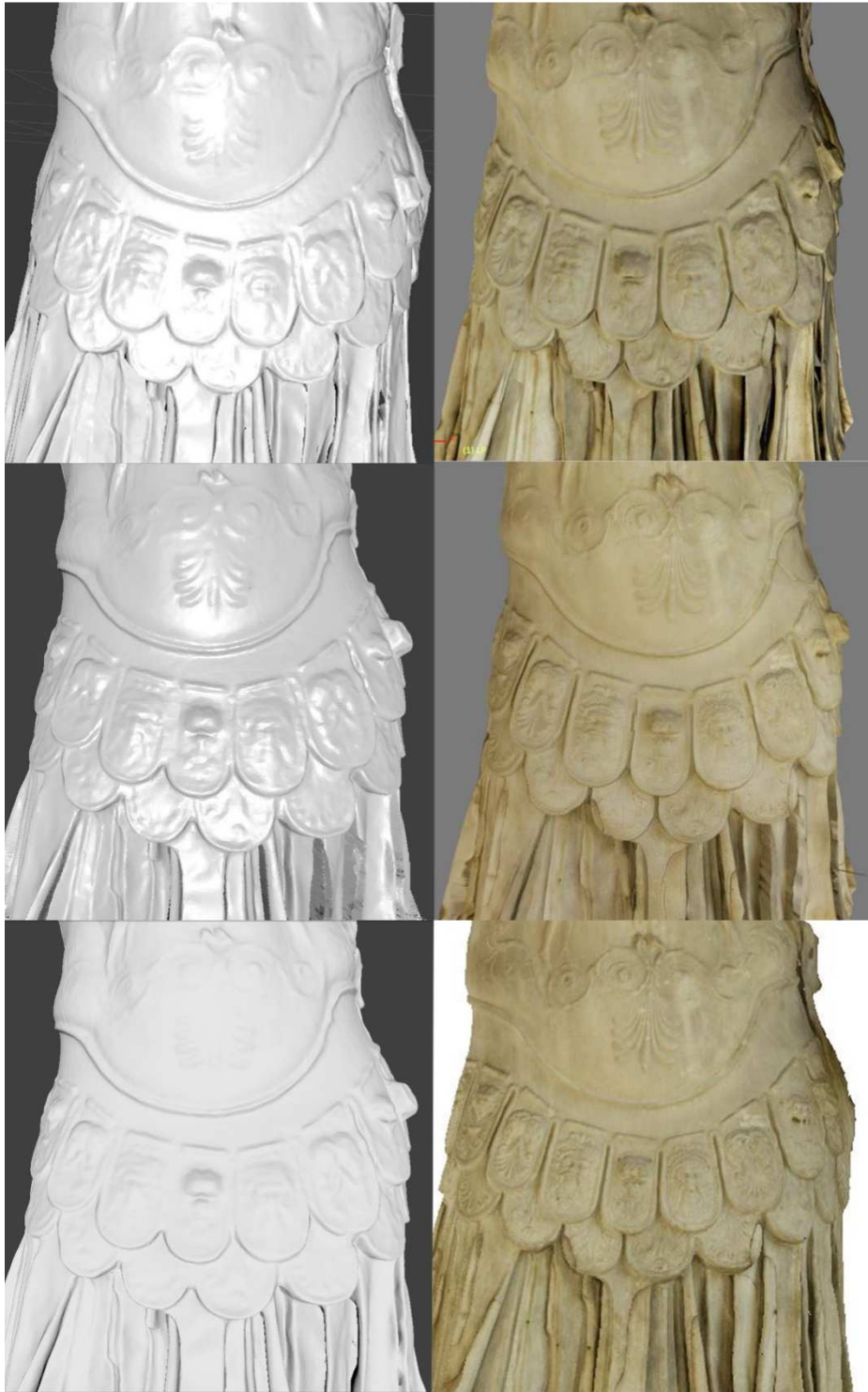


Figure 113. LP model with NM, Displaced SubDivision Surface and original HP model, without and with diffuse color texture.

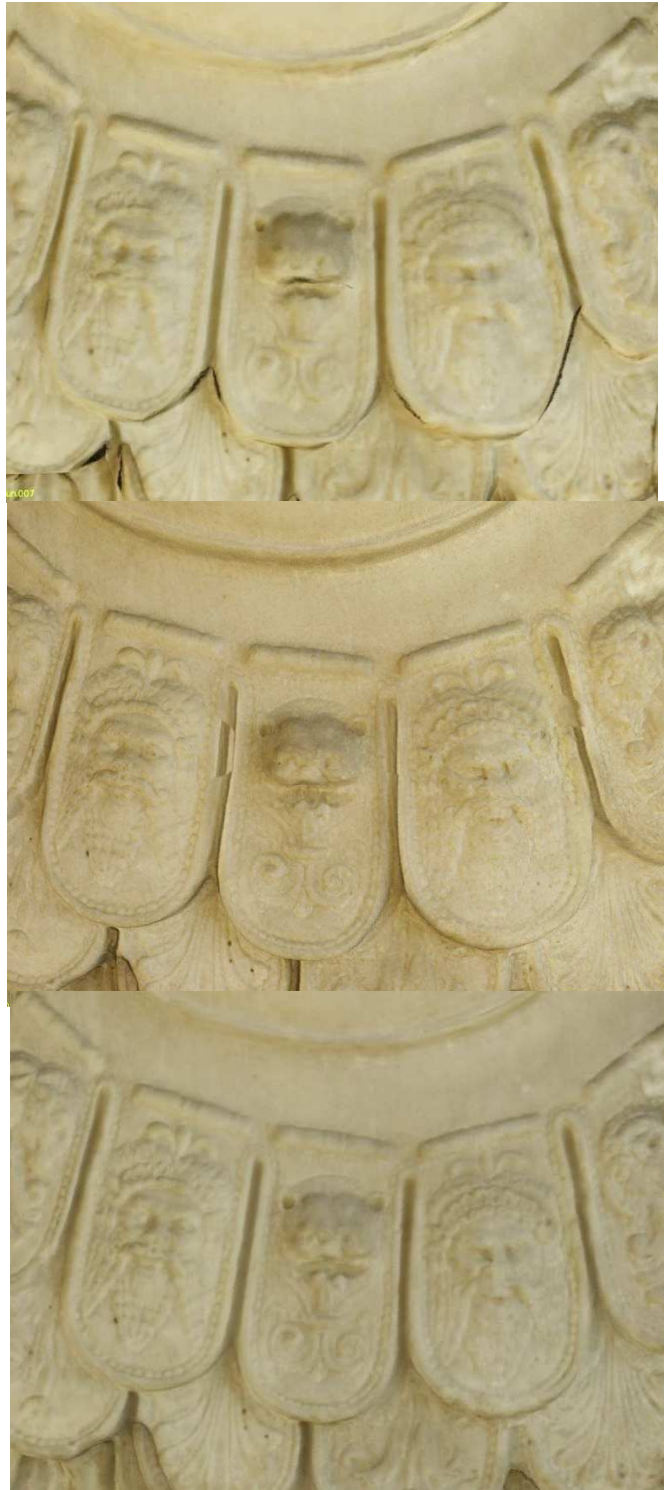


Figure 114. Zoom on LP model with NM, Displaced SubDivision Surface and original HP model.

From the comparison of (Figure 114), it is possible to notice that the LP model with the NM applied, even though shows a good level of detail considering the type of surface used, has more sharp profiles, since it is constituted by big size triangles and so the mesh is much more smoothed. The Displaced SubDivision Surface, instead, offers a higher degree of fidelity to the original HP model also from a geometrical point of view. As reported in (Figure 115), the discards between the generated displaced surface and the original HP are mostly around 0,000 m over the whole surface.

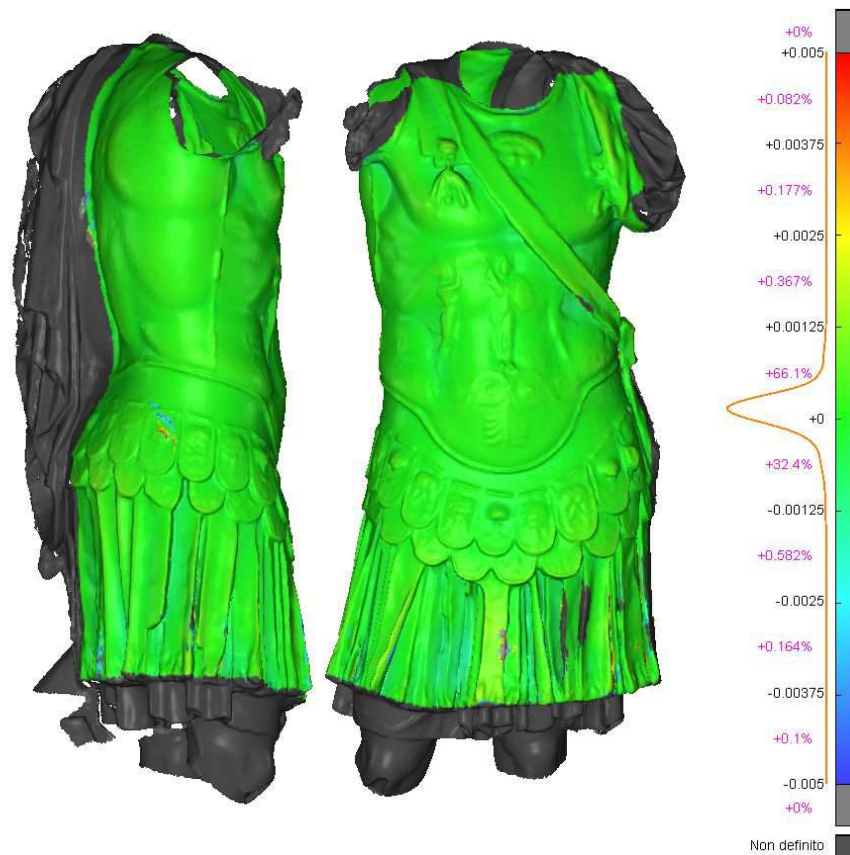
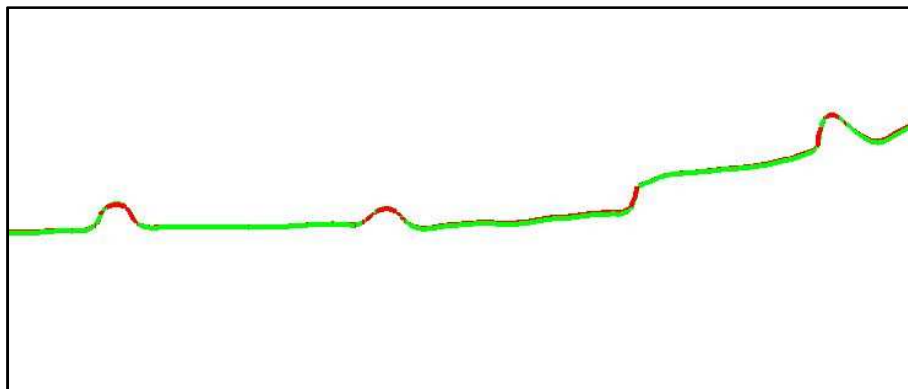
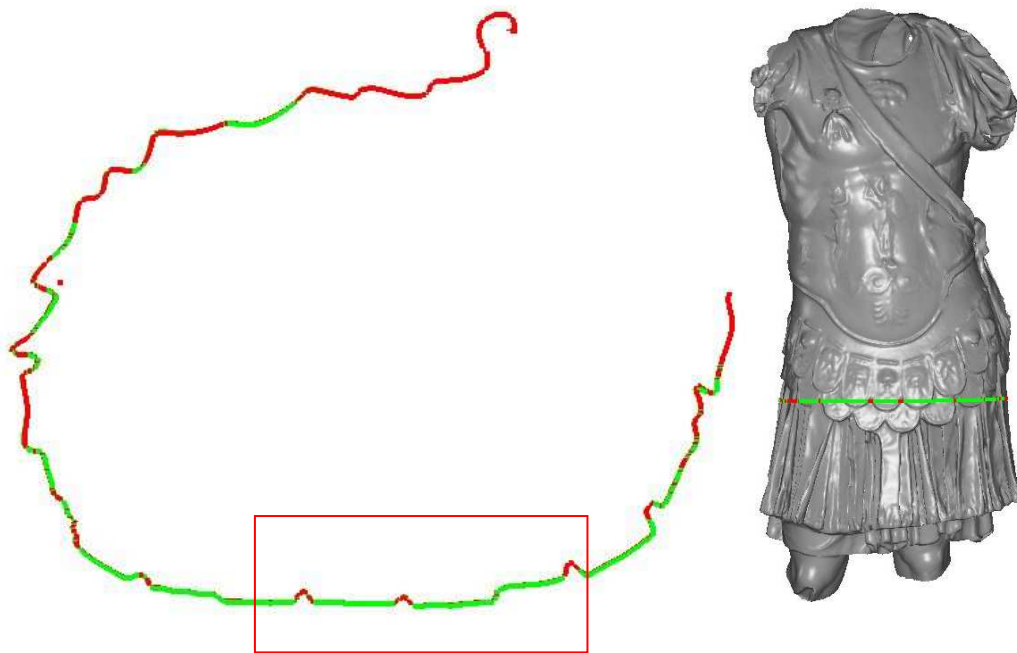


Figure 115. Displacement between the original HP model and the Displaced SubDivision Surface

This is also proved extracting some section profiles, again, from the HP and the Displaced SubDivision Surface. The two polylines totally overlap and, moreover, the displaced subdivision polyline contains a higher number of vertices (the detail is certainly not improved, in fact it is necessary to not increase too much this value in order to not generate a useless and too heavy mesh).



	N. of points
HP polyline	1811
Retopo – Displaced SubDivision Surface	2560

Figure 116. Section profiles extracted from the HP (red) and the Displaced SubDivision Surface (green) models.

5.1.3 The frieze of the Augustus arch optimization

The last optimization process applied to the frieze of the arch focused on the evaluation of the quality of orthographic views extracted from the final edited models, also in comparison to the HP ones. The main aim was to define the level of detail achievable on the optimized models connected to the possibility to extract a detailed 2D drawing from the orthophoto.

Also in this case, the workflow followed two optimization procedures, generating a LP model, with a Normal Map projected, and a Displaced Subdivision surface.

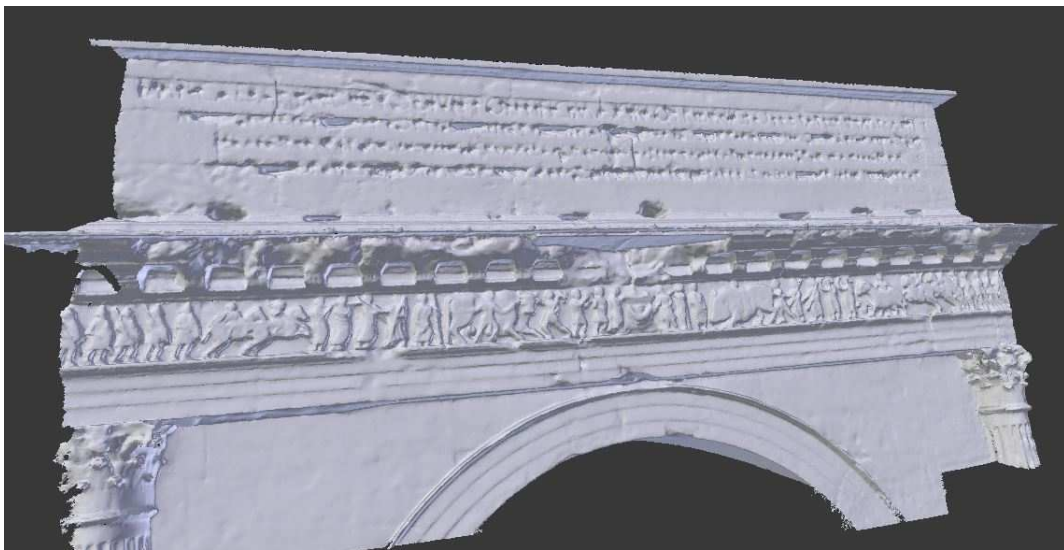


Figure 117. HP model of the north frieze.

Optimization with LP model and Normal maps

The original HP models has been edited, cleaned and topologically corrected as well as the previous test cases. Once processed a HP model lacking of topological errors, it has been imported in MeshLab and a LP model, constituted by 15.000 faces has been generated (Figure 118). A lower number of faces would produce a too smoothed LP model, not able to achieve the final desired level of detail. The LP model has been then imported in Blender and a new UV map has been computed editing the *Smart UV Project* tool. Through the baking between the HP and the decimated model, a Normal map has been computed and projected on the LP model (Figure 119 - Figure 120). A new diffuse color map has been computed in Photoscan, as in the above cases, importing the new reparametrized LP model, and then projected in Blender (Figure 119 - Figure 121).

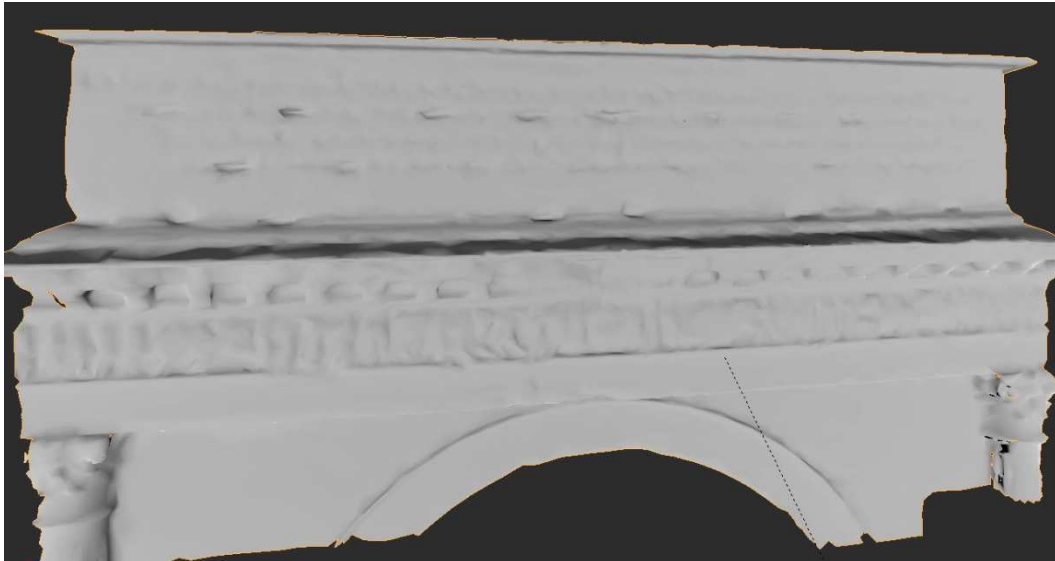


Figure 118. LP model generated in MeshLab – 15.000 faces.

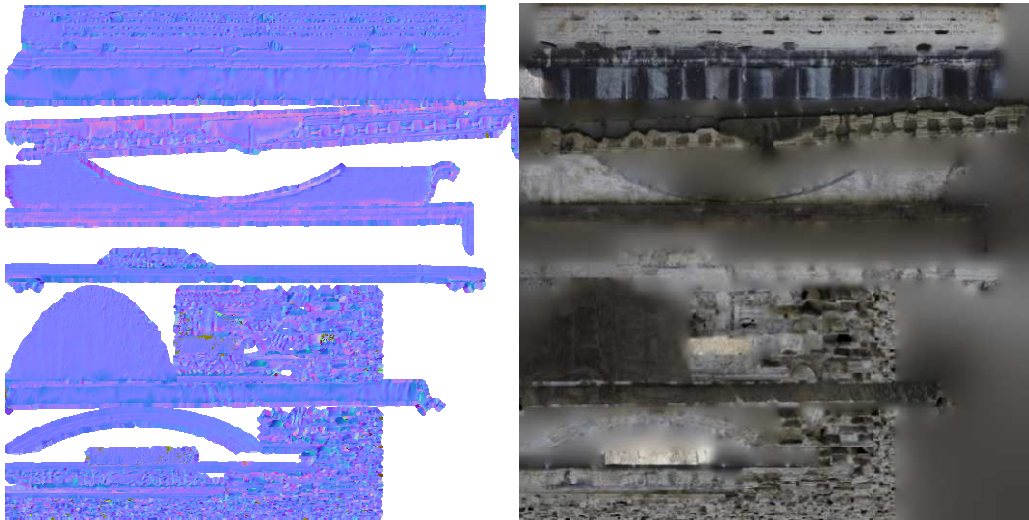


Figure 119. On the left the Normal map computed in Blender; on the right the diffuse color map recalculated in Photoscan keeping the edited UV map.

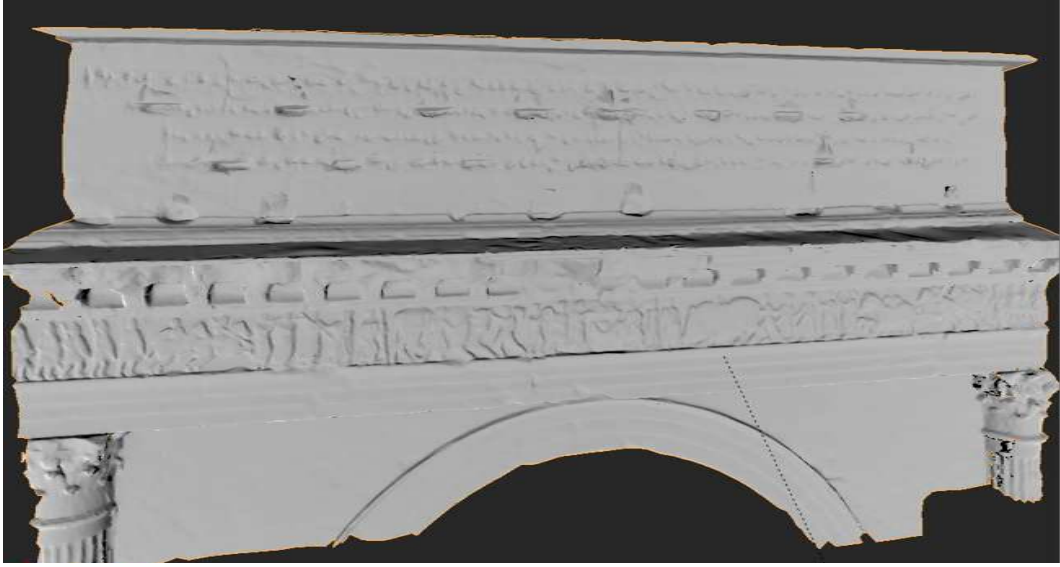


Figure 120. LP model with the NM applied.





Figure 121. Textured LP model with NM and diffuse color maps applied.

Also in this case it is evident how the Normal map is able to reproduce the missing detail, fulfilling the aims of the test. Once again the final file sizes have been compared to the original HP mesh and reported in (Table 18 - Table 19).

	N. vertices	N. of faces	KB file	% Faces reduction	% KB reduction
Original HP mesh	631.468	1.236.503	48.941	-	-
LP mesh	7.743	15.000	1.219	-98,8%	-97,5%

Table 18. Report of the file sizes involved in the optimization process as well as the KB reduction from the HP model to the LP one.

	KB file
Original HP mesh	48.941
LP mesh	1.219
Normal Map	4.610
Diffuse color map	701

Table 19. Report of the file sizes involved in the optimization process

Optimization with Displaced subdivision surface

In the second optimization process a retopology process has been manually applied over the HP model, focusing just on the illustrated frieze, which represents, in particular, 14 Gauls tribes entering the Roman world (Figure 122).

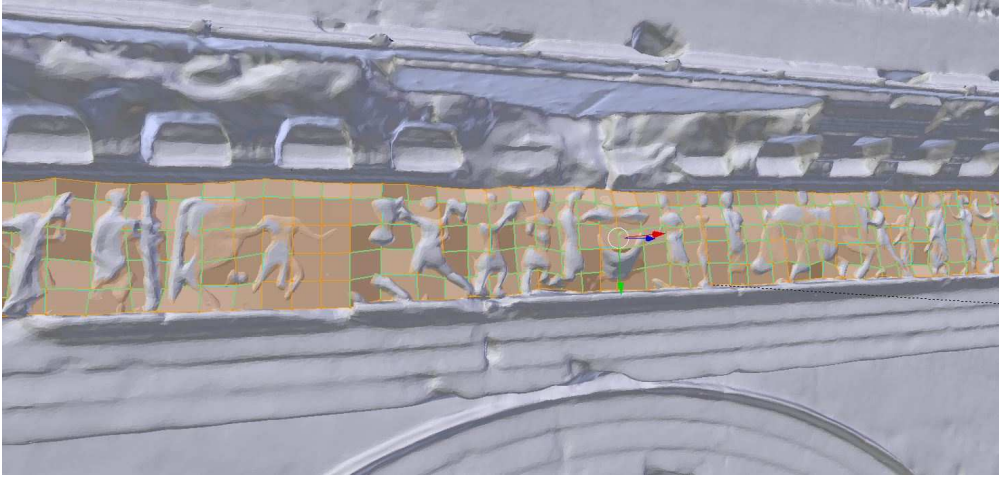


Figure 122. Retopologized mesh projected over the HP model.

Once completed the retopology process, the subdivision surface modifier has been applied to the LP model (setting Level 5) and then a displacement map has been calculated using the UV map created with the *Smart UV project* (Figure 123 - Figure 124).

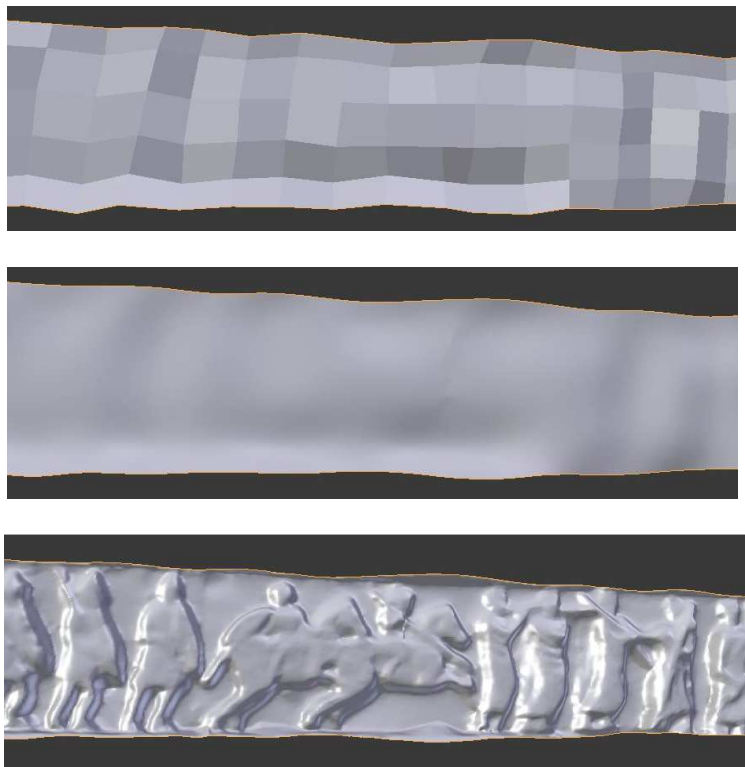


Figure 123. Above: Retopo mesh; middle: subdivided surface; below: displaced subdivision surface



Figure 124. Displacement map

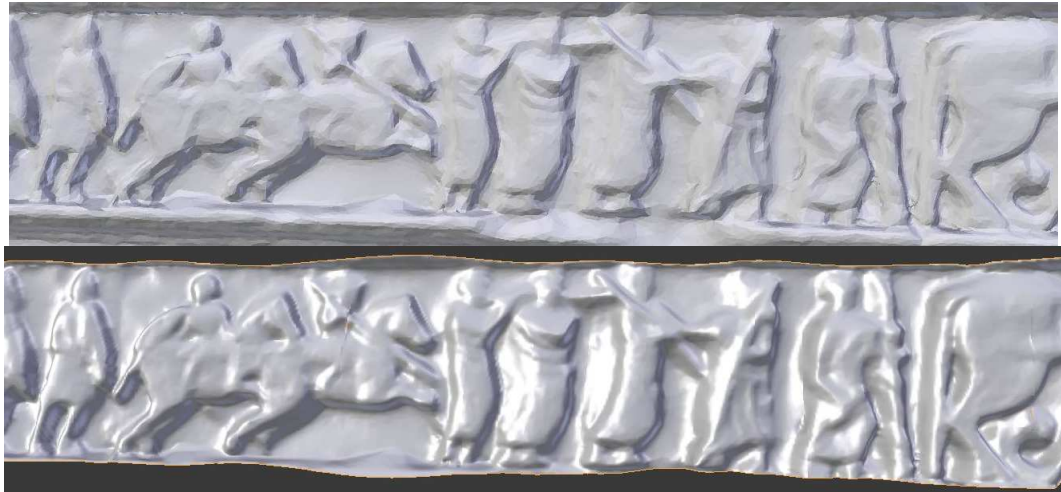


Figure 125. Above: zoom over the displaced subdivison surface; below: zoom over the HP mesh

The different file sizes are compared and reported in (Table 20 - Table 21).

	N. vertices	N. of faces	KB file	% Faces reduction	% KB reduction
Original HP mesh	58.447	115.238	4.193	-	-
Retopo mesh	502	385	52	-99,7%	-98,8%

Table 20. Comparison of the file sizes of the faces and KB reduction from the original HP model to the LP one.

	KB file
Original HP mesh	4.193
Retopo mesh	52
Displacement Map	1.352
Diffuse color map	174

Table 21. Report of the file sizes involved in the optimization process.

A new diffuse color map has been generated importing in Photoscan the retopologized and reparametrized model and then re-projected on the displaced subdivision surface. The result satisfied the aim of maintaining a high level of precision and fidelity to the HP model.



Figure 126. Final displaced subdivision surface without and with diffuse color map

Three Orthophotos have been extracted from the HP model and the optimized one, showing their high level of visual correspondence. A more thorough analysis about the information deductible from the processed model is proposed in the following paragraph.





Figure 127. Above: original HP orthophoto; middle: orthophoto from LP model without NM applied; below: orthophoto from LP model with NM applied.

Chapter 6

Additional evaluations and conclusions

6.1 Comparisons through an automatic edge detection on extracted orthographic views

The last processing tests aimed at define the quality of the optimized models through the evaluation of the type and quality of possible data extraction for a 2D representation. This test has been applied on a reduced portion of the models. From the point of view of a surveyor, a restorer, a historian, it is essential to be able to extract from 3D models specific and detailed representation of the objects of interest. Traditional 2D drawings has always a central role in any documentation phase. For this reason, a central point of interest has been the evaluation of what the final model allows to see, know, distinguish and represent, in comparison to the detailed mesh.

The aim of this test is to identify, in comparison to the HP model:

- What kind of information is it possible to extract from the optimized model?
- Which is their level of detail?
- Are them accurate enough to fulfil the conservation and documentation requests?

An output data to prove this, can be represented by a 2D traditional architectural representation, that derives from a 2D vectorialization deduced, for example, from an orthophoto.

The test here presented has focused, in particular, on the roman bust and frieze test cases, since they offer majors decorative elements and tiny details. Whereas, the Lina test case does not provide the ideal characteristics for a vectors extraction since it has a too smoothed and continuative surface, without decorative elements.

Some differences between the generated models and extractable images can be already easily detected by the naked eye and a user intended to vectorialize such representations would probably generate slightly different restitutions, depending on which 3D models is used as a source. For these reasons, but in order to provide objectives evaluations, an automatic procedure of feature extraction, which goes beyond a personal and subjective point of view, has been applied. The aim of this approach is to test which kind of 2D vectorial information can be extracted from the optimized models, following an automatic approach and comparing the results.

To do this, many automatic tools can be tested. Nowadays, many algorithms of edge detection are available (Roberts, Prewitt, Sobel and Canny operator are the most known) and many applications have studied their behaviour and have compared them to each other (Maini & Aggarwal, 2009)(Shrivakshan & Chandrasekar, 2012). Edge detection is an image processing technique that tries to find boundaries of objects within images. It works by detecting discontinuities in brightness and it is often used for image segmentation and data extraction in image processing, computer vision, and machine vision fields. For this test, MatLab software has been used and two well-known algorithms have been applied (the high performing ones):

- Canny algorithm (Canny, 1987) (Figure 128) detects edges by looking for local maxima of the gradient of I. The MatLab *edge* function calculates the gradient using the derivative of a Gaussian filter. This approach employs two thresholds to detect strong and weak edges, including weak edges in the results if they are connected to strong edges. By using two thresholds, the Canny method works better than the other methods against noise, and better detect true weak edges (<https://it.mathworks.com/help/images/ref/edge.html>).
- Sobel algorithm finds edges at those points where the gradient of the image I is maximum, using the Sobel approximation to the derivative.

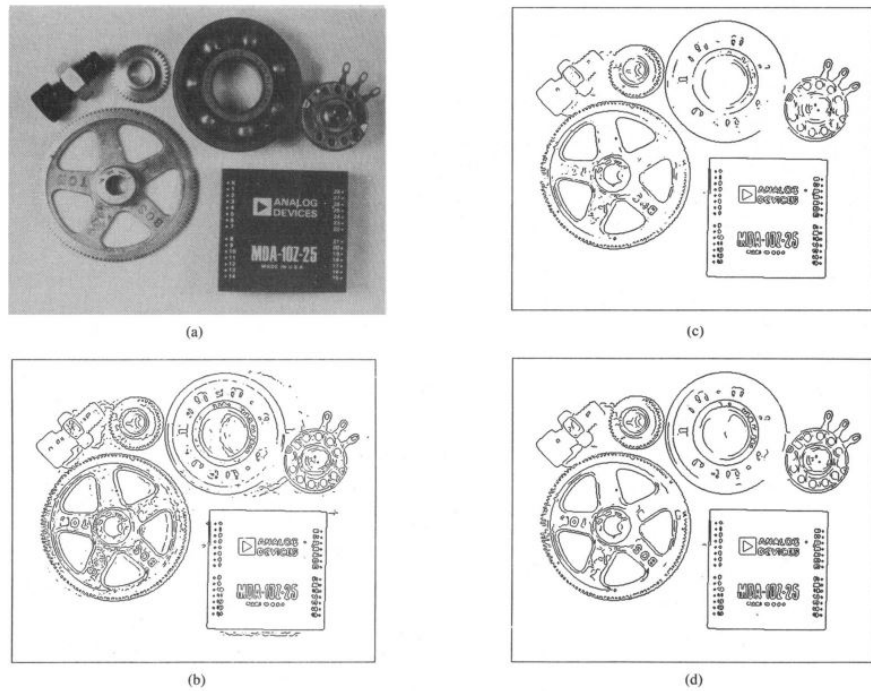


Figure 128. An example of the edge detection performed by Canny algorithm. Source: (Canny, J., 1987)

Edge detection applied to orthographic views of the optimized model

To approach this 2D restitution and comparison, several rendering views of the *pterigi* part of the roman bust have been extracted, either from the original HP model and from the optimized ones, using the same camera, positioned in the same point and with the same light (the same images have been presented also in 5.1.2). The frieze, instead, offers the chance to extract a more traditional orthophoto representation. An orthographic view has been extracted from the original Photoscan HP model, the LP with the NM applied and from the displaced subdivision surface (Figure 129).



Figure 129. Above: original HP model; middle: LP model with NM; below: displaced subdivision surface

The first step in MatLab has been the opening of the image file:

```
I = imread('LP model with NM.png');
imshow(I);
```

Then the image has been converted in a greyscale image, which is necessary to apply the edge detection filters.

```
ig = rgb2gray(IGB);
figure
imshow(ig)
```

After this commands the software opens the chosen image in greyscale.

The following step consisted in the edge detection command. The MatLab code to apply an edge detection algorithm is the following:

```
BW = edge(ig, method)
Es. BW = edge(ig, 'canny')
```

Several further information can be added to the syntax, in the case of the Canny algorithm:

```
BW = edge(ig,method,threshold)
```

Sensitivity *threshold*, specified as a 2-element vector for the 'Canny', returns all edges that are stronger than threshold. You can specify threshold as a 2-element vector of the form [low high] with low and high values in the range [0 1]. You can also specify threshold as a numeric scalar, which edge assigns to the higher threshold.

```
BW = edge(ig,method,threshold,direction)
```


Direction of edges to detect, specified as 'horizontal', 'vertical', or 'both'. The direction argument is only valid when the method is 'Sobel', 'Prewitt', or 'Roberts'.

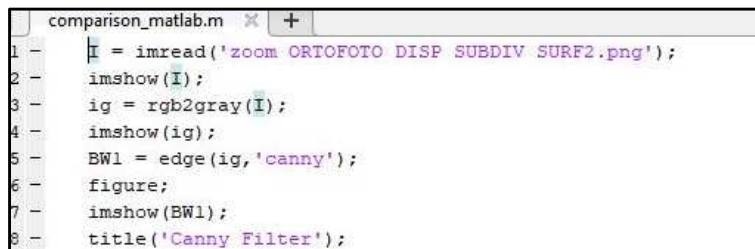
```
BW = edge(ig,method,threshold,sigma)
```

Standard deviation of the filter, specified as a scalar. The sigma argument is supported by the 'Canny' and 'log' methods only and it specifies the standard deviation of the Gaussian filter.

It is also possible to combine in the same time two edge detection algorithms. Here is an example on how to apply both the Sobel and Canny edge detectors to the image and display them for comparison.

```
BW1 = edge(I,'sobel');  
BW2 = edge(I,'canny');  
figure;  
imshowpair(BW1,BW2,'montage')  
title('Sobel Filter          Canny Filter');
```

Once ran the command, the algorithm generates a new B/W image with the edges detected. The number of edges can be controlled (increased or decreased) according to the inserted threshold and sigma values.



```
comparison_matlab.m x +  
1 - I = imread('zoom ORTOFOTO DISP SUBDIV SURF2.png');  
2 - imshow(I);  
3 - ig = rgb2gray(I);  
4 - imshow(ig);  
5 - BW1 = edge(ig,'canny');  
6 - figure;  
7 - imshow(BW1);  
8 - title('Canny Filter');
```

Figure 130. An example of the syntax applied with default values.

The first test has been applied to the *pterigi* portion. The images, after several attempts with different parameters, have been filtered using a Threshold value between 0.03-0.08 and a sigma of 0.8.

The first attempt has been processed on the HP model (Figure 131), used as reference to further compare the results of the optimized models. In this case, the model offers, of course, a high level of detail and the edge detector is able to faithfully extract all the decorative elements and figures represented.



Figure 131. Canny filter HP. Threshold [0.03 0.08] sigma (0.8).

The second test has been applied to the LP model with NM. In this case, even though the model lacks most of the 3D geometrical information, the shadows projected by the NM re-produce a sufficient level of detail for a 2D restitution and the edge detector is able to recognize and extract the main decorative elements and illustrated figures. However, as highlighted in the image with red dashed lines, some visible profiles of the model are very sharp and this influences the edge operator which, in those points, extract a wrong shape of the object.



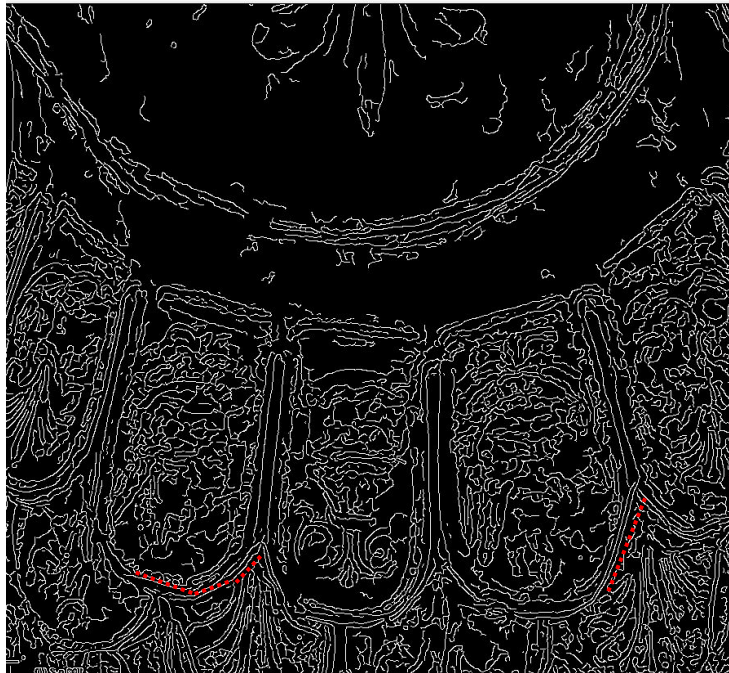


Figure 132. Canny filter - LP model with NM applied. Threshold [0.03 0.08] sigma (0.8).

The same filter with same parameters has been then applied to the Displaced SubD surface (Figure 133). In this case, it again recognizes and represents the most decorative elements of the model but also much more profiles that have to be further filtered and

deleted. It is possible to notice that this representation, if compared to the LP model with NM, is more faithful to the original HP and present fewer errors.





Figure 133. Canny filter default value – Displaced subdivision surface. Threshold [0.03 0.08] sigma (0.8).

Moreover, the Sobel filter has been also tested to the LP model with NM but with less satisfying results, since it extracts only the major profiles (Figure 134).



Figure 134. Sobel edge detection. Default value.

The orthophotos of the frieze portion have been filtered with a Threshold of 0.2 and sigma 3. The HP model provides a high level of detail and the edge detector is again able to extract the main profiles of the elements represented (Figure 135).



Figure 135. Canny edge detector applied on a zoomed portion of the frieze – HP model- Threshold 0.2, sigma 3.

The detail of the LP model with NM offers the filter the possibility to recognize and extract the main geometries of the figures. The extracted profiles allow to retrace the

sculpted elements even though they are again slightly sharp and some errors due to the coarse geometry of the model affect the representation (Figure 136).

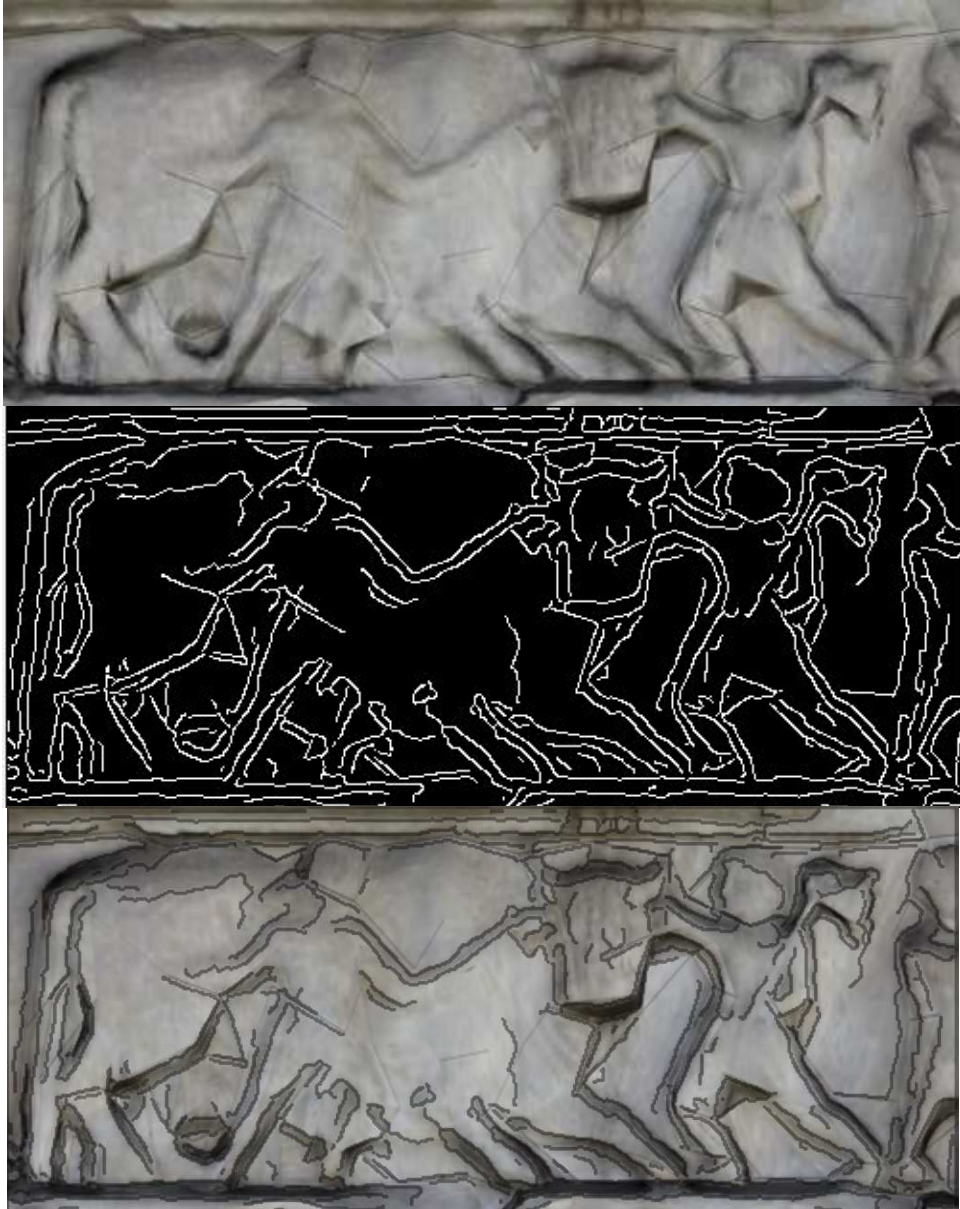


Figure 136. Canny edge detector applied on a zoomed portion of the frieze. Threshold 0.2, sigma 3.

Applying the same settings to the displaced SubD surface, it is possible to extract edges similar to those extracted from the HP model.



Figure 137. Canny edge detector applied on a zoomed portion of the frieze - Displaced subdivision surface. Threshold 0.2, sigma 3.

As visible especially in this test case, edge detector extracts all the profiles in which it recognizes a discontinuity in brightness, reason why it may generate two contour lines of the same profile, which in this case correspond to the figure profile in relief and its shadow. Furthermore, the algorithm may extract edges only visible on the diffuse color texture and not really present in the model geometry, which means that the resolution of

the radiometric information has a central role in this process. The HP models, in fact, offer a higher resolution diffuse color texture and this aspect influences the outputs. Moreover, the diffuse color texture also offers to the algorithm the chance to detect possible material damages or decay, which are essential aspects to be documented in any CH documentation process.

The results, even though do not produce a ready to be used representation, allow to point out some general interesting considerations. The edges extracted from both LP models with Normal maps applied reflect a more segmented surface. The profiles are sharper, as visible, in the case of the bust in the *pterigi* fringes contours, and, in the case of the frieze, on the outlines of the figures. Whereas the displaced subdivision surface allows to extract smoother profiles more assimilated to the original HP model. These differences are due to the greater triangles dimension of the LP model, deriving from the previous hard decimation, which influences the edge detection.

This last evaluation proves that, even though great results can be achieved optimizing a model with the projection of the normal map, a displacement map applied on a subdivided quadrangular surface stores and represents a higher level of detail, comparable to the original HP model and provides a level of information well-suited to specialistic studies usually requested in the Cultural Heritage documentation domain.

6.2 Final considerations

The obtained results allow to point out some considerations about the two pipelines tested, considering different possible aims that a 3D documentation of Cultural Heritage assets should fulfil.

The first optimization process, which foresees a hard decimation of the HP model and the computation and projection of a NM map, allows to produce a 3D object that visible looks like the original one in a very low file size. This aspect makes this model easy to be handled and shared in most portable devices, tablets or published in Internet. The so produced model, however, offers a low real geometric detail. If the user would like to extract some measures, this LP model does not provide adequate data. In this case, a simple visualization and navigation application is advisable and preferable. It is important to underline that an aggressive decimation has been applied to the original HP model, in order to test and take to extremes the potentialities of the NMs. In other test cases it is possible to process a lower decimation of the detailed model, ensuring a minimum level of geometric detail in the final optimized model. The right balance

between decimation and file size depends on a case by case basis and according to the aims of the research.

The second pipeline allows to generate a final optimized model that looks like the original ones, but in this case the similarity is both from a perceptive and geometrical point of view. From these second kind of models, it is possible to extract accurate measures, section profiles, and this characteristic makes them suitable for multipurpose metric analysis and not only for visualization applications. Another advantage offered by such models is the LoDs implementation, which can be increased or decreased according to the user need.

A further consideration concerns the diffuse color textures. The automatic texture generation of the photogrammetric pipeline does not take into consideration a further processing and correction, and it generates diffuse color maps with many unrecognisable atlas, difficult to be further edited. In the test cases presented, the possibility to generate a user-defined UV map associated to the optimized model and to further generate a new diffuse color texture according to it, enables the possibility to apply some corrections to the images, deleting, for example, shadows effects and improving their radiometric quality.

The generated optimized models, thereby, can visibly and faithfully approximate the original HP data, offering output data that for most looks like the original one, but they differ from each other if a deeper analysis is applied. As described in 6.1, slightly different information can be extracted applying an automatic vectorialization to the orthophoto or images extracted. This comparison demonstrates that the first optimization procedure is less indicated if the final aim is the extraction of drawings, sections or other traditional architectural representation, since the great dimension of the triangles cripple the perception of the shapes in some points. Whereas the second pipeline is more suitable for this aim, offering a level of detail comparable to the HP model. However, it is necessary to highlight that the resolution of the diffuse color texture may hardly influence this process. In fact, it has a central role, in particular, where the geometry of the model is very poor or for the detection of the material decay. For these reasons, it is always necessary to ensure an adequate level of the detail also from the radiometric point of view.

Moreover, the comparison between the file sizes and the number of points of extracted polylines, suggests to pay attention to two factors:

- the file size of the image textures must not be too heavy, since their projection influences the GPU memory at the rendering time;

- the level of subdivision to be applied on the retopologized model must not be too high, since it would imply a higher memory consumption without a real increase of the level of detail.

6.3 Conclusions and perspectives

This research proved once again how close range photogrammetry may offer many advantages for the CH knowledge, documentation and communication, thanks to an efficient digitization semi-automatic process, thanks to the SfM implementation, that allows to produce highly detailed textured 3D models. Such models ensure great communication capabilities, storing both detailed geometric and radiometric information and providing useful data for multipurpose aims. The photogrammetric pipeline offers great advantages, especially when a high radiometric accuracy is needed. With regard to this, as demonstrated in this research, an interesting implementation in SfM and image matching software would be the possibility to better control the parameterization procedure with the direct UV map editing and the following diffuse color texture generation process. This improvement would bring photogrammetry closer to Computer Vision applications.

Facing the challenge to easily manage big amount of data, the optimization pipeline proposed in this research demonstrates how to hardly reduce the final file sizes of detailed 3D models producing simplified mesh that, however, look like the original models but that can be easier visualized, navigated and shared. The proposed optimization tested two similar possible methodologies that offer different results that can satisfy multi-purpose applications.

This workflow represents one of the many optimization processing that today can be applied to high detailed models for their visualization and sharing, and continuous research should be encouraged, leading to the definition of a shared common standard. This is necessary also because modern sensors for 3D metric survey are more and more efficient and allow to acquire and manage more and more data so that it is further essential to be able to share and communicate them without losing important information and details, both for specialistic studies and didactic fruitions. For these reasons, it is essential to choose the best modelling and optimization method according to the needs that the model has to fulfil.

The evaluation of the final accuracy and precision of the optimized model has been an indispensable step from the metric point of view of a Geomatic scientist. The applied game engine tools borrowed from Computer Graphic field, in fact, are not born for metric

applications and the determination of the final quality of the remaining information has been essential. Many studies have already tried these tools in application to mesh model from point clouds, also in the field of CH, but in none of them a metric evaluation has been conducted on the final optimized results in order to define their accuracy and suitability for specialistic analysis. Making a comparison between the original HP, assumed as reference, with the LP models, this research proved that such tools offer great potentialities, that can be very interesting also for the Geomatic field.

Furthermore, the edge detection algorithms applied to orthophotos of the case studies represent an innovative attempt to show an objective evaluation of the results. Even though the extracted vectorialization is far to be exhaustive from the point of view of an historian or a restorer that need a representation of the decoration or of the state of decay of the object, it allowed to point out some important observations about the quality and readability of the optimized models.

Another contribution presented in the thesis is constituted by the comparison between three Normal maps generated by three different software. By now, in fact, many different algorithms allow to extract a Normal map from an image (i.e. Photoshop) but the baking process developed in Game Engine applications, that build a Normal Map through a comparison between a HP and a LP provides, as showed, a different result that lead to a different visualization of the object once projected.

Future perspectives of this work could be surely addressed on the implementation of such optimized models in multi-purpose applications (i.e. of Virtual or Augmented Reality or in web pages) in order to define the achievable output. By now, as mentioned in Chapter 3, there are already some examples of VR, AR and web sharing applications that make use of so optimized models and this kind of implementation should be encouraged and developed, with the awareness of the importance of the original metric accuracy.

Furthermore, it would be interesting to test the application of the proposed pipeline to other multiscale objects (buildings, architectural complexes, landscapes from terrestrial and aerial surveys) in order to define its potentialities and limits in comparison to other methods. The proposed tools, borrowed from Game Engine field, offer well known results if applied to small assets, such the case studies presented, but it would be interesting to apply them also to multi scale models.

The proposed optimization may also offer advantages for those applications that need to link heterogeneous and descriptive data to semantically divided 3D models (i. e. for HBIM). Rather than applying a hard simplification and segmentation to the original detailed surfaces, possibly losing lots of information, it could be interesting to test the

presented optimized models as a slight graphic base to which link multi-contents information.

References

- Adembri, B., Di Tondo, S., & Fantini, F. (2012). New advancing of the research on the architecture with concave and convex rhythms at Hadrian ' s Villa ... In *16th International Conference on "Cultural Heritage and New Technologies" (CHNT 16) Vienna, 14-16 Novembre 2011* (pp. 125–139). Vienna: Museen der Stadt WienStadtarchäologie.
- Agostoni, A., Barello, F., Borghi, A., & Compagnoni, R. (2016). The White Marble of the Arch of Augustus (Susa, North-Western Italy): Mineralogical and Petrographic Analysis for the Definition of its Origin. *Archaeometry*, *59*(3), 395–416. <https://doi.org/10.1111/arc.12251>
- Aguiaro, G., Remondino, F., Girardi, G., Von Schwerin, J., Richards-Risetto, H., & De Amicis, R. (2011). QueryArch3D: Querying and Visualising 3D Models of a Maya Archaeological Site in a Web-Based Interface. *Geoinformatics FCE CTU*, *6*(0), 10–17. <https://doi.org/10.14311/gi.6.2>
- Akca, D. (2006). 3D modeling of cultural heritage objects with a structure light system. *Mediterranean Arhaeology and Archaeometry*, *12*(1), 139–152.
- Aliaga, D. G., Bertino, E., & Valtolina, S. (2011). DECHO—a framework for the digital exploration of cultural heritage objects. *Journal on Computing and Cultural Heritage*, *3*(3), 1–26. <https://doi.org/10.1145/1921614.1921619>
- Alliez, P., Ucelli, G., Gotsman, C., & Attene, M. (2008). Recent Advances in Remeshing of Surfaces. In *Shape analysis and structuring* (pp. 53–82). IEEE Comput. Soc. https://doi.org/10.1007/978-3-540-33265-7_2
- Alsadik, B. (2016). Crowdsourced and web-published videos for 3D documentation of cultural heritage objects. *Journal of Cultural Heritage*, *21*, 899–903. <https://doi.org/10.1016/j.culher.2016.03.010>
- Auer, M., Aguiaro, G., Billen, N., Loos, L., & Zipf, A. (2014). Web-based Visualization and Query of semantically segmented multiresolution 3D Models in the Field of Cultural Heritage. *ISPRS Annals of Photogrammetry, Remote Sensing and Spatial Information Sciences*, *II-5*(June), 33–39. <https://doi.org/10.5194/isprsannals-II-5-33-2014>
- Baik, A., Alitany, A., Boehm, J., & Robson, S. (2014). Jeddah Historical Building Information Modelling "JHBIM" – Object Library. *ISPRS Annals of Photogrammetry, Remote Sensing and Spatial Information Sciences*, *II-5*(June), 41–47. <https://doi.org/10.5194/isprsannals-II-5-41-2014>

- Balletti, C., Adami, A., Guerra, F., & Vernier, P. (2012). Dal rilievo alla maquette: il caso di San Michele in Isola. *Archeomatica*, 3(2), 24–30. Retrieved from <http://mediageo.it/ojs/index.php/archeomatica/article/view/122>
- Balletti, C., D’Agnano, F., Guerra, F., & Vernier, P. (2016). From point cloud to digital fabrication: a tangible reconstruction of Ca’ Venier dei Leoni, the Guggenheim Museum in Venice. *ISPRS Annals of Photogrammetry, Remote Sensing and Spatial Information Sciences*, III-5(July), 43–49. <https://doi.org/10.5194/isprsannals-III-5-43-2016>
- Barazzetti, L., Remondino, F., & Scaioni, M. (2010). Automation in 3D reconstruction: results on different kinds of close-range blocks. *International Archives of Photogrammetry, Remote Sensing and Spatial Information Sciences*, XXXVIII(5), 55–61.
- Bay, H., Tuytelaars, T., & Van Gool, L. (2006). SURF: Speeded Up Robust Features. In *Lecture Notes in Computer Science (including subseries Lecture Notes in Artificial Intelligence and Lecture Notes in Bioinformatics)* (Vol. 3951 LNCS, pp. 404–417). Springer, Berlin, Heidelberg. https://doi.org/10.1007/11744023_32
- Behr, J., Eschler, P., Jung, Y., & Zöllner, M. (2009). X3DOM - A DOM-based HTML5/X3D Integration Model Johannes. In *Proceedings of the 14th International Conference on 3D Web Technology - Web3D ’09* (Vol. 1, p. 127). New York, New York, USA: ACM Press. <https://doi.org/10.1145/1559764.1559784>
- Beltramo, S., Donadio, E., & Spanò, A. (2018). Stratigraphic Analyses, Historical Evidences and 3D Documentation Tools. Deepening Built Heritage: New researches for historical building sites in Staffarda. In C. Inglese & A. Ippolito (Eds.), *Analysis, Conservation, and Restoration of Tangible and Intangible Cultural Heritage* (in press). IGI Global.
- Bertolini-Cestari, C., Spanò, A. T., Invernizzi, S., Donadio, E., Marzi, T., & Sammartano, G. (2016). *The role of terrestrial LiDAR for mechanical and safety evaluation of historic timber trusses*. (H. Cruz, J. Saporiti Machado, A. Campos Costa, P. Xavier Candeias, N. Ruggieri, & J. Manuel Catarino, Eds.), *Lecture Notes in Civil Engineering* (Vol. 1). Cham: Springer International Publishing. <https://doi.org/10.1007/978-3-319-39492-3>
- Blinn, J. F. (1978). Simulation of wrinkled surfaces. *ACM SIGGRAPH Computer Graphics*, 12(3), 286–292. <https://doi.org/10.1145/965139.507101>
- Bolter, J. D., & Grusin, R. A. (1996). Remediation. *Configurations*, 4(3), 311–358. <https://doi.org/10.1353/con.1996.0018>
- Bonacini, E. (2013). Communication and enhancement of Italian cultural heritage by Google *. *Palabra Clave*, 2(Cc), 49–63. Retrieved from <http://www.palabraclave.fahce.unlp.edu.ar>
- Bonfanti, C., Chiabrando, F., & Spanò, A. (2010). High Accuracy Images and Range Based Acquiring for Artistic. *International Archives of Photogrammetry, Remote Sensing and Spatial Information Sciences*, XXXVIII(5), 109–114. Retrieved from <http://www.isprs.org/proceedings/XXXVIII/part5/papers/166.pdf>
- Cadario, M. (2005). Ipotesi sulla circolazione dell’immagine loricata in età imperiale: i

- torsi giulio-claudi di Susa. In F. Slavazzi & S. Maggi (Eds.), *La scultura romana dell'Italia settentrionale. Quarant'anni dopo la mostra di Bologna. Atti del Convegno Internazionale di Studi. Pavia, 22-23 settembre 2005* (pp. 1000–1011). Firenze: All'Insegna del Giglio.
- Campana, S. (2014). 3D modelling in archaeology and cultural heritage – Theory and best practice. In F. Remondino & S. Campana (Eds.), *3D Modeling in Archaeology and Cultural Heritage Theory and Best Practices* (pp. 7–12). Archaeopress.
- Campomanes-Alvarez, B. R., Damas, S., & Cordon, O. (2012). Mesh simplification for 3D modeling using evolutionary multi-objective optimization. In *2012 IEEE Congress on Evolutionary Computation* (pp. 1–8). IEEE. <https://doi.org/10.1109/CEC.2012.6252887>
- Canciani, M., Conigliaro, E., Del Grasso, M., Papalini, P., & Saccone, M. (2016). 3D survey and augmented reality for cultural heritage. The case study of aurelian wall at Casta Praetoria in Rome. *ISPRS - International Archives of the Photogrammetry, Remote Sensing and Spatial Information Sciences, XLI-B5*, 931–937. <https://doi.org/10.5194/isprsarchives-XLI-B5-931-2016>
- Canny, J. (1987). A Computational Approach to Edge Detection. In *Readings in Computer Vision* (pp. 184–203). Elsevier. <https://doi.org/10.1016/B978-0-08-051581-6.50024-6>
- Catmull, E., & Clark, J. (1978). Recursively generated B-spline surfaces on arbitrary topological meshes. *Computer-Aided Design*, *10*(6), 350–355. [https://doi.org/10.1016/0010-4485\(78\)90110-0](https://doi.org/10.1016/0010-4485(78)90110-0)
- Chiabrandò, F., Donadio, E., Fernandez-palacios, B., Remondino, F., & Spanò, A. (2014). L 'arco di Augusto a Susa: un nuovo modello digitale per rinnovate indagini. Tecnologie innovative per il rilievo metrico terrestre. *Segusium*, *52*, 217–232.
- Chiabrandò, F., Donadio, E., & Rinaudo, F. (2015). SfM for Orthophoto to Generation: A Winning Approach for Cultural Heritage Knowledge. *ISPRS - International Archives of the Photogrammetry, Remote Sensing and Spatial Information Sciences, XL-5/W7*, 91–98. <https://doi.org/10.5194/isprsarchives-XL-5-W7-91-2015>
- Chiabrandò, F., Donadio, E., Sammartano, G., & Spanò, A. (2015). Reality based modelling training. Photomodelling and LiDAR techniques for the St. Uberto Church in Venaria Reale. In *Atti del XXXVII Convegno Internazionale dei Docenti della Rappresentazione*. Retrieved from http://porto.polito.it/2625257/1/paper_UID_eng.pdf
- Chiabrandò, F., Donadio, E., Sammartano, G., & Spanò, A. (2016). La tecnologia laser scanning per la valutazione statica delle strutture storiche. *GEOMedia*, *20*(4), 12–17. Retrieved from http://porto.polito.it/2666050/1/1332_5722_1_PB.pdf
- Chiabrandò, F., Lingua, A., Noardo, F., & Spano, A. (2014). 3D modelling of trompe l'oeil decorated vaults using dense matching techniques. *ISPRS Annals of Photogrammetry, Remote Sensing and Spatial Information Sciences, II*(5), 97–104. <https://doi.org/10.5194/isprsannals-II-5-97-2014>
- Chiabrandò, F., & Spanò, A. (2013). Point clouds generation using TLS and dense

- matching techniques. A test on approachable accuracies of different tools. *ISPRS Annals of Photogrammetry, Remote Sensing and Spatial Information Sciences, II-5/W1*(September), 67–72. <https://doi.org/10.5194/isprsannals-II-5-W1-67-2013>
- Chiabrando, F., Spanò, A., Sammartano, G., & Teppati Losè, L. (2017). UAV oblique photogrammetry and lidar data acquisition for 3D documentation of the Hercules Fountain. *Virtual Archaeology Review*, 8(16), 83. <https://doi.org/10.4995/var.2017.5961>
- Cignoni, P., Cignoni, P., Callieri, M., Callieri, M., Corsini, M., Corsini, M., ... Ranzuglia, G. (2008). MeshLab: an Open-Source Mesh Processing Tool. *Sixth Eurographics Italian Chapter Conference*, 129–136. <https://doi.org/10.2312/LocalChapterEvents/ItalChap/ItalianChapConf2008/129-136>
- Cipriani, L., & Fantini, F. (2017). Digitalization culture VS archaeological visualization: integration of pipelines and open issues. *ISPRS - International Archives of the Photogrammetry, Remote Sensing and Spatial Information Sciences, XLII-2/W3(2W3)*, 195–202. <https://doi.org/10.5194/isprs-archives-XLII-2-W3-195-2017>
- Cipriani, L., Fantini, F., & Bertacchi, S. (2014). 3D models mapping optimization through an integrated parameterization approach: cases studies from Ravenna. *ISPRS - International Archives of the Photogrammetry, Remote Sensing and Spatial Information Sciences, XL-5(5)*, 173–180. <https://doi.org/10.5194/isprsarchives-XL-5-173-2014>
- Cipriani, L., Fantini, F., & Bertacchi, S. (2014). Survey and representation of vaults and cupolas: An overview on some relevant Italian UNESCO sites. In *2014 International Conference on Virtual Systems & Multimedia (VSMM)* (pp. 50–57). IEEE. <https://doi.org/10.1109/VSMM.2014.7136682>
- Clini, P., Frapiccini, N., Mengoni, M., Nespeca, R., & Ruggeri, L. (2016). SFM technique and focus stacking for digital documentation of archaeological artifacts. In *International Archives of the Photogrammetry, Remote Sensing and Spatial Information Sciences - ISPRS Archives* (Vol. 41, pp. 229–236). <https://doi.org/10.5194/isprsarchives-XLI-B5-229-2016>
- Corns, A., Deevy, A., Devlin, G., Kennedy, L., & Shaw, R. (2015). 3D-Icons: Digitizing cultural heritage structures. *New Review of Information Networking*, 20(1), 59–65. <https://doi.org/10.1080/13614576.2015.1115232>
- D’Ayala, D., & Smars, P. (2003). *Minimum requirement for metric use of non-metric photographic documentation. University of Bath Report*. Retrieved from https://smars.yuntech.edu.tw/papers/eh_report.pdf
- Dall’Asta, E., Bruno, N., Bigliardi, G., Zerbi, A., & Roncella, R. (2016). Photogrammetric techniques for promotion of archaeological heritage: The archaeological museum of Parma (Italy). In *International Archives of the Photogrammetry, Remote Sensing and Spatial Information Sciences - ISPRS Archives* (Vol. 41, pp. 243–250). <https://doi.org/10.5194/isprsarchives-XLI-B5-243-2016>
- de la Fuente Prieto, J., Castaño Perea, E., & Labrador Arroyo, F. (2017). Augmented reality in architecture: rebuilding archaeological heritage. *ISPRS - International*

- Archives of the Photogrammetry, Remote Sensing and Spatial Information Sciences, XLII-2/W3(2W3)*, 311–315. <https://doi.org/10.5194/isprs-archives-XLII-2-W3-311-2017>
- Di Benedetto, M., Ponchio, F., Ganovelli, F., & Scopigno, R. (2010). SpiderGL. In *Proceedings of the 15th International Conference on Web 3D Technology - Web3D '10* (Vol. 1, p. 165). New York, New York, USA: ACM Press. <https://doi.org/10.1145/1836049.1836075>
- Di Pietra, V., Donadio, E., Picchi, D., Sambuelli, L., & Spanò, A. (2017). Multi-source 3D models supporting ultrasonic test to investigate an egyptian sculpture of the archaeological museum in Bologna. *The International Archives of the Photogrammetry, Remote Sensing and Spatial Information Sciences, XLII(2/W3)*, 259–266. <https://doi.org/10.5194/isprs-archives-XLII-2-W3-259-2017>
- Donadio, E. (2013). *Tecnica laser scanning e tecnologia GIS per l'analisi stratigrafica del patrimonio storico costruito: la chiesa di Santa Maria dell'Abbazia di Staffarda*. Politecnico di Torino.
- Donadio, E., Barello, F., & Mazza, R. (2016). Multimedia digital solutions from image and range based models for ancient landscapes communication. *Archeologia E Calcolatori*, 28(2), 485–496. Retrieved from http://www.kainuaproject.eu/__index.php/kainua2017/kainua17/paper/view/51
- Donadio, E., Sambuelli, L., & Spanò, A. (2018). Optimization for Multipurpose Analysis and Representation of Ancient Statues. In F. . Remondino, A. . Georgopoulos, D. . González-Aguilera, & P. Agrafiotis (Eds.), *Latest Developments in Reality-Based 3D Surveying and Modelling* (pp. 95–118). Basel: MDPI.
- Fantini, F., & Pini, S. (2011). Villa Adriana's Serapeum: Optimized 3D Models for Knowledge and Distribution of Archaeological Sites. In E. Jerem, F. Redó, & V. Szeverényi (Eds.), *On the Road to Reconstructing the Past. Computer Applications and Quantitative Methods in Archaeology (CAA). Proceedings of the 36th International Conference. Budapest, April 2-6, 2008* (pp. 340–345). Budapest: Archeolingua.
- Fernandez-Palacios, B. J., Remondino, F., Stefani, C., Lombardo, J., & De Luca, L. (2013a). Web visualization of complex reality-based 3D models with NUBES. In *2013 Digital Heritage International Congress (DigitalHeritage)* (Vol. 1, pp. 701–704). IEEE. <https://doi.org/10.1109/DigitalHeritage.2013.6743821>
- Fernandez-Palacios, B. J., Remondino, F., Stefani, C., Lombardo, J., & De Luca, L. (2013b). Web visualization of complex reality-based 3D models with NUBES. In *2013 Digital Heritage International Congress (DigitalHeritage)* (pp. 701–704). IEEE. <https://doi.org/10.1109/DigitalHeritage.2013.6743821>
- Garland, M., & Heckbert, P. S. (1997). Surface simplification using quadric error metrics. In *Proceedings of the 24th annual conference on Computer graphics and interactive techniques - SIGGRAPH '97* (pp. 209–216). <https://doi.org/10.1145/258734.258849>
- Gattet, E., Devogelaere, J., Raffin, R., Bergerot, L., Daniel, M., Jockey, P., & De Luca, L. (2015). A versatile and low-cost 3D acquisition and processing pipeline for collecting mass of archaeological findings on the field. *ISPRS - International*

- Archives of the Photogrammetry, Remote Sensing and Spatial Information Sciences*, XL-5/W4(February), 299–305. <https://doi.org/10.5194/isprsarchives-XL-5-W4-299-2015>
- Gonizzi Barsanti, S., & Guidi, G. (2017). A geometric processing workflow for transforming reality based 3D models in volumetric meshes suitable for FEA. *ISPRS - International Archives of the Photogrammetry, Remote Sensing and Spatial Information Sciences*, XLII-2/W3(2W3), 331–338. <https://doi.org/10.5194/isprs-archives-XLII-2-W3-331-2017>
- Granshaw, S. I. (2016). Photogrammetric Terminology: Third Edition. *The Photogrammetric Record*, 31(154), 210–252. <https://doi.org/10.1111/phor.12146>
- Grussenmeyer, P., Landes, T., Doneus, M., & Lerma, J.-L. (2016). Basics of range-based modelling techniques in Cultural Heritage 3D recording. In F. Remondino & S. Stylianidis (Eds.), *3D Recording, Documentation and Management in Cultural Heritage* (pp. 305–368). Whittles Publishing.
- Guarnieri, A., Pirotti, F., & Vettore, A. (2010). Cultural heritage interactive 3D models on the web: An approach using open source and free software. *Journal of Cultural Heritage*, 11(3), 350–353. <https://doi.org/10.1016/j.culher.2009.11.011>
- Guidi, G., & Angheluddu, D. (2016). Displacement Mapping as a Metric Tool for Optimizing Mesh Models Originated by 3D Digitization. *Journal on Computing and Cultural Heritage*, 9(2), 1–23. <https://doi.org/10.1145/2843947>
- Guidi, G., Gonizzi Barsanti, S., Micoli, L. L., & Russo, M. (2015). Massive 3D Digitization of Museum Contents. *Built Heritage: Monitoring Conservation Management*, 335–346. https://doi.org/10.1007/978-3-319-08533-3_28
- Guidi, G., Remondino, F., Russo, M., & Spinetti, A. (2009). Range sensors on marble surfaces: quantitative evaluation of artifacts. In F. Remondino, M. R. Shortis, & S. F. El-Hakim (Eds.) (Vol. 744703, p. 744703). <https://doi.org/10.1117/12.827251>
- Haus, G. (2016). Cultural Heritage and ICT: State of the Art and Perspectives. *DigitCult / Scientific Journal on Digital Cultures*, 1(1), 9–20. <https://doi.org/10.4399/97888548960242>
- Hindmarch, J. (2015). *Investigating the use of 3D digitisation for public facing applications in cultural heritage institutions*. University College London (UCL).
- Hirschmüller, H. (2011). Semi-Global Matching - Motivation, Developments and Applications. In D. Fritsch (Ed.), *Photogrammetric Week 11* (pp. 173–184). Wichmann. Retrieved from <http://elib.dlr.de/73119/>
- Hoppe, H. (1996). Progressive meshes. In *Proceedings of the 23rd annual conference on Computer graphics and interactive techniques - SIGGRAPH '96* (pp. 99–108). New York, New York, USA: ACM Press. <https://doi.org/10.1145/237170.237216>
- Hoppe, H., DeRose, T., Duchamp, T., McDonald, J., & Stuetzle, W. (1993). Mesh optimization. In *Proceedings of the 20th annual conference on Computer graphics and interactive techniques - SIGGRAPH '93* (Vol. d, pp. 19–26). New York, New York, USA: ACM Press. <https://doi.org/10.1145/166117.166119>
- Hoppe, H., Kazhdan, M., & Bolitho, M. (2006). Poisson surface reconstruction and its

- applications. In K. Polthier & A. Sheffer (Eds.), *Proceedings of the Eurographics Symposium on Geometry Processing 2006* (p. 10). New York, New York, USA: ACM Press. <https://doi.org/10.1145/1364901.1364904>
- Hu, J.-H., Park, J. M., Park, S., Xiao, B., Dehoff, M. H., Kim, S., ... Worley, P. F. (2010). Homeostatic Scaling Requires Group I mGluR Activation Mediated by Homer1a. *Neuron*, 68(6), 1128–1142. <https://doi.org/10.1016/j.neuron.2010.11.008>
- Jiménez Fernández-Palacios, B., Morabito, D., & Remondino, F. (2017). Access to complex reality-based 3D models using virtual reality solutions. *Journal of Cultural Heritage*, 23, 40–48. <https://doi.org/10.1016/j.culher.2016.09.003>
- Kai-browne, A., Kohlmeyer, K., Gonnella, J., & Bremer, T. (2016). *Digital Heritage. Progress in Cultural Heritage: Documentation, Preservation, and Protection*. (M. Ioannides, E. Fink, A. Moropoulou, M. Hagedorn-Saupe, A. Fresa, G. Liestøl, ... P. Grussenmeyer, Eds.) (Vol. 10059). Cham: Springer International Publishing. <https://doi.org/10.1007/978-3-319-48974-2>
- Kersten, T. P., Omelanowsky, D., & Lindstaedt, M. (2016). Investigations of low-cost systems for 3D reconstruction of small objects. In *Lecture Notes in Computer Science (including subseries Lecture Notes in Artificial Intelligence and Lecture Notes in Bioinformatics)* (Vol. 10058 LNCS, pp. 521–532). Springer International Publishing. https://doi.org/10.1007/978-3-319-48496-9_41
- Kersten, T. P., Przybilla, H.-J., Lindstaedt, M., Tschirschwitz, F., & Misgaiski-Hass, M. (2016). Comparative geometrical investigations of hand-held scanning system. *ISPRS - International Archives of the Photogrammetry, Remote Sensing and Spatial Information Sciences*, XLI-B5(June), 507–514. <https://doi.org/10.5194/isprs-archives-XLI-B5-507-2016>
- Kersten, T. P., Tschirschwitz, F., & Deggim, S. (2017). Development of a virtual museum including 4D presentation of building history in virtual reality. *ISPRS - International Archives of the Photogrammetry, Remote Sensing and Spatial Information Sciences*, XLII-2/W3(2W3), 361–367. <https://doi.org/10.5194/isprs-archives-XLII-2-W3-361-2017>
- Kivilcim, C., & Duran, Z. (2016). A semi- Automated point cloud processing methodology for 3D cultural heritage documentation. *International Archives of the Photogrammetry, Remote Sensing and Spatial Information Sciences - ISPRS Archives*, 41(July), 293–296. <https://doi.org/10.5194z>
- Koska, B., & Křemen, T. (2013). The combination of laser scanning and Structure from Motion technology for creation of accurate exterior and interior orthophotos of St. Nicholas baroque church. *ISPRS - International Archives of the Photogrammetry, Remote Sensing and Spatial Information Sciences*, XL-5/W1(February), 133–138. <https://doi.org/10.5194/isprsarchives-XL-5-W1-133-2013>
- Lachat, E., Macher, H., Landes, T., & Grussenmeyer, P. (2015). Assessment and Calibration of a RGB-D Camera (Kinect v2 Sensor) Towards a Potential Use for Close-Range 3D Modeling. *Remote Sensing*, 7(10), 13070–13097. <https://doi.org/10.3390/rs71013070>
- Lee, A., Moreton, H., & Hoppe, H. (2000). Displaced subdivision surfaces. In

- Proceedings of the 27th annual conference on Computer graphics and interactive techniques - SIGGRAPH '00* (pp. 85–94). New York, New York, USA: ACM Press. <https://doi.org/10.1145/344779.344829>
- Lerma, J. L., Navarro, S., Cabrelles, M., & Villaverde, V. (2010). Terrestrial laser scanning and close range photogrammetry for 3D archaeological documentation: the Upper Palaeolithic Cave of Parpalló as a case study. *Journal of Archaeological Science*, 37(3), 499–507. <https://doi.org/10.1016/j.jas.2009.10.011>
- Levine, S., & McLuhan, M. (1964). Understanding Media: The Extensions of Man. *American Quarterly*, 16(4), 646. <https://doi.org/10.2307/2711172>
- Lévy, B. (2001). Constrained texture mapping for polygonal meshes. In *Proceedings of the 28th annual conference on Computer graphics and interactive techniques - SIGGRAPH '01* (pp. 417–424). New York, New York, USA: ACM Press. <https://doi.org/10.1145/383259.383308>
- Lévy, B., Petitjean, S., Ray, N., & Maillot, J. (2002). Least squares conformal maps for automatic texture atlas generation. In *Proceedings of the 29th annual conference on Computer graphics and interactive techniques - SIGGRAPH '02* (p. 362). New York, New York, USA: ACM Press. <https://doi.org/10.1145/566570.566590>
- Lingua, A., Marenchino, D., & Nex, F. (2009). Performance Analysis of the SIFT Operator for Automatic Feature Extraction and Matching in Photogrammetric Applications. *Sensors*, 9(5), 3745–3766. <https://doi.org/10.3390/s90503745>
- Lo Brutto, M., Garraffa, A., Pellegrino, L., & Di Natale, B. (2015). 3D mosaic documentation using close range photogrammetry. In *Proceedings of 1st International Conference on Metrology for Archaeology Benevento, Italy* (pp. 82–87).
- Lowe, D. G. (2004a). Distinctive Image Features from Scale-Invariant Keypoints. *International Journal of Computer Vision*, 60(2), 91–110. <https://doi.org/10.1023/B:VISI.0000029664.99615.94>
- Lowe, D. G. (2004b). Distinctive Image Features from Scale-Invariant Keypoints. *International Journal of Computer Vision*, 60(2), 91–110. <https://doi.org/10.1023/B:VISI.0000029664.99615.94>
- Luhmann, T., Robson, S., Kyle, S., & Harley, I. (2006). *Close Range Photogrammetry: Principles, Techniques and Applications*. Whittles Publishing.
- Magda Ramos, M., & Remondino, F. (2015). Data fusion in cultural heritage - A review. In *International Archives of the Photogrammetry, Remote Sensing and Spatial Information Sciences - ISPRS Archives* (Vol. 40, pp. 359–363). <https://doi.org/10.5194/isprsarchives-XL-5-W7-359-2015>
- Maini, R., & Aggarwal, H. (2009). Study and comparison of various image edge detection techniques. *International Journal of Image Processing*, 3(1), 1–11. <https://doi.org/http://www.doaj.org/doaj?func=openurl&genre=article&issn=19852304&date=2009&volume=3&issue=1&spage=1>
- Manferdini, A. M., & Remondino, F. (2012). A Review of Reality-Based 3D Model Generation, Segmentation and Web-Based Visualization Methods. *International*

- Journal of Heritage in the Digital Era*, 1(1), 103–123. <https://doi.org/10.1260/2047-4970.1.1.103>
- Martin-Beaumont, N., Nony, N., Deshayes, B., Pierrot-Deseilligny, M., & De Luca, L. (2013). Photographer-Friendly Workflows for Image-Based Modelling of Heritage Artefacts. *International Archives of Photogrammetry, Remote Sensing and Spatial Information Sciences*, XL-5(W2), 421–424.
- Martina, A. (2014). *Politecnico di Torino Doctorate in Electronic Devices ZnO-based nanostructures for gas sensing applications*. Politecnico di Torino. <https://doi.org/10.6092/polito/porto/2541502>
- Matas, J., Chum, O., Urban, M., & Pajdla, T. (2004). Robust wide-baseline stereo from maximally stable extremal regions. *Image and Vision Computing*, 22(10), 761–767. <https://doi.org/10.1016/j.imavis.2004.02.006>
- Menna, F., Nocerino, E., Remondino, F., Dellepiane, M., Callieri, M., & Scopigno, R. (2016). 3D digitization of a heritage masterpiece - A critical analysis on quality assessment. *ISPRS - International Archives of the Photogrammetry, Remote Sensing and Spatial Information Sciences*, XLI-B5, 675–683. <https://doi.org/10.5194/isprsarchives-XLI-B5-675-2016>
- Merlo, A., Dalco, L., & Fantini, F. (2012). Game engine for Cultural Heritage: New opportunities in the relation between simplified models and database. In *2012 18th International Conference on Virtual Systems and Multimedia* (pp. 623–628). IEEE. <https://doi.org/10.1109/VSMM.2012.6365993>
- Merlo, A., Fantini, F., Aliperta, A., Lavoratti, G., & López Hernández, J. L. (2013). Texturing e ottimizzazione dei modelli digitali reality based: la chiesa della Compañía de Jesús Texturing and optimization of reality based digital models : the church of Compañía de Jesús. *Disegnare Con*, 6(12), 1–14.
- Merlo, A., Sánchez Belenguer, C., Vidal Vendrell, E., Fantini, F., & Aliperta, A. (2013). 3D MODEL VISUALIZATION ENHANCEMENTS IN REAL-TIME GAME ENGINES. In *ISPRS Archives – Volume of the 5th International Workshop 3D-ARCH 2013 – 3D Virtual Reconstruction and Visualization of Complex Architectures* (Vol. XL, pp. 181–188).
- Minto, S., & Remondino, F. (2014). Online Access and Sharing of Reality-based 3d Models. *SCIRES-IT - SCIENTIFIC RESEARCH AND INFORMATION TECHNOLOGY*, 4(2), 17–28. <https://doi.org/10.2423/i22394303v4n2p17>
- Murphy, M., MCGovern, E., & Pavia, S. (2009). Structural Survey Historic building information modelling (HBIM) Historic building information modelling (HBIM). *Structural Survey Structural Survey Iss Facilities*, 274(3), 311–327.
- Nicolae, C., Nocerino, E., Menna, F., & Remondino, F. (2014). Photogrammetry applied to Problematic artefacts. *ISPRS - International Archives of the Photogrammetry, Remote Sensing and Spatial Information Sciences*, XL-5(5), 451–456. <https://doi.org/10.5194/isprsarchives-XL-5-451-2014>
- Nocerino, E., Menna, F., & Remondino, F. (2014). Accuracy of typical photogrammetric networks in cultural heritage 3D modeling projects. *ISPRS - International Archives of the Photogrammetry, Remote Sensing and Spatial Information Sciences*, XL-5(5),

465–472. <https://doi.org/10.5194/isprsarchives-XL-5-465-2014>

- Nony, N., De Luca, L., Godet, A., Pierrot-Deseilligny, M., Remondino, F., Van Dongen, A., & Vincitore, M. (2012). Protocols and Assisted Tools for Effective Image-Based Modeling of Architectural Elements. In *Lecture Notes in Computer Science (including subseries Lecture Notes in Artificial Intelligence and Lecture Notes in Bioinformatics)* (Vol. 7616 LNCS, pp. 432–439). Springer, Berlin, Heidelberg. https://doi.org/10.1007/978-3-642-34234-9_44
- Oreni, D., Brumana, R., Della Torre, S., Banfi, F., Barazzetti, L., & Previtali, M. (2014). Survey turned into HBIM: the restoration and the work involved concerning the Basilica di Collemaggio after the earthquake (L'Aquila). *ISPRS Annals of Photogrammetry, Remote Sensing and Spatial Information Sciences*, II-5(June), 267–273. <https://doi.org/10.5194/isprsannals-II-5-267-2014>
- Ott, M., & Pozzi, F. (2011). Towards a new era for Cultural Heritage Education: Discussing the role of ICT. *Computers in Human Behavior*, 27(4), 1365–1371. <https://doi.org/10.1016/j.chb.2010.07.031>
- Owen Ruth, Buhalis Dimitrios, & Pletinckx Daniël. (2005). Visitors' Evaluations of ICTs Used in Cultural Heritage. In Mudge M, Ryan N, & Scopigno R (Eds.), *VAST 2005 The 6th International Symposium on Virtual Reality, Archaeology and Cultural Heritage* (pp. 129–136). Pisa: Eurographics Association.
- Pan, R., Tang, Z., Xu, S., & Da, W. (2016). Normals and texture fusion for enhancing orthogonal projections of 3D models. *Journal of Cultural Heritage*, 23, 33–39. <https://doi.org/10.1016/j.culher.2016.07.009>
- Patias, P. (2006). *Cultural heritage documentation. International summer school "Digital recording and 3D Modeling."* Retrieved from <https://pdfs.semanticscholar.org/cddb/9d9dec8d69cc25668f01c7d2c0f910220477.pdf>
- Payne, E. M. (2013). Imaging Techniques in Conservation. *Journal of Conservation and Museum Studies*, 10(2), 17–29. <https://doi.org/10.5334/jcms.1021201>
- Pepe, M., Ackermann, S., Fregonese, L., & Achille, C. (2016). 3D Point Cloud Model Color Adjustment by Combining Terrestrial Laser Scanner and Close Range Photogrammetry Datasets. *World Academy of Science, Engineering and Technology, International Journal of Computer, Electrical, Automation, Control and Information Engineering*, 10(11), 1918–1924.
- Pierdicca, R., Frontoni, E., Zingaretti, P., Malinverni, E. S., Colosi, F., & Orazi, R. (2015). *Augmented and Virtual Reality*. (L. T. De Paolis & A. Mongelli, Eds.), *Augmented and virtual reality: Second International Conference, AVR 2015* (Vol. 9254). Cham: Springer International Publishing. <https://doi.org/10.1007/978-3-319-22888-4>
- Pierrot-Deseilligny, Marc and Paparoditis, N. (2006). A Multiresolution and Optimization-Based Image Matching Approach: An Application to Surface Reconstruction from SPOT 5-HRS Stereo Imagery. *Archives of Photogrammetry, Remote Sensing and Spatial Information Sciences*, 36.
- Pierrot-Deseilligny, M., De Luca, L., & Remondino, F. (2011). Automated Image-Based

- Procedures for Accurate Artifacts 3D Modeling and Orthoimage Generation. *Geoinformatics FCE CTU*, 6, 291–299. <https://doi.org/10.14311/gi.6.36>
- Pierrot Deseilligny, M., & Clery, I. (2011). APERO, an open source Bundle Adjustment software for automatic calibration and orientation of a set of images. *ISPRS - International Archives of the Photogrammetry, Remote Sensing and Spatial Information Sciences*, XXXVIII-5(W16), 269–276. <https://doi.org/10.5194/isprsarchives-XXXVIII-5-W16-269-2011>
- Piponi, D., & Borshukov, G. (2000). Seamless texture mapping of subdivisions surfaces by nodel pelting and texture blending. *SIGGRAPH '00 Proceedings of the 27th Annual Conference on Computer Graphics and Interactive Techniques*, 471–478. <https://doi.org/http://doi.acm.org/10.1145/344779.344990>
- Ponchio, F., Callieri, M., Benedetto, M., Ponchio, F., Malomo, L., Callieri, M., ... Scopigno, R. (2014). *3D Research Challenges in Cultural Heritage*. (M. Ioannides & E. Quak, Eds.) (Vol. 8355). Berlin, Heidelberg: Springer Berlin Heidelberg. <https://doi.org/10.1007/978-3-662-44630-0>
- Potenziani, M., Callieri, M., Dellepiane, M., Corsini, M., Ponchio, F., & Scopigno, R. (2015). 3DHOP: 3D Heritage Online Presenter. *Computers & Graphics*, 52, 129–141. <https://doi.org/10.1016/j.cag.2015.07.001>
- Quattrini, R., Malinverni, E. S., Clini, P., Nespeca, R., & Orlietti, E. (2015). From TLS to HBIM. High quality semantically-aware 3D modeling of complex architecture. *ISPRS - International Archives of the Photogrammetry, Remote Sensing and Spatial Information Sciences*, XL-5/W4(5W4), 367–374. <https://doi.org/10.5194/isprsarchives-XL-5-W4-367-2015>
- Ramos, E. A., & Sadri, B. (2007). Geometric and Topological Guarantees for the Wrap Reconstruction Algorithm. In *Proceedings of the 18th annual ACM-SIAM symposium on Discrete algorithms* (pp. 1086–1095).
- Ramos, M. M., & Remondino, F. (2015). Data fusion in Cultural Heritage - A Review. *ISPRS - International Archives of the Photogrammetry, Remote Sensing and Spatial Information Sciences*, XL-5/W7(5W7), 359–363. <https://doi.org/10.5194/isprsarchives-XL-5-W7-359-2015>
- Remondino, F. (2003). From point cloud to surface: the modeling and visualization problem. *International Archives of Photogrammetry, Remote Sensing and Spatial Information Sciences*, Vol. XXXIV-5/W10, XXXIV(February), 24–28.
- Remondino, F., Del Pizzo, S., Kersten, T. P., & Troisi, S. (2012). Low cost and open source solutions for automated image orientation - A critical overview. In M. Ioannides, D. Fritsch, J. Leissner, R. Davies, R. Caffo, & F. Remondino (Eds.), *Progress in Cultural Heritage Preservation - 4th International Conference, EuroMed 2012 Limassol, Cyprus, October 29 –November 3, 2012 Proceedings* (pp. 40–55). Springer.
- Remondino, F., Nocerino, E., Toschi, I., & Menna, F. (2017). A critical review of automated photogrammetric processing of large datasets. *ISPRS - International Archives of the Photogrammetry, Remote Sensing and Spatial Information Sciences*, XLII-2/W5(September), 591–599. <https://doi.org/10.5194/isprs-archives-XLII-2->

W5-591-2017

- Remondino, F., & Rizzi, A. (2010). Reality-based 3D documentation of natural and cultural heritage sites—techniques, problems, and examples. *Applied Geomatics*, 2(3), 85–100. <https://doi.org/10.1007/s12518-010-0025-x>
- Remondino, F., Spera, M. G., Nocerino, E., Menna, F., & Nex, F. (2014). State of the art in high density image matching. *The Photogrammetric Record*, 29(146), 144–166. <https://doi.org/10.1111/phor.12063>
- Rijsdijk, M. (2014). Full Automatically Generated True Orthophotos , Sensational 3D Pointclouds and Dense Matching Techniques in Topographical Mapping Full Automatically Generated True Orthophotos , Sensational 3D Pointclouds and Dense Matching Techniques in Topographical Map. In *FIG Congress Engaging the Challenges*”. Kuala Lumpur (Malaysia) (pp. 16–21).
- Robleda, P. G., Caroti, G., Martínez-Espejo Zaragoza, I., & Piemonte, A. (2016). Computational vision in UV-mapping of textured meshes coming from photogrammetric recovery: unwrapping frescoed vaults. *ISPRS - International Archives of the Photogrammetry, Remote Sensing and Spatial Information Sciences*, XLI-B5(July), 391–398. <https://doi.org/10.5194/isprsarchives-XLI-B5-391-2016>
- Rodríguez-González, P., Nocerino, E., Menna, F., Minto, S., & Remondino, F. (2015). 3D surveying and modeling of underground passages in WWI fortifications. *ISPRS - International Archives of the Photogrammetry, Remote Sensing and Spatial Information Sciences*, XL-5/W4(February), 17–24. <https://doi.org/10.5194/isprsarchives-XL-5-W4-17-2015>
- Rodríguez Miranda, Á., Valle Melón, J. M., Calparsoro, E., & Iñáñez, J. G. (2017). Study, revalorization and virtual musealization of a ceramic kiln based on information gathered from old excavations. *Digital Applications in Archaeology and Cultural Heritage*, 7, 1–9. <https://doi.org/10.1016/j.daach.2017.08.003>
- Rothermel, M., & Wenzel, K. (2012). SURE - Photogrammetric Surface Reconstruction from Imagery. *Proceedings LC3D Workshop*, 1–21.
- Samaan, M., Héno, R., Pierrot-Deseilligny, M., Pascal, B., & France, C. (2013). Close-Range Photogrammetric Tools for Small 3D Archeological Objects. *International Archives of the Photogrammetry, Remote Sensing and Spatial Information Sciences*, Volume XL-5/W2, 1(2), 549–553.
- Sammartano, G. (2018). *Suitability Of 3D Dense Models For Rapid Mapping Strategies On Cultural Heritage Documentation And Conservation. Validation of metric and non-metric information extraction from integrated solutions*. Politecnico di Torino.
- Santos, P., Ritz, M., Tausch, R., Schmedt, H., Monroy, R., Stefano, A. De, ... Fellner, D. W. (2014). CultLab3D - On the Verge of 3D Mass Digitization. *Proceedings of the Eurographics Workshop on Graphics and Cultural Heritage*, 1–25. <https://doi.org/10.2312/gch.20141305.065-073>
- Scopigno, R., Callieri, M., Dellepiane, M., Ponchio, F., & Potenziani, M. (2017). Delivering and using 3D models on the web: are we ready? *Virtual Archaeology Review*, 8(17), 1. <https://doi.org/10.4995/var.2017.6405>

- Shrivakshan, G. T., & Chandrasekar, C. (2012). A Comparison of various Edge Detection Techniques used in Image Processing. *International Journal of Computer Science Issues (IJCSI)*, 9(5), 269–276. Retrieved from www.IJCSI.org
- Silver, M. (2016). Conservation Techniques in Cultural Heritage. In F. Remondino & E. Stylianidis (Eds.), *3D Recording, Documentation and Management of Cultural Heritage* (pp. 15–84). Whittles Publishing.
- Snavely, N. (2008). Bundler: Structure from Motion (SfM) for Unordered Image Collections.
- Spangher, A., Visintini, D., Tucci, G., & Bonora, V. (2017). Geomatic 3D modeling of a statue (also) for structural analysis and risk evaluation: the example of San Giovannino Martelli in Florence. *ISPRS - International Archives of the Photogrammetry, Remote Sensing and Spatial Information Sciences, XLII-5/W1(5W1)*, 61–68. <https://doi.org/10.5194/isprs-archives-XLII-5-W1-61-2017>
- Sužiedelytė-Visockienė, Jūratė Bagdžiūnaitė, R., Malys, N., & Malienė, V. (2015). Close-range photogrammetry enables documentation of environment-induced deformation of architectural heritage. *Environmental Engineering and Management Journal*, 14(6), 1371–1381.
- Szeliski, R. (2011a). *Computer Vision. Computer Vision: Algorithms and Applications*. London: Springer London. <https://doi.org/10.1007/978-1-84882-935-0>
- Szeliski, R. (2011b). Structure from motion. In *Computer Vision: Algorithms and Applications* (pp. 303–334). https://doi.org/10.1007/978-1-84882-935-0_7
- Tarini, M., Pietroni, N., Cignoni, P., Panozzo, D., & Puppo, E. (2010). Practical quad mesh simplification. *Computer Graphics Forum*, 29(2), 407–418. <https://doi.org/10.1111/j.1467-8659.2009.01610.x>
- Thomas Luhmann, Stuart Robson, S., & Kyle, J. B. (2014). *Close-Range Photogrammetry and 3D Imaging*.
- Tucci, G., Bonora, V., Conti, A., & Fiorini, L. (2015). Benchmarking Range-Based and Image-Based Techniques for Digitizing a Glazed Earthenware Frieze. *ISPRS Annals of Photogrammetry, Remote Sensing and Spatial Information Sciences, II-5/W3*, 315–322. <https://doi.org/10.5194/isprsannals-II-5-W3-315-2015>
- Tucci, G., Cini, D., & Nobile, A. (2011). Effective 3D digitization of archaeological artifacts for interactive virtual museum. In *Proceedings of the 4th ISPRS International Workshop 3D-ARCH* (pp. 413–420). <https://doi.org/10.5194/isprsarchives-XXXVIII-5-W16-413-2011>
- Verhoeven, G. (2011). Taking computer vision aloft - archaeological three-dimensional reconstructions from aerial photographs with photostan. *Archaeological Prospection*, 18(1), 67–73. <https://doi.org/10.1002/arp.399>
- Verhoeven, G., Taelman, D., & Vermeulen, F. (2012). Computer Vision-Based Orthophoto Mapping Of Complex Archaeological Sites: The Ancient Quarry Of Pitaranha (Portugal-Spain). *Archaeometry*, 54(6), 1114–1129. <https://doi.org/10.1111/j.1475-4754.2012.00667.x>
- Verykokou, S., Ioannidis, C., & Kontogianni, G. (2014). 3D visualization via augmented

- reality: The case of the middle stoa in the ancient agora of Athens. *Lecture Notes in Computer Science (Including Subseries Lecture Notes in Artificial Intelligence and Lecture Notes in Bioinformatics)*, 8740, 279–289. <https://doi.org/10.1007/978-3-319-13695-0>
- Vincent, M. L., Gutierrez, M. F., Coughenour, C., Manuel, V., Bendicho, L.-M., Remondino, F., & Fritsch, D. (2015). Crowd-sourcing the 3D digital reconstructions of lost cultural heritage. In *2015 Digital Heritage* (pp. 171–172). IEEE. <https://doi.org/10.1109/DigitalHeritage.2015.7413863>
- Wenzel, K., Rothermel, M., Fritsch, D., & Haala, N. (2013). Image Acquisition and Model Selection for Multi-View Stereo. *International Archives of the Photogrammetry, Remote Sensing and Spatial Information Sciences, 3D-ARCH 2013 - 3D Virtual Reconstruction and Visualization of Complex Architectures, XL(5/W1)*, 251–258. <https://doi.org/10.5194/isprsarchives-XL-5-W1-251-2013>
- Wenzel, K., Rothermel, M., Haala, N., & Fritsch, D. (2013). (read)SURE – The ifp Software for Dense Image Matching. *Photogrammetric Week 2013*, 59–70. Retrieved from <http://www.ifp.uni-stuttgart.de/publications/phowo13/index.en.html>
- Westoby, M. J., Brasington, J., Glasser, N. F., Hambrey, M. J., & Reynolds, J. M. (2012). “Structure-from-Motion” photogrammetry: A low-cost, effective tool for geoscience applications. *Geomorphology*, 179, 300–314. <https://doi.org/10.1016/j.geomorph.2012.08.021>
- Wu, C. (2011). Visual SFM: A visual structure from motion system. <Http://Ccwu.Me/Vsfm>. Retrieved from <http://ccwu.me/vsfm/doc.html>
- Zhang, L., & Gruen, A. (2006). Multi-image matching for DSM generation from IKONOS imagery. *ISPRS Journal of Photogrammetry and Remote Sensing*, 60(3), 195–211. <https://doi.org/10.1016/j.isprsjprs.2006.01.001>